**TECHNISCHE
UNIVERSITÄT
DRESDEN**

Direct dynamical tunneling in systems with a mixed phase space

Dissertation
zur Erlangung des akademischen Grades
Doctor rerum naturalium

vorgelegt von

Lars Schilling
geboren am 06.10.1977 in Hamburg

Institut für Theoretische Physik
Fachrichtung Physik
Fakultät Mathematik und Naturwissenschaften
Technische Universität Dresden

2006

Abstract

Tunneling in 1D describes the effect that quantum particles can penetrate a classically insurmountable potential energy barrier. The extension to classically forbidden transitions in phase space generalizes the tunneling concept. A typical 1D Hamiltonian system has a mixed phase space. It contains regions of regular and chaotic dynamics, the so-called regular islands and the chaotic sea. These different phase space components are classically separated by dynamically generated barriers. Quantum mechanically they are, however, connected by dynamical tunneling. We perform a semiclassical quantization of almost resonance-free regular islands and transporting island chains of quantum maps. This yields so-called quasimodes, which are used for the investigation of direct dynamical tunneling from an almost resonance-free regular island to the chaotic sea. We derive a formula which allows for the determination of dynamical tunneling rates. Good agreement between this analytical prediction and numerical results is found over several orders of magnitude for two example systems.

Zusammenfassung

Der 1D Tunneleffekt bezeichnet das Durchdringen einer klassisch nicht überwindbaren potentiellen Energiebarriere durch Quantenteilchen. Eine Verallgemeinerung des Tunnelbegriffs ist die Erweiterung auf jegliche Art von klassisch verbotenen Übergangsprozessen im Phasenraum. Der Phasenraum eines typischen 1D Hamiltonschen Systems ist gemischt. Er besteht aus Bereichen regulärer und chaotischer Dynamik, den sogenannten regulären Inseln und der chaotischen See. Während diese verschiedenen Phasenraumbereiche klassisch durch dynamisch generierte Barrieren voneinander getrennt sind, existiert quantenmechanisch jedoch eine Verknüpfung durch den dynamischen Tunnelprozess. In dieser Arbeit wird eine semiklassische Quantisierung von praktisch resonanz-freien regulären Inseln und transportierenden Inselketten von Quantenabbildungen durchgeführt. Die daraus folgenden sogenannten Quasimoden werden für die Untersuchung des direkten dynamischen Tunnelns aus einer praktisch resonanz-freien regulären Insel in die chaotische See verwendet, was auf eine Tunnelraten vorhersagende Formel führt. Ihre anschließende Anwendung auf zwei Modellsysteme zeigt eine gute Übereinstimmung zwischen Numerik und analytischer Vorhersage über viele Größenordnungen.

"Die Naturwissenschaft braucht der Mensch zum Erkennen,
 den Glauben zum Handeln."

Max Planck (1858-1947)

Contents

List of Figures

The plots in this thesis were generated with the software PYXGraph which simplifies the usage of PYX (`http://pyx.sourceforge.net/`). The programmes for numerical computations were written in Python (`http://www.python.org`) using NumPy and SciPy (`http://www.scipy.org`).

1 Introduction

In classical physics the position and the momentum of a particle can be determined as functions of time by solving equations of motion with given initial conditions. This does not hold on the quantum level anymore. There, one has the property that a quantum particle appears within a volume element with a certain probability. The corresponding probability density is given by the square of the modulus of the quantum particle wave function. This wave function itself is the solution of Schrödinger's equation, which describes the dynamics of the quantum system. A property of quantum wave functions is that they can have non-zero values in regions which are not accessible in classical physics, implying that quantum particles can enter classically forbidden regions. An interesting consequence of this observation is that quantum particles can penetrate classically insurmountable potential energy barriers. This classically unimaginable phenomenon is known as tunneling effect. Experimental examples are the α-decay of unstable nuclei, where a quantum particle escapes from a quasi-bound region, or the inversion oscillation of the NH_3-molecule, where a quantum particle performs a transition between two symmetry-related potential energy wells.

The standard textbook situation of tunneling is a particle with mass m in a static symmetric 1D double well potential energy $V(q)$ with a focus on the short wavelength or semiclassical limit. This limit can symbolically be expressed in the following manner: If one treats the system in terms of dimensionless quantities, Planck's constant h needs to be divided by a characteristic action, which is the product of a characteristic length q_0 and a characteristic momentum p_0. This yields the so-called effective Planck constant $h_{\mathrm{eff}} := h/(q_0 p_0)$. The more a system gains classical properties, the larger the characteristic length and momentum, and consequently the smaller the effective Planck constant become. The semiclassical limit is therefore associated with the limit $h_{\mathrm{eff}} \to 0$. A suitable semiclassical technique for solving Schrödinger's equation is the Wentzel-Kramers-Brillouin (WKB) ansatz [1]. It yields so-called local quasimodes by neglecting the coupling between the two wells of the potential energy. These quasimodes are semiclassical states, which are associated with certain closed quantizing phase space curves within either the left or the right well of $V(q)$. Due to the neglection of a coupling and due to the symmetry of the considered potential energy, a quasimode of the left well with e.g. a certain WKB

energy E has a partner with the same energy in the right well. They form a doublet. As the eigenstates of the Hamilton operator $\hat{H}$ of the system are symmetric or antisymmetric due to the symmetry of $V(q)$, the quasimodes of such a doublet cannot be eigenstates. But it turns out that the symmetric and antisymmetric linear combination of the doublet quasimodes are good approximations of two eigenstates of $\hat{H}$ with eigenenergies possessing the splitting

$$\Delta E(E) \;\; = \;\; \frac{\hbar_{\text{eff}}\,\omega(E)}{\pi} \exp\left(-\frac{1}{\hbar_{\text{eff}}} \int\limits_{-a(E)}^{a(E)} \mathrm{d}q \sqrt{2\left[V(q)-E\right]}\right). \tag{1.1}$$

Such a splitting is a direct consequence of the quantum mechanical tunneling process. Here $\omega(E)$ denotes the angular frequency of the considered particle within the two wells and $a(E)$ stands for the left classical turning point at energy E in the right well of the potential energy. The integral in the exponential function of equation (1.1) is performed over the classically forbidden region under the potential energy barrier, which separates the two wells from each other. The time evolution of initial states that are equal to the quasimodes of the doublet with energy E shows oscillations between the two wells of $V(q)$ with the frequency $\Delta E(E)/\hbar_{\text{eff}}$. The corresponding tunneling rate is therefore proportional to the tunnel splitting (1.1). It decreases exponentially with $1/\hbar_{\text{eff}}$, which is in agreement with the observation that tunneling does not occur in classical physics.

The notion of tunneling can be extended to any kind of classically forbidden transitions between distinct phase space regions. The investigation of these transition processes has shown that they are classically not necessarily inhibited by static potential energy barriers, but also by other constraints of the underlying classical dynamics, like e.g. integrals of motion [2, 3]. In reference [4] it is demonstrated that quantum transitions can occur between phase space regions which are classically separated by a dynamically generated barrier. In contrast to tunneling through a static potential energy barrier, this different kind of an allowed quantum transition is called dynamical tunneling. Recently, this has been observed experimentally by using cold atoms which propagate in periodically modulated optical lattices [5, 6].

The phase space structure generally influences possible transition processes [7]. Whereas the WKB ansatz is appropriate in 1D systems, it cannot easily be used for the investigation of tunneling in higher dimensions. If the underlying classical dynamics is integrable, the method of complex paths in a complexified phase space can be performed in higher dimensions [8]. But, generic 1D Hamiltonian systems have a mixed phase space with co-existing regular and chaotic regions [9]. The regular phase space components are usually

called regular islands or islands of stability, while the chaotic region forms the chaotic sea. Quantum states whose phase space representation localizes within the regular phase space part are called regular. Correspondingly, the phase space representation of chaotic states localizes in the chaotic sea.

The numerical investigation of tunneling between two symmetric regular phase space islands embedded in the chaotic sea shows that the tunnel splittings and the corresponding tunneling rates do not follow an exponential scaling with $1/\hbar_{\text{eff}}$ as in the 1D case (1.1). They rather fluctuate erratically and may be greatly enhanced [10–13]. This behaviour is described by the chaos-assisted tunneling mechanism [10, 11]. It assumes a coupling of the quasimodes of a doublet, which are associated with an invariant torus within respectively one of the two regular islands, via a chaotic state. The chaotic sea is modelled by means of a statistical ansatz and is represented by a random matrix from the Gaussian orthogonal ensemble. If the quasimodes of the considered doublet are in resonance with a chaotic state, the chaos-assisted coupling mechanism becomes very effective and yields an enhanced tunnel splitting.

The consideration of chaos-assisted tunneling in the absence of reflexion symmetry between the two regular islands is performed in reference [14]. It turned out that tunneling rates can, instead of being enhanced, also be suppressed in some cases [15, 16]. A further approach to the theoretical understanding of chaos-assisted tunneling is the evaluation of the semiclassical propagator by means of complex orbits [17–20]. It is also possible to generalize the random matrix ansatz to the tunneling-induced decay of quasi-bound states in open systems, which enables the investigation of the ionization of non-dispersive electronic wave packets in resonantly driven hydrogen atoms [21]. Chaos-assisted tunneling appears furthermore in experiments with optical cavities [22] and in microwave billiards [23, 24].

Regular islands in a phase space consist of invariant tori. They show an embedded fine structure, the so-called resonance island chains, which arise as a consequence of non-linear perturbations. These resonance island chains are responsible for plateaus or peaks in the tunnel splittings in the semiclassical limit. The resonance-assisted tunneling theory explains this observation as an effect of the coupling of regular states of the same island [25–29].

Resonance island chains within regular islands do always exist. By means of "phase space engineering" it is, however, possible to construct systems, where they are very small compared to the size of the regular island. Dynamical tunneling also occurs, when resonance island chains cannot be resolved by the effective Planck constant. This implies that apart from the resonance-assisted mechanism another tunneling process exists. Since this mechanism connects a regular state directly to a chaotic one, it will be called direct

dynamical tunneling in this thesis.

Following the early considerations in reference [30], one expects that the direct dynamical tunneling rate γ from a regular island to the surrounding chaotic sea semiclassically scales as

$$\gamma \sim \exp\left(-C\,\frac{A_{\text{reg}}}{h_{\text{eff}}}\right), \tag{1.2}$$

where A_{reg} denotes the size of the regular island and C a not universal constant. For a Wannier-Stark potential energy one obtains $C = 2\pi$ [31] and $C > 2\pi$ for rough nanowires [32]. Direct dynamical tunneling between two symmetry related regular islands embedded in the chaotic sea is studied in reference [33]. The semiclassical expansion of the corresponding tunnel splitting expression is presented in reference [29]. The transfer of this ansatz to dynamical tunneling from a regular island to the surrounding chaotic sea yields $C = 2 - \ln 4$. As is shown in reference [34], a correct implementation of the ansatz made in reference [33] actually yields $C = 3 - \ln 4$.

The direct dynamical tunneling approach in reference [33] is restricted to the regular ground state. Moreover, it does not describe our numerically determined tunneling rates in the semiclassical limit. Thus, a general theory for direct dynamical tunneling from a regular island to the chaotic sea and its semiclassical evaluation still do not exist. We address this task in this thesis and present a new approach. It yields a formula which allows for the determination of direct dynamical tunneling rates of all regular states belonging to the island, i.e. for all allowed quantum numbers at a given value of the effective Planck constant. The formula still depends on the quantum time evolution operator of the considered system and requires thus a special evaluation for every system of interest. We are able to evaluate our tunneling rate formula further for a special class of 1D kicked systems. The application of this modified formula to example systems with an elliptic harmonic oscillator-like regular island or a generic deformed regular island shows for all allowed quantum numbers a good agreement with numerically determined data over several orders of magnitude in a large domain of the effective Planck constant. The derivation of a general semiclassical formula, which expresses the tunneling rate as a function of the effective Planck constant h_{eff}, the quantum number m, and classical properties of the considered system like e.g. the area A_{reg} of the regular island or the rotation number R_m, is difficult. Using the WKB ansatz it is, however, possible to derive a semiclassical formula for direct dynamical tunneling rates from an elliptic harmonic oscillator-like regular island to the chaotic sea. Its prediction shows also a good agreement with numerical data over several orders of magnitude.

This thesis is organized as follows. In chapter 2 we recall the WKB ansatz and show

how it can be applied to static 1D potential energies with a double well shape, in order to understand 1D tunneling in the semiclassical limit. As the aim of this thesis is the derivation of a general semiclassical description of the direct dynamical tunneling process from a regular island to the surrounding chaotic sea, we need systems with a suitable phase space for numerical studies. Periodically kicked systems in 1D can easily be tailored to special needs. Their stroboscopic classical dynamics is described by a map, which possesses the area-preserving property. Chapter 3 introduces periodically kicked systems in 1D briefly and recalls their quantization. This chapter is closed with some comments on the Husimi representation. One tool for the investigation of direct dynamical tunneling from a regular island to the chaotic sea in the short wavelength limit are the quasimodes of the regular island. They are the result of a semiclassical quantization. Chapter 4 discusses the semiclassical quantization of almost resonance-free regular islands and transporting island chains of quantum maps defined on a torus. Chapter 5 presents a new theoretical approach to the understanding of direct dynamical tunneling from a regular island to the chaotic sea. Two numerical tests with 1D periodically kicked systems complete this part. The phase space of the first example shows an elliptic, harmonic oscillator-like regular island. In the second example we study the more generic case, where the regular island is deformed. The description of methods suited for the numerical determination of dynamical tunneling rates closes this chapter. Finally, a summary of the results of this thesis and an overview of open questions are given.

2 WKB approximation and 1D tunneling effect

The dynamics of a quantum particle is governed by the Schrödinger equation. It reads

$$\mathrm{i}\,\hbar\,\frac{\partial \Psi(q,t)}{\partial t} \;=\; \hat{H}\Psi(q,t) \tag{2.1}$$

in position representation in the 1D case. Here $\hat{H}$ represents the Hamilton operator, q and t denote the position and the time, and $\hbar$ stands for Planck's constant h divided by 2π. If the Hamilton operator does not explicitly depend on time, the time dependence in the wave function $\Psi(q,t)$ can be separated by means of the ansatz

$$\Psi(q,t) \;=\; \psi(q)\exp\left(-\frac{\mathrm{i}}{\hbar}Et\right), \tag{2.2}$$

where $\psi(q)$ is a solution of the time independent or stationary Schrödinger equation

$$\hat{H}\psi(q) \;=\; E\psi(q) \tag{2.3}$$

with the energy eigenvalue E.

An important property of the quantum particle Schrödinger wave function $\psi(q)$ is that its value can be different from zero in classically not accessible regions. Since the square of the modulus of $\psi(q)$ is equal to the quantum mechanical probability density of finding the quantum particle in a certain volume element, a quantum particle can enter classically forbidden regions. This is completely unimaginable in classical physics. A classically forbidden region exists e.g. under a 1D potential energy barrier, if the energy of a particle is smaller than the barrier height. A non-zero residence probability under the barrier also enables quantum particles to penetrate it. This quantum phenomenon without a classical analogue is known as 1D tunneling effect. It has already been experimentally observed. Examples are the α-decay of unstable nuclei, where a quantum particle escapes from a quasi-bound region, or the inversion oscillation of the NH_3-molecule, where a quantum particle performs a transition between two symmetry-related potential energy wells sepa-

rated by an energetic barrier.

Following Bohr's correspondence principle one expects a gradual transition from quantum to classical mechanics in the so-called semiclassical limit, where the de Broglie wave length of a particle becomes small with respect to the typical length of a considered system. The study of the 1D tunneling effect in the semiclassical limit requires a semiclassical technique for solving Schrödinger's equation. One important approach is the WKB approximation, which is named after its developers Wentzel, Kramers, and Brillouin.

In section 2.1 we give a brief account of the WKB approximation. The application to the harmonic oscillator and some remarks on uniform approximations close this section. The WKB approximation is an important tool for the understanding of the 1D tunneling effect in the semiclassical limit, which is recalled in section 2.2. Finally, we continue with the discussion of a double well example in section 2.3.

2.1 WKB approximation

The WKB approximation provides a semiclassical solution of the stationary Schrödinger equation. The following brief consideration of this method follows the textbook by Landau and Lifschitz [1].

2.1.1 WKB method

The Hamilton operator of a spinless particle with mass m moving in a stationary 1D potential energy $V(q)$ reads

$$\hat{H} \;\; = \;\; -\frac{\hbar^2}{2m}\frac{\mathrm{d}^2}{\mathrm{d}q^2} + V(\hat{q}). \tag{2.4}$$

For theoretical considerations it is often helpful to deal with dimensionless quantities. An explanation of the necessary steps for making a considered physical 1D system dimensionless can be found in appendix A.1. Following these instructions, one finds

$$\hat{\tilde{H}} \;\; = \;\; -\frac{\hbar_{\mathrm{eff}}^2}{2}\frac{\mathrm{d}^2}{\mathrm{d}\tilde{q}^2} + \tilde{V}(\hat{\tilde{q}}) \tag{2.5}$$

as dimensionless analogue of equation (2.4). The tilde on a quantity denotes that it is dimensionless. It will be omitted in the following. The dimensionless Planck constant, the so-called effective Planck constant, will be denoted by h_{eff}. The effective Planck constant is equal to the ratio of h and a typical action of the system, which itself is given by the product of a typical length and a typical momentum. As the latter two quantities grow

in the semiclassical limit, it can symbolically be denoted by the limit $h_{\text{eff}} \to 0$.

With the expression (2.5) one can start to solve the time independent Schrödinger equation (2.3) semiclassically using the WKB approximation. Since a spinless particle is considered, the eigenfunction $\psi(q)$ of the Hamilton operator (2.5) must be scalar. As it is in general complex, the decomposition into an amplitude $A(q)$ and a phase $\varphi(q)$ multiplied with $\hbar_{\text{eff}}$ is appropriate

$$\psi(q) \;\; = \;\; A(q) \exp\left(\frac{\mathrm{i}}{\hbar_{\text{eff}}}\varphi(q)\right). \tag{2.6}$$

With $\sigma(q) = \varphi(q) + (\hbar_{\text{eff}}/\mathrm{i})\ln(A(q))$ one has

$$\psi(q) \;\; = \;\; \exp\left(\frac{\mathrm{i}}{\hbar_{\text{eff}}}\sigma(q)\right) \tag{2.7}$$

and its insertion into equation (2.3) yields

$$\frac{1}{2}\left(\frac{\mathrm{d}\sigma(q)}{\mathrm{d}q}\right)^2 - \frac{\mathrm{i}\,\hbar_{\text{eff}}}{2}\frac{\mathrm{d}^2\sigma(q)}{\mathrm{d}q^2} \;\; = \;\; E - V(q). \tag{2.8}$$

Since the semiclassical limit is studied, an expansion of $\sigma(q)$ into a power series in $\hbar_{\text{eff}}/\mathrm{i}$,

$$\sigma(q) \;\; = \;\; \sum_n \left(\frac{\hbar_{\text{eff}}}{\mathrm{i}}\right)^n \sigma_n(q), \tag{2.9}$$

is performed. By inserting (2.9) in leading order of $\hbar_{\text{eff}}$ into equation (2.8) and neglecting[1] the second term on the left-hand side of equation (2.8), which is proportional to $\hbar_{\text{eff}}$, one finds

$$\sigma_0(q) \;\; = \;\; \pm \int\limits_c^q \mathrm{d}q' \; \sqrt{2[E - V(q')]}. \tag{2.10}$$

The meaning of the constant c will be explained in the next paragraph. The integrand of (2.10) is equal to the modulus of the momentum of the particle in the classically allowed region, where $E \geq V(q)$ holds,

$$p(q) \;\; = \;\; \sqrt{2[E - V(q)]}, \tag{2.11}$$

---

[1]This neglection will be justified later.

so that one has

$$\sigma_0(q) \ = \ \pm \int\limits_{c}^{q} dq' \, p(q').   \tag{2.12}$$

In order to determine $\sigma_1(q)$ in equation (2.9), $\sigma(q)$ is expanded up to $O(\hbar_{\mathrm{eff}})$ and inserted into the Schrödinder equation (2.8). The comparison of the terms of $O(\hbar_{\mathrm{eff}})$ yields

$$\frac{d\sigma_1(q)}{dq} \ = \ -\frac{\left(d^2\sigma_0(q)/dq^2\right)}{2\,\left(d\sigma_0(q)/dq\right)} \ = \ -\frac{1}{2\,p(q)}\,\frac{dp(q)}{dq},   \tag{2.13}$$

what leads to

$$\sigma_1(q) \ = \ -\frac{1}{2}\ln\left(p(q)\right)   \tag{2.14}$$

apart from an integration constant. After the insertion of $\sigma_0(q)$ and $\sigma_1(q)$ into equation (2.7) one obtains a semiclassical expression for the wave function $\psi(q)$ which solves the stationary Schrödinger equation (2.3) in $O(\hbar_{\mathrm{eff}})$

$$\psi(q) \ = \ \frac{N_1}{\sqrt{p(q)}}\,\exp\left(\frac{i}{\hbar_{\mathrm{eff}}}\int\limits_{c_1}^{q} dq'\,p(q')\right) + \frac{N_2}{\sqrt{p(q)}}\,\exp\left(-\frac{i}{\hbar_{\mathrm{eff}}}\int\limits_{c_2}^{q} dq'\,p(q')\right).   \tag{2.15}$$

The normalization constants N_1 and N_2 will be determined later.

The neglection of the second term on the left-hand side of equation (2.8), which was performed in order to obtain an analytical expression for σ_0, is justified only, if

$$\hbar_{\mathrm{eff}}\left|\frac{\frac{d^2\sigma(q)}{dq^2}}{\left(\frac{d\sigma(q)}{dq}\right)^2}\right| \ \ll \ 1.   \tag{2.16}$$

With the definition of the de Broglie wave length $\lambda(q) = h_{\mathrm{eff}}/p(q)$ and

$$\frac{d\sigma(q)}{dq} \ \approx \ \frac{d\sigma_0(q)}{dq} \ = \ \pm\,p(q)   \tag{2.17}$$

one obtains

$$\frac{1}{2\,\pi}\,\lambda(q)\left|\frac{dp(q)}{dq}\right| \ \ll \ p(q)   \tag{2.18}$$

from equation (2.16). The performed neglection is therefore justified only, if the change of the momentum over one de Broglie wave length is small compared to the momentum itself. This condition can alternatively be expressed in the following way: The potential energy $V(q)$ is allowed to have only minimal changes on the scale given by the de Broglie wave length. Thus, the WKB solution (2.15) breaks down where the potential energy $V(q)$ is steep and especially where the momentum $p(q)$ vanishes, i.e. at classical turning points, where

$$V(q) \;=\; E. \tag{2.19}$$

The momentum of the considered particle becomes purely imaginary in classically forbidden regions, where $V(q) > E$, so that the exponents of the WKB wave function (2.15) become real. With the definition

$$|p(q)| \;:=\; \sqrt{2[V(q) - E]} \tag{2.20}$$

one obtains

$$\psi(q) \;=\; \frac{N_1'}{\sqrt{|p(q)|}} \, \exp\left(-\frac{1}{\hbar_{\text{eff}}} \int\limits_{c_1'}^{q} \mathrm{d}q' \, |p(q')|\right) + \frac{N_2'}{\sqrt{|p(q)|}} \, \exp\left(\frac{1}{\hbar_{\text{eff}}} \int\limits_{c_2'}^{q} \mathrm{d}q' \, |p(q')|\right) \tag{2.21}$$

for the WKB wave function approximation in classically forbidden regions in contrast to equation (2.15). In the scope of the semiclassical approximation it is not justified to keep an exponentially small term and an exponentially large one at the same time. It is therefore generally not allowed to take both contributions of equation (2.21) into account.

2.1.2 Connection formulae

A classically allowed and a classically forbidden region are separated by a turning point in 1D. The energy E of the considered particle is equal to the potential energy at such a point. Figure 2.1 illustrates a 1D turning point at $q = a$ for a monotonous potential energy function $V(q)$. The classically allowed region extends over the domain $q < a$, whereas the classically forbidden region is given by $q > a$. Based on this sketch the connection between the normalization constants of the WKB wave functions (2.15) and (2.21) left and right to the classical turning point will be considered in the following.

In the classically forbidden region the wave function must decrease. Sufficiently away
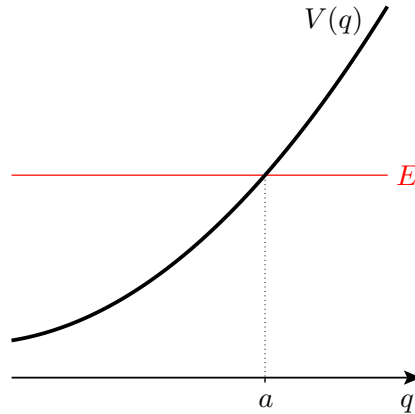
Figure 2.1: A classical turning point at $q = a$ for a monotonous potential energy function $V(q)$: The region $q < a$ is classically allowed $\big(E > V(q)\big)$, whereas the region $q > a$ is classically forbidden $\big(E < V(q)\big)$.

from the turning point it can semiclassically be approximated by

$$\psi(q) \;=\; \frac{N}{2\,\sqrt{|p(q)|}}\;\exp\left(-\,\frac{1}{\hbar_{\text{eff}}}\int\limits_{a}^{q} \mathrm{d}q'\,|p(q')|\,\right), \qquad (2.22)$$

according to the first summand of equation (2.21), where a factor $1/2$ was separated from the normalization constant. In the classically allowed region, located left with respect to a, the wave function is given by equation (2.15)

$$\psi(q) \;=\; \frac{N_1}{\sqrt{p(q)}}\;\exp\left(\frac{\mathrm{i}}{\hbar_{\text{eff}}}\int\limits_{a}^{q}\mathrm{d}q'\,p(q')\right) + \frac{N_2}{\sqrt{p(q)}}\;\exp\left(-\frac{\mathrm{i}}{\hbar_{\text{eff}}}\int\limits_{a}^{q}\mathrm{d}q'\,p(q')\right). \quad (2.23)$$

From (2.22) and (2.23) it becomes clear that the lower limit of the integrals in the exponential functions of the general WKB wave functions (2.15) and (2.21) is equal to the turning point with respect to which the wave functions are considered.

In order to find the connection between N, N_1, and N_2, the behaviour of the WKB wave function $\psi(q)$ needs to be studied in the vicinity of the turning point a, e.g. along the line from $q = a + \rho$ to $q = a - \rho$ with positive ρ, see figure 2.2. However, this path is not appropriate due to the divergence of the WKB wave functions (2.22) and (2.23) at the position of the classical turning point $q = a$. In reference [35] the wave function $\psi(q)$ is considered as a function of the complex variable q and the study of its behaviour from $q = a + \rho$ to $q = a - \rho$ is performed along a semicircle with radius ρ, e.g. in the upper half

of the complex q plane. Since the WKB wave function approximations (2.22) and (2.23) are not valid at $q = a$, the radius ρ must be chosen so large that equations (2.22) and (2.23) can be regarded as good approximations of the actual wave functions. The potential energy is additionally expanded into a Taylor series around $q = a$ in reference [35]. It is also shown that it is at the same time possible to choose ρ so small that contributions of $O\left((q - a)^2\right)$ can be neglected

$$V(q) \;\approx\; E + (q - a)F_a \quad \text{with} \quad F_a \;=\; \left.\frac{\mathrm{d}V(q)}{\mathrm{d}q}\right|_{q=a} > 0. \tag{2.24}$$

Using equation (2.24) the WKB wave function in the classically forbidden region, equation (2.22), becomes

$$\psi(q) \;=\; \frac{N}{2\,(2F_a)^{1/4}}\,\frac{1}{(q - a)^{1/4}}\,\exp\left(-\frac{1}{\hbar_{\text{eff}}}\int\limits_a^q \mathrm{d}q'\,\sqrt{2F_a(q' - a)}\right). \tag{2.25}$$

The integral in the exponent of (2.25) from a to q can be determined along the red path in figure 2.2 by using polar coordinates, $q - a = \rho\exp(\mathrm{i}\varphi)$, which leads to

$$\int\limits_a^q \mathrm{d}q'\,\sqrt{q - a} \;=\; \frac{2}{3}\,\rho^{3/2}\left[\cos\left(\frac{3\varphi}{2}\right) + \mathrm{i}\,\sin\left(\frac{3\varphi}{2}\right)\right]. \tag{2.26}$$
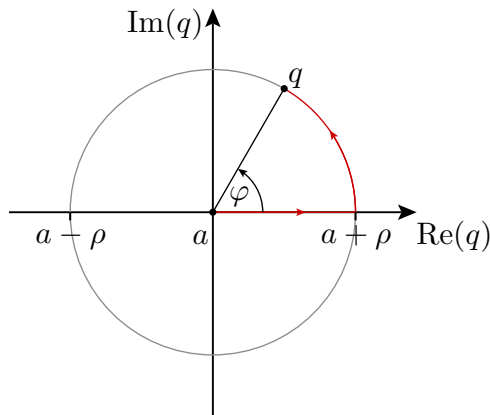
Figure 2.2: Extension of the real line to the complex plane: The classically allowed region is given by $\mathrm{Re}(q) < a$ and the classically forbidden one by $\mathrm{Re}(q) > a$.

The phase φ changes from 0 to π along the semicircle in the upper half of the complex q plane. At $\varphi = \pi$ the exponent of (2.25) is equal to

$$-\frac{i}{\hbar_{\mathrm{eff}}} \int\limits_a^q dq' \, \sqrt{2F_a(a - q')} \;=\; -\frac{i}{\hbar_{\mathrm{eff}}} \int\limits_a^q dq' \, p(q'). \tag{2.27}$$

Since the integration path was chosen in the upper half of the complex q plane, the prefactor of equation (2.25) needs to be replaced as follows

$$(q - a)^{-1/4} \;\rightarrow\; (a - q)^{-1/4} \exp\left(-i\frac{\pi}{4}\right). \tag{2.28}$$

The expression of the wave function (2.22) transfers therefore into the second summand of equation (2.23) with

$$N_2 \;=\; \frac{N}{2} \exp\left(-i\frac{\pi}{4}\right). \tag{2.29}$$

Similarly, one finds

$$N_1 \;=\; \frac{N}{2} \exp\left(i\frac{\pi}{4}\right) \tag{2.30}$$

by studying the behaviour of the WKB wave function along a semicircle with radius ρ in the lower half of the complex q plane. Using equations (2.29) and (2.30) the wave function in the classically allowed region (2.23) becomes

$$\psi(q) \;=\; \frac{N}{\sqrt{p(q)}} \cos\left(\frac{1}{\hbar_{\mathrm{eff}}} \int\limits_a^q dq' \, p(q') + \frac{\pi}{4}\right). \tag{2.31}$$

In the case, which is studied here, the classically forbidden region lies right to the turning point. A formulation, which is independent of the relative order of the classically allowed and forbidden region, was found by Kramers

   classically forbidden region: classically allowed region:

$$\frac{N}{2\sqrt{|p(q)|}} \exp\left(-\frac{1}{\hbar_{\mathrm{eff}}} \left|\int\limits_a^q dq' \, p(q')\right|\right) \;\rightarrow\; \frac{N}{\sqrt{p(q)}} \cos\left(\frac{1}{\hbar_{\mathrm{eff}}} \left|\int\limits_a^q dq' \, p(q')\right| - \frac{\pi}{4}\right). \tag{2.32}$$

One should note that the connection between the normalization constants N, N_1, and N_2 can only be determined by starting in the classically forbidden region. The reason is that

one knows that there the wave function must decrease exponentially. The direction of the arrow in equation (2.32) must thus not be changed.

2.1.3 Bohr-Sommerfeld quantization condition and normalization

The semiclassical quantization condition will be repeated in this section. For this purpose it is helpful to consider a bound state of a particle with energy E in a simple potential well, e.g. the one in figure 2.3(a). The classically allowed region is given by $a \leq q \leq b$. According to equation (2.32), the wave function of the particle with respect to the left turning point $q = a$ reads

$$\psi(q) \;=\; \frac{N}{\sqrt{p(q)}} \; \cos\left(\frac{1}{\hbar_{\text{eff}}} \int\limits_{a}^{q} \mathrm{d}q' \, p(q') - \frac{\pi}{4} \right). \qquad (2.33)$$

But $\psi(q)$ can also be determined with respect to the right turning point

$$\psi(q) \;=\; \frac{N'}{\sqrt{p(q)}} \; \cos\left(\frac{1}{\hbar_{\text{eff}}} \int\limits_{q}^{b} \mathrm{d}q' \, p(q') - \frac{\pi}{4} \right). \qquad (2.34)$$

These two expressions must be equal apart from their signs. Consequently, $N' = (-1)^z N$ with $z \in \mathbb{Z}$ must hold. Thus, the sum of the arguments of the cos functions of (2.33) and
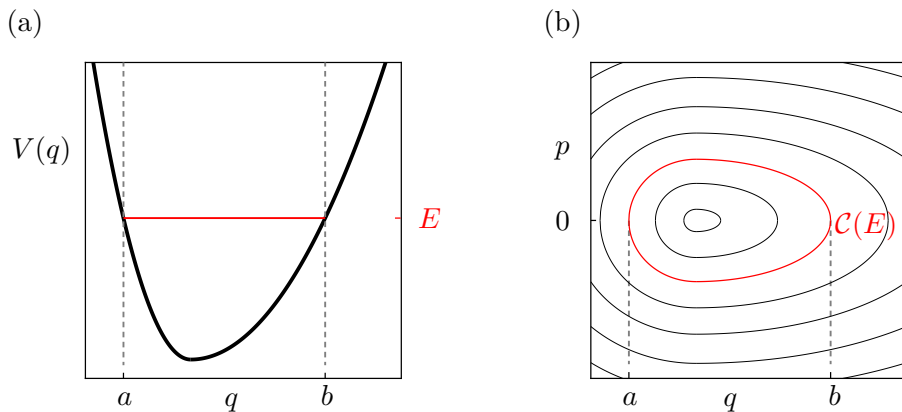
Figure 2.3: (a) A particle with energy E in a simple potential well. The classical turning points are a and b. (b) The motion displayed in phase space: A bound state with energy E is associated with a closed curve $\mathcal{C}(E)$.

(2.34) must be equal to $z\pi$

$$\frac{1}{\hbar_{\text{eff}}} \int\limits_{a}^{b} \mathrm{d}q'\, p(q') - \frac{\pi}{2} \;=\; z\pi \qquad \text{with} \qquad z \in \mathbb{Z}\,. \tag{2.35}$$

The quantity z can be interpreted as a quantum number. Here only non-negative quantum numbers are meaningful, so that one replaces $z \in \mathbb{Z}$ by $m \in \mathbb{N}_0$. Equation (2.35) selects certain momenta which depend on the energy. Consequently, the energy must be quantized: $E \to E_m$. Similarly, the turning points a and b are replaced by a_m and b_m. For each m there are two branches of the momentum, $\pm p(q, E_m)$, which fulfill equation (2.35). If one plots them as a function of q, one gets closed curves $\mathcal{C}_m := \mathcal{C}(E_m)$, see figure 2.3(b). One therefore obtains

$$\oint\limits_{\mathcal{C}_m} \mathrm{d}q\, p(q) \;=\; S_m \;=\; 2\pi\hbar_{\text{eff}} \left(m + \frac{1}{2} \right) \qquad \text{with} \qquad m \in \mathbb{N}_0 \tag{2.36}$$

from (2.35), where S_m is the classical action enclosed by $\mathcal{C}_m$. This is the well-known Bohr-Sommerfeld quantization condition.

One usually knows the closed invariant tori $\mathcal{C}_m$ fulfilling the Bohr-Sommerfeld quantization condition, but not the corresponding quantized energies E_m. With b_m as the position coordinate of the right turning point belonging to the closed curve $\mathcal{C}_m$, the quantized energy E_m follows from[2]

$$E_m \;=\; \int\limits_{0}^{b_m} \mathrm{d}q\, \frac{1}{T(q)} \frac{\mathrm{d}S(q)}{\mathrm{d}q}. \tag{2.37}$$

In this formula $S(q)$ denotes the action which is enclosed by a curve with the right turning point at the position q. The quantity $T(q)$ stands for the classical period which is required to pass the corresponding closed curve.

The question of the normalization of the WKB wave function $\psi_m(q)$ with the quantum number m is still open. Since it decreases exponentially in the classically forbidden regions $q < a_m$ and $q > b_m$, it is sufficient to perform the normalization in the classically allowed region $a_m \leq q \leq b_m$

$$1 \;\overset{!}{=}\; \int\limits_{a_m}^{b_m} \mathrm{d}q\, |\psi_m(q)|^2. \tag{2.38}$$

---

[2]The proof can be found in appendix A.2.

Now one inserts the WKB expression for $\psi_m(q)$, equation (2.33). It contains a cos function, which rapidly oscillates in the semiclassical limit due to the $1/\hbar_{\text{eff}}$ dependence. The factor $|\psi_m(q)|^2$ can therefore be approximated by its mean value $1/2$

$$
\begin{aligned}
1 &= \frac{N_m^2}{2} \int\limits_{a_m}^{b_m} \frac{\mathrm{d}q}{p(q)} \\
&= \frac{N_m^2}{2} \frac{T_m}{2} \\
&= N_m^2 \frac{\pi}{2\omega_m}.
\end{aligned} \tag{2.39}
$$

In equation (2.39) the angular frequency $\omega_m := 2\pi/T_m$ of the classical periodic motion was introduced, so that one finally obtains

$$
N_m = \sqrt{\frac{2\omega_m}{\pi}} \tag{2.40}
$$

as normalization constant[3].

2.1.4 Example: Harmonic oscillator

Now we apply the WKB theory to the harmonic oscillator with the dimensionful Hamiltonian

$$
H(q, p) = \frac{p^2}{2m} + \frac{1}{2} m\omega^2 q^2 \tag{2.41}
$$

with the angular frequency ω. In order to treat the system in the scope of dimensionless quantities, we introduce a characteristic energy V_0 and a characteristic length q_0 according to the procedure described in appendix A.1. By means of equations (A.3) and (A.4) we find expressions for the characteristic momentum p_0 and time t_0, which finally enable us to set up the dimensionless Hamiltonian

$$
\tilde{H}(\tilde{q}, \tilde{p}) = \frac{1}{2} \left(\tilde{p}^2 + \tilde{\omega}^2 \tilde{q}^2 \right) \tag{2.42}
$$

with the dimensionless angular frequency $\tilde{\omega}$. In order to distinguish between the dimensionless and the dimensionful Hamiltonian, we temporarily introduced the tilde. Since we will only use the dimensionless system in the following, we omit it from now on. The

---

[3]The negative square root on the right-hand side of equation (2.40) is mathematically also correct. However, it is physically not sensible.

WKB prediction for the quantized energies,

$$E_m \;=\; \hbar_{\text{eff}}\,\omega\left(m+\frac{1}{2}\right) \qquad \text{with} \qquad m \in \mathbb{N}_0, \tag{2.43}$$

follows immediately from equations (2.36) and (2.37). We remark that equation (2.43) is accidentally equal to the exact quantum mechanical formula. By means of equations (2.42) and (2.43) the left and the right turning point belonging to the quantum number m read

$$-a_m \;=\; \sqrt{2\frac{h_{\text{eff}}}{\omega}\left(m+\frac{1}{2}\right)} \;=\; b_m. \tag{2.44}$$

With this knowledge we can determine the three parts of the WKB wave function according to equations (2.22) and (2.31)

$$\psi_m(q) \;=\; \begin{cases} \begin{aligned} &\sqrt{\frac{1}{2\pi}}\,\frac{1}{\left[q^2-2\frac{\hbar_{\text{eff}}}{\omega}\left(m+\frac{1}{2}\right)\right]^{1/4}} \\ &\cdot \exp\left(\frac{\omega}{2\hbar_{\text{eff}}}q\sqrt{q^2-2\frac{\hbar_{\text{eff}}}{\omega}\left(m+\frac{1}{2}\right)}+(m+\tfrac{1}{2})\text{arcosh}\left(-\sqrt{\frac{\omega}{2\hbar_{\text{eff}}(m+1/2)}}q\right)\right) \\[6pt] &\sqrt{\frac{2}{\pi}}\,\frac{1}{\left[2\frac{\hbar_{\text{eff}}}{\omega}\left(m+\frac{1}{2}\right)-q^2\right]^{1/4}} \\ &\cdot \cos\left(\frac{\omega}{2\hbar_{\text{eff}}}q\sqrt{2\frac{\hbar_{\text{eff}}}{\omega}\left(m+\frac{1}{2}\right)-q^2}+(m+\tfrac{1}{2})\arcsin\left(\sqrt{\frac{\omega}{2\hbar_{\text{eff}}(m+1/2)}}q\right)+m\tfrac{\pi}{2}\right) \\[6pt] &\sqrt{\frac{1}{2\pi}}\,\frac{1}{\left[q^2-2\frac{\hbar_{\text{eff}}}{\omega}\left(m+\frac{1}{2}\right)\right]^{1/4}} \\ &\cdot \exp\left(-\frac{\omega}{2\hbar_{\text{eff}}}q\sqrt{q^2-2\frac{\hbar_{\text{eff}}}{\omega}\left(m+\frac{1}{2}\right)}+(m+\tfrac{1}{2})\text{arcosh}\left(\sqrt{\frac{\omega}{2\hbar_{\text{eff}}(m+1/2)}}q\right)\right) \end{aligned} \end{cases}$$

$$\text{for} \quad \begin{cases} q < a_m \\[12pt] a_m < q < b_m \\[12pt] q > b_m \end{cases}.$$

Figure 2.4 shows the squares of the WKB wave functions for $m = 0$ by $m = 8$ for $h_{\text{eff}} = 1/60$ in comparison with the analytical quantum mechanical results. We clearly see the divergences of the WKB wave functions at the classical turning points and that the WKB approximation is worse in their immediate vicinity. It becomes, however, better for higher excited states.
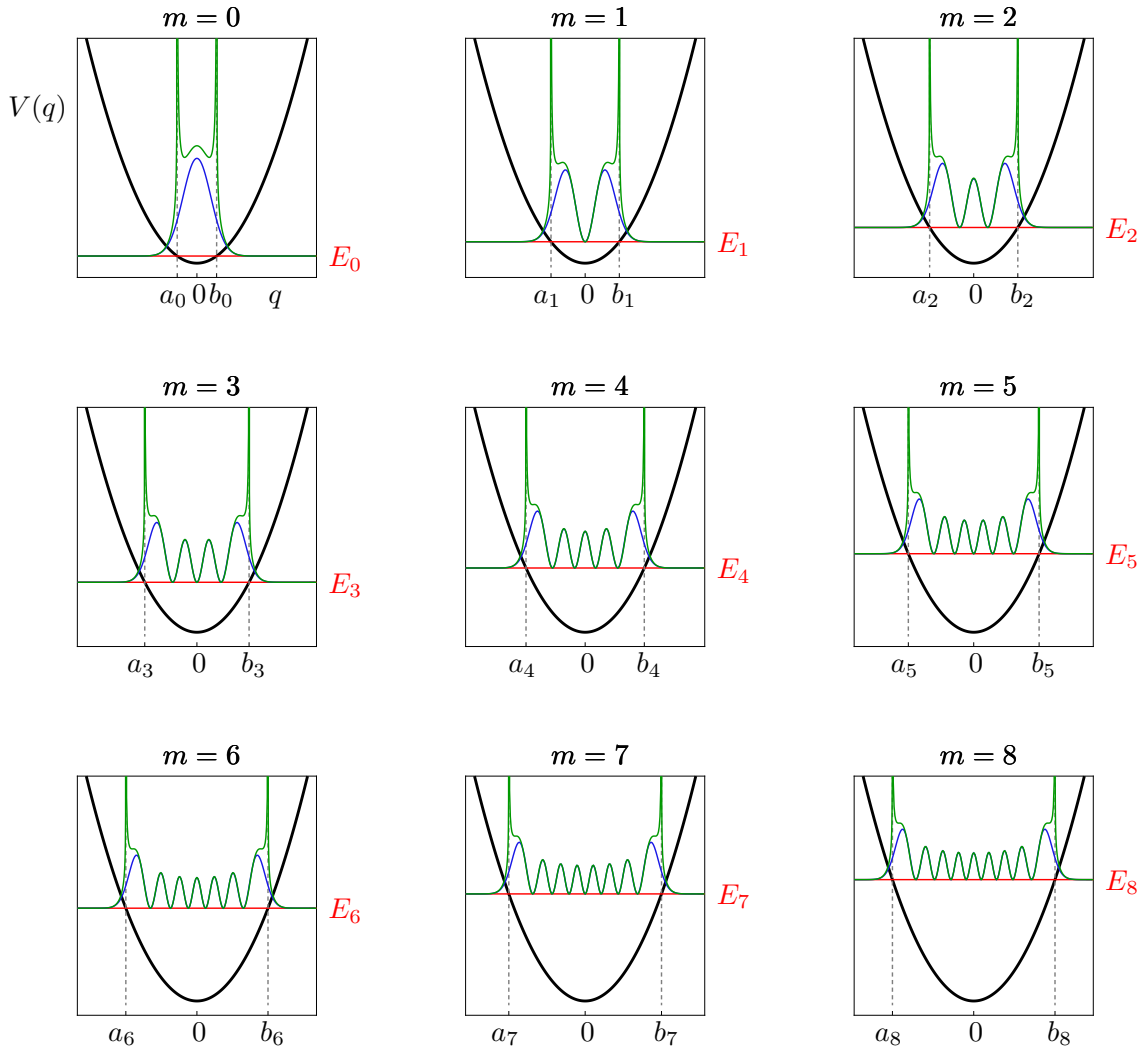
Figure 2.4: Squares of the WKB wave functions (2.45) of the harmonic oscillator (green) compared with the squares of the exact wave functions (blue) for $h_{\text{eff}} = 1/60$ and $m = 0$ by $m = 8$. The wave functions are plotted with respect to the quantum energy E_m. One clearly sees the divergences at the classical turning points a_m and b_m, and that the WKB approximation becomes better for higher excited states.

2.1.5 Uniform approximation

A lack of the WKB approximation is that it breaks down in the vicinity of classical turning points. A first approach to get rid of the divergences of the WKB wave functions in these regions was suggested in references [36] and [37]. It uses that the stationary Schrödinger equation,

$$-\frac{\hbar_{\text{eff}}^2}{2}\frac{\mathrm{d}^2\psi(q)}{\mathrm{d}q^2} + [V(q) - E]\,\psi(q) \;=\; 0, \tag{2.45}$$

is a linear second-order differential equation. The idea consists of introducing

$$-\frac{\hbar_{\text{eff}}^2}{2}\frac{\mathrm{d}^2\phi(q)}{\mathrm{d}q^2} + \Gamma(q)\phi(q) \;=\; 0, \tag{2.46}$$

where $\Gamma(q)$ is chosen in a similar manner to $V(q) - E$ such that the solutions $\phi(q)$ are known on the whole q domain without divergences. This implies that the wave function $\psi(q)$ can be expressed in terms of $\phi(q)$ by stretching or contracting. A good summary of this method of a uniform approximation, which is known as the "method of comparison equations", can be found in reference [38]. The question is, whether a simple comparison function $\Gamma(q)$ does always exist in the whole q domain. The general answer is, however, "no".

A modification of the method of comparison equations is the restriction of the search for a comparison potential energy to the vicinity of a classical turning point of $V(q)$. This requires a matching of the divergence-free comparison wave function $\phi(q)$ to the WKB wave function parts on both sides of the classical turning point. The matching must be performed such that the resulting wave function is continuously differentiable. The most often used comparison potential energy for this purpose is the first order expansion of $V(q)$ with respect to the position of the classical turning point. The reason is that the corresponding Schrödinger equation

$$-\frac{\hbar_{\text{eff}}^2}{2}\frac{\mathrm{d}^2\phi(q)}{\mathrm{d}q^2} + \left(c_1 q - c_2\right)\phi(q) \;=\; 0 \qquad \text{with} \quad c_1,\, c_2 \in \mathbb{R} \tag{2.47}$$

is equal to the Airy equation, see e.g. equation (10.4.1) in reference [39], with the two independent Airy functions $\mathrm{Ai}(q)$ and $\mathrm{Bi}(q)$ as solutions. This kind of uniform approximation was first introduced in the references [40] and [41]. The method of Airy uniformization cannot be applied in general. It fails especially in those cases, where two different classical turning points lie close to each other.

This implies that the concept of uniform approximations is complicated. In this thesis we do not need WKB functions in the vicinity of classical turning points. We therefore do not continue the description of uniform approximations beyond this point. For a further reading reference [42] and the references therein are a good starting point.

2.2 1D tunneling effect

The standard 1D tunneling effect example, which can be found in textbooks, is a potential energy with a symmetric double well shape. It describes e.g. the inversion oscillation of the NH_3-molecule. Tunneling in 1D is, however, not only restricted to the case of full symmetry.

Let us consider the time independent position space Schrödinger equation of a 1D system,

$$E_n \psi_n(q, \kappa) \;=\; -\frac{\hbar_{\mathrm{eff}}^2}{2}\frac{\mathrm{d}^2}{\mathrm{d}q^2}\psi_n(q, \kappa) + V(q, \kappa)\psi_n(q, \kappa) \tag{2.48}$$

$$=:\; \hat{H}(\kappa)\psi_n(q, \kappa), \tag{2.49}$$

with the potential energy

$$V(q, \kappa) \;:=\; q^4 - q^2 + \kappa q \qquad \text{with} \qquad \kappa \in \mathbb{R}. \tag{2.50}$$

The system-specific parameter κ can be varied. For $\kappa = 0$ the potential energy (2.50) is symmetric with respect to $q = 0$ and consists of two wells, which are separated by a potential energy barrier. The potential energy has still a double well shape for $\kappa \neq 0$, but an asymmetric one. The shape of $V(q, \kappa)$ is illustrated in figure 2.5 for three different values of κ: (a) $\kappa < 0$, (b) $\kappa = 0$, and (c) $\kappa > 0$.

For any value of the parameter κ the potential energy barrier, which separates the two wells from each other, has a certain height. If the energy of a particle is smaller than this barrier height, the motion is classically restricted to either the left or the right well of $V(q, \kappa)$. Semiclassically one assumes that a coupling between the two wells of
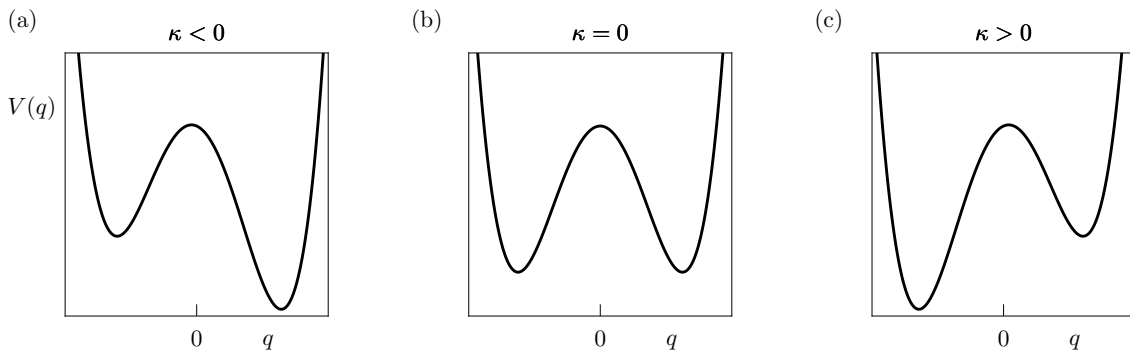
Figure 2.5: The double well shaped potential energy $V(q, \kappa)$ given by equation (2.50) for three different values of the system-specific parameter κ: (a) $\kappa < 0$, (b) $\kappa = 0$, and (c) $\kappa > 0$. $V(q, \kappa)$ is symmetric with respect to $q = 0$ in case (b).

the potential energy can approximately be neglected and performs WKB quantizations in the left and the right well independently of each other. With m_L and m_R as allowed WKB quantum numbers in the left and the right well, one finds quantizing curves $\mathcal{C}_{m_L}(\kappa)$ and $\mathcal{C}_{m_R}(\kappa)$ by means of the Bohr-Sommerfeld quantization condition (2.36). Figure 2.6 gives an image of the phase space contour lines of the considered system for $\kappa = 0$. The quantizing curve for a certain quantum number m_L, $\mathcal{C}_{m_L}(\kappa = 0)$, is highlighted in red, and $\mathcal{C}_{m_R}(\kappa = 0)$ as corresponding curve for a certain quantum number m_R is plotted in blue. Equation (2.37) finally assigns WKB energies $E_{m_L}(\kappa)$ and $E_{m_R}(\kappa)$ to these quantizing curves. Corresponding semiclassical states $|\psi_{m_L}(\kappa)\rangle$ and $|\psi_{m_R}(\kappa)\rangle$ can be constructed by means of the WKB theory.

Because of the neglection of a coupling between the two wells of the potential energy, it is obvious that a left and a right well WKB energy, e.g. $E_{m_L}(\kappa)$ and $E_{m_R}(\kappa)$, can become equal at a certain parameter value κ^* under the variation of the system-specific parameter κ: $E_{m_L}(\kappa^*) = E_{m_R}(\kappa^*)$. This implies that the WKB energies $E_{m_L}(\kappa)$ and $E_{m_R}(\kappa)$ can cross. In the considered example crossings with $m_L = m_R$ can only occur for $\kappa = 0$ due to the choice of the potential energy (2.50). For $\kappa \neq 0$ crossings do appear for $m_L \neq m_R$. Figure 2.7(a) illustrates the behaviour of certain energies $E_{m_L}(\kappa)$ and $E_{m_R}(\kappa)$ in the vicinity of $\kappa = \kappa^*$. It is emphasized again that the crossing between the WKB energies $E_{m_L}(\kappa)$ and $E_{m_R}(\kappa)$ results from the previously assumed neglection of any coupling between the two wells of the potential energy. Is this assumption really
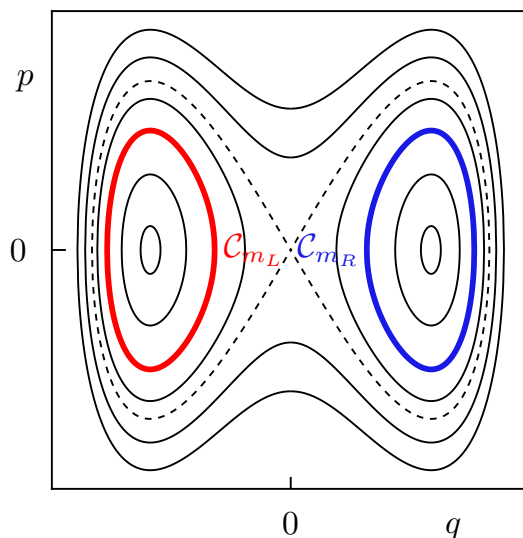
Figure 2.6: Phase space contour lines of the considered double well system (2.50) for the parameter value $\kappa = 0$. Red and blue coloured contour line: Quantizing curves $\mathcal{C}_{m_L}(\kappa = 0)$ in the left and $\mathcal{C}_{m_R}(\kappa = 0)$ in the right well. The dashed line belongs to the energy equal to the height of the potential energy barrier.
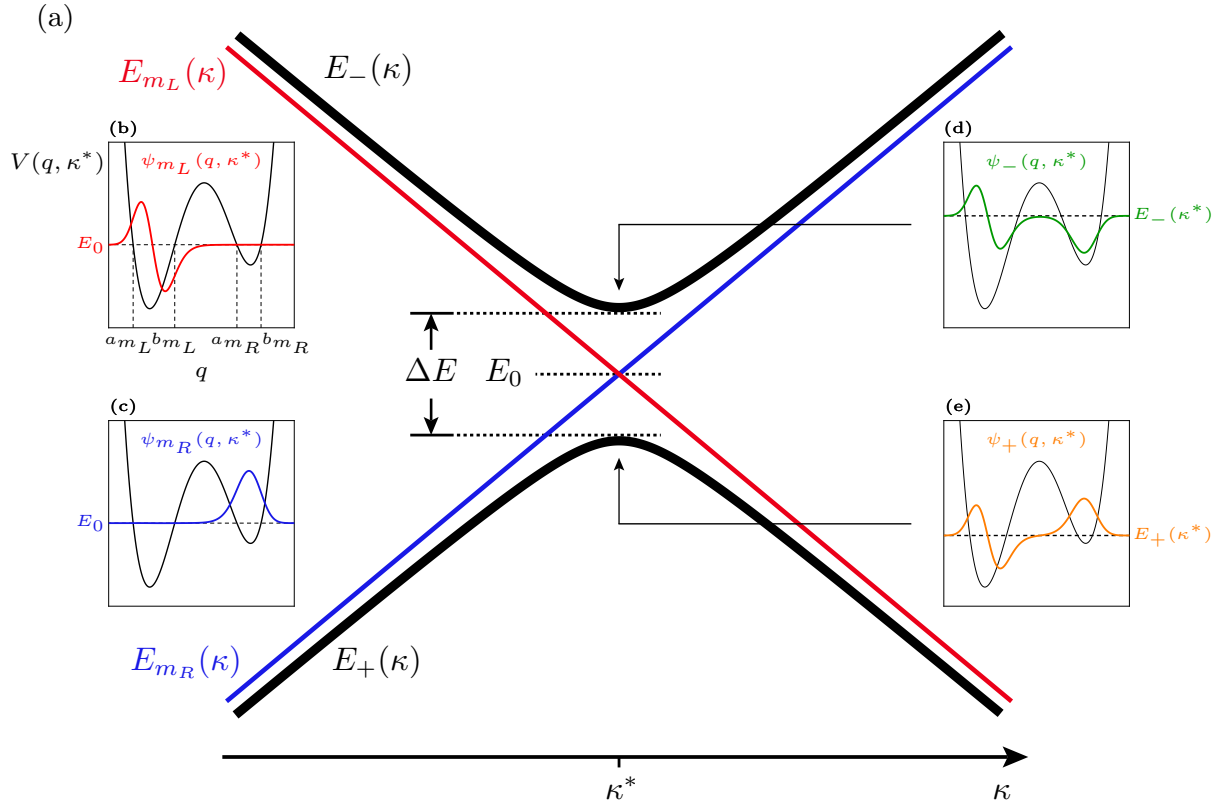
Figure 2.7: (a) The eigenenergies $E_+(\kappa)$ and $E_-(\kappa)$ of the Hamilton operator $\hat{H}(\kappa)$ show an avoided crossing at $\kappa = \kappa^*$ due the coupling of the left and right well of the potential energy by the barrier tunneling effect. An independent treatment of the left and the right well in the scope of the WKB theory yields functions $E_{m_L}(\kappa)$ (red) and $E_{m_R}(\kappa)$ (blue), which cross at $\kappa = \kappa^*$ and which are asymptotes to $E_+(\kappa)$ and $E_-(\kappa)$ sufficiently away from the avoided crossing. ΔE denotes the tunnel splitting, whereas E_0 is the value of the left and the right well WKB energy at the avoided crossing. The insets (b) and (c) show images of the WKB wave functions $\psi_{m_L}(q, \kappa = \kappa^*)$ and $\psi_{m_R}(q, \kappa = \kappa^*)$. The parts (d) and (e) of the figure illustrate the eigenfunctions $\psi_-(q, \kappa = \kappa^*)$ and $\psi_+(q, \kappa = \kappa^*)$ of the Hamilton operator belonging to the eigenvalues $E_+(\kappa^*)$ and $E_-(\kappa^*)$.

justified? An answer to this question gives the determination of the eigenvalues of the Hamilton operator $\hat{H}(\kappa)$. Its numerical diagonalization yields two functions $E_+(\kappa)$ and $E_-(\kappa)$, which the functions[4] $E_{m_L}(\kappa)$ and $E_{m_R}(\kappa)$ are asymptotes to, see figure 2.7(a). The most important observation is that $E_+(\kappa)$ and $E_-(\kappa)$ do not cross at $\kappa = \kappa^*$. They rather show an avoided crossing. This observation is a consequence of the quantum mechanically allowed connection of the two wells of $V(q, \kappa)$ by the tunneling effect. In order to distinguish this tunneling phenomenon, which involves a 1D potential energy

---

[4]At first view it appears strange to label the lower energy with a "+" and the higher one with a "−". The choice of the labels follows a generally accepted convention and will become clear later.

barrier, from the dynamical tunneling process, that will be investigatd in chapter 5, it is named 1D barrier tunneling. Whenever one encounters an avoided crossing between two eigenenergies of a system under the variation of a system-specific parameter, a tunneling process is involved.

The task in the remaining part of this section is to find a semiclassical expression for the so-called tunnel splitting $\Delta E := E_-(\kappa = \kappa^*) - E_+(\kappa = \kappa^*)$ by means of analytical considerations. For this purpose one concentrates on an avoided crossing, e.g. the one at $\kappa = \kappa^*$ and fixes

$$
\begin{aligned}
\hat{H} &:= \hat{H}(\kappa = \kappa^*), \\
E_+ &:= E_+(\kappa = \kappa^*), \\
E_- &:= E_-(\kappa = \kappa^*), \\
E_0 &:= E_{m_L}(\kappa = \kappa^*) = E_{m_R}(\kappa = \kappa^*), \\
V(q) &:= V(q, \kappa^*).
\end{aligned}
\tag{2.51}
$$

With $|\psi_+\rangle$ and $|\psi_-\rangle$ as eigenstates of the Hamilton operator $\hat{H}$ belonging to the energies E_+ and E_-, one has the eigenvalue equations

$$
\hat{H} |\psi_\pm\rangle = E_\pm |\psi_\pm\rangle .
\tag{2.52}
$$

Since the states $|\psi_+\rangle$ and $|\psi_-\rangle$ belong to an avoided crossing, their weights in the left as well as in the right well are equal to $1/2$.

One now focuses on the construction of the WKB wave functions $\psi_{m_L}(q)$ and $\psi_{m_R}(q)$ belonging to the WKB energy E_0 and defines a_{m_L} and b_{m_L} as classical turning points in the left well and correspondingly a_{m_R} and b_{m_R} in the right well, see figure 2.7(b). At first one can concentrate e.g. on $\psi_{m_L}(q)$. Using the WKB theory and a connection formula derived by Langer in reference [43], one can determine $\psi_{m_L}(q)$. It has the correct physical behaviour in the domain $q < a_{m_R}$, except for the classical turning points. The WKB wave function $\psi_{m_L}(q)$ shows oscillations for $a_{m_R} < q < b_{m_R}$ and an exponential growth for $q > b_{m_R}$ as is illustrated in reference [11] by Tomsovic and Ullmo. The resulting WKB wave function $\psi_{m_L}(q)$ defined on $\mathbb{R}$ is consequently not normalizable and thus unphysical. In order to get the physically expected exponential decrease of the semiclassical wave function $\psi_{m_L}(q)$ in the domain $q > a_{m_R}$, $\psi_{m_L}(q)$ can be multiplied with an appropriate smooth function $\varphi_{m_L}(q)$

$$
\bar{\psi}_{m_L}(q) := \varphi_{m_L}(q)\psi_{m_L}(q).
\tag{2.53}
$$

The function $\varphi_{m_L}(q)$ has to be chosen such that it does not change $\psi_{m_L}(q)$ for $q < a_{m_R}$, i.e. that $\bar{\psi}_{m_L}(q)$ and $\psi_{m_L}(q)$ are equal for $q < a_{m_R}$. A similar treatment yields a normalizable WKB wave function $\bar{\psi}_{m_R}(q)$ by introducing an appropriate smooth function $\varphi_{m_R}(q)$. Tomsovic and Ullmo show also in reference [11] that the resulting semiclassical formula for the tunnel splitting[5] is independent of the special choice of the functions $\varphi_{m_L}(q)$ and $\varphi_{m_R}(q)$. In the following we will omit the bars and regard $\psi_{m_L}(q)$ and $\psi_{m_R}(q)$ as physical WKB wave functions with quantum numbers m_L and m_R, respectively. The construction of a WKB wave function $\psi_{m_L}(q)$ with the correct physical properties is equivalent to the definition of a smooth potential energy $V_L(q)$, which is equal to the actual function $V(q)$ for $q \leq a_{m_R}$. For $q > a_{m_R}$ it is continued such that it fulfills $V_L(q) > E_0$. Since, as has been mentioned above, the final semiclassical formula for the tunnel splitting is independent of the functions $\varphi_{m_L}(q)$ and $\varphi_{m_R}(q)$, the exact shape of $V_L(q)$ does not matter as long as $V_L(q)$ is smooth and $V_L(q) > E_0$. Otherwise $\psi_{m_L}(q)$ would not decrease exponentially in the domain $q > a_{m_R}$. Similarly, one can define a smooth potential energy $V_R(q)$, which is equal to $V(q)$ for $q > b_{m_L}$ and which fulfills $V_R(q) > E_0$ for $q < b_{m_L}$.

The normalized states $|\psi_{m_L}\rangle$ and $|\psi_{m_R}\rangle$ can then be regarded as eigenstates of Hamilton operators $\hat{H}_{\mathrm{L}}$ and $\hat{H}_{\mathrm{R}}$,

$$\hat{H}_{\mathrm{L}} \ := \ \frac{\hat{p}^2}{2} + V_L(\hat{q})\,, \tag{2.54}$$

$$\hat{H}_{\mathrm{R}} \ := \ \frac{\hat{p}^2}{2} + V_R(\hat{q})\,, \tag{2.55}$$

with

$$\hat{H}_{\mathrm{L}}|\psi_{m_L}\rangle \ = \ E_0|\psi_{m_L}\rangle\,, \tag{2.56}$$

$$\hat{H}_{\mathrm{R}}|\psi_{m_R}\rangle \ = \ E_0|\psi_{m_R}\rangle\,. \tag{2.57}$$

The insets (b) and (c) of figure 2.7 illustrate $\psi_{m_L}(q)$ and $\psi_{m_R}(q)$ plotted with respect to the reference line $E = E_0$. The parts (d) and (e) of this figure show the numerically determined eigenfunctions $\psi_+(q)$ and $\psi_-(q)$ with respect to the reference lines $E = E_+$ and $E = E_-$, respectively. They live, in contrast to $\psi_{m_L}(q)$ and $\psi_{m_R}(q)$, in both wells of the potential energy $V(q)$. An assumption which one usually finds in textbooks on quantum mechanics is that the overlap of a left and a right well WKB state, $\langle \psi_{m_L}|\psi_{m_R}\rangle$, becomes negligible in the semiclassical limit. This assumption can be analytically confirmed for a symmetric double well potential energy which consists of two connected harmonic oscillators [44].

---

[5]This is equation (2.77) of this section.

Thus, $|\psi_{m_L}\rangle$ and $|\psi_{m_R}\rangle$ are approximately orthogonal in the semiclassical limit and one obtains therefore

$$|\psi_\pm\rangle \;\approx\; \frac{1}{\sqrt{2}}\Big(|\psi_{m_L}\rangle \pm |\psi_{m_R}\rangle\Big),\tag{2.58}$$

in the lowest order of a perturbative treatment. Now the choice of the labels of the energies E_+ and E_- becomes clear: The eigenstates, which belong to the eigenvalues E_+ and E_-, are approximately the symmetric and the anti-symmetric linear combination of $|\psi_{m_L}\rangle$ and $|\psi_{m_R}\rangle$. It is a convention to label E_+ and E_- with the sign which appears between the two WKB states on the right-hand side of equation (2.58).

In order to determine a semiclassical expression for the tunnel splitting ΔE, one can, according to an idea presented in reference [7], consider

$$
\begin{aligned}
E_\pm \;&=\; \Big\langle \psi_\pm \Big| \hat{H} \Big| \psi_\pm \Big\rangle \\
&\overset{(2.58)}{\approx}\; \frac{1}{2}\Big\langle \psi_{m_L} \pm \psi_{m_R} \Big| \hat{H} \Big| \psi_{m_L} \pm \psi_{m_R} \Big\rangle \\
&=\; \frac{1}{2}\Bigg[\Big\langle \psi_{m_L} \Big| \hat{H} \Big| \psi_{m_L} \Big\rangle + \Big\langle \psi_{m_R} \Big| \hat{H} \Big| \psi_{m_R} \Big\rangle \pm \Big\langle \psi_{m_L} \Big| \hat{H} \Big| \psi_{m_R} \Big\rangle \\
&\qquad\qquad \pm \Big\langle \psi_{m_R} \Big| \hat{H} \Big| \psi_{m_L} \Big\rangle \Bigg].
\end{aligned}\tag{2.59}
$$

Due to the hermiticity of $\hat{H}$ and the reality of $\psi_{m_L}(q)$ and $\psi_{m_R}(q)$ one has $\big\langle \psi_{m_L}\big|\hat{H}\big|\psi_{m_R}\big\rangle = \big\langle \psi_{m_R}\big|\hat{H}\big|\psi_{m_L}\big\rangle$, which yields

$$
\begin{aligned}
E_\pm \;&\approx\; \frac{1}{2}\Bigg[\Big\langle \psi_{m_L} \Big| \hat{H} \Big| \psi_{m_L} \Big\rangle + \Big\langle \psi_{m_R} \Big| \hat{H} \Big| \psi_{m_R} \Big\rangle \pm 2 \Big\langle \psi_{m_L} \Big| \hat{H} \Big| \psi_{m_R} \Big\rangle \Bigg] \\
&=\; \frac{1}{2}\Bigg[\Big\langle \psi_{m_L} \Big| \hat{H}_{\mathrm{L}} \Big| \psi_{m_L} \Big\rangle + \Big\langle \psi_{m_R} \Big| \hat{H}_{\mathrm{R}} \Big| \psi_{m_R} \Big\rangle + \Big\langle \psi_{m_L} \Big| \hat{H} - \hat{H}_{\mathrm{L}} \Big| \psi_{m_L} \Big\rangle \\
&\qquad\quad + \Big\langle \psi_{m_R} \Big| \hat{H} - \hat{H}_{\mathrm{R}} \Big| \psi_{m_R} \Big\rangle \pm 2 \Big\langle \psi_{m_R} \Big| \hat{H} - \hat{H}_{\mathrm{L}} \Big| \psi_{m_L} \Big\rangle \\
&\qquad\quad \pm 2 \Big\langle \psi_{m_R} \Big| \hat{H}_{\mathrm{L}} \Big| \psi_{m_L} \Big\rangle \Bigg].
\end{aligned}\tag{2.60}
$$

By means of equations (2.56) and (2.57), and the semiclassically correct assumption $\langle \psi_{m_L} | \psi_{m_R} \rangle \approx 0$ equation (2.60) becomes

$$
\begin{aligned}
E_\pm &\approx E_0 + \frac{1}{2} \left\langle \psi_{m_L} \left| \hat{H} - \hat{H}_L \right| \psi_{m_L} \right\rangle + \frac{1}{2} \left\langle \psi_{m_R} \left| \hat{H} - \hat{H}_R \right| \psi_{m_R} \right\rangle \\
&\quad \pm \left\langle \psi_{m_R} \left| \hat{H}_L \right| \psi_{m_L} \right\rangle \pm \left\langle \psi_{m_R} \left| \hat{H} - \hat{H}_L \right| \psi_{m_L} \right\rangle
\end{aligned}
\tag{2.61}
$$

$$
\begin{aligned}
&= E_0 + \frac{1}{2} \left\langle \psi_{m_L} \left| \hat{H} - \hat{H}_L \right| \psi_{m_L} \right\rangle + \frac{1}{2} \left\langle \psi_{m_R} \left| \hat{H} - \hat{H}_R \right| \psi_{m_R} \right\rangle \\
&\quad \pm E_0 \left\langle \psi_{m_R} \middle| \psi_{m_L} \right\rangle \pm \left\langle \psi_{m_R} \left| \hat{H} - \hat{H}_L \right| \psi_{m_L} \right\rangle
\end{aligned}
\tag{2.62}
$$

$$
\approx E_0 \pm \left\langle \psi_{m_R} \left| \hat{H} - \hat{H}_L \right| \psi_{m_L} \right\rangle .
\tag{2.63}
$$

The neglection of the term $\langle \psi_{m_L} | \hat{H} - \hat{H}_L | \psi_{m_L} \rangle$ is justified, because $\hat{H} - \hat{H}_L$ is different from zero, where $\psi_{m_L}(q)$ is already exponentially small. With a similar reasoning the contribution $\langle \psi_{m_R} | \hat{H} - \hat{H}_R | \psi_{m_R} \rangle$ is also negligible. One thus has

$$
\begin{aligned}
\Delta E &:= E_- - E_+ \\
&\approx -2 \left\langle \psi_{m_R} \left| \hat{H} - \hat{H}_L \right| \psi_{m_L} \right\rangle
\end{aligned}
\tag{2.64}
$$

$$
\overset{(2.56)}{=} -2 \left\langle \psi_{m_R} \left| \hat{H} \right| \psi_{m_L} \right\rangle + E_0 \left\langle \psi_{m_R} | \psi_{m_L} \right\rangle
\tag{2.65}
$$

$$
\Rightarrow \quad \Delta E \approx -2 \left\langle \psi_{m_R} \left| \hat{H} \right| \psi_{m_L} \right\rangle
\tag{2.66}
$$

for the tunnel splitting and

$$
\left\langle \psi_{m_R} \left| \hat{H} \right| \psi_{m_L} \right\rangle \approx -\frac{\Delta E}{2}
\tag{2.67}
$$

for the coupling matrix element, where the overlap of the states $|\psi_{m_L}\rangle$ and $|\psi_{m_R}\rangle$ was again neglected in the step from equation (2.65) to (2.66). By means of this coupling matrix element and

$$
\begin{aligned}
\left\langle \psi_{m_L/m_R} \left| \hat{H} \right| \psi_{m_L/m_R} \right\rangle &\overset{(2.58)}{\approx} \frac{1}{2} \left\langle \psi_+ \pm \psi_- \left| \hat{H} \right| \psi_+ \pm \psi_- \right\rangle \\
&= \frac{1}{2} \left(\left\langle \psi_+ \left| \hat{H} \right| \psi_+ \right\rangle + \left\langle \psi_- \left| \hat{H} \right| \psi_- \right\rangle \pm 2 \left\langle \psi_+ \left| \hat{H} \right| \psi_- \right\rangle \right) \\
&= \frac{1}{2} \left(E_+ + E_- \right) \\
&= E_0,
\end{aligned}
\tag{2.68}
$$

one obtains the projection

$$\hat{H}_{(2)} \;=\; \begin{pmatrix} E & -\frac{\Delta E}{2} \\ -\frac{\Delta E}{2} & E \end{pmatrix}. \tag{2.69}$$

of the Hamilton operator $\hat{H}$ onto the two-dimensional space $\left\{\,|\psi_{m_L}\rangle\,\right\} \bigoplus \left\{\,|\psi_{m_R}\rangle\,\right\}$. Its diagonalization yields the tunnel splitting ΔE and the eigenstates (2.58) [45].

It turns out that equation (2.66) is not suited for an analytical consideration of the tunnel splitting and that it is better to start with the eigenequations

$$\hat{H}\psi_+(q) \;=\; E_+\psi_+(q), \tag{2.70}$$

$$\hat{H}\psi_-(q) \;=\; E_-\psi_-(q). \tag{2.71}$$

Multiplying equation (2.70) with $\psi_-(q)$ and (2.71) with $\psi_+(q)$ from the left and taking the difference yields

$$\psi_-(q)\hat{H}\psi_+(q) - \psi_+(q)\hat{H}\psi_-(q) \;=\; (E_+ - E_-)\,\psi_+(q)\psi_-(q). \tag{2.72}$$

Equation (2.72) holds for all values of q. But the eigenfunctions $\psi_+(q)$ and $\psi_-(q)$ are semiclassically not exactly known. One therefore integrates equation (2.72) over the interval $[q,\infty]$, where q is an arbitrary position under the tunnel barrier $[b_{m_L}, a_{m_R}]$. By performing this integration, the uncertainty of the functions $\psi_+(q)$ and $\psi_-(q)$ becomes unimportant

$$
\begin{aligned}
(E_+ - E_-) & \int\limits_q^\infty \mathrm{d}q'\; \psi_+(q')\psi_-(q') \\[2mm]
&= \int\limits_q^\infty \mathrm{d}q'\, \Big(\psi_-(q')\hat{H}\psi_+(q') - \psi_+(q')\hat{H}\psi_-(q') \Big) \\[2mm]
&\overset{(2.5)}{=} -\frac{\hbar_{\mathrm{eff}}^2}{2} \int\limits_q^\infty \mathrm{d}q'\, \left(\psi_-(q')\frac{\mathrm{d}^2\psi_+(q')}{\mathrm{d}q'^2} - \psi_+(q')\frac{\mathrm{d}^2\psi_-(q')}{\mathrm{d}q'^2} \right) \\[2mm]
&= -\frac{\hbar_{\mathrm{eff}}^2}{2} \left[\psi_-(q')\frac{\mathrm{d}\psi_+(q')}{\mathrm{d}q'} - \psi_+(q')\frac{\mathrm{d}\psi_-(q')}{\mathrm{d}q'} \right]_q^\infty \\[2mm]
&\quad +\frac{\hbar_{\mathrm{eff}}^2}{2} \int\limits_q^\infty \mathrm{d}q'\, \left(\frac{\mathrm{d}\psi_-(q')}{\mathrm{d}q'}\frac{\mathrm{d}\psi_+(q')}{\mathrm{d}q'} - \frac{\mathrm{d}\psi_+(q')}{\mathrm{d}q'}\frac{\mathrm{d}\psi_-(q')}{\mathrm{d}q'} \right)
\end{aligned} \tag{2.73}
$$

Since square integrable wave functions vanish at $q = \infty$, the evaluation of the first term of equation (2.73) at the upper border yields zero. The integrand of the term in the second line of this equation is already equal to zero. It remains

$$
(E_+ - E_-) \int\limits_q^\infty \mathrm{d}q'\ \psi_+(q')\psi_-(q')
$$
$$
= \frac{\hbar_{\mathrm{eff}}^2}{2} \left(\psi_-(q) \left.\frac{\mathrm{d}\psi_+(q')}{\mathrm{d}q'}\right|_{q'=q} - \psi_+(q) \left.\frac{\mathrm{d}\psi_-(q')}{\mathrm{d}q'}\right|_{q'=q} \right). \qquad (2.74)
$$

The demonstrated procedure works, however, only for Hamilton operators with the special form like in equation (2.5). Using equation (2.58) one has

$$
\int\limits_q^\infty \mathrm{d}q'\ \psi_+(q')\psi_-(q') \ \approx\ \frac{1}{2} \int\limits_q^\infty \mathrm{d}q'\ \left(|\psi_{m_R}(q')|^2 - |\psi_{m_L}(q')|^2 \right) \ \approx\ \frac{1}{2} \qquad (2.75)
$$

and therefore

$$
\Delta E \ =\ E_- - E_+
$$
$$
=\ \hbar_{\mathrm{eff}}^2 \left(\psi_{m_L}(q) \left.\frac{\mathrm{d}\psi_{m_R}(q')}{\mathrm{d}q'}\right|_{q'=q} - \psi_{m_R}(q) \left.\frac{\mathrm{d}\psi_{m_L}(q')}{\mathrm{d}q'}\right|_{q'=q} \right). \qquad (2.76)
$$

The wave functions and their derivatives, which appear in (2.76), are evaluated at a position q in the classically forbidden region under the potential energy barrier. The insertion of the corresponding WKB wave function expressions for $\psi_{m_L}(q)$ and $\psi_{m_R}(q)$, equation (2.21), yields finally a semiclassical expression for the tunnel splitting

$$
\Delta E(E_0) \ =\ \frac{\hbar_{\mathrm{eff}}}{2} N_{m_L} N_{m_R} \exp\left(-\frac{1}{\hbar_{\mathrm{eff}}} \int\limits_{b_{m_L}}^{a_{m_R}} \mathrm{d}q\ |p(q, E_0)| \right). \qquad (2.77)
$$

Equation (2.77) is independent of the left and the right well WKB wave functions. This observation supports the former assumption that the continuation of the potential energies $V_L(q)$ and $V_R(q)$ does not matter, provided that they are smooth and that $V_L(q) > E_0$ for $q > a_{m_R}$ and $V_R(q) > E_0$ for $q < b_{m_L}$. The larger the WKB energy E_0 is, the smaller the integral in the exponential function of (2.77) becomes. Tunnel splittings therefore increase with increasing energy E_0, and thus with increasing quantum number. Initial states prepared as $\psi_{m_L}(q)$ or $\psi_{m_R}(q)$ belonging to the energy E_0 undergo oscillations between the two wells with the frequency $\Delta E(E_0)/\hbar_{\mathrm{eff}}$.

2.3 Double well versus scattering system

As example we choose the 1D potential energy

$$
V(q) \quad := \quad \begin{cases} \frac{1}{2}\omega^2 q^2 + V_{\mathrm{H}} & \text{for} \quad q \leq 1 \\ V_{\mathrm{B}} & \text{for} \quad 1 < q \leq 1 + L \\ \infty & \text{for} \quad 1 + L < q \end{cases} , \tag{2.78}
$$

where the angular frequency ω, the length L, and the energy shifts V_{H} and V_{B} are real parameters. Figure 2.8 illustrates that the potential energy $V(q)$ consists of two asymmetric wells, which are separated by an energy barrier of height $V(1) = V_{\mathrm{H}} + \omega^2/2$. The shape of the left well is a part of a harmonic oscillator and the right well is similar to a box. With an energy $E < V_{\mathrm{H}} + \omega^2/2$, we have the classical turning points $\pm\sqrt{2(E - V_{\mathrm{H}})}/\omega$ in the left well, and 1 and $1 + L$ in the right one. We remark that the latter two turning points are independent of E.

A system with a potential energy $V(q)$ like equation (2.78) is called closed. It possesses the property that the spectrum of its Hamilton operator consists of discrete real eigenenergies. The corresponding eigenfunctions are square integrable and vanish at $q = \pm\infty$. If the length L in the potential energy (2.78) is infinitely large, the system resembles an open system, see figure 2.9. The most important property of an open system is that it possesses a continuous energy spectrum. A quantum particle which is initially located in the harmonic oscillator-like well of the open system eventually tunnels through the energy barrier after a certain time and escapes to infinity. The quantum state which is associated with this particle is thus a scattering state and the system is consequently called scattering
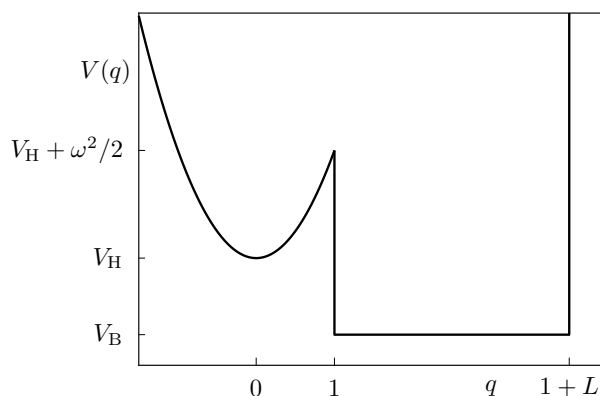
Figure 2.8: Illustration of the asymmetric double well potential energy defined by equation (2.78). The shape of the left well resembles that of a harmonic oscillator and the right well is similar to a box.

system. Since such a state behaves as if it were bounded for a certain time, it is named metastable or it is sometimes regarded as a quasi-bound state [46]. The domain, where a metastable state initially localizes, is usually called quasi-bound region. The energy of a quasi-bound state is equal to a resonance energy of the scattering system [1]. Possible resonance energies E lie between V_{H} and $V_{\mathrm{H}} + \omega^2/2$ with $\pm\sqrt{2(E - V_{\mathrm{H}})}/\omega$ as corresponding classical turning points in the considered example. The tunneling process through the 1D energy barrier in a scattering system occurs with a certain probability, which is called decay or tunneling rate $\gamma(E)$. Gamow studied the tunneling rate semiclassically and argued that it is equal to the product of the rate at which the particle appears at the right classical turning point $\sqrt{2(E - V_{\mathrm{H}})}/\omega$ and the probability of penetrating the barrier at energy E, see e.g. reference [47]. As the angular frequency of a harmonic oscillator is energy independent, the rate is here just given by $\omega/(2\pi)$. The rate would otherwise be a function of the energy E. The probability of penetrating the potential energy barrier is in general equal to the square of the exponential function which appears in equation (2.77), so that Gamow's formula for tunneling rates reads

$$\gamma(E) \;\; = \;\; \frac{\omega}{2\pi} \exp\left(-\frac{2}{\hbar_{\mathrm{eff}}} \int\limits_{\sqrt{2(E-V_{\mathrm{H}})}/\omega}^{1} \mathrm{d}q \, |p(q, E)| \right). \tag{2.79}$$

It is in agreement with the following simple considerations. The larger the angular frequency ω is, the more frequent does the considered particle appear at the right turning point per unit time, implying a larger $\gamma(E)$. And the smaller the length of the tunneling path under the energy barrier is, the larger should the probability of penetrating it be. This implies that the tunneling rate increases with an increasing energy E. Both expec-
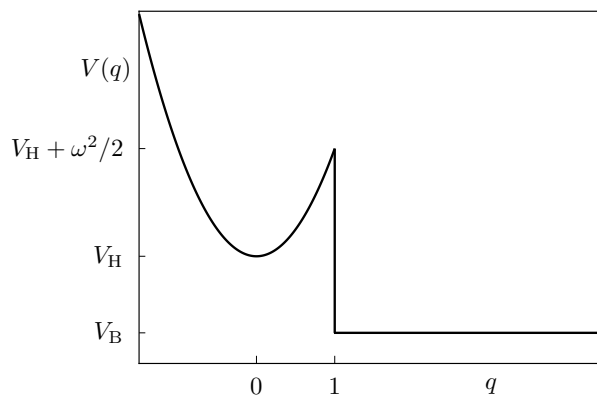
Figure 2.9: Double well potential energy of the example system (2.78) with infinite length L. This system is similar to a scattering system.

tations are confirmed by equation (2.79). We finally remark that the exponential function in equation (2.79) is also known as Gamow factor.

Before we will investigate tunneling through the potential energy barrier in the example (2.78), we show that Gamow's formula for tunneling rates can also be derived via Fermi's golden rule.

2.3.1 Gamow's formula and Fermi's golden rule

We return to the closed system with the double well shaped potential energy (2.78). If the left well had been a pure harmonic oscillator,

$$E_{m_L} \;\; = \;\; \hbar_{\mathrm{eff}}\,\omega\left(m_L + \frac{1}{2}\right) \qquad \text{with} \qquad m_L \in \mathbb{N}_0 \qquad\qquad (2.80)$$

would have been the left well WKB energy belonging to the quantum number m_L. Similarly,

$$E_{m_R} \;\; = \;\; \frac{\hbar_{\mathrm{eff}}^2 \pi^2}{2L^2}(m_R + 1)^2 + V_{\mathrm{B}} \qquad \text{with} \qquad m_R \in \mathbb{N}_0 \qquad\qquad (2.81)$$

would have been the right well WKB energy prediction, if the right well had been a box of length L with infinitely high walls. The two wells are, however, separated by a static potential energy barrier of the finite height $V(1) = V_{\mathrm{H}} + \omega^2/2$. The smaller E_{m_L} and E_{m_R} are compared to this height, the better the WKB approximations (2.80) and (2.81) are.
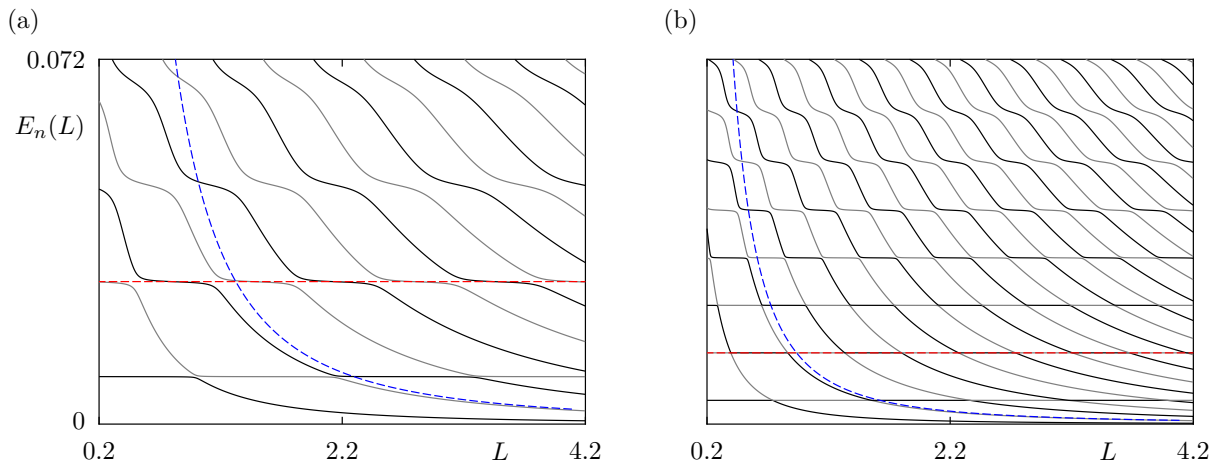
Figure 2.10: Numerically determined eigenvalues of the Hamilton operator $\hat{H}$ under the variation of the system-specific length L of the right well in the interval $[0.2, 4.2]$ for (a) $\hbar_{\mathrm{eff}} = 1/20$ and (b) $\hbar_{\mathrm{eff}} = 1/40$ with $V_{\mathrm{H}} = V_{\mathrm{B}} = 0$ and $\omega = 0.375$. The dashed lines represent the WKB energies $E_{m_L}(L)$ (red) and $E_{m_R}(L)$ (blue) for $m_L = m_R = 1$.

We now consider the spectrum of the corresponding Hamilton operator $\hat{H}$ under the variation of the system-specific length L of the right box shaped well. We define that we label its eigenenergies with the index n: $E_n(L)$. Figure 2.10 shows the spectra for (a) $\hbar_{\text{eff}} = 1/20$ and (b) $\hbar_{\text{eff}} = 1/40$ with $V_{\text{H}} = V_{\text{B}} = 0$ and $\omega = 0.375$. These parameter values will be kept fixed in the following. The larger the energy becomes, the better we can see avoided crossings. This reflects the prediction of equation (2.77). We furthermore notice approximate horizontal lines and hyperbolae in the spectra. The horizontal lines represent the WKB energies of the left harmonic oscillator-shaped well given by equation (2.80) and the hyperbolae represent the WKB energies (2.81) of the box shaped right well. For the purpose of illustration, the energy functions $E_{m_L}(L)$ and $E_{m_R}(L)$ are additionally plotted for $m_L = m_R = 1$ in figures 2.10(a) and (b) as red and blue dashed lines, respectively. The deviations of the actual spectrum, especially from the blue hyperbolae, become larger with increasing energy. The reason is the growing influence of the finite height of the left wall of the box shaped well on the spectrum of the Hamilton operator with increasing energy.

Fermi's golden rule provides a formula which allows for the determination of the tunneling rate of an initial metastable state with energy E_{i} through e.g. an energy barrier to a final state whose energy E_{f} belongs to a continuous spectrum [48]. It relates the tunneling rate with the coupling matrix element V_{fi} with respect to the initial and the final state

$$\gamma_{\text{i}\to\text{f}} \;\; = \;\; \frac{2\pi}{\hbar_{\text{eff}}} \, |V_{\text{fi}}|^2 \, \rho(E_{\text{f}}). \tag{2.82}$$

Here $\rho(E_{\text{f}})$ denotes the density of the final states. Fermi's golden rule is thus in principle only applicable to systems with a continuous spectrum. The spectrum of the closed double well system (2.78) is, however, discrete. Heisenberg's energy-time-uncertainty relation

$$\Delta E \, \Delta t \;\; \geq \;\; h_{\text{eff}} \tag{2.83}$$

states that the resolution of a certain energy interval requires a certain time. A typical energy interval of a closed system is the mean level spacing $\Delta E_{\text{discrete}}$ of its discrete eigenenergies. Its resolution requires the Heisenberg time $\tau_{\text{H}} := h_{\text{eff}}/\Delta E_{\text{discrete}}$. A closed system behaves therefore like a system with a continuous spectrum up to τ_{H}, so that Fermi's golden rule is also applicable for $t < \tau_{\text{H}}$ in a closed system.

Figure 2.10 shows the spectra of the considered closed system as a function of the system-specific parameter L. The Heisenberg time increases with increasing L. Every avoided crossing along the line $E_{m_L}(L) = \text{const.}$, where the quantum number m_L does not change, gives rise to a coupling of the state $|\psi_{m_L}\rangle$ to the states $|\psi_{m_R}\rangle$ with diffe-

rent quantum numbers m_R. These couplings are characterized by the matrix elements $\langle \psi_{m_L} | \hat{H} | \psi_{m_R} \rangle$. As Fermi's golden rule is applicable to a closed system for $t < \tau_{\mathrm{H}}$, we insert these coupling matrix elements into equation (2.82)

$$
\begin{aligned}
\gamma_{m_L \to m_R} &= \frac{2\pi}{\hbar_{\mathrm{eff}}} \left| \left\langle \psi_{m_L} \left| \hat{H} \right| \psi_{m_R} \right\rangle \right|^2 \rho_R(E_{m_R}) \\
&\overset{(2.67)}{=} \frac{2\pi}{\hbar_{\mathrm{eff}}} \left| \frac{\Delta E_{m_L, m_R}}{2} \right|^2 \rho_R(E_{m_R}),
\end{aligned}
\tag{2.84}
$$

where $\rho_R(E_{m_R})$ stands for the density of the WKB states which localize in the right well. Formula (2.84) assigns a tunneling rate to each avoided crossing along the line $E_{m_L}(L) = \mathrm{const.}$ The resonance energies E of the corresponding open system, which is illustrated in figure 2.9, are approximately equal to the allowed WKB energies in the left well of the closed system: $E \approx E_{m_L}$. We therefore believe that the average over all the corresponding tunneling rates of the closed system along the line $E_{m_L}(L) = \mathrm{const.}$ is approximately equal to the tunneling rate of a metastable state with energy E_{m_L}, which initially localizes in the quasi-bound region of the scattering system for a certain time.

The density $\rho_R(E_{m_R})$ is equal to the inverse mean level spacing $\Delta(E_{m_R})$ of the WKB states in the right well

$$
(\rho_R(E_{m_R}))^{-1} = \Delta(E_{m_R}) = \frac{\mathrm{d}E_{m_R}}{\mathrm{d}m_R} = \frac{\hbar_{\mathrm{eff}}^2 \pi^2}{L^2}(m_R + 1).
\tag{2.85}
$$

At an avoided crossing we have $E_0 := E_{m_L} = E_{m_R}$ and thus

$$
(\rho_R(E_{m_R}))^{-1} \overset{(2.81)}{=} \frac{h_{\mathrm{eff}}\pi}{L}\sqrt{2\left(E_0 - V_{\mathrm{B}}\right)}.
\tag{2.86}
$$

The insertion of (2.86) into (2.84) yields

$$
\gamma_{m_L \to m_R} = \frac{\sqrt{2}}{4\hbar_{\mathrm{eff}}^2} \frac{L\left|\Delta E\right|^2}{\sqrt{E_0 - V_{\mathrm{B}}}}.
\tag{2.87}
$$

Now we insert the WKB expression for the tunnel splitting, equation (2.77), with

$$
N_{m_L} = \sqrt{\frac{2\omega_{m_L}}{\pi}} = \sqrt{\frac{2\omega}{\pi}},
\tag{2.88}
$$

$$
N_{m_R} = \sqrt{\frac{2\omega_{m_R}}{\pi}} = \sqrt{\frac{2}{L}\sqrt{2\left(E_0 - V_{\mathrm{B}}\right)}}
\tag{2.89}
$$

into (2.87) and obtain

$$\gamma_{m_L \to m_R} \quad = \quad \frac{\omega}{2\pi} \exp\left(-\frac{2}{\hbar_{\text{eff}}} \int\limits_{\sqrt{2E_{L,m}/\omega}}^{1} dq \sqrt{\omega^2 q^2 - 2E_{L,m}} \right). \qquad (2.90)$$

This formula is identical with Gamow's formula for the tunneling rate γ_{m_L}, equation (2.79), for $|p(q, E_{L,m})| = \sqrt{\omega^2 q^2 - 2E_{L,m}}$. The performed steps show that it is possible to derive Gamow's formula via Fermi's golden rule. Both approaches are thus consistent.

2.3.2 Numerical and analytical consideration

With E_{m_L} given by equation (2.80) we can evaluate the semiclassical equation (2.90) analytically

$$\gamma_{m_L} \quad := \quad \gamma_{m_L \to m_R} \quad = \quad \frac{\omega}{2\pi} \exp\left(-\frac{\omega}{\hbar_{\text{eff}}} \sqrt{1 - \frac{\hbar_{\text{eff}}}{\omega}(2m_L + 1)} \right.$$
$$\left. + (2m_L + 1) \operatorname{arcosh}\left(\sqrt{\frac{\omega}{\hbar_{\text{eff}}(2m_L + 1)}} \right) \right). \qquad (2.91)$$

We now want to compare this analytical prediction for tunneling rates with numerically determined data. We consider the example system (2.78) under the variation of the length L and pass along the line $E_{L,m}(L) = \text{const.}$ in figure 2.10. By means of Fermi's golden rule, equation (2.87), we get a tunneling rate for every avoided crossing. In order to determine these tunneling rates numerically, we have to measure the avoided crossings in the spectrum.

A simple method is the determination of the minimal distance between the two eigenergies which are involved in the avoided crossing of interest by means of a nested interval algorithm. The advantage of this procedure is that it is very precise. It can, however, be very time consuming.

Another method is performing a fit through numerically determined data points on a coarse grid. For this purpose we need general expressions for the energy curves being involved in the avoided crossing. Von Neumann and Wigner treated this problem in reference [45]. They showed that

$$E_{\pm}(L) \quad = \quad E + (L - L_0)v \pm \sqrt{\left(\frac{\Delta E}{2}\right)^2 + (L - L_0)^2 u^2} \qquad (2.92)$$

holds in the vicinity of an avoided crossing. This implies that the eigenenergies lie on hyperbola branches. The parameters L_0, E, u, v, and the tunnel splitting ΔE are fit parameters. Here L_0 denotes the position of the avoided crossing. The energy E stands for the WKB energy of the left and the right well at the avoided crossing. The matrix elements $\langle \psi_- |V(\hat{q})| \psi_+ \rangle$ and $\langle \psi_+ |V(\hat{q})| \psi_+ \rangle$ are represented by the parameters u and v. Compared to a nested interval algorithm, this method yields acceptable results on a less fine L grid. As long as no further avoided crossing is located close to the one of interest, the hyperbola shape of the two eigenenergy branches of the Hamilton operator is not disturbed and fits through the numerically determined discrete data points can successfully be performed by means of equation (2.92). Since this is fulfilled in the considered example, see figure 2.10, we focused on this method.

Equation (2.87) contains a factor L in the numerator of its right-hand side. But, for fixed m_L the tunneling rate belonging to the coupling of the state $|\psi_{m_L}\rangle$ to states $|\psi_{m_R}\rangle$ with different quantum numbers m_R should be constant. We therefore expect that $\sqrt{L}\,\Delta E(L, E_{m_L}) = \text{const.}$ holds. Figure 2.11 supports this assumption numerically.

For $\hbar_{\text{eff}} = 1/20$ and $\hbar_{\text{eff}} = 1/40$ tables 2.1 and 2.2 contain tunneling rates obtained via the WKB-like Gamow formula (2.91) and from numerically determined tunnel splittings inserted into Fermi's golden rule (2.87). The above choice of $\omega = 0.375$ allows four WKB states in the left harmonic oscillator-like well in the first and eight in the second case. Let us label the avoided crossings in the spectra of figure 2.10 by the pair of WKB quantum numbers (m_L, m_R). For fixed m_L the numerically determined tunneling rates were obtained by averaging over the ten avoided crossings with $m_R = 0$ by $m_R = 9$ along the line $E_{m_L}(L) = \text{const.}$ in each case. The relative error $\left|\gamma_{m_L}^{\text{WKB}} - \gamma_{m_L}^{\text{num}}\right| / \left|\gamma_{m_L}^{\text{WKB}}\right|$ is illustrated as a function of the quantum number m_L in the figures 2.12(a) and (b). We realize that the relative error grows when the quantum number m_L increases. This
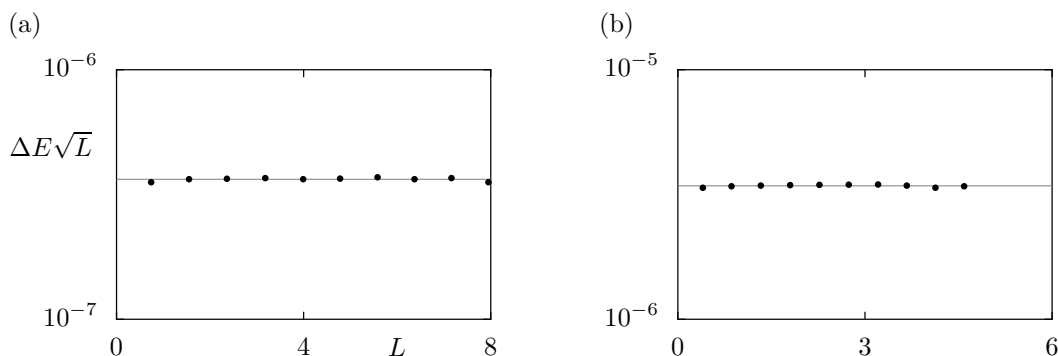
Figure 2.11: The product $\Delta E(L, E_{m_L})\sqrt{L}$ for the ten avoided crossings labelled by the WKB quantum numbers (m_L, m_R) for $m_R = 0$ by $m_R = 9$ and (a) $m_L = 0$ and (b) $m_L = 1$. The data were determined for $\hbar_{\text{eff}} = 1/40$.

observation has two reasons. The first one is that the WKB approximation becomes worse with increasing energy due to a steeper shape of the potential energy at the classical turning points. I.e. that Gamow's formula becomes less accurate with increasing quantum number m_L. The second reason is that the numerical determination of avoided crossings becomes more difficult, and thus less accurate, with increasing m_L.
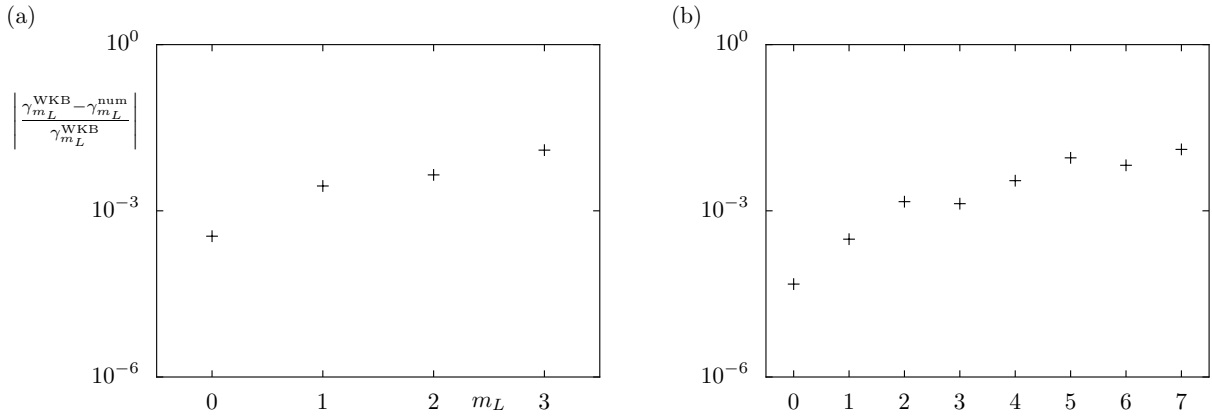
Figure 2.12: Relative error $\left|\gamma_{m_L}^{\text{WKB}} - \gamma_{m_L}^{\text{num}}\right| / \left|\gamma_{m_L}^{\text{WKB}}\right|$ as a function of the quantum number m_L for (a) $\hbar_{\text{eff}} = 1/20$ and (b) $\hbar_{\text{eff}} = 1/40$.

m_L	$\gamma_{m_L}^{\text{WKB}}$	$\gamma_{m_L}^{\text{num}}$
0	$2.92993 \cdot 10^{-4}$	$2.92891 \cdot 10^{-4}$
1	$3.95401 \cdot 10^{-3}$	$3.96511 \cdot 10^{-3}$
2	$2.11432 \cdot 10^{-2}$	$2.12373 \cdot 10^{-2}$
3	$5.46966 \cdot 10^{-2}$	$5.40152 \cdot 10^{-2}$

Table 2.1: Comparison of tunneling rates obtained via Gamow's formula (2.90), second column, and from numerically determined tunnel splittings inserted into Fermi's golden rule (2.87), last column. The data were determined for $\hbar_{\text{eff}} = 1/20$. The choice $\omega = 0.375$ allows four WKB energy levels in the left well. The numerically determined tunneling rates are a result of an average over ten single values along the line $E_{m_L} = const$.

m_L	$\gamma_{m_L}^{\mathrm{WKB}}$	$\gamma_{m_L}^{\mathrm{num}}$
0	$2.31194 \cdot 10^{-7}$	$2.31183 \cdot 10^{-7}$
1	$6.76189 \cdot 10^{-6}$	$6.75981 \cdot 10^{-6}$
2	$8.82730 \cdot 10^{-5}$	$8.81439 \cdot 10^{-5}$
3	$6.97773 \cdot 10^{-4}$	$6.96834 \cdot 10^{-4}$
4	$3.71248 \cdot 10^{-3}$	$3.72548 \cdot 10^{-3}$
5	$1.38550 \cdot 10^{-2}$	$1.37297 \cdot 10^{-2}$
6	$3.61761 \cdot 10^{-2}$	$3.59361 \cdot 10^{-2}$
7	$5.96831 \cdot 10^{-2}$	$5.89162 \cdot 10^{-2}$

Table 2.2:   The same comparison as in table 2.1 for $\hbar_{\mathrm{eff}} = 1/40$. This corresponds to eight allowed WKB energy levels in the left well.

3 Periodically kicked systems in 1D

In quantum chaos one studies quantum systems whose classical limit is in some sense chaotic. In section 3.1 we introduce classical periodically kicked 1D systems on a torus. Stroboscopically, their classical dynamics is described by a map, which possesses the area-preserving property. Since area-preserving maps show different dynamical behaviour like e.g. integrable motion, mixed dynamics, or ergodicity, they are helpful for the investigation of classical chaos.

Kicked systems in 1D have furthermore attracted much attention especially due to their simple quantization, which is demonstrated in section 3.2. While time evolution is classically described by certain equations of motion, one has a unitary time evolution operator on the quantum level. In order to visualize its eigenstates in phase space and in order to compare them with the phase space structures of the corresponding classical map, the concept of the Husimi function is explained in section 3.3. We close this chapter with the introduction of an example map in section 3.4. We will use this map for numerical studies and illustrations in the remaining part of the thesis.

3.1 Classical periodically kicked systems in 1D and area-preserving maps

The two-torus $\mathbb{T}^2$ is defined by the product manifold

$$\mathbb{T}^2 \; := \; S^1 \times S^1, \tag{3.1}$$

where

$$S^1 \; := \; \left\{ z \in \mathbb{C} \, \middle| \, |z| = 1 \right\} = \left\{ e^{2\pi i \varphi} \, \middle| \, \varphi \in \mathbb{R} \right\} \tag{3.2}$$

denotes the unit circle. This implies that the points $(q, p) \in \mathbb{R}^2$ and $(q', p') \in \mathbb{R}^2$ are identified with each other

$$(q, p) \; \equiv \; (q', p'), \tag{3.3}$$

if

$$q - q' \in \mathbb{Z} \quad \text{and} \quad p - p' \in \mathbb{Z}. \qquad (3.4)$$

The two-torus $\mathbb{T}^2$ is isomorphic to the quotient manifold $\mathbb{R}^2 \backslash \mathbb{Z}^2$ [49]. Its natural representation is the unit square $[0,1] \times [0,1]$, where opposite sides are identified. The identification of $p = 0$ with $p = 1$ yields a cylinder, which becomes a torus by additionally identifying $q = 0$ with $q = 1$. The term torus is thus justified for the manifold (3.1). In this thesis we will also consider maps on the torus $[0, M_q] \times [0, M_p]$ with $M_q \in \mathbb{N}$ and $M_p \in \mathbb{N}$. Here $q = 0$ is identified with $q = M_q$ as well as $p = 0$ with $p = M_p$.

A map P on the two-torus $\mathbb{T}^2$, which has the Lebesgue measure $\mathrm{d}\mu := \mathrm{d}q\mathrm{d}p$ as natural invariant measure, is formally defined by

$$
\begin{aligned}
P: \quad \mathbb{T}^2 &\rightarrow \quad \mathbb{T}^2 \\
(q,p) &\mapsto \quad (q',p').
\end{aligned}
\qquad (3.5)
$$

If the determinant of the matrix which represents the linearization DP of the map P is equal to one, it is area-preserving.

The dimensionless Hamiltonian of a periodically kicked particle in 1D with kicking period τ possesses the property $H(q,p,t) = H(q,p,t+\tau)$ and is given by

$$H(q,p,t) \;=\; T(p) + \tau\, V(q) \sum_{n \in \mathbb{Z}} \delta(t - n\tau), \qquad (3.6)$$

where $T(p)$ and $V(q)$ denote the kinetic and the potential energy, respectively [50]. For simplicity one usually sets the kicking period equal to one

$$H(q,p,t) \;=\; T(p) + V(q) \sum_{n \in \mathbb{Z}} \delta(t - n). \qquad (3.7)$$

The δ-function in equations (3.6) and (3.7) ensures that the particle is subject to the potential energy instantaneously once per kicking period.

The time evolution of a classical system is e.g. governed by Hamilton's equations of motion: $\dot{q} = \partial H(q,p,t)/\partial p$ and $\dot{p} = -\partial H(q,p,t)/\partial q$, where the dot denotes the time derivative. Their stroboscopic evaluation immediately after the nth kick yields [50]

$$
\begin{aligned}
q_{n+1} &= q_n + T'(p_n), \qquad &(3.8)\\
p_{n+1} &= p_n - V'\big(q_n + T'(p_n)\big). \qquad &(3.9)
\end{aligned}
$$

The primes in equations (3.8) and (3.9) stand for the p or q derivative. In order to ensure that the mapped point (q_{n+1}, p_{n+1}) remains on the two-torus $\mathbb{T}^2$, it is necessary to incorporate a periodic boundary condition in q as well as in p direction. They are mathematically reflected by the modulo operation

$$
\begin{pmatrix} q_{n+1} \\ p_{n+1} \end{pmatrix} = \begin{pmatrix} q_n + T'(p_n) \\ p_n - V'\big(q_n + T'(p_n)\big) \end{pmatrix} \mod 1, \tag{3.10}
$$

so that one obtains the classical map

$$
P: \quad \mathbb{T}^2 \quad \to \quad \mathbb{T}^2
$$

$$
\begin{pmatrix} q_n \\ \\ p_n \end{pmatrix} \mapsto \begin{pmatrix} q_n + T'(p_n) \\ \\ p_n - V'\big(q_n + T'(p_n)\big) \end{pmatrix} \mod 1 \text{ with } n \in \mathbb{Z}. \tag{3.11}
$$

The phase space of the periodically kicked system which is characterized by the Hamiltonian (3.7) is thus equal to the two-torus $\mathbb{T}^2$. With an initial point $(q_0, p_0) \in \mathbb{T}^2$, the sequence of the phase space points[1] $(q_n, p_n) = P^n(q_0, p_0) \in \mathbb{T}^2$, with $n \in \mathbb{Z}$, builds an orbit. The point (q_n, p_n) is also called the nth iterate of the initial point (q_0, p_0). The linearization DP of the map P around a phase space point $(\bar{q}, \bar{p})$,

$$
DP: \quad \mathbb{T}^2 \quad \to \quad \mathbb{T}^2
$$

$$
\begin{pmatrix} q \\ p \end{pmatrix} \mapsto \begin{pmatrix} q' \\ p' \end{pmatrix} = M \begin{pmatrix} q \\ p \end{pmatrix} \mod 1, \tag{3.12}
$$

is represented by the so-called monodromy matrix

$$
\begin{aligned}
M &:= \begin{pmatrix} \dfrac{\partial q_{n+1}(q_n, p_n)}{\partial q_n} & \dfrac{\partial q_{n+1}(q_n, p_n)}{\partial p_n} \\[2mm] \dfrac{\partial p_{n+1}(q_n, p_n)}{\partial q_n} & \dfrac{\partial p_{n+1}(q_n, p_n)}{\partial p_n} \end{pmatrix} \Bigg|_{(q_n, p_n) = (\bar{q}, \bar{p})} \\[4mm]
&= \begin{pmatrix} 1 & T''(\bar{p}) \\[3mm] -V''\big(\bar{q} + T'(\bar{p})\big) & 1 - V''\big(\bar{q} + T'(\bar{p})\big) T''(\bar{p}) \end{pmatrix}.
\end{aligned} \tag{3.13}
$$

---

[1] P^n denotes the n-fold application of the map P.

It fulfills $\det(M) = 1$. This implies that the map which is defined by equation (3.11) and which follows from the time dependent Hamiltonian (3.7) is area-preserving.

A phase space region, where the distance between the iterates of two orbits with close initial points (q_0, p_0) and (q_0', p_0') grows exponentially as a function of time, is called chaotic or chaotic sea. A phase space component is called regular, if this distance does not grow exponentially. Regular iterates lie on so-called invariant tori.

The linearization of a map is an important tool for the stability analysis of fixed points [51]. A point (q^*, p^*) is called a fixed point of the map P, if $P(q^*, p^*) = (q^*, p^*)$ holds. The fixed point is stable, if the modulus of the trace of the monodromy matrix evaluated at the fixed point,

$$\left| \mathrm{Tr}\big(M(q^*, p^*)\big) \right| \; = \; \left| 2 - V''(q^* + T'(p^*)) \, T''(p^*) \right|, \tag{3.14}$$

is smaller than two. In this case the eigenvalues of the monodromy matrix are complex, see equation (B.12) in appendix B, and an orbit with an initial point taken from a small vicinity of the fixed point lies thus on an elliptic invariant torus. A stable fixed point is therefore also called elliptic. The iterates perform R revolutions along the ellipse per kicking period, where R denotes the so-called rotation number. This number is constant for all elliptic invariant tori of the linearized map around the stable fixed point. The multiplication of R with the full angle 2π yields the winding number $\vartheta := 2\pi R$. The residue of an elliptic fixed point [52],

$$\mathrm{Res} \; = \; \frac{2 - \mathrm{Tr}\big(M(q^*, p^*)\big)}{4}, \tag{3.15}$$

is equal to $\sin^2(\vartheta/2)$ [52], so that one obtains

$$R \; = \; \frac{1}{\pi} \arcsin\left(\sqrt{\frac{2 - \mathrm{Tr}\big(M(q^*, p^*)\big)}{4}} \right) \; = \; \frac{1}{2\pi} \arccos\left(\frac{\mathrm{Tr}\big(M(q^*, p^*)\big)}{2} \right) \tag{3.16}$$

for the rotation number.

Characteristic quantities of an ellipse are their tilting angle θ with respect to the q axis of the phase space and the aspect ratio $\sigma = b/a$, where a and b are the semi axes of the ellipse, see figure 3.1. They follow from the monodromy matrix

$$\theta \; = \; \frac{1}{2}\arctan\left(\frac{M_{22} - M_{11}}{M_{12} - M_{21}} \right), \tag{3.17}$$

$$\sigma \; = \; \sqrt{\frac{|M_{12} - M_{21} + c|}{|M_{12} - M_{21} - c|}} \quad \text{with} \quad c = \sqrt{(M_{12} + M_{21})^2 + (M_{22} - M_{11})^2}, \tag{3.18}$$
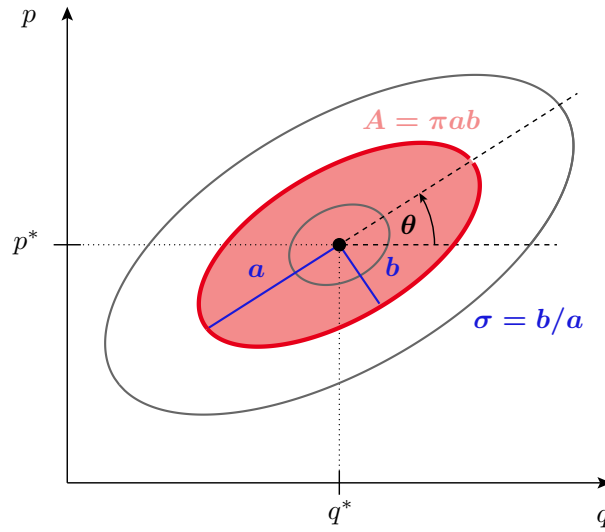
Figure 3.1: Elliptic invariant tori of the linearized map DP with tilting angle θ around a stable fixed point (q^*, p^*) in phase space. The red ellipse encloses the area $A = \pi ab$, where a and b are their semi-axes. The aspect ratio is $\sigma = b/a$.

what is demonstrated in appendix B. If $\left|\text{Tr}\big(M(q^*, p^*)\big)\right| > 2$, the fixed point (q^*, p^*) is unstable. For $\text{Tr}\big(M(q^*, p^*)\big) > 2$ it is called hyperbolic, and inverse hyperbolic for $\text{Tr}\big(M(q^*, p^*)\big) < 2$.

With $k \in \mathbb{N}$, (q^*, p^*) is similarly called a fixed point of the k-fold applied map P^k, if $P^k(q^*, p^*) = (q^*, p^*)$ holds. Its stability analysis can be performed in the same manner as above after replacing the trace $\text{Tr}\big(M(q^*, p^*)\big)$ by $\text{Tr}\big(M^k(q^*, p^*)\big)$.

The closed invariant tori around elliptic fixed points form so-called regular islands. They coexist with the chaotic sea in typical Hamiltonian systems [9]. Both phase space components are classically, however, separated by dynamically generated barriers, i.e. that transitions between them are classically impossible.

A simple example of an area-preserving map is the standard map [53]. Its definition reads

$$P : \quad \mathbb{T}^2 \quad \rightarrow \quad \mathbb{T}^2$$

$$\begin{pmatrix} q_n \\ p_n \end{pmatrix} \mapsto \begin{pmatrix} q_n + p_n \\ p_n - \frac{\kappa}{2\pi} \sin(2\pi[q_n + p_n]) \end{pmatrix} \quad \text{mod} \ 1 \ \text{ with } \ n \in \mathbb{Z}, \qquad (3.19)$$

where $\kappa \in \mathbb{R}^+$ denotes a perturbation parameter. Figure 3.2 shows phase space orbits of the standard map for different initial points for the perturbation parameter values (a)

$\kappa = 0.0$, (b) $\kappa = 0.5$, (c) $\kappa = 1.0$, and (d) $\kappa = 3.0$. For $\kappa = 0$ the orbits lie on horizontal lines for every initial point (q_0, p_0). The iterates rotate along these lines in q direction with the frequency p_0. They fill each invariant torus densely for irrational p_0, whereas the iterates lie on single points for rational p_0. This can be seen in figure 3.2(a) for $p_0 = 1/2$. While the dynamics is integrable for $\kappa = 0$, this does not hold for $\kappa > 0$. Most of the initial invariant tori still exist for a small value of κ, albeit in a distorted manner. The invariant tori with rational p_0 break up. According to the Poincaré-Birkhoff-fixed-point theorem [54] a sequence of alternating stable and unstable fixed points remains. A regular island evolves around every stable fixed point.
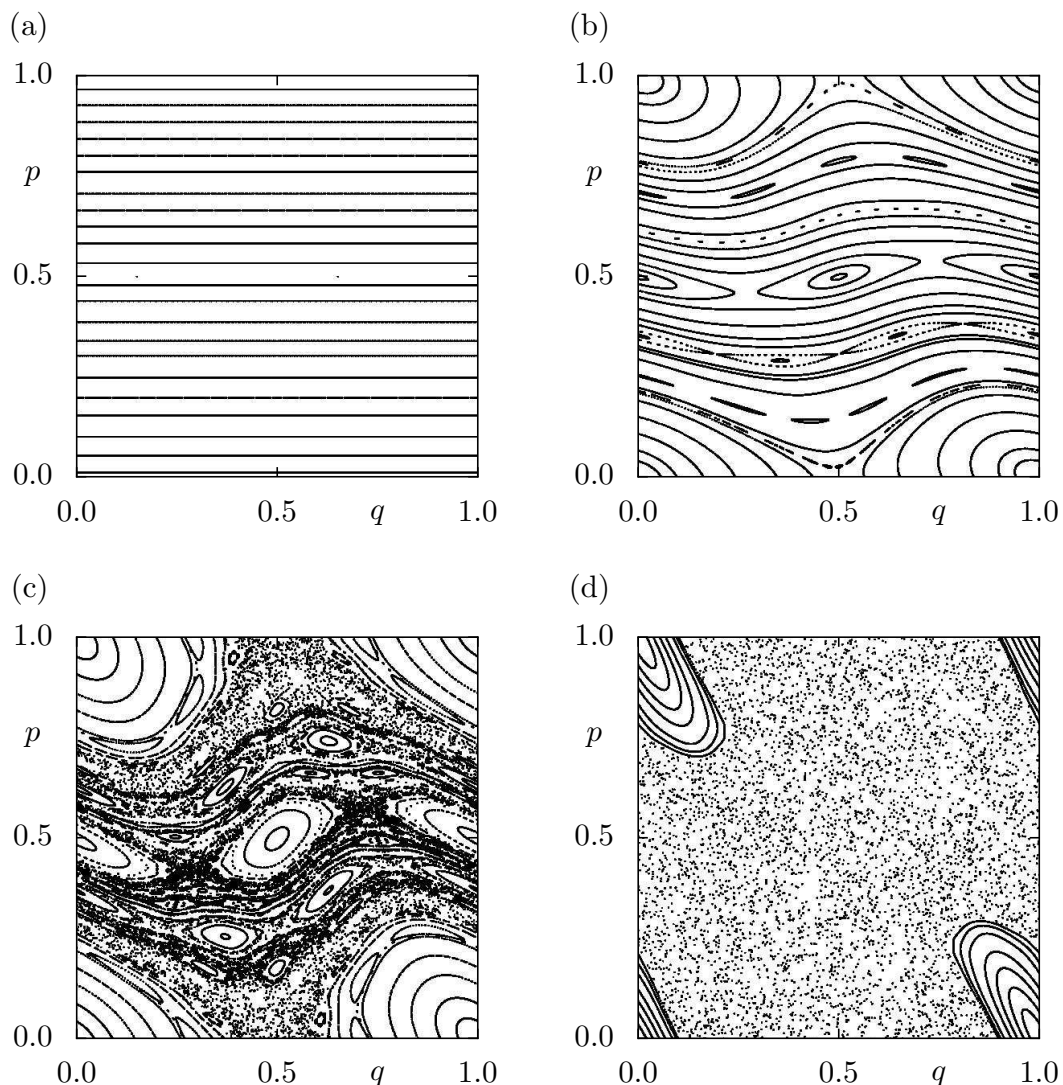
Figure 3.2: Phase space of the standard map for (a) $\kappa = 0.0$, (b) $\kappa = 0.5$, (c) $\kappa = 1.0$, and (d) $\kappa = 3.0$.

As a whole, these islands form a chain with layers of chaotic dynamics, see figure 3.2(b). According to the Kolmogorov-Arnol'd-Moser (KAM) theorem the formation of such an island chain is theoretically understood for small values of the perturbation parameter κ. They are a consequence of resonances and are therefore called resonance island chains. For increasing values of the perturbation parameter more and more invariant tori break up and the chaotic phase space component grows, see figure 3.2(c). For $\kappa = 3.0$, figure 3.2(d), one clearly sees a regular island which coexists with the chaotic sea. This demonstrates that a system whose dynamics is described by the standard map can show mixed dynamics.

A phase space region is called ergodic, if the time average of the iterates (q_n, p_n) of almost all initial points (q_0, p_0) from this region is equal to the phase space average. Whether the dynamics in the chaotic sea of the phase space of the standard map is ergodic for any perturbation parameter value, is still an unsolved mathematical problem.

3.2   Quantization of periodically kicked systems

Area-preserving maps, which describe the dynamics of 1D periodically kicked systems defined on a torus, have been considered on the classical level up to this point. Their quantization is demonstrated in this section. While time evolution is classically described by means of a map following from certain equations of motion, it is quantum mechanically represented by a unitary operator.

3.2.1   Time evolution operator of periodically kicked systems

Given a classical 1D Hamiltonian $H(q, p, t)$, the quantum mechanical time evolution operator is equal to

$$\hat{U}(t, t_0) \;=\; \hat{O} \exp\left(-\frac{\mathrm{i}}{\hbar_{\mathrm{eff}}} \int_{t_0}^{t} \mathrm{d}t' \, H(\hat{q}, \hat{p}, t') \right), \qquad (3.20)$$

where t_0 is a reference time and $\hat{O}$ the time ordering operator.

Classically, the time evolution of a periodically kicked system is stroboscopically studied e.g. immediately after the nth kick. Consequently, one would like to know the associated time evolution operator at those times, which are equal to an integer multiple of the kicking period τ. For its derivation one can follow e.g. reference [55]. One replaces at first

the δ-function in equation (3.6) temporarily by a pulse of finite width $\Delta\tau$ and height $1/\Delta\tau$

$$
\bar{H}(q,p,t) \;=\; \begin{cases} T(p) & \text{for} \quad n\tau \le t < (n+1)\tau - \Delta\tau \\ T(p) + \frac{\tau}{\Delta\tau}V(q) & \text{for} \quad (n+1)\tau - \Delta\tau \le t < (n+1)\tau \end{cases} \quad , \quad (3.21)
$$

with $n \in \mathbb{Z}$. The Hamiltonian (3.21) is piecewise constant. After the restriction to one kicking period one has

$$
\hat{\bar{U}}(t) \;=\; \exp\left(-\frac{\mathrm{i}}{\hbar_{\text{eff}}}T(\hat{p})t\right) \tag{3.22}
$$

for $0 \le t < \tau - \Delta\tau$, and

$$
\begin{aligned}
\hat{\bar{U}}(t) \;&=\; \exp\left(-\frac{\mathrm{i}}{\hbar_{\text{eff}}}\left[T(\hat{p}) + \frac{\tau}{\Delta\tau}V(\hat{q})\right](t-\tau+\Delta\tau)\right)\hat{\bar{U}}(t-\Delta\tau) \\
&=\; \exp\left(-\frac{\mathrm{i}}{\hbar_{\text{eff}}}\left[T(p) + \frac{\tau}{\Delta\tau}V(\hat{q})\right](t-\tau+\Delta\tau)\right) \\
&\quad \cdot \exp\left(-\frac{\mathrm{i}}{\hbar_{\text{eff}}}T(\hat{p})(t-\Delta\tau)\right)
\end{aligned} \tag{3.23}
$$

for $\tau - \Delta\tau \le t < \tau$. Thus,

$$
\hat{U}(\tau) \;:=\; \lim_{\Delta\tau \to 0}\hat{\bar{U}}(\tau) = \exp\left(-\frac{\mathrm{i}}{\hbar_{\text{eff}}}V(\hat{q})\tau\right)\exp\left(-\frac{\mathrm{i}}{\hbar_{\text{eff}}}T(\hat{p})\tau\right) \tag{3.24}
$$

follows immediately for the time evolution operator at $t = \tau$. It is usually called Floquet operator [55] and can be understood as a successive application of an operator, which describes the free evolution of the system, and an operator, which corresponds to a kick at $t = \tau$. By setting $\tau = 1$ as in the classical case, one finally obtains

$$
\hat{U} \;=\; \exp\left(-\frac{2\pi\mathrm{i}}{h_{\text{eff}}}V(\hat{q})\right)\exp\left(-\frac{2\pi\mathrm{i}}{h_{\text{eff}}}T(\hat{p})\right). \tag{3.25}
$$

The systems which will be considered in this thesis are defined on a torus, where opposite sides are identified with each other. Before one is able to evaluate equation (3.25) e.g. in position or momentum representation, one needs to know how the toroidal topology influences the quantization of the position and the momentum variable. This will be studied in the next section.

3.2.2 Quasi-periodicity in q and p direction

The opposite sides of the torus $[0, M_q] \times [0, M_p]$, with $M_q \in \mathbb{N}$ and $M_p \in \mathbb{N}$ are identified with each other, what implies a spatial periodicity in q as wells as in p direction. The quantum mechanical consequences of these periodicities will be studied in the following.

One starts with the phase space translation operator,

$$\hat{T}(q,p) \;=\; \mathrm{e}^{\frac{\mathrm{i}}{\hbar_{\mathrm{eff}}}(p\,\hat{q} - q\,\hat{p})}, \tag{3.26}$$

which fulfills

$$\hat{T}^{\dagger}(q,p) \;=\; \hat{T}(-q,-p) \;. \tag{3.27}$$

It performs a translation by the distances q and p in position and momentum direction, respectively. Using the operator identities

$$\mathrm{e}^{\hat{A}}\,\mathrm{e}^{\hat{B}} \;=\; \mathrm{e}^{\hat{A}+\hat{B}}\,\mathrm{e}^{\frac{1}{2}[\hat{A},\hat{B}]}, \tag{3.28}$$

$$\mathrm{e}^{\hat{A}}\,\mathrm{e}^{\hat{B}} \;=\; \mathrm{e}^{\hat{B}}\,\mathrm{e}^{\hat{A}}\,\mathrm{e}^{[\hat{A},\hat{B}]}, \tag{3.29}$$

which hold for $[\hat{A},[\hat{A},\hat{B}]] = 0$ and $[\hat{B},[\hat{A},\hat{B}]] = 0$, one finds

$$\hat{T}(q,p) \;=\; \mathrm{e}^{-\frac{\mathrm{i}}{2\hbar_{\mathrm{eff}}}pq}\,\mathrm{e}^{\frac{\mathrm{i}}{\hbar_{\mathrm{eff}}}p\hat{q}}\,\mathrm{e}^{-\frac{\mathrm{i}}{\hbar_{\mathrm{eff}}}q\hat{p}} \tag{3.30}$$

$$=\; \mathrm{e}^{-\frac{\mathrm{i}}{2\hbar_{\mathrm{eff}}}pq}\,\hat{T}(0,p)\,\hat{T}(q,0) \tag{3.31}$$

$$=\; \mathrm{e}^{\frac{\mathrm{i}}{2\hbar_{\mathrm{eff}}}pq}\,\mathrm{e}^{-\frac{\mathrm{i}}{\hbar_{\mathrm{eff}}}q\hat{p}}\,\mathrm{e}^{\frac{\mathrm{i}}{\hbar_{\mathrm{eff}}}p\hat{q}} \tag{3.32}$$

$$=\; \mathrm{e}^{\frac{\mathrm{i}}{2\hbar_{\mathrm{eff}}}pq}\,\hat{T}(q,0)\,\hat{T}(0,p). \tag{3.33}$$

In the following the action of the operator $\hat{T}(\varepsilon,0)$ on the state $|q\rangle$ will be important. With the knowledge that $|q\rangle$ is an eigenstate of the operator $\hat{q}$ with the eigenvalue q, one has by exploiting the formula $[\hat{q}, f(\hat{p})] = \mathrm{i}\,\hbar_{\mathrm{eff}}\,f'(\hat{p})$, see e.g. reference [56],

$$\hat{q}\,\hat{T}(\varepsilon,0)|q\rangle \;=\; \hat{q}\,\mathrm{e}^{-\frac{\mathrm{i}}{\hbar_{\mathrm{eff}}}\varepsilon\hat{p}}|q\rangle$$

$$=\; \mathrm{e}^{-\frac{\mathrm{i}}{\hbar_{\mathrm{eff}}}\varepsilon\hat{p}}\,\hat{q}|q\rangle + \mathrm{i}\,\hbar_{\mathrm{eff}}\left(-\frac{\mathrm{i}}{\hbar_{\mathrm{eff}}}\right)\varepsilon\,\mathrm{e}^{-\frac{\mathrm{i}}{\hbar_{\mathrm{eff}}}\varepsilon\hat{p}}|q\rangle$$

$$=\; \hat{T}(\varepsilon,0)\,\hat{q}|q\rangle + \varepsilon\,\hat{T}(\varepsilon,0)|q\rangle$$

$$=\; (q+\varepsilon)\,\hat{T}(\varepsilon,0)|q\rangle. \tag{3.34}$$

Thus, $\hat{T}(\varepsilon,0)|q\rangle$ is an eigenstate of the operator $\hat{q}$ with the eigenvalue $q + \varepsilon$, i.e.

$$\hat{T}(\varepsilon,0)|q\rangle \;=\; |q+\varepsilon\rangle, \tag{3.35}$$

and consequently

$$\langle q|\hat{T}(\varepsilon,0) \;=\; \langle q-\varepsilon|. \tag{3.36}$$

The action of the operator $\hat{T}(0,\delta)$ on the state $|p\rangle$ is also important. The state $|p\rangle$ is an eigenstate of the operator $\hat{p}$ with the eigenvalue p. By means of the formula $[\hat{p},g(\hat{q})] = -\,\mathrm{i}\,\hbar_{\mathrm{eff}}\,g'(\hat{q})$, see also e.g. reference [56], one derives

$$
\begin{aligned}
\hat{p}\,\hat{T}(0,\delta)|p\rangle &= \hat{p}\,\mathrm{e}^{\frac{\mathrm{i}}{\hbar_{\mathrm{eff}}}\delta\hat{q}}|p\rangle \\
&= \mathrm{e}^{\frac{\mathrm{i}}{\hbar_{\mathrm{eff}}}\delta\hat{q}}\,\hat{p}|p\rangle - \mathrm{i}\,\hbar_{\mathrm{eff}}\,\frac{\mathrm{i}}{\hbar_{\mathrm{eff}}}\,\delta\,\mathrm{e}^{\frac{\mathrm{i}}{\hbar_{\mathrm{eff}}}\,\delta\,\hat{q}}|p\rangle \\
&= \hat{T}(0,\delta)\,\hat{p}|p\rangle + \delta\,\hat{T}(0,\delta)|p\rangle \\
&= (p+\delta)\,\hat{T}(0,\delta)|p\rangle.
\end{aligned}
\tag{3.37}
$$

The state $\hat{T}(0,\delta)|p\rangle$ is consequently an eigenstate of the operator $\hat{p}$ with the eigenvalue $p+\delta$, i.e.

$$\hat{T}(0,\delta)|p\rangle \;=\; |p+\delta\rangle, \tag{3.38}$$

and therefore

$$\langle p|\hat{T}(0,\delta) \;=\; \langle p-\delta|. \tag{3.39}$$

As has already been mentioned, a system with a toroidal phase space $[0,\,M_q]\times[0,\,M_p]$ possesses a spatial periodicity with the distances M_q and M_p in q and in p direction, respectively. This property must also be reflected on the quantum level. One therefore has

$$\langle q+\mu\,M_q\,|\psi\rangle \;=\; \mathrm{e}^{2\pi\mathrm{i}\mu\theta_q}\langle q|\psi\rangle, \tag{3.40}$$

$$\langle p+\nu\,M_p\,|\psi\rangle \;=\; \mathrm{e}^{-2\pi\mathrm{i}\nu\theta_p}\langle p|\psi\rangle, \tag{3.41}$$

for an arbitrary quantum state $|\psi\rangle$ with $\mu\in\mathbb{Z}$ and $\nu\in\mathbb{Z}$. The constant Bloch phases θ_q and θ_p are system-specific parameters. The choice of the signs in the exponential functions of equations (3.40) and (3.41) will become clear later. The two equations (3.40) and (3.41) are usually called quasi-periodicity conditions.

By replacing ε in equation (3.35) by $\mu\,M_q$, one finds

$$|q+\mu\,M_q\rangle \;=\; \hat{T}(\mu\,M_q,0)\,|q\rangle \tag{3.42}$$

and therefore

$$\langle q + \mu\, M_q| \;=\; \langle q|\, \hat{T}^\dagger(\mu\, M_q, 0). \tag{3.43}$$

This implies

$$
\begin{aligned}
\langle q + \mu\, M_q|\, \psi\rangle \;&=\; \langle q|\, \hat{T}^\dagger(\mu\, M_q, 0)\, |\psi\rangle \\
&\overset{(3.40)}{=}\; \mathrm{e}^{2\pi\mathrm{i}\mu\theta_q}\langle q|\psi\rangle.
\end{aligned}
\tag{3.44}
$$

As $\langle q|$ is arbitrary, one can deduce

$$
\begin{aligned}
\hat{T}^\dagger(\mu\, M_q, 0)\, |\psi\rangle \;&=\; \mathrm{e}^{2\pi\mathrm{i}\mu\theta_q}|\psi\rangle, \tag{3.45}\\
\Rightarrow\qquad \hat{T}(\mu\, M_q, 0)\, |\psi\rangle \;&=\; \mathrm{e}^{-2\pi\mathrm{i}\mu\theta_q}|\psi\rangle. \tag{3.46}
\end{aligned}
$$

Similarly, one finds

$$|p + \nu\, M_p\rangle \;=\; \hat{T}(0, \nu\, M_p)\, |p\rangle \tag{3.47}$$

by replacing δ in (3.38) by $\nu\, M_p$ and therefore

$$\langle p + \nu\, M_p| \;=\; \langle p|\, \hat{T}^\dagger(0, \nu\, M_p). \tag{3.48}$$

Equation (3.48) implies

$$
\begin{aligned}
\langle p + \nu\, M_p|\, \psi\rangle \;&=\; \langle p|\hat{T}^\dagger(0, \nu\, M_p)|\psi\rangle \\
&\overset{(3.41)}{=}\; \mathrm{e}^{-2\pi\mathrm{i}\nu\theta_p}\langle p|\psi\rangle.
\end{aligned}
\tag{3.49}
$$

With arbitrary $\langle p|$ one thus has

$$
\begin{aligned}
\hat{T}^\dagger(0, \nu\, M_p)\, |\psi\rangle \;&=\; \mathrm{e}^{-2\pi\mathrm{i}\nu\theta_p}|\psi\rangle, \tag{3.50}\\
\Rightarrow\qquad \hat{T}(0, \nu M_p)\, |\psi\rangle \;&=\; \mathrm{e}^{2\pi\mathrm{i}\nu\theta_p}|\psi\rangle. \tag{3.51}
\end{aligned}
$$

Quasi-periodicity conditions in q as well as in p direction at the same time influence the allowed values which can be assigned to the effective Planck constant. In order to

demonstrate this, one considers

$$
\begin{aligned}
\mathrm{e}^{-2\pi\mathrm{i}\theta_q}\,\mathrm{e}^{2\pi\mathrm{i}\theta_p}|\psi\rangle \quad &\overset{(3.51)}{=} \quad \mathrm{e}^{-2\pi\mathrm{i}\theta_q}\,\hat{T}(0, M_p)|\psi\rangle \\
&= \quad \hat{T}(0, M_p)\,\mathrm{e}^{-2\pi\mathrm{i}\theta_q}\,|\psi\rangle \\
&\overset{(3.46)}{=} \quad \hat{T}(0, M_p)\,\hat{T}(M_q, 0)|\psi\rangle \\
&\overset{(3.31),(3.33)}{=} \quad \mathrm{e}^{\frac{\mathrm{i}}{\hbar_{\mathrm{eff}}}M_q M_p}\,\hat{T}(M_q, 0)\,\hat{T}(0, M_p)|\psi\rangle \\
&\overset{(3.51)}{=} \quad \mathrm{e}^{\frac{2\pi\mathrm{i}}{\hbar_{\mathrm{eff}}}M_q M_p}\,\hat{T}(M_q, 0)\,\mathrm{e}^{2\pi\mathrm{i}\theta_p}|\psi\rangle \\
&= \quad \mathrm{e}^{2\pi\mathrm{i}\frac{M_q M_p}{\hbar_{\mathrm{eff}}}}\,\mathrm{e}^{2\pi\mathrm{i}\theta_p}\,\hat{T}(M_q, 0)|\psi\rangle \\
&= \quad \mathrm{e}^{2\pi\mathrm{i}\frac{M_q M_p}{\hbar_{\mathrm{eff}}}}\,\mathrm{e}^{2\pi\mathrm{i}\theta_p}\,\mathrm{e}^{-\mathrm{i}2\pi\theta_q}|\psi\rangle \\
&\overset{(3.46)}{=} \quad \mathrm{e}^{2\pi\mathrm{i}\frac{M_q M_p}{\hbar_{\mathrm{eff}}}}\,\mathrm{e}^{-\mathrm{i}2\pi\theta_q}\,\mathrm{e}^{2\pi\mathrm{i}\theta_p}|\psi\rangle.
\end{aligned}
\tag{3.52}
$$

Since h_{eff} is a positive quantity, one obtains

$$
\frac{M_q M_p}{h_{\mathrm{eff}}} \;=\; N \quad \text{with} \ \ N \in \mathbb{N} \tag{3.53}
$$

from the comparison of both sides of equation (3.52). The effective Planck constant of a system, which is quasi-periodic in q and in p direction, can therefore have the values

$$
h_{\mathrm{eff}} \;=\; \frac{M_q M_p}{N}, \tag{3.54}
$$

only. An interesting question is that for the consequence of quasi-periodicity in q direction. Using equation (3.45), one realizes

$$
\begin{aligned}
\left\langle p \middle| \hat{T}^\dagger(M_q, 0) \middle| \psi \right\rangle \quad &= \quad \left\langle \hat{T}(M_q, 0)\,p \middle| \psi \right\rangle \\
&= \quad \left\langle \mathrm{e}^{-\frac{\mathrm{i}}{\hbar_{\mathrm{eff}}}M_q \hat{p}}\,p \middle| \psi \right\rangle \\
&= \quad \left\langle \mathrm{e}^{-\frac{\mathrm{i}}{\hbar_{\mathrm{eff}}}M_q p}\,p \middle| \psi \right\rangle \\
&= \quad \mathrm{e}^{\frac{\mathrm{i}}{\hbar_{\mathrm{eff}}}M_q p}\,\langle p|\psi\rangle \tag{3.55} \\
&\overset{(3.45)}{=} \quad \mathrm{e}^{2\pi\mathrm{i}\theta_q}\,\langle p|\psi\rangle. \tag{3.56}
\end{aligned}
$$

From (3.55) and (3.56) one deduces

$$
\mathrm{e}^{\frac{\mathrm{i}}{\hbar_{\mathrm{eff}}}M_q p} \;=\; \mathrm{e}^{2\pi\mathrm{i}\theta_q}\,\mathrm{e}^{2\pi\mathrm{i}m} \quad \text{with} \ \ m \in \mathbb{Z}. \tag{3.57}
$$

The insertion of the allowed values of h_{eff}, equation (3.54), yields the allowed values of

the momentum variable

$$p \quad \rightarrow \quad p_m \;=\; \frac{M_p}{N}(m + \theta_q) \quad \text{with} \quad m \in \mathbb{Z}_N, \tag{3.58}$$

with the definition $\mathbb{Z}_N := \{0, 1, ..., N - 1\}$. Quasi-periodicity in q direction therefore requires a quantization of the p variable. It remains the investigation of the consequence of quasi-periodicity in p direction. With (3.50) one finds

$$
\begin{aligned}
\left\langle q \middle| \hat{T}^\dagger(0, M_p) \middle| \psi \right\rangle \;&=\; \left\langle \hat{T}(0, M_p)\, q \middle| \psi \right\rangle \\
&=\; \left\langle \mathrm{e}^{\frac{\mathrm{i}}{\hbar_{\text{eff}}} M_p \hat{q}}\, q \middle| \psi \right\rangle \\
&=\; \left\langle \mathrm{e}^{\frac{\mathrm{i}}{\hbar_{\text{eff}}} M_p q}\, q \middle| \psi \right\rangle \\
&=\; \mathrm{e}^{-\frac{\mathrm{i}}{\hbar} M_p q} \left\langle q | \psi \right\rangle \tag{3.59} \\
&\overset{(3.50)}{=}\; \mathrm{e}^{-2\pi \mathrm{i} \theta_p} \left\langle q | \psi \right\rangle. \tag{3.60}
\end{aligned}
$$

and concludes

$$\mathrm{e}^{\frac{\mathrm{i}}{\hbar} M_p q} \;=\; \mathrm{e}^{2\pi \mathrm{i} \theta_p}\, \mathrm{e}^{2\pi \mathrm{i} n} \quad \text{with} \quad n \in \mathbb{Z}, \tag{3.61}$$

from (3.59) and (3.60). Consequently,

$$q \quad \rightarrow \quad q_n \;=\; \frac{M_q}{N}(n + \theta_p) \qquad \text{with} \quad n \in \mathbb{Z}_N, \tag{3.62}$$

must hold. The quasi-periodicity in p direction requires thus a quantization of the q variable.

From the formulae (3.58) and (3.62) immediately follows that the parameter N is equal to the size of the Hilbert space. Equations (3.58) and (3.62) are discrete complete sets of states in momentum and position representation, respectively. These two representations are connected by a discrete Fourier transform $\mathcal{F}$

$$|p_m\rangle \;=\; \sum_{j=0}^{N-1} \left(\mathcal{F}^{-1}\right)_{j,m} |q_j\rangle \;=\; \frac{1}{\sqrt{N}} \sum_{j=0}^{N-1} \mathrm{e}^{\frac{2\pi \mathrm{i}}{N}(j + \theta_p)(m + \theta_q)} |q_j\rangle. \tag{3.63}$$

One therefore has the scalar product

$$
\begin{aligned}
\langle q_k | p_m \rangle \;&=\; \frac{1}{\sqrt{N}}\, \mathrm{e}^{\mathrm{i} \frac{p_m q_k}{\hbar_{\text{eff}}}} \tag{3.64} \\
&=\; \frac{1}{\sqrt{N}}\, \mathrm{e}^{\frac{2\pi \mathrm{i}}{N}(k + \theta_p)(m + \theta_q)}. \tag{3.65}
\end{aligned}
$$

Finally, we remark that the choice of the signs in the exponential functions of equations (3.40) and (3.41) is such that the Bloch phases θ_q and θ_p appear with positive signs in equations (3.58) and (3.62).

Given an allowed value for the effective Planck constant h_{eff}, one knows the allowed position (3.62) and momentum (3.58) values. By means of them it is possible to evaluate the time evolution operator of a periodically kicked system, equation (3.25), e.g. in position representation.

3.2.3 Time evolution operator of periodically kicked systems in position representation

The unitary time evolution operator over one kicking period of periodically kicked systems, equation (3.25), reads

$$
\left\langle q_k \left| \hat{U} \right| q_l \right\rangle \;=\; \sum_{m=0}^{N-1}\sum_{n=0}^{N-1} \left\langle q_k \left| e^{-\frac{2\pi i}{h_{\text{eff}}}V(\tilde{q})} \right| q_m \right\rangle \left\langle q_m \left| e^{-\frac{2\pi i}{h_{\text{eff}}}T(\tilde{p})} \right| p_n \right\rangle \left\langle p_n \middle| q_l \right\rangle
$$

$$
\overset{(3.65)}{=}\; \frac{1}{N}\, e^{-\frac{2\pi i}{h_{\text{eff}}}V(q_k)} \sum_{m=0}^{N-1} e^{\frac{2\pi i}{N}(k-l)(m+\theta_q)}\, e^{-\frac{2\pi i}{h_{\text{eff}}}T(p_m)} \tag{3.66}
$$

in position representation.

Instead of considering the torus $[0,\,M_q]\times[0,\,M_p]$, with $M_q\in\mathbb{N}$ and $M_p\in\mathbb{N}$, one can introduce shifts in q and p direction, $q_{\min}$ and $p_{\min}$, which yield the torus $[q_{\min},\,M_q+q_{\min}]\times[p_{\min},\,M_p+p_{\min}]$. This modifies the quantized positions (3.62) and momenta (3.58) slightly,

$$
q_n \;=\; \frac{M_q}{N}(n+\theta_p)+q_{\min} \qquad \text{with } n\in\mathbb{Z}_N, \tag{3.67}
$$

$$
p_m \;=\; \frac{M_p}{N}(m+\theta_q)+p_{\min} \qquad \text{with } m\in\mathbb{Z}_N, \tag{3.68}
$$

as well as the time-evolution operator (3.66)

$$
\left\langle q_k \left| \hat{U} \right| q_l \right\rangle \;=\; \frac{1}{N}\, e^{-\frac{2\pi i}{h_{\text{eff}}}V(q_k)} \sum_{m=0}^{N-1} e^{\frac{2\pi i}{N}(k-l)(m+\theta_q)}\, e^{\frac{2\pi i}{M_p}(k-l)p_{\min}}\, e^{-\frac{2\pi i}{h_{\text{eff}}}T(p_m)}. \tag{3.69}
$$

One could have introduced the shifts $q_{\min}$ and $p_{\min}$ from the very beginning in section 3.2.2. This might, however, have caused a distraction from the crucial contents.

Irrespective of the representation, the basic task is to solve the eigenequation

$$\hat{U} \left| \psi_n \right\rangle = z_n \left| \psi_n \right\rangle , \tag{3.70}$$

where $\left| \psi_n \right\rangle$ is an eigenstate of the time evolution operator $\hat{U}$ with the eigenvalue z_n. Since $\hat{U}$ is unitary, its eigenvalues must lie on the unit circle

$$\hat{U} \left| \psi_n \right\rangle = \mathrm{e}^{\mathrm{i}\varphi_n} \left| \psi_n \right\rangle , \tag{3.71}$$

with the so-called quasi-energies φ_n.

The semiclassical eigenfunction hypothesis [57–59] states that the phase space representation of a quantum mechanical eigenstate of the time evolution operator $\hat{U}$ concentrates on those phase space regions in the semiclassical limit which a typical classical orbit explores in the long-time limit. As is discussed in section 3.1, such an orbit is either regular or chaotic. In order to visualize eigenstates of $\hat{U}$ and in order to compare them with the structures of the phase space of the corresponding classical map, one needs a phase space representation. The concept of the Husimi function is appropriate and will therefore be considered in the next paragraph.

3.3 Husimi representation

The Husimi function or the Husimi representation $H_{\left| \psi \right\rangle}(q, p)$ enables a phase space representation of the state $\left| \psi \right\rangle$. It is given by the square of the modulus of its projection onto a coherent state $\left| C_{q,p} \right\rangle$ centered at the phase space point (q, p) on the considered torus [60]

$$
\begin{aligned}
H_{\left| \psi \right\rangle}(q, p) \quad &:= \quad \left| \left\langle C_{q,p} \,\middle|\, \psi \right\rangle \right|^2 \\
&= \quad \left| \sum_{j=0}^{N-1} \langle C_{q,p} | q_j \rangle \langle q_j | \psi \rangle \right|^2 \\
&= \quad \left| \sum_{j=0}^{N-1} (2N)^{\frac{1}{4}} \mathrm{e}^{-\pi N(q^2 - \mathrm{i}pq)} \, \mathrm{e}^{\pi N(-q_j^2 + 2(q - \mathrm{i}p)q_j)} \right. \\
&\qquad\qquad \left. \cdot \, \vartheta_3 \left(\mathrm{i}\pi N \left(q_j - \frac{\mathrm{i}\theta_q}{N} - q + \mathrm{i}p \right) \middle| \mathrm{i}N \right) \psi(q_j) \right|^2 .
\end{aligned}
\tag{3.72}
$$

The function $\vartheta_3(Z|\tau)$ is the Jacobi-Theta function, which is defined by

$$\vartheta_3(Z|\tau) \quad := \sum_{n \in \mathbb{Z}} \mathrm{e}^{\mathrm{i}\pi\tau n^2 + \mathrm{i}2nZ} \qquad \text{with} \quad Z, \tau \in \mathbb{C} \ \text{ and } \ \mathrm{Im}(\tau) > 0. \tag{3.73}$$

It represents one possibility to ensure the periodic boundary conditions on the torus.

In order to determine the time evolution operator $\hat{U}$ over one kicking period, equation (3.69), for the standard map, one has to insert $T(p) = p^2/2$ and $V(q) = -\kappa/(2\pi)^2 \cos(2\pi q)$ according to equation (3.19). As an example figure 3.3 shows Husimi functions of two eigenstates of the time evolution operator of the quantum version standard map (3.19) for $\kappa = 3.0$. The first Husimi function concentrates on an invariant torus of the regular island (a) and the other one lives in the chaotic sea (b). The corresponding classical phase space, figure 3.2(d), is plotted as background for the purpose of comparison. Both illustrated Husimi functions are in agreement with the statement of the semiclassical eigenfunction hypothesis.
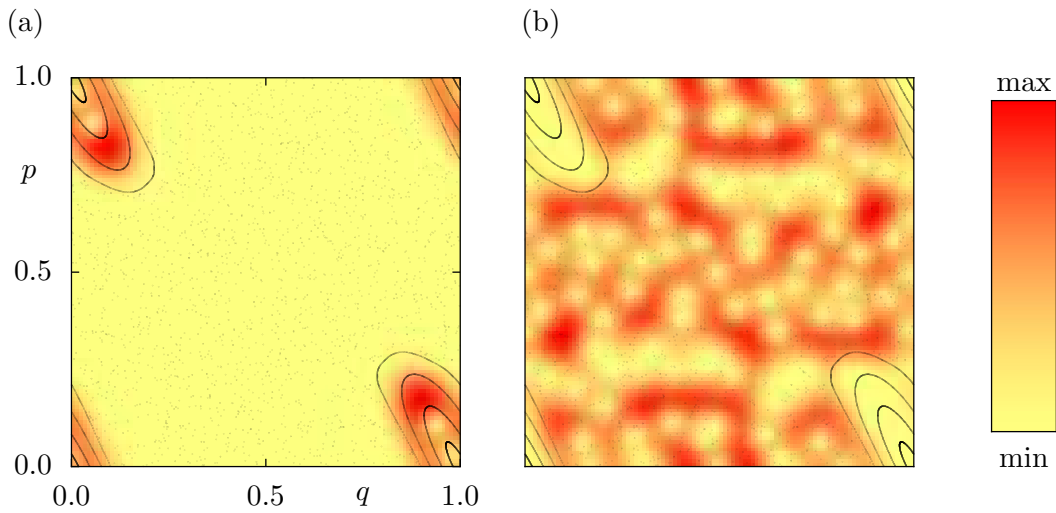
Figure 3.3: Husimi functions of two eigenstates of the time evolution operator of the quantum version standard map for $\kappa = 3.0$ as perturbation parameter. (a) Concentration on an invariant torus of the regular island. (b) Localization in the chaotic sea. The classical phase space, which has already been shown in figure 3.2(d), is plotted as background.

3.4 Example map P_{ex}

The periodically kicked system which will be considered in the following was first introduced in reference [61]. For $q \in [-1/2, M_q - 1/2]$ and $p \in [-1/2, 1/2]$ with $M_q \in \mathbb{N}$ one starts with the piecewise defined linear derivatives of the kinetic and the potential energy function

$$t'(p) \;=\; \frac{s}{4} + \big(A - s\,(p - \lfloor p + 1/2\rfloor)\big)\,\mathrm{sign}\,(p - \lfloor p + 1/2\rfloor)\,, \tag{3.74}$$

$$v'(q) \;=\; -rq - (1 - r)\lfloor q + 1/2\rfloor, \tag{3.75}$$

where $\lfloor\cdot\rfloor$ denotes the floor function. The system-specific parameters $r \in \mathbb{R}$ and $s \in \mathbb{R}$ determine the properties of the regular and the chaotic phase space components. The influence of the parameter $A \in \mathbb{Z}$ will be explained in section 3.4.2. Using a Gaussian smoothing

$$G_\varepsilon(z) := \frac{1}{\sqrt{2\pi}\varepsilon}\, \mathrm{e}^{-\frac{z^2}{2\varepsilon^2}}, \tag{3.76}$$

where ε is a positive real parameter, one obtains the analytical functions

$$T'(p) \;=\; \int\limits_{-\infty}^{\infty} \mathrm{d}z\, t'(p) G_\varepsilon(p - z), \tag{3.77}$$

$$V'(q) \;=\; \int\limits_{-\infty}^{\infty} \mathrm{d}z\, v'(q) G_\varepsilon(q - z). \tag{3.78}$$

By means of equations (3.77) and (3.78) one can, similar to definition (3.11), set up the classical map P_{ex} defined on the torus $[-1/2, M_q - 1/2] \times [-1/2, 1/2]$. Apart from a few exceptions, we will consider the "standard" parameters $A = 1$, $r = 0.65$, $s = 2.0$, and $\varepsilon = 0.015$ for plots and numerical investigations in the remaining part of this thesis. The phase space of this map extends over M_q unit cells in q direction, which will be labelled from 0 by $M_q - 1$. It is illustrated in figure 3.4. Figure 3.5(a) shows its restriction to $M_q = 3$ unit cells. The corresponding functions $t'(p)$ and $T'(p)$ are shown in part (b), and $v'(q)$ and $V'(q)$ are presented in part (c). For any integer k the smoothed functions possess the periodicity properties

$$T'(p + k) \;=\; T'(p), \tag{3.79}$$

$$V'(q + k) \;=\; V'(q) - k. \tag{3.80}$$
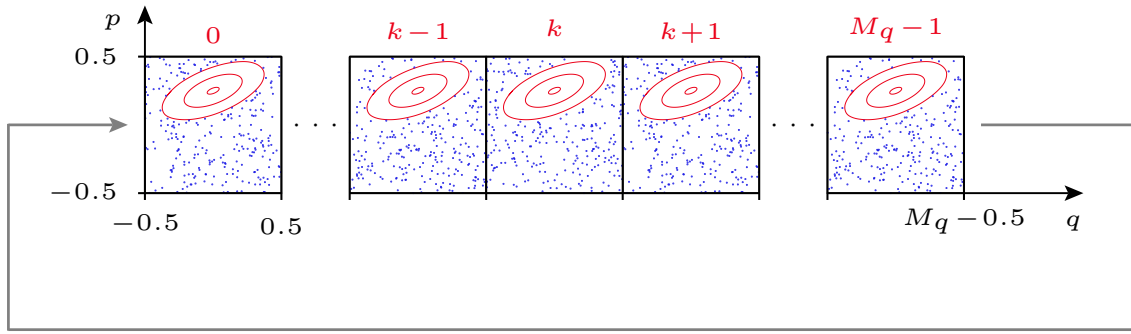
Figure 3.4: Phase space of the example map defined on the torus $[-1/2, M_q - 1/2] \times [-1/2, 1/2]$, where $q = -1/2$ is identified with $q = M_q - 1/2$, as well as $p = -1/2$ with $p = 1/2$. Red labels denote the numbers of the M_q unit cells. As parameters $A = 1.0$, $r = 0.65$, $s = 2.0$, and $\varepsilon = 0.015$ are used.
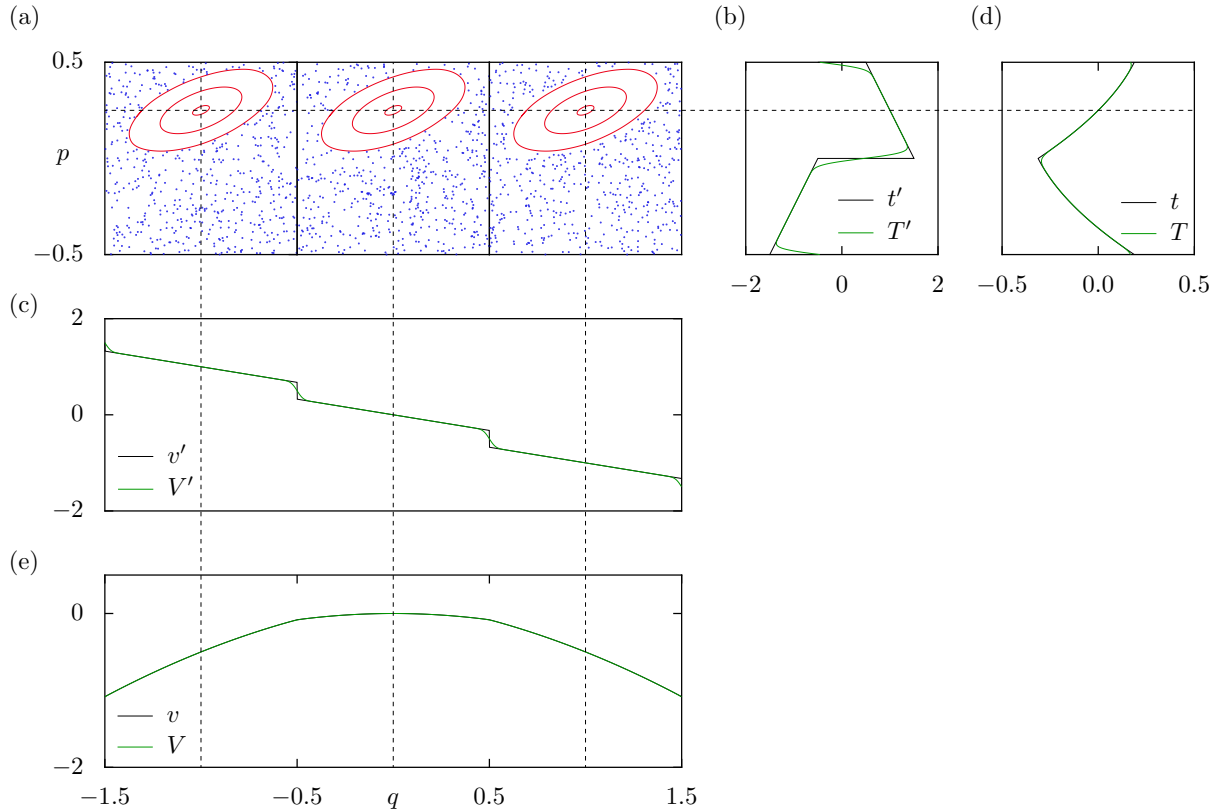
Figure 3.5: (a) Phase space of the example map for three unit cells ($M_q = 3$). (b) Discontinuous (3.74) and smoothed derivative (3.77) of the kinetic energy. (c) Discontinuous (3.75) and smoothed derivative (3.78) of the potential energy. (d) and (e) illustrate the primitive functions of (b) and (c). The integration constants are chosen such that $V(q = 0) = 0$ and $T(p = 1/4) = 0$. In order to illustrate the symmetry of the function $V(q)$ with respect to $q = 0$, the q domain is chosen accordingly as $[-1.5, 1.5]$.

In order to write down explicit expressions for the kinetic and the potential energy function and their derivatives, one starts with the definition of the error function,

$$\text{erf}(x) = \frac{2}{\sqrt{\pi}} \int_0^x \mathrm{d}t \, \mathrm{e}^{-t^2}, \tag{3.81}$$

and uses it to define

$$\text{Erf}_\varepsilon(z) := \frac{1}{2} \left(1 + \text{erf}\left(\frac{z}{\sqrt{2}\varepsilon} \right) \right), \tag{3.82}$$

with $\lim_{\varepsilon \to 0} \text{Erf}_\varepsilon(z) = \theta(z)$, where $\theta(z)$ stands for the Heaviside step function. Now one defines

$$\hat{q} := \left(q + \frac{1}{2} \right) \bmod 1 - \frac{1}{2} \quad \in \left[-\frac{1}{2}, \frac{1}{2} \right], \tag{3.83}$$

$$\hat{m} := q - \hat{q} \in \mathbb{Z}, \tag{3.84}$$

where $\hat{m}$ is a unit cell label. With these definitions one obtains

$$T'(p) = \begin{cases} \frac{A}{2} - \tilde{T}'\left(p + \frac{1}{2}\right) & \text{for} & -\frac{1}{2} \le p < -\frac{1}{4} \\ \tilde{T}'(p) & \text{for} & -\frac{1}{4} \le p < \frac{1}{4} \\ \frac{A}{2} - \tilde{T}'\left(p - \frac{1}{2}\right) & \text{for} & \frac{1}{4} \le p < \frac{1}{2} \end{cases} \tag{3.85}$$

after some algebraic steps with

$$\tilde{T}'(p) = \frac{s}{4} - (A - sp)\left[1 - 2\text{Erf}_\varepsilon(p)\right] - 2As\varepsilon^2 G_\varepsilon(p), \tag{3.86}$$

and

$$V'(q) = -\left\{ \hat{m} + r\hat{q} + (1 - r)\,\text{sign}(\hat{q})\,\text{Erf}_\varepsilon\left(|\hat{q}| - \frac{1}{2} \right) \right\}. \tag{3.87}$$

Whereas the derivatives (3.85) and (3.87) are required for the classical example map P_{ex} on the torus $q \in [-1/2, M_q - 1/2]$ and $p \in [-1/2, 1/2]$, one needs the functions $T(p)$ and $V(q)$ for the quantum map according to equation (3.25). The integration of equations (3.85) and (3.87) yields

$$T(p) = \begin{cases} \frac{A}{2} - \tilde{T}\left(p + \frac{1}{2}\right) + c_T & \text{for} & -\frac{1}{2} \le p < -\frac{1}{4} \\ \tilde{T}(p) + c_T & \text{for} & -\frac{1}{4} \le p < \frac{1}{4} \\ \frac{A}{2} - \tilde{T}\left(p - \frac{1}{2}\right) + c_T & \text{for} & \frac{1}{4} \le p < \frac{1}{2} \end{cases} \tag{3.88}$$

with

$$
\begin{aligned}
\tilde{T}(p) \;=\; & -\left(A - \frac{s}{4}\right)p + \frac{1}{2}\,sp^2 + (2A - sp)\left[p\,\mathrm{Erf}_\varepsilon(p) + \varepsilon^2 G_\varepsilon(p)\right] \\
& -As\varepsilon^2\left[\mathrm{Erf}_\varepsilon(p) - \frac{1}{2}\right]
\end{aligned}
\tag{3.89}
$$

for the kinetic energy and

$$
\begin{aligned}
V(q) \;=\; c_V - \Bigg\{ & \frac{1}{2}\hat{m}^2 + \hat{m}\hat{q} + \frac{1}{2}\,r\hat{q}^2 \\
& + (1-r)\left[\left(|\hat{q}| - \frac{1}{2}\right)\,\mathrm{Erf}_\varepsilon\left(|\hat{q}| - \frac{1}{2}\right) + \varepsilon^2 G_\varepsilon\left(|\hat{q}| - \frac{1}{2}\right)\right] \Bigg\}
\end{aligned}
\tag{3.90}
$$

for the potential energy. The possible integration constants are chosen as $c_T = -s/32 - A/4$ and $c_V = 0$ which leads to $T(p = 1/4) = 0$ and $V(q = 0) = 0$. Figure 3.5(d) shows the function $T(p)$ in comparison with the discontinuous kinetic energy $t(p)$. Part (e) of the same figure compares $V(p)$ with $v(q)$. For any integer k one has the following periodicity properties

$$
\begin{aligned}
T(p + k) \;&=\; T(p), & (3.91) \\
V(q + k) \;&=\; V(q) - kq - \frac{1}{2}k^2. & (3.92)
\end{aligned}
$$

Each of the M_q phase space unit cells contains one large almost resonance-free regular island with center $(q_c, p_c) = (k, 1/4)$, $0 \le k \le M_q - 1$, embedded in a homogeneous chaotic sea. These islands are equal and have the relative area $A_{\mathrm{reg}} \approx 0.215$. Figure 3.6 shows the phase space of one unit cell. The magnification gives an image of the hierarchical region of the regular island. One clearly sees that it is very narrow, i.e. that the boundary of the island is rather sharp with only very small resonance islands due to non-linear perturbations.

The regular islands of the example map are by construction elliptic. An elliptic island possesses the property that the rotation numbers of all of its invariant tori are constant. The fine structure in the hierarchical region should, however, influence the rotation number. This influence will be investigated in the next paragraph.
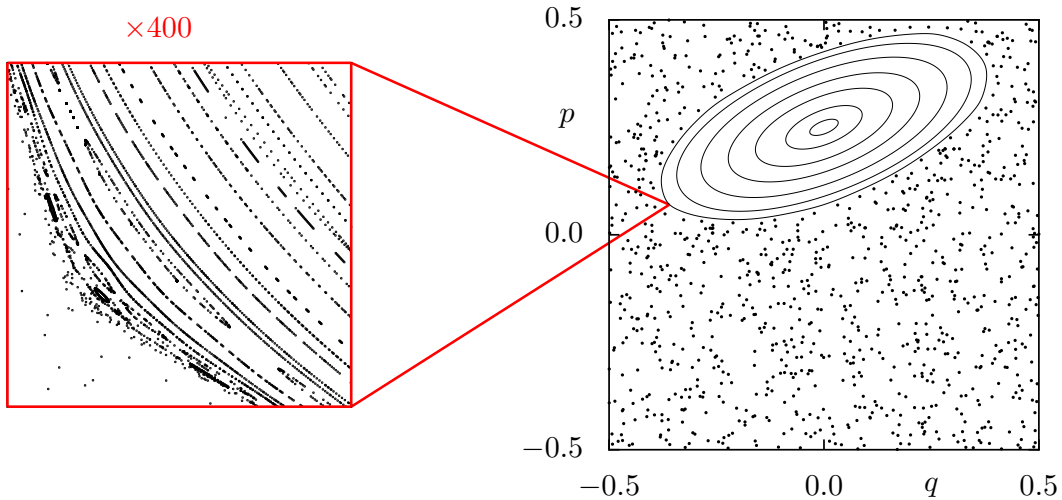
Figure 3.6: Phase space of one unit cell. The magnification shows the very narrow hierarchical region of the large regular island.

3.4.1 Rotation number

Since all of the M_q regular islands are equal, it is sufficient to investigate the rotation number R of the invariant tori of one of them, e.g. the one around the elliptic fixed point $(q_c, p_c) = (0, 1/4)$. Figure 3.7(a) shows R of the invariant tori as a function of the area enclosed by them. It was determined numerically using the frequency map analysis algorithm [62, 63]. We see that R starts to vary close to the border of the regular island. This reflects the immediate influence of the smoothing of the piecewise linear functions $t'(p)$ and $v'(q)$ with a Gaussian. The smoothing becomes less important the more the center of the regular island is approached. In the vicinity of the elliptic fixed point in the island center the dynamics of the example map can be approximated by the linearized map, which is given by the monodromy matrix evaluated at $(q_c, p_c) = (0, 1/4)$

$$M(q_c, p_c) \;\; = \;\; \begin{pmatrix} 1 & -s \\ r & 1 - rs \end{pmatrix}. \tag{3.93}$$

According to equation (3.16) the analytical value of the rotation number in the center of the island reads

$$R_c \;\; = \;\; \frac{1}{\pi} \arcsin \left(\frac{\sqrt{rs}}{2} \right) \approx 0.193091 \,. \tag{3.94}$$

Figure 3.7(b) shows the modulus of the difference of the numerically determined rotation number and the reference value (3.94) in the center of the island. This difference plot reveals the increasing influence of the smoothing close to the border of the regular island
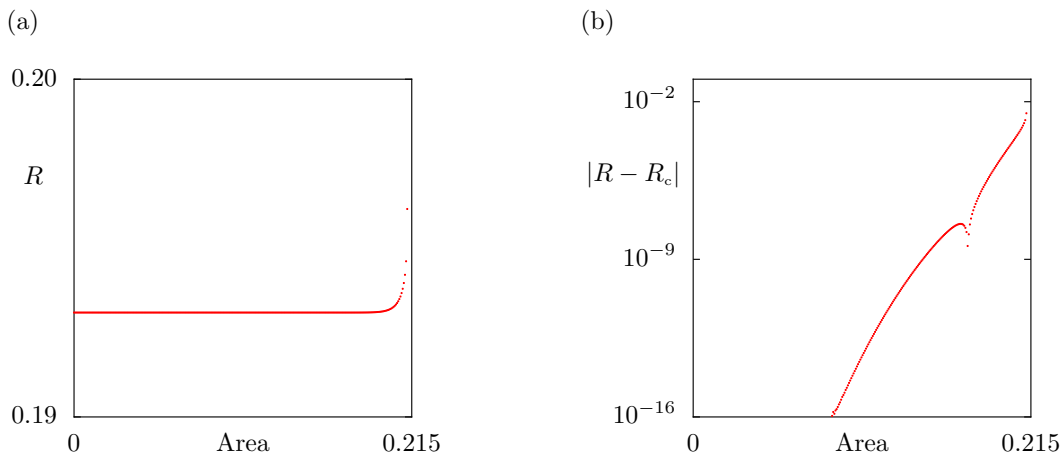
Figure 3.7: (a) Rotation number of the regular island as a function of the area enclosed by the invariant tori. (b) Modulus of the difference of figure (a) and the analytically determined value of the rotation number in the center of the island (3.94) in a logarithmic-linear plot.

much better than figure 3.7(a). We also notice a local "collapse" in the difference plot. We assumed at first that it is due to a small resonance island chain. The rotation number is, however, constant while passing a resonance island chain [62,63], so that this assumption is obviously wrong. As a zoom into the phase space of the classical map at the corresponding elliptic invariant tori does not yield a reasonable explanation, we leave the reason for this observation as an open question.

3.4.2 Regular and chaotic transport properties

The considered map is defined on the torus $[-1/2, M_q - 1/2] \times [-1/2, 1/2]$. It possesses the property that a point on an invariant torus of the regular island in unit cell k, which encloses a certain area, is mapped to the invariant torus of the regular island in unit cell $k + A$, that encloses the same area. The parameter $A \in \mathbb{Z}$ in the definition of the discontinuous kinetic energy (3.74) is thus a shift parameter. This reflects a regular transport to the right with velocity $v_{\mathrm{reg}} = A$ for positive A. A further property of the map is then that the chaotic sea possesses a mean drift to the left with the velocity $v_{\mathrm{ch}} < 0$. The green arrows in figure 3.8 illustrate the regular transport, while the mean chaotic drift is indicated by a blue arrow. According to the considerations in reference [64], the chaotic drift velocity must fulfill

$$
\begin{aligned}
A_{\mathrm{ch}} v_{\mathrm{ch}} + A_{\mathrm{reg}} v_{\mathrm{reg}} &= 0 \\
\Leftrightarrow \qquad v_{\mathrm{ch}} &= -\frac{A_{\mathrm{reg}}}{1 - A_{\mathrm{reg}}} v_{\mathrm{reg}}.
\end{aligned}
\tag{3.95}
$$

Here A_{reg} and $A_{\text{ch}} = 1 - A_{\text{reg}}$ are the relative areas of the regular and the chaotic phase space components. For the used parameter set one has $A_{\text{reg}} \approx 0.215$ per regular island and therefore $v_{\text{ch}} \approx -0.274A$. Due to the spatial periodicity after M_q unit cells in q direction, points within the regular island of unit cell $M_q - 1$ are mapped to the island of unit cell 0. The connection of the last with the first unit cell is indicated by the grey arrow in figure 3.4. We will later see that the regular and the chaotic transport properties of this map allow for the determination of decay or dynamical tunneling rates of regular states from a regular island to the chaotic sea by means of the wave packet dynamics method.
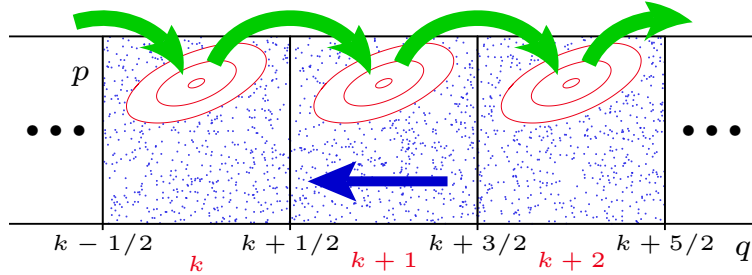
Figure 3.8: Shown are three of the M_q phase space unit cells of the system. For $A = 1$ a point within the red coloured regular island in cell k is mapped to the island in cell $k + 1$ (green arrows). The chaotic sea has a mean drift to the left (blue arrow). Due to the periodic boundary conditions, the last cell with index $M_q - 1$ is connected to the first one with index 0. The black q labels denote position coordinates, whereas the red labels stand for unit cell numbers.

3.4.3 Quantum map and constraints on the Bloch phases θ_q and θ_p

The position space time evolution operator over one kicking period of the corresponding quantum map can be determined according to equation (3.69). Using equations (3.67) and (3.68) with $M_q \geq 1$ and $M_p = 1$ and $q_{\min} = p_{\min} = -1/2$ the quantized positions and momenta are

$$q_n = \frac{M_q}{N}(n + \theta_p) - \frac{1}{2} \qquad \text{with} \qquad n \in \mathbb{Z}_N, \qquad (3.96)$$

$$p_m = \frac{1}{N}(m + \theta_q) - \frac{1}{2} \qquad \text{with} \qquad m \in \mathbb{Z}_N. \qquad (3.97)$$

Furthermore, we have $h_{\text{eff}} = M_q/N$, which follows from equation (3.54). It remains the question, which values can be assigned to the Bloch phases θ_q and θ_p. To answer this, we write down the time evolution operator in position representation

$$\left\langle q_k | \hat{U} | q_l \right\rangle = \frac{1}{N} \, e^{-iV(q_k)/\hbar_{\text{eff}}} \sum_{m=0}^{N-1} e^{\frac{2\pi i}{N}(k-l)(m+\theta_q)} \, e^{\frac{2\pi i}{M_p}(k-l)p_{\min}} \, e^{-iT(p_m)/\hbar_{\text{eff}}}. \qquad (3.98)$$

In order to keep the quasi-periodicity in q direction, the relation

$$\langle q_k|\hat{U}|q_l\rangle \overset{!}{=} \langle q_{k+N}|\hat{U}|q_{l+N}\rangle \tag{3.99}$$

must hold, with

$$q_{k+N} = q_k + M_q. \tag{3.100}$$

The potential energy function (3.90) can be separated into a unit cell independent part $\mathcal{V}(\hat{q}_k)$ and a sum of terms depending on the index of the unit cell $\hat{m}$

$$V(q_k) = -\frac{1}{2}\hat{m}^2 - \hat{m}\hat{q}_k + \mathcal{V}(\hat{q}_k). \tag{3.101}$$

The evaluation of the potential energy function at q_{k+N} yields

$$\begin{aligned}
V(q_{k+N}) = V(q_k + M_q) &= -\frac{1}{2}(\hat{m} + M_q)^2 - \hat{m}\hat{q}_k - M_q\hat{q}_k + \mathcal{V}(\hat{q}_k) \\
&= -\hat{m}M_q - \frac{1}{2}M_q^2 - M_q\hat{q}_k + V(q_k) \\
&\overset{(3.84)}{=} -\frac{1}{2}M_q^2 - M_q q_k + V(q_k).
\end{aligned} \tag{3.102}$$

From (3.98) we find after inserting (3.102) and (3.96)

$$\begin{aligned}
\hat{U}_{k+N,l+N} &= \hat{U}_{k,l}\, \mathrm{e}^{\frac{\mathrm{i}}{2\hbar_{\mathrm{eff}}}M_q^2}\, \mathrm{e}^{\frac{\mathrm{i}}{\hbar_{\mathrm{eff}}}M_q q_k} \tag{3.103} \\
&= \hat{U}_{k,l}\, \mathrm{e}^{\pi\mathrm{i}NM_q}\, \underbrace{\mathrm{e}^{2\pi\mathrm{i}M_q k}}_{=1}\, \mathrm{e}^{2\pi\mathrm{i}M_q\theta_p}\, \mathrm{e}^{-\pi\mathrm{i}N}. \tag{3.104}
\end{aligned}$$

In order to fulfill condition (3.99), we deduce

$$\theta_p = \begin{cases} \frac{2\nu+1}{2M_q} & \text{for } N \text{ odd and } M_q \text{ even} \\ \frac{\nu}{M_q} & \text{otherwise} \end{cases} \tag{3.105}$$

with $\nu \in \mathbb{Z}_{M_q}$, since $\theta_p \in [0;1)$. The phase θ_q does not appear in this consideration and can therefore be chosen arbitrarily within the interval $[0;1)$. An alternative consideration of the time evolution operator in momentum representation yields the same result.

4 Semiclassical quantization of regular islands of quantum maps

Let us now consider a periodically kicked system in 1D on a torus. Stroboscopically the classical dynamics is described by a map. For the corresponding quantum map represented by the time evolution operator $\hat{U}$ over one kicking period we have the eigenvalue equation

$$\hat{U}|\psi_n\rangle = \mathrm{e}^{\mathrm{i}\varphi_n}|\psi_n\rangle, \tag{4.1}$$

where the index n distinguishes different eigenstates $|\psi_n\rangle$ and quasi-energies φ_n. For a given size $N \in \mathbb{N}$ of the Hilbert space we have $n \in \mathbb{Z}_N$ and the value of the effective Planck constant h_{eff} is fixed by equation (3.54).

We want to consider a regular island with negligible embedded resonances. The Husimi functions of the eigenstates of $\hat{U}$ show in the semiclassical limit localization either in the chaotic sea or on certain closed curves in the regular island according to the semiclassical eigenfunction hypothesis [57–59]. In the following we will concentrate on the regular eigenstates of $\hat{U}$. The closed curve $\mathcal{C}_m$, on which the Husimi function of the mth regular eigenstate localizes, encloses an action determined by the quantization condition [65]

$$\oint_{\mathcal{C}_m} \mathrm{d}q\, p(q) \;=\; \left(m + \frac{1}{2}\right) h_{\mathrm{eff}}. \tag{4.2}$$

The largest possible quantum number m_{max} at a given value of the effective Planck constant is governed by the size A_{reg} of the regular island

$$m_{\mathrm{max}} \;=\; \left\lfloor \frac{A_{\mathrm{reg}}}{h_{\mathrm{eff}}} - \frac{1}{2} \right\rfloor. \tag{4.3}$$

In reference [66] it is demonstrated that the WKB-type quantization rule (4.2) is not a sufficient condition. It is shown that

$$\gamma_m < \frac{1}{\tau_H} \tag{4.4}$$

is a second necessary criterion for the existence of a regular eigenstate whose Husimi function localizes on the mth quantizing torus $\mathcal{C}_m$. Here $\tau_H = h_{\text{eff}}/\Delta_{\text{ch}}$ is the Heisenberg time of the chaotic sea with the mean level spacing Δ_{ch}, and γ_m is the decay rate of the mth regular state if the chaotic sea were infinite.

Provided that m is an allowed quantum number according to conditions (4.2) and (4.4), the regular state $|\psi_m\rangle$ and its quasi-energy φ_m are the central quantities. A semiclassical quantization of regular islands consists therefore of two steps:

1.) Determination of a semiclassical approximation $|\psi_m^{\text{sc}}\rangle$ of the regular eigenstate $|\psi_m\rangle$.

2.) Derivation of a semiclassical approximation φ_m^{sc} of the corresponding quasi-energy φ_m.

The pair $(|\psi_m^{\text{sc}}\rangle, \varphi_m^{\text{sc}})$ is called quasimode [67].

The semiclassical quantization of regular islands of quantum maps of periodically kicked 1D systems, whose phase space is equal to $\mathbb{R}^2$, is studied in reference [65]. In section 4.1 we present a similar approach, which also accounts for a regular transport between equal regular islands in $\mathbb{R}^2$. It turns out that the result for the semiclassical approximation of the regular quasi-energies obtained in reference [65] is contained in our formula as a special case. The semiclassical quantization of a single regular island on a torus is more demanding due to the periodic boundary conditions in q and in p direction. It is performed in section 4.2. The numerical investigation of the quasimodes of two examples closes this section. Finally, we address the semiclassical quantization of a chain of equal transporting regular islands on a torus in section 4.3.

4.1 Transporting regular island in the phase space $\mathbb{R}^2$

We can consider the example map P_{ex}, which was introduced in section 3.4, also without periodic boundary conditions in q as well as in p direction. The phase space of the system is then equal to $\mathbb{R}^2$ instead of the torus $[-1/2, M_q - 1/2] \times [-1/2, 1/2]$ and consists of an infinite number of unit cells. Figure 4.1 illustrates a part of it for the standard parameter set. Let us label the unit cell $[r_q - 1/2, r_q + 1/2] \times [r_p - 1/2, r_p + 1/2]$, where r_q and r_p are integer values, by $\langle r_q, r_p \rangle$. All unit cells contain equal regular islands with the centers $(r_q, r_p + 1/4)$.
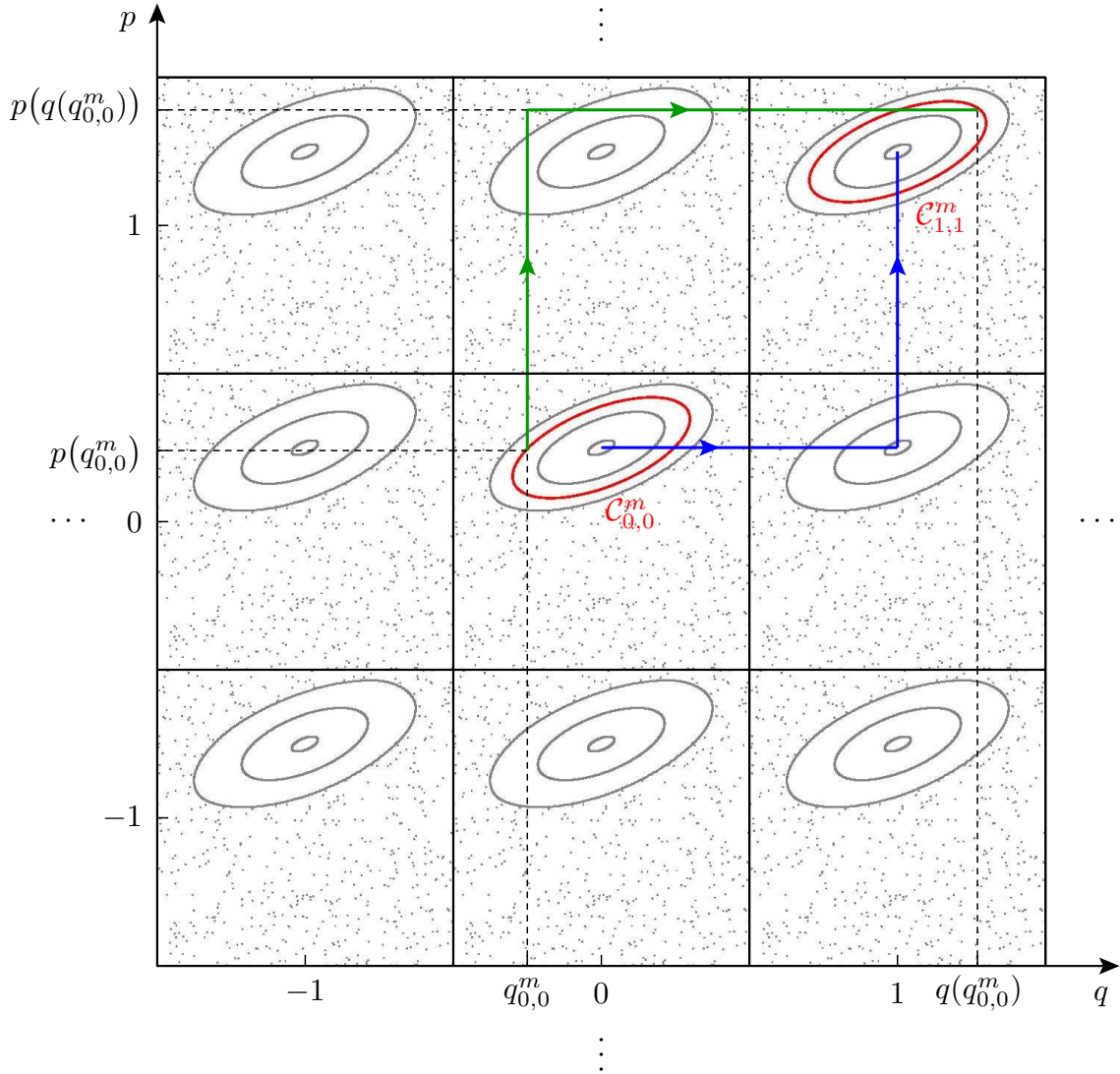
Figure 4.1: Part of the infinite phase space of the example map P_{ex} in the absence of periodic boundary conditions in q and in p direction. Due to regular transport the center of the regular island in unit cell $\langle r_q, r_p \rangle$ is mapped one cell to the right and $r_q + 1$ cells up. A point on the closed quantizing curve $\mathcal{C}^m_{r_q,r_p}$ is correspondingly mapped to a point on the curve $\mathcal{C}^m_{r_q,r_p+r_q+1}$. The blue arrow indicates e.g. the mapping of the center of the regular island in unit cell $\langle 0, 0 \rangle$ and the green arrow illustrates the mapping of the point $\bigl(q^m_{0,0}, p(q^m_{0,0})\bigr)$ on $\mathcal{C}^m_{0,0}$.

The map, which describes the stroboscopic classical dynamics, has the structure

$$P_{\mathrm{ex}}:\ \mathbb{R}^2\ \rightarrow\ \mathbb{R}^2$$

$$\begin{pmatrix} q_n \\ p_n \end{pmatrix} \ \mapsto\ \begin{pmatrix} q_{n+1} \\ p_{n+1} \end{pmatrix} = \begin{pmatrix} q_n + T'(p_n) \\ p_n - V'(q_{n+1}) \end{pmatrix}. \tag{4.5}$$

The functions $T'(p)$ and $V'(q)$ of the example map possess the properties

$$
\begin{aligned}
T'(p+k) &= T'(p), & (4.6) \\
V'(q+k) &= V'(q) - k, & (4.7)
\end{aligned}
$$

where $k \in \mathbb{Z}$. The linearization of a map with respect to the center of a regular island approximates the classical dynamics in a small vicinity of the island center. The derivative of the corresponding kinetic energy function $T_L(p)$ is linear in p. For the linearized version of the example map around the center of the regular island in the unit cell $\langle r_q, r_p \rangle$ the function $T'_L(p)$ is given by equation (3.74) and reads

$$
T'_L(p) = \frac{s}{4} + \left(A - s \left(p - \lfloor p + 1/2 \rfloor \right) \right) \operatorname{sign} \left(p - \lfloor p + 1/2 \rfloor \right), \quad (4.8)
$$

where $A \in \mathbb{Z}$. Its insertion into equation (4.5) shows that the position coordinate r_q of the center of the regular island in the unit cell $\langle r_q, r_p \rangle$ is mapped to $r_q + A$. This shows again that the system-specific parameter A leads to a regular transport in q direction. By equation (4.7), which also holds for the corresponding function $V'_L(q)$, the momentum coordinate $r_p + 1/4$ of the center of the regular island in the same unit cell is transported to $r_p + 1/4 + r_q + A$. The center is thus mapped A cells in q direction and $r_q + A$ cells up

$$
P_{\text{ex}} \begin{pmatrix} r_q \\ r_p + \frac{1}{4} \end{pmatrix} = \begin{pmatrix} r_q + A \\ r_p + \frac{1}{4} + r_q + A \end{pmatrix}. \quad (4.9)
$$

Correspondingly, all invariant tori around the center of the regular island in the unit cell $\langle r_q, r_p \rangle$ show the same regular transport in q as well as in p direction, see figure 4.1.

We now consider periodically kicked systems in 1D without periodic boundary conditions, whose functions $T(p)$ and $V(q)$ fulfill

$$
\begin{aligned}
T(p+k) &= T(p), & (4.10) \\
V(q+k) &= V(q) - kq + d(k), & (4.11)
\end{aligned}
$$

where $d(k)$ is a certain function and $k \in \mathbb{Z}$. The example map P_{ex} belongs to this class of systems with $d(k) = -(1/2)k^2$. The phase space of such a system is equal to $\mathbb{R}^2$. For an appropriate choice of $T(p)$ and $V(q)$ all unit cells contain again one equal and almost resonance-free regular island, see figure 4.2. This will be assumed in the following. Using the derivatives of the kinetic and the potential energy we construct a classical map P similar to equation (4.5). Now we concentrate on the unit cell $\langle r_q, r_p \rangle$ and consider the linearization of the classical map around the center of its regular island with the

corresponding functions $T_L(p)$ and $V_L(q)$. As the derivative $T'_L(p)$ is linear in p, we have

$$T_L(p) \;=\; ap^2 + (b + s_q)p + c \qquad \text{with } a, b, c \in \mathbb{R}, \tag{4.12}$$

where $s_q \in \mathbb{Z}$ separates that contribution of the coefficient in front of the summand linear in p, which yields a regular transport in q direction. Also $T_L(p)$ fulfills equation (4.10), so that s_q needs to be constant. The parameters a, b, and c contain the information about a shift of the island center in p direction. The special shape of the function $V_L(q)$ will not be needed in the following. Using equation (4.12) we find

$$DP: \;\; \mathbb{R}^2 \;\; \rightarrow \;\; \mathbb{R}^2$$

$$\begin{pmatrix} q_n \\ p_n \end{pmatrix} \;\mapsto\; \begin{pmatrix} q_{n+1} \\ p_{n+1} \end{pmatrix} = \begin{pmatrix} q_n + 2ap_n + b + s_q \\ p_n - V'_L(q_{n+1}) \end{pmatrix}. \tag{4.13}$$

for the linearized map around the center of the regular island in the unit cell $\langle r_q, r_p \rangle$. We see that there is a regular transport from the regular island of this unit cell to the regular island in the unit cell $\langle r_q + s_q, r_p + r_q + s_q \rangle$, since also $V_L(q)$ fulfills (4.11).

We let $\big| \phi^{\mathrm{sc},m}_{r_q,r_p} \big\rangle$ be a semiclassical state, whose Husimi function localizes on the mth quantizing torus $\mathcal{C}^m_{r_q,r_p}$ in the regular island of unit cell $\langle r_q, r_p \rangle$. The quantum version of the classical map (4.13) must also reflect this regular transport property

$$\hat{U} \big| \phi^{\mathrm{sc},m}_{r_q,r_p} \big\rangle \;\approx\; \mathrm{e}^{\mathrm{i}\omega^{\mathrm{sc},m}_{r_q,r_p}} \big| \phi^{\mathrm{sc},m}_{r_q+s_q,r_p+r_q+s_q} \big\rangle, \tag{4.14}$$

where $\omega^{\mathrm{sc},m}_{r_q,r_p}$ is a certain phase. Its semiclassical determination will be performed in the following.

Using the general time evolution operator of periodically kicked 1D systems, equation (3.25), and the functions $T_L(p)$ and $V_L(q)$ we can determine $\hat{U}$ at least for regular states, whose quantizing curves lie close to the center of the regular island in the unit cell $\langle r_q, r_p \rangle$. It reads

$$\langle q | \hat{U} | q' \rangle \;=\; \frac{1}{2\sqrt{|a|\pi\hbar_{\mathrm{eff}}}} \, \mathrm{e}^{\mathrm{i}\frac{\pi}{4}\mathrm{sign}(-a)} \, \mathrm{e}^{-\frac{\mathrm{i}}{\hbar_{\mathrm{eff}}}c} \, \mathrm{e}^{-\frac{\mathrm{i}}{\hbar_{\mathrm{eff}}}V_L(q)} \, \mathrm{e}^{\frac{\mathrm{i}}{4a\hbar_{\mathrm{eff}}}\left(b+s_q-q+q'\right)^2} \tag{4.15}$$

in position representation. Since the map is defined on $\mathbb{R}^2$, the values which can be assigned to the effective Planck constant are no longer restricted by equation (3.54). As the subscript of the state on the right-hand side of equation (4.14) is very long, we will use the abbreviations "$i := r_q, r_p$" for initial and "$f := r_q + s_q, r_p + r_q + s_q$" for final quantities in the following. The states $\big| \phi^{\mathrm{sc},m}_i \big\rangle$ and $\big| \phi^{\mathrm{sc},m}_f \big\rangle$ in equation (4.14) are associated with the

closed quantizing curves $\mathcal{C}_i^m$ and $\mathcal{C}_f^m$, respectively. With $q_{\mathrm{ref},i}^m$ and $q_{\mathrm{ref},f}^m$ as arbitrary phase reference levels, see figure 4.2, we make the usual semiclassical ansatz

$$\phi_i^{\mathrm{sc},m}(q) \;=\; a_i^m(q) \, \exp\left(\frac{\mathrm{i}}{\hbar_{\mathrm{eff}}} \int\limits_{q_{\mathrm{ref},i}^m}^{q} \mathrm{d}q_i \, p_i(q_i) \right) \qquad (4.16)$$
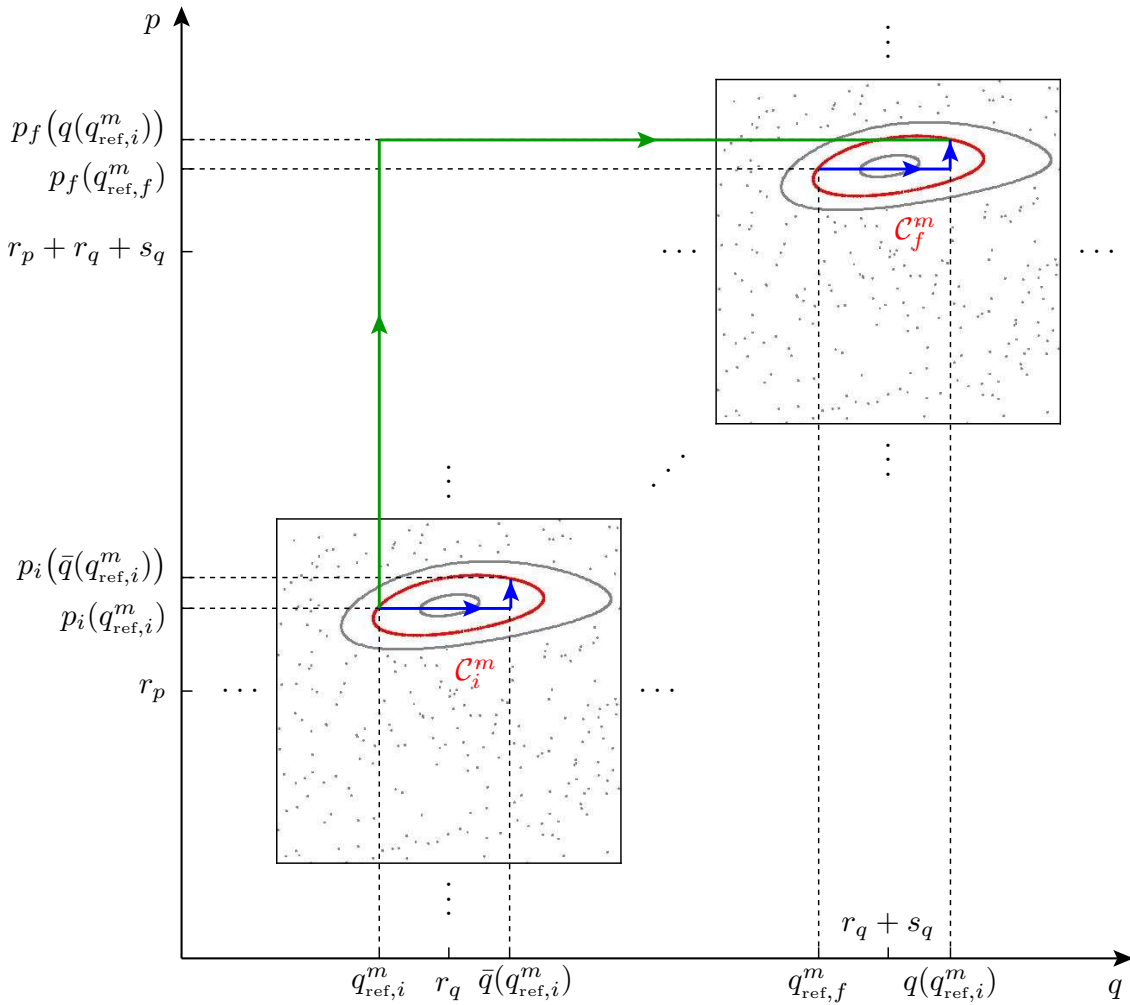
Figure 4.2: Part of the infinite phase space of the map P. Due to regular transport in q as well as in p direction the center of the regular island in the unit cell $\langle r_q, r_p \rangle$ is mapped s_q cells to the right and $r_q + s_q$ cells up. A point on the quantizing curve $\mathcal{C}_i^m$ is consequently mapped to a point on the corresponding curve $\mathcal{C}_f^m$. The blue arrow indicates the mapping of the point $\big(q_{\mathrm{ref},i}^m, p_i(q_{\mathrm{ref},i}^m)\big)$. If no transport is present, this point is mapped as is indicated by the blue arrow.

and

$$\phi_f^{\mathrm{sc},m}(q) \;=\; a_f^m(q)\,\exp\!\left(\frac{\mathrm{i}}{\hbar_{\mathrm{eff}}}\int\limits_{q_{\mathrm{ref},f}^m}^{q}\mathrm{d}q_f\,p_f(q_f)\right) \tag{4.17}$$

according to reference [68]. The prefactors $a_i^m(q)$ and $a_f^m(q)$ are smooth densities along $\mathcal{C}_i^m$ and $\mathcal{C}_f^m$, respectively. We remark that we can set $q_{\mathrm{ref},f}^m = q_{\mathrm{ref},i}^m + s_q$, since the regular islands in all unit cells are equal. Using equations (4.14) and (4.15) we find

$$\mathrm{e}^{\mathrm{i}\omega_i^{\mathrm{sc},m}}\,\phi_f^{\mathrm{sc},m}(q) \;\approx\; \big\langle q\big|\hat{U}\big|\phi_i^{\mathrm{sc},m}\big\rangle \tag{4.18}$$

$$=\;\frac{1}{2\sqrt{|a|\pi\hbar_{\mathrm{eff}}}}\,\mathrm{e}^{\mathrm{i}\frac{\pi}{4}\mathrm{sign}(-a)}\,\mathrm{e}^{-\frac{\mathrm{i}}{\hbar_{\mathrm{eff}}}c}\,\mathrm{e}^{-\frac{\mathrm{i}}{\hbar_{\mathrm{eff}}}V_L(q)}$$

$$\cdot\int\limits_{-\infty}^{\infty}\mathrm{d}q'\,a_i^m(q')\mathrm{e}^{\frac{\mathrm{i}}{4a\hbar_{\mathrm{eff}}}\left(b+s_q-q+q'\right)^2}\exp\!\left(\frac{\mathrm{i}}{\hbar_{\mathrm{eff}}}\int\limits_{q_{\mathrm{ref},i}^m}^{q'}\mathrm{d}q_i\,p_i(q_i)\right). \tag{4.19}$$

The argument of the exponential function in the integrand of equation (4.19) oscillates rapidly in the semiclassical limit due to the $1/\hbar_{\mathrm{eff}}$ dependence. It becomes stationary at the value $\xi(q)$ which fulfills

$$q \;=\; \xi(q) + 2ap_i\left(\xi(q)\right) + b + s_q. \tag{4.20}$$

A comparison of equation (4.20) with (4.13) shows that q is the spatial coordinate of the mapped point $P\big(\xi(q), p\left(\xi(q)\right)\big)$. Solving the integral by the method of stationary phase yields

$$\mathrm{e}^{\mathrm{i}\omega_i^{\mathrm{sc},m}}\,\phi_f^{\mathrm{sc},m}(q) \;\approx\; a_i^m\left(\xi(q)\right)\left|\frac{\mathrm{d}\xi(q)}{\mathrm{d}q}\right|^{\frac{1}{2}}\mathrm{e}^{\mathrm{i}\frac{\pi}{4}\left[\mathrm{sign}(-a)+\mathrm{sign}(a(\mathrm{d}\xi(q)/\mathrm{d}q))\right]}\,\mathrm{e}^{\frac{\mathrm{i}}{\hbar_{\mathrm{eff}}}S^m(q)}\,\mathrm{e}^{-\frac{\mathrm{i}}{\hbar_{\mathrm{eff}}}c}, \tag{4.21}$$

where the abbreviation

$$S^m(q) \;:=\; \int\limits_{q_{\mathrm{ref},i}^m}^{\xi(q)}\mathrm{d}q_i\,p_i(q_i) + ap_i^2\left(\xi(q)\right) - V_L(q) \tag{4.22}$$

is used. If more than one stationary point solves equation (4.20), we have to sum over the different contributions. The phase $\pi/4\left[\mathrm{sign}(-a)+\mathrm{sign}(a(\mathrm{d}\xi(q)/\mathrm{d}q))\right]$ in equation (4.21) distinguishes proper mappings, where $\mathrm{d}\xi(q)$ and $\mathrm{d}q$ have the same sign, from those with opposite signs. The examples considered in this thesis are throughout proper, so that this

phase disappears. The point (q_i, p_i) on the curve $\mathcal{C}_i^m$ is mapped to (q_f, p_f) on $\mathcal{C}_f^m$ according to equation (4.13). The point $\big(q_{\mathrm{ref},i}^m, p_i(q_{\mathrm{ref},i}^m)\big)$ is mapped to $\big(q(q_{\mathrm{ref},i}^m), p_f(q(q_{\mathrm{ref},i}^m))\big)$. This is indicated by the green arrow in figure 4.2. A replacement of $\mathrm{d}q_i$ and $p_i(q_i)$ in the integrand of equation (4.22) by means of the classical mapping (4.13) yields

$$
S^m(q) \;=\; \int\limits_{q(q_{\mathrm{ref},i}^m)}^{q} \mathrm{d}q_f\, p_f(q_f) + V_L(q) - V_L\big(q(q_{\mathrm{ref},i}^m)\big) - a p_i^2\big(\xi(q)\big) + a p_i^2(q_{\mathrm{ref},i}^m). \tag{4.23}
$$

After the insertion of equation (4.23) into equation (4.21) we have

$$
\begin{aligned}
\mathrm{e}^{\mathrm{i}\omega_i^{\mathrm{sc},m}} \phi_f^m(q) \;\approx\;\; & a_i^m\,(\xi(q)) \left|\frac{\mathrm{d}\xi(q)}{\mathrm{d}q}\right|^{\frac{1}{2}} \exp\left(-\frac{\mathrm{i}}{\hbar_{\mathrm{eff}}}c\right) \\[4pt]
& \cdot \exp\left(\frac{\mathrm{i}}{\hbar_{\mathrm{eff}}}\left[\int\limits_{q(q_{\mathrm{ref},i}^m)}^{q} \mathrm{d}q_f\, p_f(q_f) + a p_i^2(q_{\mathrm{ref},i}^m) - V_L\big(q(q_{\mathrm{ref},i}^m)\big)\right]\right) \\[6pt]
=\;\; & a_f^m(q)\, \exp\left(\frac{\mathrm{i}}{\hbar_{\mathrm{eff}}} \int\limits_{q_{\mathrm{ref},f}^m}^{q} \mathrm{d}q_f\, p_f(q_f)\right) \\[4pt]
& \cdot \frac{a_i^m\,(\xi(q))}{a_f^m(q)}\left|\frac{\mathrm{d}\xi(q)}{\mathrm{d}q}\right|^{\frac{1}{2}} \exp\left(-\frac{\mathrm{i}}{\hbar_{\mathrm{eff}}}c\right) \\[4pt]
& \cdot \exp\left(\frac{\mathrm{i}}{\hbar_{\mathrm{eff}}}\left[-\int\limits_{q_{\mathrm{ref},f}^m}^{q(q_{\mathrm{ref},f}^m)} \mathrm{d}q_f\, p_f(q_f) + a p_i^2(q_{\mathrm{ref},i}^m) - V_L\big(q(q_{\mathrm{ref},i}^m)\big)\right]\right) \\[6pt]
\overset{(4.17)}{=}\;\; & \phi_f^m(q)\, \frac{a_i^m\,(\xi(q))}{a_f^m(q)}\left|\frac{\mathrm{d}\xi(q)}{\mathrm{d}q}\right|^{\frac{1}{2}} \exp\left(-\frac{\mathrm{i}}{\hbar_{\mathrm{eff}}}c\right) \\[4pt]
& \cdot \exp\left(\frac{\mathrm{i}}{\hbar_{\mathrm{eff}}}\left[-\int\limits_{q_{\mathrm{ref},f}^m}^{q(q_{\mathrm{ref},i}^m)} \mathrm{d}q_f\, p_f(q_f) + a p_i^2(q_{\mathrm{ref},i}^m) - V_L\big(q(q_{\mathrm{ref},i}^m)\big)\right]\right) \tag{4.24}
\end{aligned}
$$

With

$$
a_f^m(q) \;\equiv\; a_i^m\,(\xi(q)) \left|\frac{\mathrm{d}\xi(q)}{\mathrm{d}q}\right|^{\frac{1}{2}} \tag{4.25}
$$

due to stationarity [65], we obtain

$$
\exp\left(\mathrm{i}\omega_i^{\mathrm{sc},m}\right) \;\approx\; \exp\left(\frac{\mathrm{i}}{\hbar_{\mathrm{eff}}}\left[-\int\limits_{q_{\mathrm{ref},f}^m}^{q(q_{\mathrm{ref},i}^m)}\mathrm{d}q_f\,p_f(q_f) + ap_i^2(q_{\mathrm{ref},i}^m) - V_L\big(q(q_{\mathrm{ref},i}^m)\big) - c\right]\right). \,(4.26)
$$

We can therefore deduce

$$
\begin{aligned}
\omega_i^{\mathrm{sc},m} \;\approx\;& \frac{1}{\hbar_{\mathrm{eff}}}\left[-\int\limits_{q_{\mathrm{ref},f}^m}^{q(q_{\mathrm{ref},i}^m)}\mathrm{d}q_f\,p_f(q_f) + ap_i^2(q_{\mathrm{ref},i}^m) - V_L\big(q(q_{\mathrm{ref},i}^m)\big) - c\right] \\[2mm]
\overset{(4.12)}{=}\;& \frac{1}{\hbar_{\mathrm{eff}}}\left[-\int\limits_{q_{\mathrm{ref},f}^m}^{q(q_{\mathrm{ref},i}^m)}\mathrm{d}q_f\,p_f(q_f) + T_L\big(p_i(q_{\mathrm{ref},i}^m)\big) - V_L\big(q(q_{\mathrm{ref},i}^m)\big)\right. \\[3mm]
& \left. - bp_i(q_{\mathrm{ref},i}^m) - s_q p_i(q_{\mathrm{ref},i}^m) - 2c\right].
\end{aligned}\tag{4.27}
$$

The point $\big(q_{\mathrm{ref},i}^m, p_i(q_{\mathrm{ref},i}^m)\big)$ lies on the mth quantizing torus $\mathcal{C}_i^m$ in the unit cell $\langle r_q, r_p\rangle$. Its map, $\big(q(q_{\mathrm{ref},i}^m), p_f(q(q_{\mathrm{ref},i}^m))\big)$, lies on the curve $\mathcal{C}_f^m$ in the unit cell $\langle r_q + s_q, r_p + r_q + s_q\rangle$. If there had been no regular transport, the point $\big(q_{\mathrm{ref},i}^m, p_i(q_{\mathrm{ref},i}^m)\big)$ would have been mapped to a point on the curve $\mathcal{C}_i^m$: $\big(\bar{q}(q_{\mathrm{ref},i}^m), p_i(\bar{q}(q_{\mathrm{ref},i}^m))\big)$. Since all regular islands are equal and since they lie at the same position in each unit cell, we have $\bar{q}(q_{\mathrm{ref},i}^m) = q(q_{\mathrm{ref},i}^m) - s_q$, see figure 4.2. In the next step we use the property (4.11), which also holds for the function $V_L(q)$

$$
\begin{aligned}
\omega_i^{\mathrm{sc},m} \;\approx\;& \frac{1}{\hbar_{\mathrm{eff}}}\left[-\int\limits_{q_{\mathrm{ref},f}^m}^{q(q_{\mathrm{ref},i}^m)}\mathrm{d}q_f\,p_f(q_f) + T_L\big(p_i(q_{\mathrm{ref},i}^m)\big) - V_L\big(\bar{q}(q_{\mathrm{ref},i}^m) + s_q\big)\right. \\[3mm]
& \left. - bp_i(q_{\mathrm{ref},i}^m) - s_q p_i(q_{\mathrm{ref},i}^m) - 2c\right] \\[3mm]
=\;& \frac{1}{\hbar_{\mathrm{eff}}}\left[-\int\limits_{q_{\mathrm{ref},f}^m}^{q(q_{\mathrm{ref},i}^m)}\mathrm{d}q_f\,p_f(q_f) + T_L\big(p_i(q_{\mathrm{ref},i}^m)\big) - V_L\big(\bar{q}(q_{\mathrm{ref},i}^m)\big)\right. \\[3mm]
& \left. - bp_i(q_{\mathrm{ref},i}^m) - s_q p_i(q_{\mathrm{ref},i}^m) + s_q \bar{q}(q_{\mathrm{ref},i}^m) - d(s_q) - 2c\right].
\end{aligned}\tag{4.28}
$$

As all regular islands in the phase space are equal, the integral in the first summand of equation (4.28), which is performed in the unit cell $\langle r_q + s_q, r_p + r_q + s_q \rangle$, can also be determined in the unit cell $\langle r_q, r_p \rangle$

$$
\omega_i^{\mathrm{sc},m} \approx \frac{1}{\hbar_{\mathrm{eff}}} \left[- \int_{q_{\mathrm{ref},i}^m}^{\bar{q}(q_{\mathrm{ref},i}^m)} \mathrm{d}q_i \, p_i(q_i) + T_L\big(p_i(q_{\mathrm{ref},i}^m)\big) - V_L\big(\bar{q}(q_{\mathrm{ref},i}^m)\big) \right.
$$
$$
\left. - bp_i(q_{\mathrm{ref},i}^m) - s_q p_i(q_{\mathrm{ref},i}^m) + s_q \bar{q}(q_{\mathrm{ref},i}^m) - d(s_q) - 2c \right]. \qquad (4.29)
$$

All positions and momenta appearing in equation (4.29) belong to points in the same unit cell. In the following we will consider only this unit cell with periodic boundary conditions in q and in p direction. Then, the point $\big(\bar{q}(q_{\mathrm{ref},i}^m), p_i(\bar{q}(q_{\mathrm{ref},i}^m))\big)$ is the mapped point of $\big(q_{\mathrm{ref},i}^m, p_i(q_{\mathrm{ref},i}^m)\big)$. Let us denote the latter point by $\big(q_0, p(q_0)\big)$ and the former one by $\big(q_1, p(q_1)\big)$. With this notation equation (4.29) becomes

$$
\omega_i^{\mathrm{sc},m} \approx \frac{1}{\hbar_{\mathrm{eff}}} \left[- \int_{q_0}^{q_1} \mathrm{d}q \, p(q) + T_L\big(p(q_0)\big) - V_L(q_1) \right.
$$
$$
\left. - bp(q_0) - s_q p(q_0) + s_q q_1 - d(s_q) - 2c \right]. \qquad (4.30)
$$

Now we resubstitute the abbreviation "i" by "r_q, r_p". The dependence of $\omega_i^{\mathrm{sc},m} = \omega_{r_q,r_p}^{\mathrm{sc},m}$ on the constant phase reference level q_0 is not nice. In order to get rid of it, we perform the same procedure as in reference [65]. It exploits that the iterates (q_k, p_k) of the initial point (q_0, p_0) will eventually cover the quantizing curve $\mathcal{C}_{r_q,r_p}^m$ for an irrational rotation number R_m. Averaging over these iterates yields

$$
\omega_{r_q,r_p}^{\mathrm{sc},m} \approx \lim_{N \to \infty} \frac{1}{N} \sum_{k=0}^{N} \frac{1}{\hbar_{\mathrm{eff}}} \left[- \int_{q_k}^{q_{k+1}} \mathrm{d}q \, p(q) + T_L\big(p(q_k)\big) - V_L(q_{k+1}) \right.
$$
$$
\left. - bp(q_k) - s_q p(q_k) + s_q q_{k+1} - d(s_q) - 2c \right]. \qquad (4.31)
$$

The first term involves successive areas which are enclosed by $\mathcal{C}_{r_q,r_p}^m$. Using the rotation number R_m associated with $\mathcal{C}_{r_q,r_p}^m$ and the quantization condition (4.2), we obtain

$$
\begin{aligned}
\omega_{r_q,r_p}^{\mathrm{sc},m} &\approx 2\pi R_m \left(m + \frac{1}{2} \right) + \frac{1}{\hbar_{\mathrm{eff}}} \Big\langle T_L(p) - V_L(q) \Big\rangle_{\mathcal{C}_{r_q,r_p}^m} \\
&\quad - \frac{1}{\hbar_{\mathrm{eff}}} \left[b \Big\langle p \Big\rangle_{\mathcal{C}_{r_q,r_p}^m} + s_q \Big\langle p \Big\rangle_{\mathcal{C}_{r_q,r_p}^m} - s_q \Big\langle q \Big\rangle_{\mathcal{C}_{r_q,r_p}^m} + d(s_q) + 2c \right],
\end{aligned} \tag{4.32}
$$

where $\langle f \rangle_{\mathcal{C}_{r_q,r_p}^m}$ denotes the average of the function f along the invariant curve $\mathcal{C}_{r_q,r_p}^m$. The expression $\langle q \rangle_{\mathcal{C}_{r_q,r_p}^m}$ is thus equal to the position coordinate of the center of the regular island in the unit cell $\langle r_q, r_p \rangle$ and $\langle p \rangle_{\mathcal{C}_{r_q,r_p}^m}$ represents the corresponding momentum coordinate.

Using the linearized map, which already contains the information about the regular transport, enabled the previous analytical consideration. Since this information is reflected by the second line of equation (4.32), we are allowed to replace the functions $T_L(p)$ and $V_L(q)$ by the actual functions $T(p)$ and $V(q)$ and obtain finally

$$
\begin{aligned}
\omega_{r_q,r_p}^{\mathrm{sc},m} &\approx 2\pi R_m \left(m + \frac{1}{2} \right) + \frac{1}{\hbar_{\mathrm{eff}}} \Big\langle T(p) - V(q) \Big\rangle_{\mathcal{C}_{r_q,r_p}^m} \\
&\quad - \frac{1}{\hbar_{\mathrm{eff}}} \left[b \Big\langle p \Big\rangle_{\mathcal{C}_{r_q,r_p}^m} + s_q \Big\langle p \Big\rangle_{\mathcal{C}_{r_q,r_p}^m} - s_q \Big\langle q \Big\rangle_{\mathcal{C}_{r_q,r_p}^m} + d(s_q) + 2c \right].
\end{aligned} \tag{4.33}
$$

We thus have a general semiclassical prediction for the phase $\omega_{r_q,r_p}^{\mathrm{sc},m}$ for systems with equal transporting regular islands, where the kinetic and the potential energy function fullfill the conditions (4.10) and (4.11), respectively.

In reference [65] the semiclassical quantization of a single regular island is studied in the absence of regular transport. This corresponds to setting $s_q = 0$. The kinetic energy is chosen as $T(p) = p^2/2$, what implies $a = 1/2$ and $b = c = 0$ for our formula. Consequently, only the first line of equation (4.33) remains, which is exactly the formula obtained in reference [65].

Equation (4.33) provides a semiclassical expression for the phase $\omega_{r_q,r_p}^{\mathrm{sc},m}$. As semiclassical approximation for the wave function $\phi_{r_q,r_p}^{\mathrm{sc},m}(q)$, whose Husimi function localizes on the mth quantizing torus $\mathcal{C}_{r_q,r_p}^m$, equation (4.16) has been used so far. It is, however, only valid for the classically allowed region at a given quantum number m. In order to find a semiclassical approximation $\phi_{r_q,r_p}^{\mathrm{sc},m}(q)$ valid on $\mathbb{R}$, one can continue the regular dynamics from the island to the chaotic sea. This can be done by determining a time independent 1D Hamiltonian $H_{\mathrm{reg}}(q,p)$ which interpolates the dynamics of the regular island in the mixed system. By means of this time independent 1D Hamiltonian the continuation of

the regular island to the chaotic sea is possible. A suitable method for this purpose is the Lie transform, which is briefly explained in appendix C.1. After the symmetrization of the time independent interpolating 1D Hamiltonian $H_{\text{reg}}(q,p)$, a quantization leads to a Hamilton operator $\hat{H}_{\text{reg}}(q,p)$. Some of its eigenstates are the states $\left| \phi_{r_q,r_p}^{\text{sc},m} \right\rangle$. The smaller the effect of resonance island chains within the regular island of the actual mixed system is, the more precise can $H_{\text{reg}}(q,p)$ be determined. If the regular dynamics within the island of the actually considered mixed system is perfectly known, there should be exactly one possible continuation of the regular island to the chaotic sea.

4.2 Single regular island on a torus

The phase space of the periodically kicked system in the previous section is equal to $\mathbb{R}^2$. It consists of an infinite number of unit cells $[r_q + q_{\min}, r_q + q_{\min} + 1] \times [r_p + p_{\min}, r_p + p_{\min} + 1]$, where r_q and r_p are integers. Each unit cell contains an almost resonance-free regular island and all islands are by construction equal.

Now we focus on one of these unit cells, e.g. the one which is labelled by $\langle r_q, r_p \rangle = \langle 0, 0 \rangle$: $[q_{\min}, q_{\min} + 1] \times [p_{\min}, p_{\min} + 1]$. The introduction of periodic boundary conditions in q and in p direction assigns the properties of a torus to the unit cell, i.e. that $q_{\min}$ becomes identified with $q_{\min} + 1$, as well as $p_{\min}$ with $p_{\min} + 1$.

The quantum time evolution of this kicked system is described by the unitary time evolution operator $\hat{U}$ over one kicking period. The solution of the eigenvalue equation

$$\hat{U}|\psi_n\rangle = \mathrm{e}^{\mathrm{i}\varphi_n}|\psi_n\rangle \tag{4.34}$$

provides the eigenstates $|\psi_n\rangle$ and the corresponding quasi-energies φ_n. In the following we will demonstrate the semiclassical quantization of the regular island of the quantum map that is defined on the torus $[q_{\min}, q_{\min} + 1] \times [p_{\min}, p_{\min} + 1]$. The size A_{reg} of the regular island determines the maximum quantum number of regular eigenstates of $\hat{U}$ according to equation (4.3). At the beginning of this chapter we agreed to label regular eigenstates of $\hat{U}$ with the quantum number m, i.e. that the Husimi function of the eigenstate $|\psi_m\rangle$ localizes on the mth quantizing torus $\mathcal{C}_{0,0}^m$ within the regular island.

The semiclassical quantization of a regular island consists of determining semiclassical approximations $|\psi_m^{\text{sc}}\rangle$ and φ_m^{sc} of the eigenstates $|\psi_m\rangle$ and the corresponding quasi-energies φ_m. The regular island in the considered unit cell with periodic boundary conditions is equal to the regular island in the corresponding unit cell of the infinite phase space in the previous section. We therefore use the semiclassical state $\left| \phi_{0,0}^{\text{sc},m} \right\rangle$ of the previous section as starting point for the determination of $|\psi_m^{\text{sc}}\rangle$. As the state $\left| \phi_{0,0}^{\text{sc},m} \right\rangle$ is an eigenstate of

the Hamiltonian $\hat{H}_{\mathrm{reg}}$ of a completely regular system with a phase space equal to $\mathbb{R}^2$, it needs to be adapted to the torus, i.e. that it has to be modified such that it fulfills the quasi-periodicity conditions (3.40) and (3.41). We therefore introduce a periodization operator in q direction [69]

$$\hat{P}_q(\theta_q) := \sum_{\mu=-\infty}^{\infty} \mathrm{e}^{2\pi\mathrm{i}\mu\theta_q}\hat{T}(\mu M_q, 0), \tag{4.35}$$

as well as in p direction

$$\hat{P}_p(\theta_p) := \sum_{\nu=-\infty}^{\infty} \mathrm{e}^{-2\pi\mathrm{i}\nu\theta_p}\hat{T}(0, \nu M_p). \tag{4.36}$$

With

$$\hat{P}(\theta_q, \theta_p) := \hat{P}_q(\theta_q)\hat{P}_p(\theta_p) \tag{4.37}$$

we get the operator which yields doubly periodized states on the considered torus. Since we treat the case of a single unit cell here, we set $M_q = M_p = 1$. For an arbitrary quantum state $|\psi\rangle$ in an infinite Hilbert space we will denote the doubly periodized one on the torus by

$$\big|\tilde{\psi}\big\rangle := \hat{P}(\theta_q, \theta_p)\big|\psi\big\rangle. \tag{4.38}$$

Later we will also need states which are only periodized in p direction. We will denote them by

$$\big|\bar{\psi}\big\rangle := \hat{P}_p(\theta_p)\big|\psi\big\rangle. \tag{4.39}$$

This implies

$$\big|\tilde{\psi}\big\rangle = \hat{P}_q(\theta_q)\big|\bar{\psi}\big\rangle. \tag{4.40}$$

Interesting observations are the commutation relations [69]

$$[\hat{U}, \hat{P}_q(\theta_q)] = 0, \tag{4.41}$$

$$[\hat{U}, \hat{P}_p(\theta_p)] = 0, \tag{4.42}$$

and

$$[\hat{U}, \hat{P}(\theta_q, \theta_p)] \;=\; 0, \tag{4.43}$$

which hold in general for $h_{\mathrm{eff}} = M_q M_p / N$, where $M_q \in \mathbb{N}$ and $M_p = 1$ or $M_q = 1$ and $M_p \in \mathbb{N}$. With $|\psi_m^{\mathrm{sc}}\rangle := |\tilde{\phi}_{0,0}^{\mathrm{sc},m}\rangle$ the semiclassical approximation of the mth regular eigenstate of the time evolution operator $\hat{U}$ is performed. Now we continue with the determination of the semiclassical approximation φ_m^{sc} of the corresponding quasi-energy φ_m.

In the next section we will consider a system whose phase space is equal to the torus $[q_{\min}, q_{\min} + M_q] \times [p_{\min}, p_{\min} + 1]$. It consists of $M_q > 1$ unit cells in q direction, where $q_{\min}$ is identified with $q_{\min} + M_q$, as well as $p_{\min}$ with $p_{\min} + 1$. Each of the M_q unit cells contains one regular island and all islands are assumed to be equal again. The following consideration is also useful for this case. We will therefore perform it for $M_q \in \mathbb{N}$. Given the state $|\tilde{\phi}_{0,0}^{\mathrm{sc},m}\rangle$, we define at first the shifted state

$$\left|\phi_{k,j}^{\mathrm{sc},m}\right\rangle \;:=\; \hat{T}(k,0)\,\hat{T}(0,j)\left|\phi_{0,0}^{\mathrm{sc},m}\right\rangle \qquad \text{with } k,\, j \in \mathbb{Z}, \tag{4.44}$$

where the translation operator (3.26) is used. We then have

$$
\begin{aligned}
\hat{U}\left|\tilde{\phi}_{k,0}^{\mathrm{sc},m}\right\rangle &\overset{(4.38)}{=} \hat{U}\,\hat{P}(\theta_q, \theta_p)\left|\phi_{k,0}^{\mathrm{sc},m}\right\rangle \\[4pt]
&\overset{(4.43)}{=} \hat{P}(\theta_q, \theta_p)\,\hat{U}\left|\phi_{k,0}^{\mathrm{sc},m}\right\rangle \\[4pt]
&\overset{(4.14)}{\approx} \hat{P}(\theta_q, \theta_p)\,\mathrm{e}^{\mathrm{i}\omega_{k,0}^{\mathrm{sc},m}}\left|\phi_{k+s_q,k+s_q}^{\mathrm{sc},m}\right\rangle \\[4pt]
&\overset{(4.44)}{=} \mathrm{e}^{\mathrm{i}\omega_{k,0}^{\mathrm{sc},m}}\,\hat{P}(\theta_q, \theta_p)\,\hat{T}(k+s_q,0)\,\hat{T}(0,k+s_q)\left|\phi_{0,0}^{\mathrm{sc},m}\right\rangle \\[4pt]
&\overset{(3.31),(3.33)}{=} \mathrm{e}^{\mathrm{i}\omega_{k,0}^{\mathrm{sc},m}}\,\mathrm{e}^{-\frac{\mathrm{i}}{\hbar_{\mathrm{eff}}}(k+s_q)^2}\,\hat{P}(\theta_q, \theta_p)\,\hat{T}(0,k+s_q)\,\hat{T}(k+s_q,0)\left|\phi_{0,0}^{\mathrm{sc},m}\right\rangle \\[4pt]
&\overset{(4.44)}{=} \mathrm{e}^{\mathrm{i}\omega_{k,0}^{\mathrm{sc},m}}\,\mathrm{e}^{-\frac{\mathrm{i}}{\hbar_{\mathrm{eff}}}(k+s_q)^2}\,\hat{P}(\theta_q, \theta_p)\,\hat{T}(0,k+s_q)\left|\phi_{k+s_q,0}^{\mathrm{sc},m}\right\rangle \\[4pt]
&\overset{(4.37)}{=} \mathrm{e}^{\mathrm{i}\omega_{k,0}^{\mathrm{sc},m}}\,\mathrm{e}^{-\frac{\mathrm{i}}{\hbar_{\mathrm{eff}}}(k+s_q)^2}\,\hat{P}_q(\theta_q)\,\hat{P}_p(\theta_p)\,\hat{T}(0,k+s_q)\left|\phi_{k+s_q,0}^{\mathrm{sc},m}\right\rangle. \tag{4.45}
\end{aligned}
$$

As $s_q \in \mathbb{Z}$, the sum $k + s_q$ is also integer valued. Now we consider

$$
\begin{aligned}
\hat{P}_p(\theta_p)\,\hat{T}(0,k+s_q) &\overset{(4.36)}{=} \sum_{\nu=-\infty}^{\infty} \mathrm{e}^{-2\pi\mathrm{i}\nu\theta_p}\,\hat{T}(0,\nu)\,\hat{T}(0,k+s_q) \\[4pt]
&= \sum_{\nu=-\infty}^{\infty} \mathrm{e}^{-2\pi\mathrm{i}\nu\theta_p}\,\hat{T}(0,\nu+k+s_q)
\end{aligned}
$$

$$\Leftrightarrow \quad \hat{P}_p(\theta_p)\,\hat{T}(0, k+s_q) \overset{\nu':=\nu+k+s_q}{=} \mathrm{e}^{2\pi\mathrm{i}(k+s_q)\theta_p} \sum_{\nu'=-\infty}^{\infty} \mathrm{e}^{-2\pi\mathrm{i}\nu'\theta_p}\,\hat{T}(0,\nu')$$

$$\overset{(4.36)}{=} \quad \mathrm{e}^{2\pi\mathrm{i}(k+s_q)\theta_p}\,\hat{P}_p(\theta_p). \tag{4.46}$$

The insertion of equation (4.46) into (4.45) yields

$$\hat{U}\big|\tilde{\phi}_{k,0}^{\mathrm{sc},m}\big\rangle \quad \approx \quad \mathrm{e}^{\mathrm{i}\omega_{k,0}^{\mathrm{sc},m}}\,\mathrm{e}^{-\frac{\mathrm{i}}{\hbar_{\mathrm{eff}}}(k+s_q)^2}\,\mathrm{e}^{2\pi\mathrm{i}(k+s_q)\theta_p}\,\hat{P}_q(\theta_q)\,\hat{P}_p(\theta_p)\big|\phi_{k+s_q,0}^{\mathrm{sc},m}\big\rangle$$

$$\overset{(4.39)}{=} \quad \mathrm{e}^{\mathrm{i}\omega_{k,0}^{\mathrm{sc},m}}\,\mathrm{e}^{-\frac{\mathrm{i}}{\hbar_{\mathrm{eff}}}(k+s_q)^2}\,\mathrm{e}^{2\pi\mathrm{i}(k+s_q)\theta_p}\,\hat{P}_q(\theta_q)\big|\bar{\phi}_{k+s_q,0}^{\mathrm{sc},m}\big\rangle. \tag{4.47}$$

With the abbreviation $a(k) := (k+s_q)/M_q$ we have

$$\hat{P}_q(\theta_q)\big|\bar{\phi}_{k+s_q,0}^{\mathrm{sc},m}\big\rangle \overset{(4.44)}{=} \hat{P}_q(\theta_q)\,\hat{T}(k+s_q,0)\big|\bar{\phi}_{0,0}^{\mathrm{sc},m}\big\rangle$$

$$= \hat{P}_q(\theta_q)\,\hat{T}\big(\lfloor a(k)\rfloor\,M_q,0\big)\,\hat{T}\big((k+s_q)\bmod M_q,0\big)\big|\bar{\phi}_{0,0}^{\mathrm{sc},m}\big\rangle \tag{4.48}$$

$$\overset{(4.44)}{=} \hat{P}_q(\theta_q)\,\hat{T}\big(\lfloor a(k)\rfloor\,M_q,0\big)\big|\bar{\phi}_{(k+s_q)\bmod M_q,0}^{\mathrm{sc},m}\big\rangle. \tag{4.49}$$

In the step from equation (4.48) to equation (4.49) we used $k+s_q = \lfloor a(k)\rfloor\,M_q + (k+s_q)\bmod M_q$. The reason for this replacement will become clear soon. Moreover, we consider

$$\hat{P}_q(\theta_q)\,\hat{T}\big(\lfloor a(k)\rfloor\,M_q,0\big) \overset{(4.35)}{=} \sum_{\mu=-\infty}^{\infty} \mathrm{e}^{2\pi\mathrm{i}\mu\theta_q}\,\hat{T}(\mu M_q,0)\,\hat{T}\big(\lfloor a(k)\rfloor\,M_q,0\big)$$

$$= \sum_{\mu=-\infty}^{\infty} \mathrm{e}^{2\pi\mathrm{i}\mu\theta_q}\,\hat{T}\big((\mu+\lfloor a(k)\rfloor)M_q,0\big)$$

$$\overset{\mu':=\mu+\lfloor a(k)\rfloor}{=} \mathrm{e}^{-2\pi\mathrm{i}\lfloor a(k)\rfloor\theta_q} \sum_{\mu'=-\infty}^{\infty} \mathrm{e}^{2\pi\mathrm{i}\mu'\theta_q}\,\hat{T}(\mu'M_q,0)$$

$$\overset{(4.35)}{=} \mathrm{e}^{-2\pi\mathrm{i}\lfloor a(k)\rfloor\theta_q}\,\hat{P}_q(\theta_q). \tag{4.50}$$

The insertion of (4.49) and (4.50) into equation (4.47) yields

$$\hat{U}\big|\tilde{\phi}_{k,0}^{\mathrm{sc},m}\big\rangle \quad \approx \quad \mathrm{e}^{\mathrm{i}\omega_{k,0}^{\mathrm{sc},m}}\,\mathrm{e}^{-\frac{\mathrm{i}}{\hbar_{\mathrm{eff}}}(k+s_q)^2}\,\mathrm{e}^{2\pi\mathrm{i}(k+s_q)\theta_p}\,\mathrm{e}^{-2\pi\mathrm{i}\lfloor a(k)\rfloor\theta_q}\,\hat{P}_q(\theta_q)\big|\bar{\phi}_{(k+s_q)\bmod M_q,0}^{\mathrm{sc},m}\big\rangle$$

$$\overset{(4.40)}{=} \quad \mathrm{e}^{\mathrm{i}\omega_{k,0}^{\mathrm{sc},m}}\,\mathrm{e}^{-\frac{\mathrm{i}}{\hbar_{\mathrm{eff}}}(k+s_q)^2}\,\mathrm{e}^{2\pi\mathrm{i}(k+s_q)\theta_p}\,\mathrm{e}^{-2\pi\mathrm{i}\lfloor a(k)\rfloor\theta_q}\big|\tilde{\phi}_{(k+s_q)\bmod M_q,0}^{\mathrm{sc},m}\big\rangle. \tag{4.51}$$

Let us discuss equation (4.51). The regular island in the unit cell $\langle k,0\rangle$ of the phase space of the kicked system is transported by the distance s_q in q direction and by $k+s_q$ in p direction per kicking period, if periodic boundary conditions are neglected. The corresponding quantum map reflects the same property. For $k \in \mathbb{Z}_{M_q}$ the application

of the time evolution operator $\hat{U}$ over one kicking period to the non-periodized state $\left|\phi_{k,0}^{\mathrm{sc},m}\right\rangle$ yields the state $\left|\phi_{k+s_q,k+s_q}^{\mathrm{sc},m}\right\rangle$ apart from a phase factor, see equation (4.14). As the considered system is, however, equal to the torus $[q_{\min}, q_{\min} + M_q] \times [p_{\min}, p_{\min} + 1]$, we have to take the periodic boundary conditions into account. They are ensured by the periodization of the state $\left|\phi_{k,0}^{\mathrm{sc},m}\right\rangle$ in q as well as in p direction. The periodization in p direction yields the state $\left|\bar{\phi}_{k,0}^{\mathrm{sc},m}\right\rangle$. After the application of $\hat{U}$ we have the state $\left|\bar{\phi}_{k+s_q,0}^{\mathrm{sc},m}\right\rangle$. However, the application of the time evolution operator results in passing the line $p = p_{\min}+1$ of the torus $k + s_q$ times, what yields the additional phase $2\pi(k+s_q)\theta_p$ in equation (4.51) according to the quasi-periodicity condition (3.41). From the additional periodization of the state $\left|\bar{\phi}_{k,0}^{\mathrm{sc},m}\right\rangle$ in q direction we obtain the doubly periodized state $\left|\tilde{\phi}_{k,0}^{\mathrm{sc},m}\right\rangle$. The application of $\hat{U}$ maps it by the distance s_q in q direction. If $k + s_q \geq M_q$, it passed the line $q = q_{\min} + M_q$ of the torus $\lfloor a(k) \rfloor = \lfloor (k + s_q)/M_q \rfloor$ times leading to the phase $-2\pi \lfloor a(k) \rfloor \theta_q$ in equation (4.51) according to the quasi-periodicity condition (3.40). Then, the mapped state localizes in the unit cell $\langle (k + s_q) \bmod M_q, 0 \rangle$. These considerations also explain the replacement $k + s_q = \lfloor a(k) \rfloor M_q + (k + s_q) \bmod M_q$ in the step from equation (4.48) to (4.49).

We have

$$\hat{U}\left|\tilde{\phi}_{k,0}^{\mathrm{sc},m}\right\rangle \approx \mathrm{e}^{\mathrm{i}\tilde{\omega}_{k,0}^{\mathrm{sc},m}}\left|\tilde{\phi}_{(k+s_q)\bmod M_q,0}^{\mathrm{sc},m}\right\rangle \tag{4.52}$$

similar to (4.14) and thus

$$\tilde{\omega}_{k,0}^{\mathrm{sc},m} = \omega_{k,0}^{\mathrm{sc},m} - \frac{1}{\hbar_{\mathrm{eff}}}(k + s_q)^2 - 2\pi \left\lfloor \frac{k + s_q}{M_q} \right\rfloor \theta_q + 2\pi(k + s_q)\theta_p \tag{4.53}$$

from equation (4.51). In this section we consider the case $M_q = M_p = 1$. We therefore have $k \equiv 0$ and the approximate eigenvalue equation

$$\hat{U}\left|\tilde{\phi}_{0,0}^{\mathrm{sc},m}\right\rangle \approx \mathrm{e}^{\mathrm{i}\tilde{\omega}_{0,0}^{\mathrm{sc},m}}\left|\tilde{\phi}_{0,0}^{\mathrm{sc},m}\right\rangle. \tag{4.54}$$

As $\left|\tilde{\phi}_{0,0}^{\mathrm{sc},m}\right\rangle$ is the semiclassical approximation of the mth regular eigenstate $|\psi_m\rangle$ of the time evolution operator $\hat{U}$, $\tilde{\omega}_{0,0}^{\mathrm{sc},m}$ is the semiclassical approximation φ_m^{sc} of the corresponding quasi-energy φ_m. We then have

$$\varphi_m^{\mathrm{sc}} \approx \omega_{0,0}^{\mathrm{sc},m} - \frac{1}{\hbar_{\mathrm{eff}}}s_q^2 - 2\pi s_q \theta_q + 2\pi s_q \theta_p.$$

Now we insert equation (4.33) and obtain finally

$$
\begin{aligned}
\varphi_m^{\text{sc}} \quad &\approx \quad 2\pi R_m \left(m + \frac{1}{2} \right) + \frac{1}{\hbar_{\text{eff}}} \Big\langle T(p) - V(q) \Big\rangle_{\mathcal{C}_{0,0}^m} \\
&\quad - \frac{1}{\hbar_{\text{eff}}} \left[b \Big\langle p \Big\rangle_{\mathcal{C}_{0,0}^m} + s_q \Big\langle p \Big\rangle_{\mathcal{C}_{0,0}^m} - s_q \Big\langle q \Big\rangle_{\mathcal{C}_{0,0}^m} + d(s_q) + 2c \right] \\
&\quad - \frac{1}{\hbar_{\text{eff}}} s_q^2 - 2\pi s_q \theta_q + 2\pi s_q \theta_p \\
&\stackrel{(3.54)}{=} 2\pi R_m \left(m + \frac{1}{2} \right) + 2\pi N \Big\langle T(p) - V(q) \Big\rangle_{\mathcal{C}_{0,0}^m} \\
&\quad - 2\pi N \left[b \Big\langle p \Big\rangle_{\mathcal{C}_{0,0}^m} + s_q \Big\langle p \Big\rangle_{\mathcal{C}_{0,0}^m} - s_q \Big\langle q \Big\rangle_{\mathcal{C}_{0,0}^m} + d(s_q) + 2c \right] \\
&\quad - 2\pi N s_q^2 - 2\pi s_q \theta_q + 2\pi s_q \theta_p.
\end{aligned}
\tag{4.55}
$$

If no regular transport is present, the terms which are proportional to s_q vanish. The factors b and c describe a shift of the center of the regular island in p direction. A shift in q direction can be effected by shifting the potential energy $V(q)$. This influences the average along the curve $\mathcal{C}_{0,0}^m$ and thus the quasi-energy $\tilde{\varphi}_m^{\text{sc}}$.

In the following we will apply the results of the semiclassical quantization of a regular island of a quantum map defined on a torus to the example map P_{ex} with the standard parameters $r = 0.65$, $s = 2.0$, and $\varepsilon = 0.015$. The parameter A will be adapted accordingly, depending on whether regular transport should or should not occur.

Example map P_{ex} without transport

The center of the regular island of the example map in the unit cell $\langle 0, 0 \rangle$ reads $(q_{\text{c}}, p_{\text{c}}) = (0, 1/4)$. To obtain a map without transport, we set $A = 0$. This is equal to setting $s_q = 0$, so that we have

$$
T_L(p) \quad = \quad -p^2 + \frac{1}{2}p - \frac{1}{16}
\tag{4.56}
$$

for the linearized kinetic energy function determined with respect to the momentum coordinate of the center of the regular island. From the comparison of equation (4.56) with (4.12) we find $a = -1$, $b = 1/2$, and $c = -1/16$. For the evaluation of the quasi-energy formula (4.55) we also need the function $d(s_q)$. The comparison of equation (4.11) with (3.92) yields $d(s_q) = -(1/2)s_q^2 = 0$.

As $\langle q \rangle_{\mathcal{C}_{0,0}^m} = q_{\text{c}}$ and $\langle p \rangle_{\mathcal{C}_{0,0}^m} = p_{\text{c}}$, the contribution in the second line of equation (4.55)

becomes equal to zero. We thus have

$$\varphi_m^{\mathrm{sc}} \quad \approx \quad 2\pi R_m \left(m + \frac{1}{2} \right) + 2\pi N \Big\langle T(p) - V(q) \Big\rangle_{\mathcal{C}_{0,0}^m}. \tag{4.57}$$

The functions $T(p)$ and $V(q)$ are by construction quadratic in p or in q almost up to the border of the regular island. As these two functions are furthermore constructed such that they vanish in the center of the regular island, the average along the curve $\mathcal{C}_{0,0}^m$ vanishes approximately for small quantum numbers. The smoothing with a Gaussian mainly influences the border region of the regular island, see section 3.4. The energies $T(p)$ and $V(q)$ are different from quadratic functions there. The average $\langle \cdot \rangle_{\mathcal{C}_{0,0}^m}$ becomes thus important for states whose quantizing curve $\mathcal{C}_{0,0}^m$ is close to the border of the regular island. Figures 4.3(a) and (b) show the quasi-energy spectrum φ_n of the operator $\hat{U}$ for $N = 10$ and $N = 20$ as a function of $\theta_q \in [0,1)$, as there is no restriction for the Bloch phase θ_q in the case of the example map, see section 3.4.3. According to (3.105) we can set the other Bloch phase θ_p equal to zero for both values of N. For the size $A_{\mathrm{reg}} = 0.215$ of the regular island we expect two regular eigenstates in the former and five in the latter case according to equation (4.3). The semiclassical prediction of their quasi-energies (4.57) is also plotted for $m = 0$ by $m = m_{\mathrm{max}}$ with different colours. As it is independent of θ_q, we observe horizontal lines. We furthermore realize that, apart from avoided crossings, respectively one quasi-energy of the spectrum of $\hat{U}$ lies on the semiclassically determined curves. In figure 4.4 we show the modulus of the difference of the quasi-energies φ_m and φ_m^{sc} as a function of $1/h_{\mathrm{eff}}$ for the quantum numbers $m = 0$ by $m = 10$. This difference decreases with increasing h_{eff} implying that the semiclassical approximations φ_m^{sc} of the quasi-energies φ_m become better in the semiclassical limit $h_{\mathrm{eff}} \to 0$. The observable fluctuations in figure 4.4 result from avoided crossings between regular and chaotic quasi-energies of $\hat{U}$, see figure 4.3.

The regular island of the example map is elliptic and almost resonance-free. These properties suggest that harmonic oscillator eigenstates are appropriate for the semiclassical approximation of the regular eigenstates $|\psi_m\rangle$. In textbooks on quantum mechanics the 1D harmonic oscillator problem is typically solved in the normal coordinate system, where the semi-axes of the elliptic invariant tori lie parallel to the phase space axes. In our case the island is, however, tilted with respect to the q axis of the phase space and somehow stretched. By means of the aspect ratio and the tilting angle, which follow from the monodromy matrix of the corresponding classical map of $\hat{U}$, see section 3.1, it is possible to solve the tilted harmonic oscillator problem. This technical derivation is presented in appendix B for the case, where the center of the elliptic island coincides with the origin of the phase space. It yields the eigenstates $|\phi_{\mathrm{ho}}^m\rangle$. As the center of the regular

island is equal to $(0, 1/4)$ in our example, we shift $|\phi_{\mathrm{ho}}^m\rangle$ accordingly and find

$$|\psi_m^{\mathrm{sc}}\rangle = \hat{P}(\theta_q, \theta_p)\,\hat{T}(0, 1/4)|\phi_{\mathrm{ho}}^m\rangle \tag{4.58}$$

for the semiclassical approximation of the regular eigenstates of $\hat{U}$. Figure 4.5(a) shows the phase space of the example map for the considered unit cell. The phase space of the accordingly tilted harmonic oscillator is the plane $\mathbb{R}^2$. Its restriction to the same unit cell is illustrated in part (b) of the same figure. In part (c) we compare the moduli of the regular eigenstates $|\psi_m\rangle$ of the time evolution operator $\hat{U}$ with the moduli of the semiclassical eigenstates $|\psi_m^{\mathrm{sc}}\rangle$ of the tilted harmonic oscillator in position representation for $m = 0$ by $m = 2$ and $N = 100$. The modulus of their difference is shown in figure
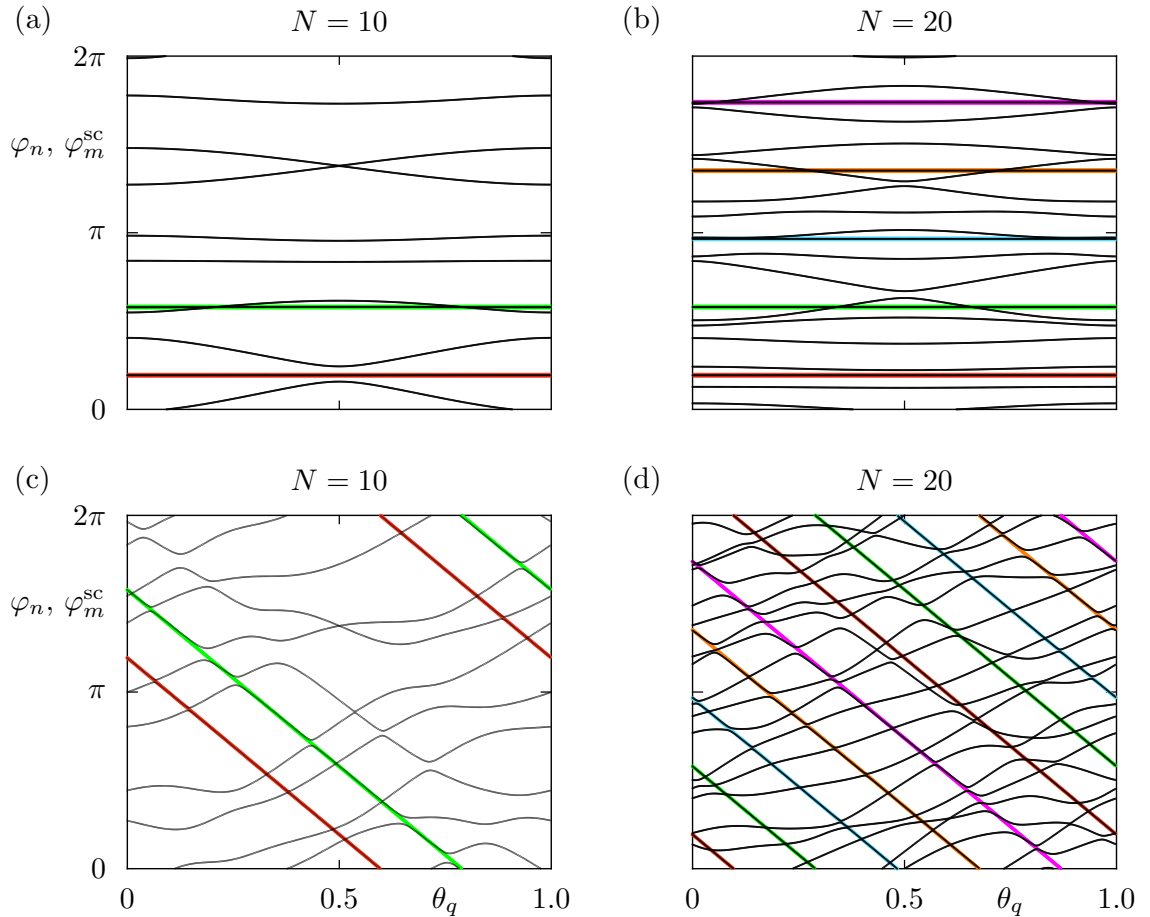
Figure 4.3: Quasi-energy spectrum of the time evolution operator $\hat{U}$ of the example map for $N = 10$ (a,c) and $N = 20$ (b,d) as a function of the Bloch phase θ_q. In contrast to figures (c) and (d), there is no regular transport in figures (a) and (b). The semiclassical prediction for the quasi-energies (4.57) is plotted with colours in the background using the following code: $m = 0$ (red), $m = 1$ (green), $m = 2$ (blue), $m = 3$ (orange), and $m = 4$ (magenta).

4.5(d). The borders of the regular island in q direction are additionally plotted. The agreement of $|\psi_m\rangle$ and $|\psi_m^{\mathrm{sc}}\rangle$ is very good within the regular region. With increasing quantum number m it becomes less good. The reason is the already noticed influence of the smoothing on the kinetic and the potential energy function in the border region of the regular island. We furthermore notice that the tails of $|\psi_m^{\mathrm{sc}}\rangle$ decrease rapidly outside the regular island.

The pair $(|\psi_m^{\mathrm{sc}}\rangle, \varphi_m^{\mathrm{sc}})$ is called quasimode [67] and the quantity

$$|\varepsilon_m\rangle \quad := \quad \hat{U}|\psi_m^{\mathrm{sc}}\rangle - \hat{\mathbb{1}}\mathrm{e}^{\mathrm{i}\varphi_m^{\mathrm{sc}}}|\psi_m^{\mathrm{sc}}\rangle \tag{4.59}$$

is the quasimode-error-vector. The accuracy of the quasimode is measured by the norm of $|\varepsilon_m\rangle$

$$\||\varepsilon_m\rangle\| \quad = \quad \left\|\hat{U}|\psi_m^{\mathrm{sc}}\rangle - \hat{\mathbb{1}}\mathrm{e}^{\mathrm{i}\varphi_m^{\mathrm{sc}}}|\psi_m^{\mathrm{sc}}\rangle\right\|, \tag{4.60}$$

the so-called quasimode error. The better the constructed quasimode is, the smaller the quasimode error becomes. In the semiclassical limit, $h_{\mathrm{eff}} \to 0$, the accuracy of the semiclassical quantities $|\psi_m^{\mathrm{sc}}\rangle$ and φ_m^{sc} becomes better. We thus expect that $\||\varepsilon_m(h_{\mathrm{eff}})\rangle\|$
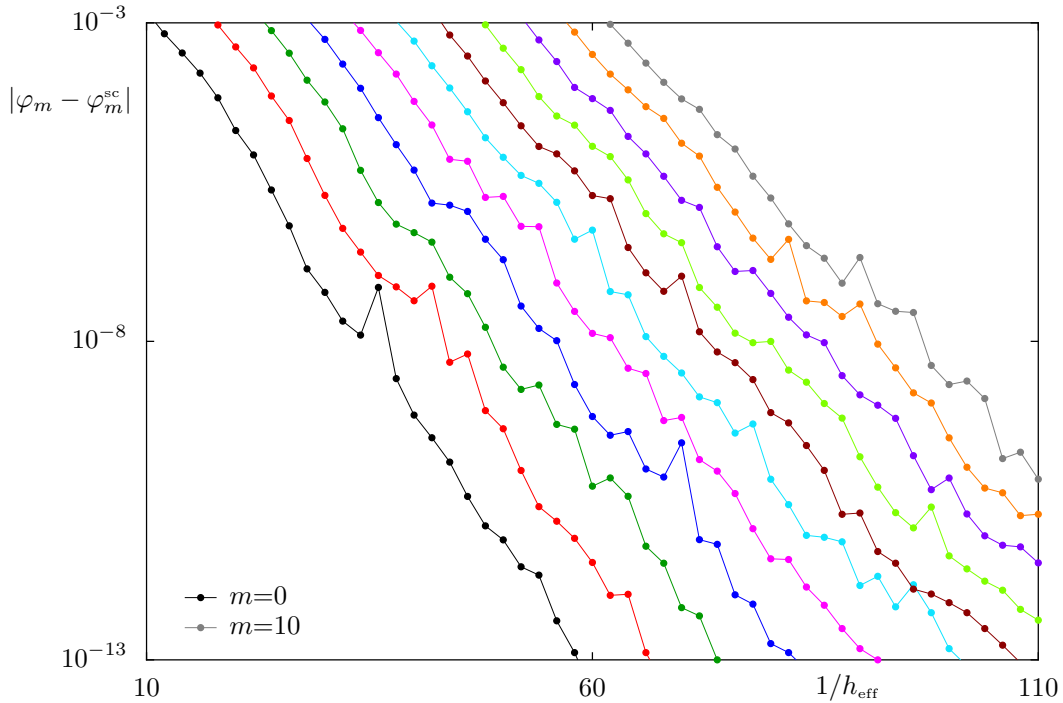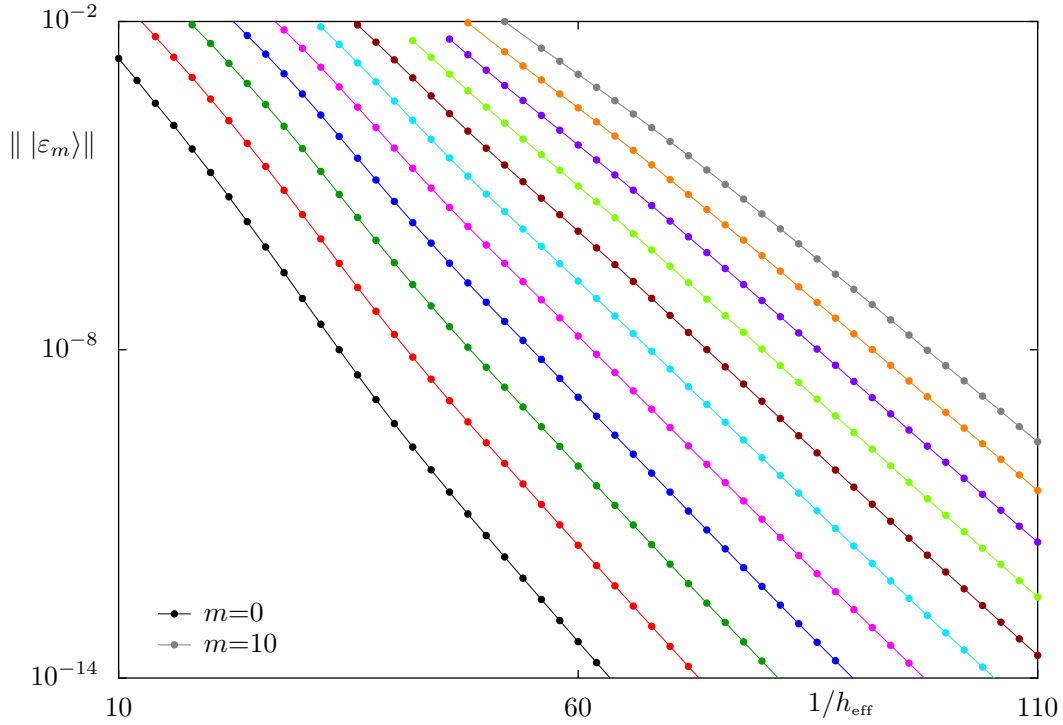

Figure 4.4: Difference $|\varphi_m - \varphi_m^{\mathrm{sc}}|$ for the quantum numbers $m = 0$ by $m = 10$ as a function of the inverse effective Planck constant evaluated for the example map. The lines are a guide to the eye.

decreases monotonically for a fixed quantum number m in this limit. Figure 4.6 confirms this expectation numerically. We used $\|f(q)\| := \sqrt{\sum_{k=0}^{N-1} |f(q_k)|^2}$ for numerical studies, where the vector f is determined in position representation on the grid (3.67).
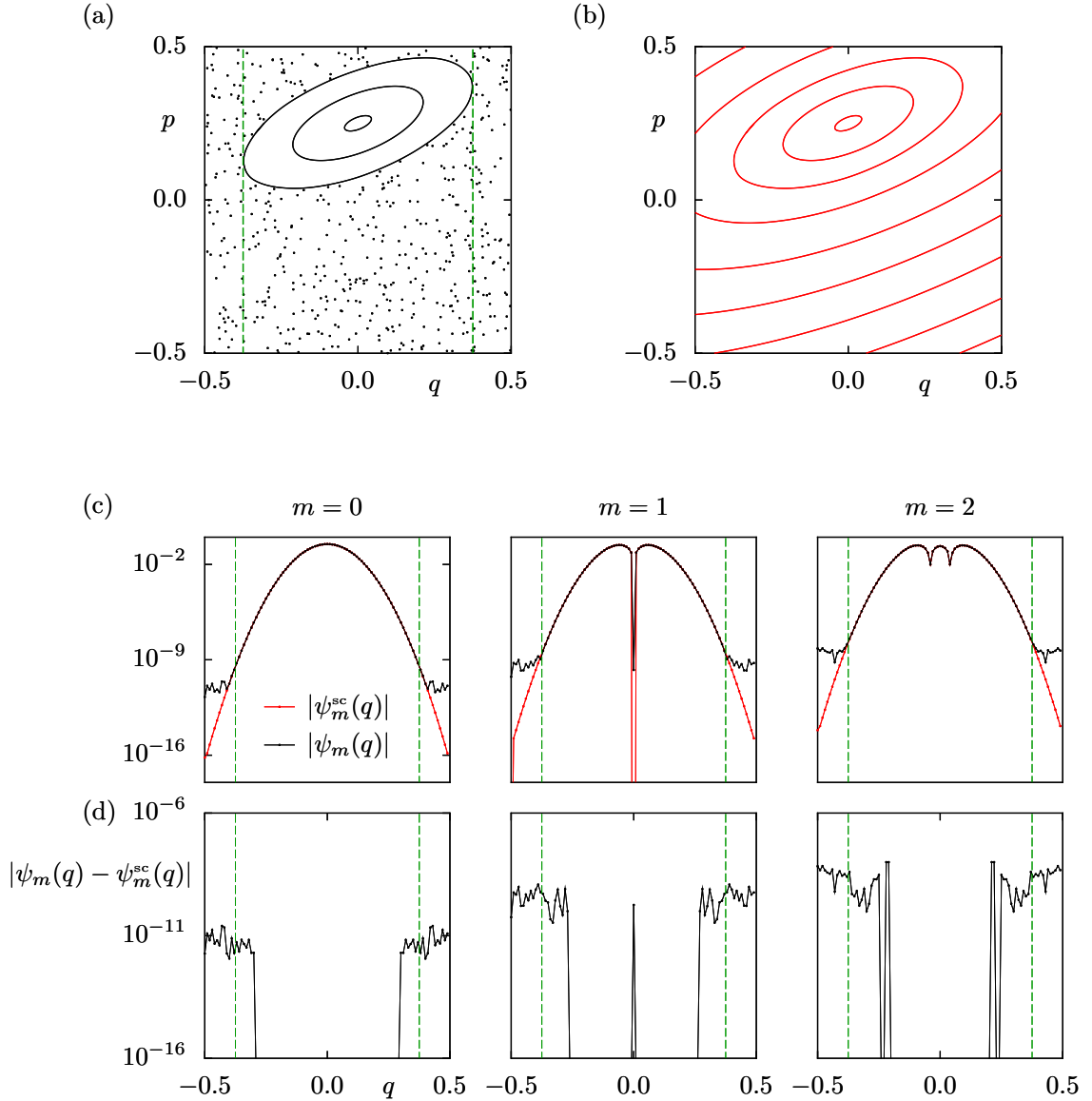
Figure 4.5: (a) Mixed phase space of the example map for one unit cell. The dashed green lines indicate the borders of the regular island in position space. (b) Phase space of the accordingly shifted and tilted harmonic oscillator restricted to the same unit cell. (c) Comparison of the regular eigenstates $|\psi_m\rangle$ of $\hat{U}$ with the corresponding tilted harmonic oscillator eigenstates $|\psi_m^{\mathrm{sc}}\rangle$ in position representation for $m = 0$ by $m = 2$. (d) Modulus of the difference of $\psi_m(q)$ and $\psi_m^{\mathrm{sc}}(q)$. The size of the Hilbert space is chosen as $N = 100$.

Figure 4.6: Quasimode error $\||\varepsilon_m\rangle\|$ for the quantum numbers $m = 0$ by $m = 10$ as a function of the inverse effective Planck constant evaluated for the example map. The lines are a guide to the eye.

Example map P_{ex} with transport

In this paragraph we want to study the example map with transport and set therefore $A = 1$. This is equal to setting $s_q = 1$, so that we obtain

$$T_L(p) \;=\; -p^2 + \left(\frac{1}{2} + 1\right) p - \frac{5}{16} \tag{4.61}$$

for the linearized kinetic energy function determined with respect to the momentum coordinate of the center of the regular island. From the comparison of equation (4.61) with (4.12) we find $a = -1$, $b = 1/2$, and $c = -5/16$. We furthermore have $d(s_q) = -(1/2)s_q^2 = -1/2$, what follows from the comparison of equation (4.11) with (3.92). From equation (4.55) we thus deduce

$$
\begin{aligned}
\varphi_m^{\text{sc}} \;\approx\; & 2\pi R_m \left(m + \frac{1}{2}\right) + 2\pi N \Big\langle T(p) - V(q) \Big\rangle_{\mathcal{C}_{0,0}^m} \\
& + \frac{3}{2}\pi N - 2\pi N - 2\pi\theta_q + 2\pi\theta_p.
\end{aligned}
\tag{4.62}
$$

As $N \in \mathbb{N}$ and $\varphi_m^{\mathrm{sc}} \in [0, 2\pi]$, the contribution $-2\pi N$ has no effect and can thus be neglected. In contrast to equation (4.57) we see a dependence on the Bloch phases θ_q and θ_p. Figures 4.3(c) and (d) show the quasi-energy spectrum φ_n of the operator $\hat{U}$ again for $N = 10$ and $N = 20$ as a function of $\theta_q \in [0, 1)$. For both values of N the Bloch phase θ_p can be chosen equal to zero according to equation (3.105), so that

$$\varphi_m^{\mathrm{sc}} \approx 2\pi R_m \left(m + \frac{1}{2} \right) + 2\pi N \Big\langle T(p) - V(q) \Big\rangle_{\mathcal{C}_{0,0}^m} + \frac{3}{2} \pi N - 2\pi \theta_q \qquad (4.63)$$

becomes the semiclassical prediction of the regular quasi-energies of $\hat{U}$. They are plotted with colours in figures 4.3(c) and (d) for all allowed quantum numbers m. We see again that, apart from avoided crossings, respectively one quasi-energy of the spectrum of $\hat{U}$ lies on the semiclassically determined curves. Besides the contribution $-2\pi\theta_q$, equation (4.63) also contains an additional phase $\varphi_{\mathrm{add}} := (3/2)\pi N$ in contrast to the corresponding formula (4.57) in the non-transporting case. As quasi-energies are defined up to integer multiples of 2π, we expect $\varphi_{\mathrm{add}} = \pi$ for $N = 10$ and $\varphi_{\mathrm{add}} = 0$ for $N = 20$. These expectations are confirmed by figures 4.3(c) and (d). Since the semiclassical approximation of the regular eigenstates of $\hat{U}$ is the same as in the non-transporting case, we finish the semiclassical approximation of a single transporting regular island of a quantum map defined on a torus at this point.

4.3 Chain of transporting regular islands on a torus

For $M_q > 1$ we now consider a system whose phase space is equal to the torus $[q_{\min}, q_{\min} + M_q] \times [p_{\min}, p_{\min} + 1]$. This phase space consists of M_q unit cells in q direction, where $q_{\min}$ is identified with $q_{\min} + M_q$, as well as $p_{\min}$ with $p_{\min} + 1$. It is assumed that each of the M_q unit cells contains one regular island and that all islands are equal. We furthermore assume a regular transport with $s_q = 1$. The M_q regular islands form thus a transporting chain with the regular transport velocity $v_{\mathrm{reg}} = 1$.

Since we have $M_q > 1$, there are M_q different regular eigenstates of the time evolution operator $\hat{U}$ for an allowed quantum number m. Their Husimi functions localize on corresponding quantizing tori within the M_q regular islands in phase space at the same time. Furthermore, these M_q Husimi functions are almost identical. In order to distinguish the M_q different regular eigenstates of the time evolution operator $\hat{U}$, which belong to the same quantum number m, we introduce a further index $k \in \mathbb{Z}_{M_q}$ and write

$$\hat{U} |\psi_k^m\rangle = \mathrm{e}^{\mathrm{i}\varphi_k^m} |\psi_k^m\rangle \qquad (4.64)$$

for the eigenvalue equation. In the following we will demonstrate how semiclassical approximations $|\psi_k^{\mathrm{sc},m}\rangle$ and $\varphi_k^{\mathrm{sc},m}$ of the eigenstates $|\psi_k^m\rangle$ and the corresponding quasi-energies φ_k^m can be found based on the results of the previous sections. They fulfill the semiclassical eigenvalue equation

$$\hat{U}\,|\psi_k^{\mathrm{sc},m}\rangle \quad \approx \quad \mathrm{e}^{\mathrm{i}\varphi_k^{\mathrm{sc},m}}\,|\psi_k^{\mathrm{sc},m}\rangle. \tag{4.65}$$

We let $\big|\tilde{\phi}_k^{\mathrm{sc},m}\big\rangle := \big|\tilde{\phi}_{k,0}^{\mathrm{sc},m}\big\rangle$ be the doubly periodized semiclassical state, whose Husimi function localizes on the mth quantizing torus $\mathcal{C}_k^m := \mathcal{C}_{k,0}^m$ in the regular island of unit cell k. The set of states $\big\{\big|\tilde{\phi}_k^{\mathrm{sc},m}\big\rangle\big\}$ with $k \in \mathbb{Z}_{M_q}$ and m extending over all allowed quantum numbers builds an approximate basis for the regular region of the torus

$$\hat{\mathbb{1}}_{\mathrm{reg}} \quad \approx \quad \sum_m \sum_{k=0}^{M_q-1} \big|\tilde{\phi}_k^{\mathrm{sc},m}\big\rangle\big\langle\tilde{\phi}_k^{\mathrm{sc},m}\big|. \tag{4.66}$$

The sum over m extends over all possible quantum numbers of regular states. Since this number depends on the effective Planck constant according to equation (4.3), we omit the limits of summation. The investigation of the example map in the previous section showed that the tails of the semiclassical states $\big|\tilde{\phi}_k^{\mathrm{sc},m}\big\rangle$ decrease rapidly outside the regular island of unit cell k. We therefore assume that the states of the set $\big\{\big|\tilde{\phi}_k^{\mathrm{sc},m}\big\rangle\big\}$ are approximately orthogonal

$$\big\langle\tilde{\phi}_k^{\mathrm{sc},m}\big|\tilde{\phi}_l^{\mathrm{sc},n}\big\rangle \quad \approx \quad \delta^{m,n}\,\delta_{k,l}. \tag{4.67}$$

The application of the time evolution operator $\hat{U}$ to the state $\big|\tilde{\phi}_k^{\mathrm{sc},m}\big\rangle$ transports it to the unit cell $(k+1)\bmod M_q$ according to equation (4.52)

$$\hat{U}\big|\tilde{\phi}_k^{\mathrm{sc},m}\big\rangle \quad \approx \quad \mathrm{e}^{\mathrm{i}\tilde{\omega}_k^{\mathrm{sc},m}}\big|\tilde{\phi}_{(k+1)\bmod M_q}^{\mathrm{sc},m}\big\rangle, \tag{4.68}$$

where we defined

$$\tilde{\omega}_k^{\mathrm{sc},m} \quad := \quad \tilde{\omega}_{k,0}^{\mathrm{sc},m} \quad = \quad \omega_{k,0}^{\mathrm{sc},m} - \frac{1}{\hbar_{\mathrm{eff}}}(k+1)^2 - 2\pi\theta_q\delta_{k,M_q-1} + 2\pi(k+1)\theta_p \tag{4.69}$$

using equation (4.53). As the set of states $\big\{\big|\tilde{\phi}_k^{\mathrm{sc},m}\big\rangle\big\}$ with $k \in \mathbb{Z}_{M_q}$ builds an approximate basis for the regular region of the torus, the M_q different semiclassical approximations $|\psi_k^{\mathrm{sc},m}\rangle$ of the regular eigenstates of $\hat{U}$ belonging to the quantum number m can be written

as a linear combination of them

$$|\psi_k^{\text{sc},m}\rangle \;:=\; \sum_{j=0}^{M_q-1} \alpha_{k,j}^m |\tilde{\phi}_j^{\text{sc},m}\rangle. \tag{4.70}$$

Since we consider a chain of equal islands, $\left|\alpha_{k,j}^m\right|^2 = 1/M_q$ follows immediately from the normalization of the eigenstates of $\hat{U}$. In order to complete the determination of the states $|\psi_k^{\text{sc},m}\rangle$, we now need to determine the expansion coefficients $\alpha_{k,j}^m$. For their derivation it is helpful to investigate the relation between the semiclassical quasi-energies $\varphi_k^{\text{sc},m}$ and the phases $\tilde{\omega}_k^{\text{sc},m}$. We will therefore focus on this relation before we will return to the determination of the expansion coefficients.

Relation between the quasi-energies $\varphi_k^{\text{sc},m}$ and the phases $\tilde{\omega}_k^{\text{sc},m}$

On the one hand the M_q-fold application of $\hat{U}$ to an approximated regular eigenstate with quantum number m yields

$$\hat{U}^{M_q} |\psi_k^{\text{sc},m}\rangle \;\overset{(4.70)}{=}\; \hat{U}^{M_q} \sum_{j=0}^{M_q-1} \alpha_{k,j}^m |\tilde{\phi}_j^{\text{sc},m}\rangle$$

$$=\; \sum_{j=0}^{M_q-1} \alpha_{k,j}^m \hat{U}^{M_q} |\tilde{\phi}_j^{\text{sc},m}\rangle \tag{4.71}$$

$$\overset{(4.68)}{\approx}\; \sum_{j=0}^{M_q-1} \alpha_{k,j}^m \exp\left(\mathrm{i} \sum_{l=0}^{M_q-1} \tilde{\omega}_l^m \right) |\tilde{\phi}_j^{\text{sc},m}\rangle. \tag{4.72}$$

On the other hand we have

$$\hat{U}^{M_q} |\psi_k^{\text{sc},m}\rangle \;\approx\; \mathrm{e}^{\mathrm{i}M_q\varphi_k^{\text{sc},m}} |\psi_k^{\text{sc},m}\rangle \tag{4.73}$$

according to equation (4.65). Comparing (4.72) with (4.73) we find

$$\varphi_k^{\text{sc},m} \;\approx\; \frac{\sum_{l=0}^{M_q-1} \tilde{\omega}_l^{\text{sc},m}}{M_q} + z_k^m \frac{2\pi}{M_q} \qquad \text{with } z_k^m \in \mathbb{Z}. \tag{4.74}$$

The parameter z_k^m can in principle be any integer number. In order to investigate, whether certain values are physically equal, we consider the matrix element of $\hat{U}^r$, $r \in \mathbb{Z}_{M_q}$, with respect to the semiclassical states belonging to the quantum number m localizing in the

unit cells $k \in \mathbb{Z}_{M_q}$ and $l \in \mathbb{Z}_{M_q}$

$$
\langle \tilde{\phi}_l^{\mathrm{sc},m} | \hat{U}^r | \tilde{\phi}_k^{\mathrm{sc},m} \rangle \stackrel{(4.68)}{\approx} \langle \tilde{\phi}_l^{\mathrm{sc},m} | \mathrm{e}^{\mathrm{i}\left(\tilde{\omega}_k^{\mathrm{sc},m} + \tilde{\omega}_{(k+1)\,\mathrm{mod}\,M_q}^{\mathrm{sc},m} + \cdots + \tilde{\omega}_{(k+r-1)\,\mathrm{mod}\,M_q}^{\mathrm{sc},m}\right)} | \tilde{\phi}_{(k+r)\,\mathrm{mod}\,M_q}^{\mathrm{sc},m} \rangle
$$

$$
\approx \mathrm{e}^{\mathrm{i}\left(\tilde{\omega}_k^{\mathrm{sc},m} + \tilde{\omega}_{(k+1)\,\mathrm{mod}\,M_q}^{\mathrm{sc},m} + \cdots + \tilde{\omega}_{(k+r-1)\,\mathrm{mod}\,M_q}^{\mathrm{sc},m}\right)} \delta_{l,(k+r)\,\mathrm{mod}\,M_q}. \tag{4.75}
$$

As the set of states $\{|\psi_k^{\mathrm{sc},m}\rangle\}$ is also an approximate basis for the regular region of the torus, we can write

$$
\langle \tilde{\phi}_l^{\mathrm{sc},m} | \hat{U}^r | \tilde{\phi}_k^{\mathrm{sc},m} \rangle \approx \sum_{j=0}^{M_q-1} \sum_n \langle \tilde{\phi}_l^{\mathrm{sc},m} | \hat{U}^r | \psi_j^{\mathrm{sc},n} \rangle \langle \psi_j^{\mathrm{sc},n} | \tilde{\phi}_k^{\mathrm{sc},m} \rangle
$$

$$
\stackrel{(4.65)}{\approx} \sum_{j=0}^{M_q-1} \sum_n \mathrm{e}^{\mathrm{i}r\varphi_j^{\mathrm{sc},n}} \langle \tilde{\phi}_l^{\mathrm{sc},m} | \psi_j^{\mathrm{sc},n} \rangle \langle \psi_j^{\mathrm{sc},n} | \tilde{\phi}_k^{\mathrm{sc},m} \rangle
$$

$$
\stackrel{(4.67),(4.70)}{\approx} \sum_{j=0}^{M_q-1} \sum_n \mathrm{e}^{\mathrm{i}r\varphi_j^{\mathrm{sc},n}} \alpha_{j,l}^m \left(\alpha_{j,k}^m\right)^* \delta^{m,n}
$$

$$
\approx \sum_{j=0}^{M_q-1} \mathrm{e}^{\mathrm{i}r\varphi_j^{\mathrm{sc},m}} \alpha_{j,l}^m \left(\alpha_{j,k}^m\right)^*. \tag{4.76}
$$

Comparing (4.75) with (4.76), we have for $l = k$, $r \in \mathbb{Z}_{M_q} \backslash \{0\}$, and $|\alpha_{j,k}^m|^2 = 1/M_q$

$$
\sum_{j=0}^{M_q-1} \left|\alpha_{j,k}^m\right|^2 \mathrm{e}^{\mathrm{i}r\varphi_j^{\mathrm{sc},m}} = 0 \quad \Rightarrow \quad \sum_{j=0}^{M_q-1} \mathrm{e}^{\mathrm{i}r\varphi_j^{\mathrm{sc},m}} = 0. \tag{4.77}
$$

Inserting equation (4.74) and taking into account that its first summand leads to a non-zero prefactor, yields

$$
\sum_{j=0}^{M_q-1} \mathrm{e}^{2\pi\mathrm{i}r z_j^m/M_q} = 0. \tag{4.78}
$$

For $r = 0$ we similarly have

$$
\sum_{j=0}^{M_q-1} \mathrm{e}^{2\pi\mathrm{i}r z_j^m/M_q} = M_q, \tag{4.79}
$$

and consequently for $t \in \mathbb{Z}_{M_q}$

$$
\sum_{r=0}^{M_q-1} \sum_{j=0}^{M_q-1} \mathrm{e}^{-2\pi\mathrm{i}r t/M_q} \mathrm{e}^{2\pi\mathrm{i}r z_j^m/M_q} = M_q. \tag{4.80}
$$

Rewriting equation (4.80) we get

$$M_q = \sum_{j=0}^{M_q-1} \left[\sum_{r=0}^{M_q-1} e^{2\pi i r/M_q(z_j^m - t)} \right] = \sum_{j=0}^{M_q-1} M_q \delta_{t,z_j^m}. \tag{4.81}$$

This yields

$$\sum_{j=0}^{M_q-1} \delta_{t,z_j^m} = 1 \tag{4.82}$$

for $t \in \mathbb{Z}_{M_q}$. Thus, for every t there exists exactly one j such that $t = z_j^m$. We have therefore, apart from permutations, $z_j^m = j$ and equation (4.74) becomes

$$\varphi_k^{\mathrm{sc},m} \approx \frac{\sum_{l=0}^{M_q-1} \tilde{\omega}_l^{\mathrm{sc},m}}{M_q} + k \frac{2\pi}{M_q}. \tag{4.83}$$

We could have taken $t \in \mathbb{N}$. But this would not have lead to new results, because quasi-energies are defined up to integer multiples of 2π. With this relation between the quasi-energies $\varphi_k^{\mathrm{sc},m}$ and the phases $\tilde{\omega}_k^{\mathrm{sc},m}$ we return to the task of determining the expansion coefficients $\alpha_{k,j}^m$, in order to complete the semiclassical approximation of the regular eigenstates of the time evolution operator $\hat{U}$.

Determination of the expansion coefficients $\alpha_{k,j}^m$

First we consider

$$
\begin{aligned}
\langle \tilde{\phi}_l^{\mathrm{sc},m} | \hat{U} | \psi_k^{\mathrm{sc},m} \rangle \;&\overset{(4.65)}{\approx}\; e^{i\varphi_k^{\mathrm{sc},m}} \langle \tilde{\phi}_l^{\mathrm{sc},m} | \psi_k^{\mathrm{sc},m} \rangle \\
&\overset{(4.70)}{=}\; e^{i\varphi_k^{\mathrm{sc},m}} \sum_{r=0}^{M_q-1} \alpha_{k,r}^m \langle \tilde{\phi}_l^{\mathrm{sc},m} | \tilde{\phi}_r^m \rangle \\
&\overset{(4.67)}{\approx}\; e^{i\varphi_k^{\mathrm{sc},m}} \sum_{r=0}^{M_q-1} \alpha_{k,r}^m \delta_{l,r} \\
&=\; e^{i\varphi_k^{\mathrm{sc},m}} \alpha_{k,l}^m.
\end{aligned}
\tag{4.84}
$$

But we also have for $l \neq 0$

$$\langle \tilde{\phi}_l^{\mathrm{sc},m} | \hat{U} | \psi_k^{\mathrm{sc},m} \rangle \;\overset{(4.66)}{\approx}\; \sum_n \sum_{r=0}^{M_q-1} \langle \tilde{\phi}_l^{\mathrm{sc},m} | \hat{U} | \tilde{\phi}_r^{\mathrm{sc},n} \rangle \langle \tilde{\phi}_r^{\mathrm{sc},n} | \psi_k^{\mathrm{sc},m} \rangle \tag{4.85}$$

Using equation (4.68) yields

$$
\begin{aligned}
\langle \tilde{\phi}_l^{\mathrm{sc},m} | \hat{U} | \psi_k^{\mathrm{sc},m} \rangle \quad &\approx \quad \sum_{n=0}^{M_q-1} \sum_{r=0}^{M_q-1} \mathrm{e}^{\mathrm{i}\tilde{\omega}_r^{\mathrm{sc},n}} \langle \tilde{\phi}_l^{\mathrm{sc},m} | \tilde{\phi}_{(r+1)\,\mathrm{mod}\,M_q}^{\mathrm{sc},n} \rangle \langle \tilde{\phi}_r^{\mathrm{sc},n} | \psi_k^{\mathrm{sc},m} \rangle \\[2mm]
&\overset{(4.67),(4.70)}{=} \quad \sum_{r=0}^{M_q-1} \mathrm{e}^{\mathrm{i}\tilde{\omega}_r^{\mathrm{sc},m}} \langle \tilde{\phi}_l^{\mathrm{sc},m} | \tilde{\phi}_{(r+1)\,\mathrm{mod}\,M_q}^{\mathrm{sc},m} \rangle \alpha_{k,r}^m \\[2mm]
&\overset{(4.67)}{\approx} \quad \sum_{r=0}^{M_q-1} \mathrm{e}^{\mathrm{i}\tilde{\omega}_r^{\mathrm{sc},m}} \alpha_{k,r}^m \delta_{l,(r+1)\,\mathrm{mod}\,M_q}^m \\[2mm]
&\overset{l\neq 0}{=} \quad \sum_{r=0}^{M_q-1} \mathrm{e}^{\mathrm{i}\tilde{\omega}_r^{\mathrm{sc},m}} \alpha_{k,r}^m \delta_{l,r+1} \\[2mm]
&= \quad \sum_{r=0}^{M_q-1} \mathrm{e}^{\mathrm{i}\tilde{\omega}_r^{\mathrm{sc},m}} \alpha_{k,r}^m \delta_{r,l-1} \\[2mm]
&= \quad \mathrm{e}^{\mathrm{i}\tilde{\omega}_{l-1}^{\mathrm{sc},m}} \alpha_{k,l-1}^m.
\end{aligned}
\tag{4.86}
$$

From the comparison of equations (4.84) and (4.86) we derive a recursion relation for the expansion coefficients

$$
\alpha_{k,l+1}^m \quad = \quad \mathrm{e}^{\mathrm{i}\left(\tilde{\omega}_l^{\mathrm{sc},m} - \varphi_k^{\mathrm{sc},m}\right)} \alpha_{k,l}^m.
\tag{4.87}
$$

Since $\left|\alpha_{k,l}^m\right|^2 = 1/M_q$, we can define

$$
\alpha_{k,0}^m \quad := \quad \frac{1}{\sqrt{M_q}},
\tag{4.88}
$$

apart from an irrelevant global phase. With this we find

$$
\alpha_{k,j}^m \quad = \quad \frac{1}{\sqrt{M_q}} \exp\left(\mathrm{i} \left[\sum_{r=0}^{j-1} \tilde{\omega}_r^{\mathrm{sc},m} - j\varphi_k^{\mathrm{sc},m} \right] \right)
\tag{4.89}
$$

for $j = 1$ by $j = M_q - 1$. Now we insert equation (4.83) into (4.89)

$$
\alpha_{k,j}^m \quad = \quad \frac{1}{\sqrt{M_q}} \exp\left(\mathrm{i} \left[\sum_{r=0}^{j-1} \tilde{\omega}_r^{\mathrm{sc},m} - \frac{j}{M_q} \sum_{r=0}^{M_q-1} \tilde{\omega}_r^{\mathrm{sc},m} - jk\frac{2\pi}{M_q} \right] \right).
\tag{4.90}
$$

From this we obtain

$$
\begin{aligned}
\alpha_{k,j}^m \;=\; & \frac{1}{\sqrt{M_q}} \exp\left(\mathrm{i} \left[\sum_{r=0}^{j-1} (\tilde{\omega}_r^{\mathrm{sc},m} - \tilde{\omega}_0^{\mathrm{sc},m}) - \frac{j}{M_q} \sum_{r=0}^{M_q-1} (\tilde{\omega}_r^{\mathrm{sc},m} - \tilde{\omega}_0^{\mathrm{sc},m}) \right] \right) \\
& \cdot \exp\left(-\mathrm{i} j k \frac{2\pi}{M_q} \right) \exp\left(\mathrm{i} \left[\underbrace{ \sum_{r=0}^{j-1} \tilde{\omega}_0^{\mathrm{sc},m} - \frac{j}{M_q} \sum_{r=0}^{M_q-1} \tilde{\omega}_0^{\mathrm{sc},m} }_{=0} \right] \right) \\
\;=\; & \frac{1}{\sqrt{M_q}} \exp\left(\mathrm{i} \left[\sum_{r=0}^{j-1} (\tilde{\omega}_r^{\mathrm{sc},m} - \tilde{\omega}_0^{\mathrm{sc},m}) - \frac{j}{M_q} \sum_{r=0}^{M_q-1} (\tilde{\omega}_r^{\mathrm{sc},m} - \tilde{\omega}_0^{\mathrm{sc},m}) - j k \frac{2\pi}{M_q} \right] \right) . \quad (4.91)
\end{aligned}
$$

We realize that the expansion coefficients $\alpha_{k,j}^m$ depend on the phase differences $\tilde{\omega}_r^{\mathrm{sc},m} - \tilde{\omega}_0^{\mathrm{sc},m}$, only. Let us rewrite this difference. We start with the non-periodized state

$$
\left| \phi_{r_q,r_p}^{\mathrm{sc},m} \right\rangle \;:=\; \hat{T}(r_q,0)\,\hat{T}(0,r_p) \left| \phi_{0,0}^{\mathrm{sc},m} \right\rangle . \quad (4.92)
$$

The application of $\hat{U}$ to this state yields

$$
\hat{U} \left| \phi_{r_q,r_p}^{\mathrm{sc},m} \right\rangle \;\approx\; \mathrm{e}^{\mathrm{i}\omega_{r_q,r_p}^{\mathrm{sc},m}} \left| \phi_{r_q+1,r_p+r_q+1}^{\mathrm{sc},m} \right\rangle \quad (4.93)
$$

according to equation (4.14) with $s_q = 1$. Let us now consider the application more precisely

$$
\begin{aligned}
\hat{U} \left| \phi_{r_q,r_p}^{\mathrm{sc},m} \right\rangle \;\overset{(4.92)}{=}\;\; & \hat{U}\,\hat{T}(r_q,0)\,\hat{T}(0,r_p) \left| \phi_{0,0}^{\mathrm{sc},m} \right\rangle \\
\overset{(3.25)}{=}\;\; & \mathrm{e}^{-\frac{\mathrm{i}}{\hbar_{\mathrm{eff}}}V(\hat{q})}\, \mathrm{e}^{-\frac{\mathrm{i}}{\hbar_{\mathrm{eff}}}T(\hat{p})}\, \hat{T}(r_q,0)\,\hat{T}(0,r_p) \left| \phi_{0,0}^{\mathrm{sc},m} \right\rangle \\
=\;\; & \hat{T}(r_q,0)\,\hat{T}(0,r_p)\, \mathrm{e}^{-\frac{\mathrm{i}}{\hbar_{\mathrm{eff}}}V(\hat{q}+r_q\hat{\mathbb{1}})}\, \mathrm{e}^{-\frac{\mathrm{i}}{\hbar_{\mathrm{eff}}}T(\hat{p}+r_p\hat{\mathbb{1}})} \left| \phi_{0,0}^{\mathrm{sc},m} \right\rangle \\
\overset{(4.10),(4.11)}{=}\;\; & \hat{T}(r_q,0)\,\hat{T}(0,r_p)\mathrm{e}^{-\frac{\mathrm{i}}{\hbar_{\mathrm{eff}}}V(\hat{q})}\, \mathrm{e}^{\frac{\mathrm{i}}{\hbar_{\mathrm{eff}}}r_q\hat{q}}\, \mathrm{e}^{-\frac{\mathrm{i}}{\hbar_{\mathrm{eff}}}d(r_q)}\, \mathrm{e}^{-\frac{\mathrm{i}}{\hbar_{\mathrm{eff}}}T(\hat{p})} \left| \phi_{0,0}^{\mathrm{sc},m} \right\rangle \\
=\;\; & \mathrm{e}^{-\frac{\mathrm{i}}{\hbar_{\mathrm{eff}}}d(r_q)}\, \hat{T}(r_q,0)\,\hat{T}(0,r_p)\mathrm{e}^{-\frac{\mathrm{i}}{\hbar_{\mathrm{eff}}}V(\hat{q})}\, \hat{T}(0,r_q)\, \mathrm{e}^{-\frac{\mathrm{i}}{\hbar_{\mathrm{eff}}}T(\hat{p})} \left| \phi_{0,0}^{\mathrm{sc},m} \right\rangle \\
=\;\; & \mathrm{e}^{-\frac{\mathrm{i}}{\hbar_{\mathrm{eff}}}d(r_q)}\, \hat{T}(r_q,0)\,\hat{T}(0,r_p)\,\hat{T}(0,r_q)\mathrm{e}^{-\frac{\mathrm{i}}{\hbar_{\mathrm{eff}}}V(\hat{q})}\, \mathrm{e}^{-\frac{\mathrm{i}}{\hbar_{\mathrm{eff}}}T(\hat{p})} \left| \phi_{0,0}^{\mathrm{sc},m} \right\rangle \\
\overset{(3.25)}{=}\;\; & \mathrm{e}^{-\frac{\mathrm{i}}{\hbar_{\mathrm{eff}}}d(r_q)}\, \hat{T}(r_q,0)\,\hat{T}(0,r_p+r_q)\, \hat{U} \left| \phi_{0,0}^{\mathrm{sc},m} \right\rangle \\
\overset{(4.93)}{\approx}\;\; & \mathrm{e}^{-\frac{\mathrm{i}}{\hbar_{\mathrm{eff}}}d(r_q)}\, \hat{T}(r_q,0)\,\hat{T}(0,r_p+r_q)\, \mathrm{e}^{\mathrm{i}\omega_{0,0}^{\mathrm{sc},m}} \left| \phi_{1,1}^{\mathrm{sc},m} \right\rangle \\
\overset{(4.92)}{=}\;\; & \mathrm{e}^{\mathrm{i}\omega_{0,0}^{\mathrm{sc},m}}\, \mathrm{e}^{-\frac{\mathrm{i}}{\hbar_{\mathrm{eff}}}d(r_q)}\, \hat{T}(r_q,0)\,\hat{T}(0,r_p+r_q) \\
& \cdot \hat{T}(1,0)\,\hat{T}(0,1) \left| \phi_{0,0}^{\mathrm{sc},m} \right\rangle \quad (4.94)
\end{aligned}
$$

Using equations (3.31) and (3.33) leads to

$$
\begin{aligned}
\hat{U}\big|\phi^{\mathrm{sc},m}_{r_q,r_p}\big\rangle &= \mathrm{e}^{\mathrm{i}\omega^{\mathrm{sc},m}_{0,0}}\mathrm{e}^{-\frac{\mathrm{i}}{\hbar_{\mathrm{eff}}}d(r_q)} \\
&\quad \cdot \hat{T}(r_q,0)\,\mathrm{e}^{\frac{\mathrm{i}}{\hbar_{\mathrm{eff}}}(r_q+r_p)}\,\hat{T}(1,0)\,\hat{T}(0,r_p+r_q)\,\hat{T}(0,1)\big|\phi^{\mathrm{sc},m}_{0,0}\big\rangle \\
&= \mathrm{e}^{\mathrm{i}\omega^{\mathrm{sc},m}_{0,0}}\mathrm{e}^{-\frac{\mathrm{i}}{\hbar_{\mathrm{eff}}}d(r_q)}\mathrm{e}^{\frac{\mathrm{i}}{\hbar_{\mathrm{eff}}}(r_q+r_p)} \\
&\quad \hat{T}(r_q+1,0)\,\hat{T}(0,r_p+r_q+1)\big|\phi^{\mathrm{sc},m}_{0,0}\big\rangle \\
&\overset{(4.92)}{=} \mathrm{e}^{\mathrm{i}\left[\omega^{\mathrm{sc},m}_{0,0}+\frac{r_p}{\hbar_{\mathrm{eff}}}+\frac{r_q}{\hbar_{\mathrm{eff}}}-\frac{1}{\hbar_{\mathrm{eff}}}d(r_q)\right]}\big|\phi^{\mathrm{sc},m}_{r_q+1,r_p+r_q+1}\big\rangle.
\end{aligned}
\tag{4.95}
$$

From the comparison of equations (4.95) and (4.93) we deduce

$$
\omega^{\mathrm{sc},m}_{r_q,r_p} = \omega^{\mathrm{sc},m}_{0,0} + \frac{1}{\hbar_{\mathrm{eff}}}\big(r_p + r_q - d(r_q)\big).
\tag{4.96}
$$

Using this result and equation (4.69) we get

$$
\begin{aligned}
\tilde{\omega}^{\mathrm{sc},m}_k &= \omega^{\mathrm{sc},m}_{0,0} - \frac{1}{\hbar_{\mathrm{eff}}}\big(k^2+k+d(k)+1\big) - 2\pi\theta_q\delta_{k,M_q-1} + 2\pi(k+1)\theta_p \\
&\overset{(4.33)}{=} 2\pi R_m\left(m+\frac{1}{2}\right) + \frac{1}{\hbar_{\mathrm{eff}}}\big\langle T(p)-V(q)\big\rangle_{\mathcal{C}^m_0} \\
&\quad - \frac{1}{\hbar_{\mathrm{eff}}}\left[b\big\langle p\big\rangle_{\mathcal{C}^m_0} + \big\langle p\big\rangle_{\mathcal{C}^m_0} - \big\langle q\big\rangle_{\mathcal{C}^m_0} + d(1) + 2c\right] \\
&\quad - \frac{1}{\hbar_{\mathrm{eff}}}\big(k^2+k+d(k)+1\big) - 2\pi\theta_q\delta_{k,M_q-1} + 2\pi(k+1)\theta_p \\
&\overset{(3.54)}{=} 2\pi R_m\left(m+\frac{1}{2}\right) + \frac{2\pi N}{M_q}\big\langle T(p)-V(q)\big\rangle_{\mathcal{C}^m_0} \\
&\quad - \frac{2\pi N}{M_q}\left[b\big\langle p\big\rangle_{\mathcal{C}^m_0} + \big\langle p\big\rangle_{\mathcal{C}^m_0} - \big\langle q\big\rangle_{\mathcal{C}^m_0} + d(1) + 2c\right] \\
&\quad - \frac{2\pi N}{M_q}\big(k^2+k+d(k)+1\big) - 2\pi\theta_q\delta_{k,M_q-1} + 2\pi(k+1)\theta_p
\end{aligned}
\tag{4.97}
$$

and the difference

$$
\begin{aligned}
\tilde{\omega}^{\mathrm{sc},m}_k - \tilde{\omega}^{\mathrm{sc},m}_0 &= -\frac{1}{\hbar_{\mathrm{eff}}}\big(k^2+k+d(k)-d(0)\big) \\
&\quad - 2\pi\theta_q\delta_{k,M_q-1} + 2\pi k\theta_p \\
&\overset{(3.54)}{=} -\frac{2\pi N}{M_q}\big(k^2+k+d(k)-d(0)\big) \\
&\quad - 2\pi\theta_q\delta_{k,M_q-1} + 2\pi k\theta_p.
\end{aligned}
\tag{4.98}
$$

After the insertion of equation (4.98) into (4.91) we know the expansion coefficients $\alpha^m_{k,j}$. Their insertion into equation (4.70) completes the semiclassical approximation of the

regular eigenstates $|\psi_k^m\rangle$ of the time evolution operator $\hat{U}$. Using formula (4.97) for the phases $\tilde{\omega}_k^{\mathrm{sc},m}$ we get a semiclassical approximation of the corresponding quasi-energies φ_k^m by inserting it into equation (4.83).

As the formulae for the difference $\tilde{\omega}_k^{\mathrm{sc},m} - \tilde{\omega}_0^{\mathrm{sc},m}$ and for the phase $\tilde{\omega}_k^{\mathrm{sc},m}$ depend on the function $d(k)$, which appears in the relation (4.11), we cannot write down an explicit expression for the quasimode $(|\psi_k^{\mathrm{sc},m}\rangle, \varphi_k^{\mathrm{sc},m})$. In the following we will consider the example map P_{ex} for the standard parameters $r = 0.65$, $s = 2.0$, $\varepsilon = 0.015$ and $A = s_q = 1$. There we have $d(k) = -(1/2)k^2$.

Application to example map P_{ex}

The analytical evaluation of formula (4.83) yields

$$
\begin{aligned}
\varphi_k^{\mathrm{sc},m} \approx\ & 2\pi R_m \left(m + \frac{1}{2} \right) + \frac{2\pi N}{M_q} \Big\langle T(p) - V(q) \Big\rangle_{\mathcal{C}_0^m} \\
& -\frac{2N\pi}{M_q} \left(b \big\langle p \big\rangle_{\mathcal{C}_0^m} + \big\langle p \big\rangle_{\mathcal{C}_0^m} - \big\langle q \big\rangle_{\mathcal{C}_0^m} - \frac{1}{2} + 2c \right) \\
& -\frac{N\pi}{6M_q} (7 + 3M_q + 2M_q^2) \\
& + k\frac{2\pi}{M_q} - \frac{2\pi}{M_q}\theta_q + (M_q + 1)\pi\theta_p
\end{aligned}
\tag{4.99}
$$

and the expansion coefficients (4.91) become

$$
\begin{aligned}
\alpha_{k,j}^m =\ & \frac{1}{\sqrt{M_q}} \exp\left(\mathrm{i}\frac{j\pi N}{6M_q}(M_q - j)(2M_q + 2j + 3) \right) \\
& \cdot \exp\left(\mathrm{i}\pi j \left[\frac{2}{M_q}(\theta_q - k) + (j - M_q)\theta_p \right] \right).
\end{aligned}
\tag{4.100}
$$

The latter are required for the determination of the semiclassical approximation (4.70)

$$
|\psi_k^{\mathrm{sc},m}\rangle = \sum_{j=0}^{M_q-1} \alpha_{k,j}^m |\tilde{\phi}_j^{\mathrm{sc},m}\rangle
\tag{4.101}
$$

of the regular eigenstate $|\psi_k^m\rangle$. As the center of the regular island in the jth unit cell is equal to $(j, 1/4)$, we use

$$
|\tilde{\phi}_j^{\mathrm{sc},m}\rangle = \hat{P}(\theta_q, \theta_p)\,\hat{T}(j, 1/4)|\phi_{\mathrm{ho}}^m\rangle,
\tag{4.102}
$$

where $|\phi_{\mathrm{ho}}^m\rangle$ is again the mth eigenstate of an accordingly squeezed and tilted harmonic oscillator, whose center is equal to $(0, 0)$.

Since the averages in formula (4.99) are performed in the unit cell 0, we can use the parameters $b = 1/2$ and $c = -5/16$ as in the example in the previous section, which deals with a single transporting regular island. We then obtain

$$
\begin{aligned}
\varphi_k^{\mathrm{sc},m} \;=\; & 2\pi R_m \left(m + \frac{1}{2} \right) + \frac{2\pi N}{M_q} \Big\langle T(p) - V(q) \Big\rangle_{\mathcal{C}_0^m} \\
& + \frac{3N\pi}{2M_q} - \frac{N\pi}{6M_q} \left(7 + 3M_q + 2M_q^2 \right) \\
& + k\frac{2\pi}{M_q} - \frac{2\pi}{M_q}\,\theta_q + (M_q + 1)\pi\theta_p.
\end{aligned}
\tag{4.103}
$$

Apart from an irrelevant phase $-2N\pi$, this formula reduces to equation (4.62) for $M_q = 1$. Let us consider $M_q = 5$ and the Hilbert space size $N = 48$, where we have $h_{\mathrm{eff}} = 5/48$. As the regular island in each of the five unit cells has a relative area $A_{\mathrm{reg}} = 0.215$, the maximum quantum number is $m_{\max} = 1$ according to equation (4.3). Figure 4.10 shows the quasi-energy spectrum φ_n of the corresponding time evolution operator $\hat{U}$ as a function of $\theta_q \in [0, 1)$. The choice $\theta_p = 0$ is appropriate according to equation (3.105). The semiclassical regular quasi-energies (4.103) are plotted for $k = 0$ by $k = 4$ with colours in the background. We notice that respectively one quasi-energy of the spectrum of $\hat{U}$ lies on them apart from avoided crossings. Since numerical studies showed the same good accuracy of the quasimodes as in the case of one unit cell, we omit their discussion here.

As a final numerical test we consider the case $M_q = 5$ and $N = 198$ which yields $h_{\mathrm{eff}} = 5/198$. According to equation (4.3) we expect $m_{\max} = 7$. Figure 4.7 shows the square of the modulus of one of the respective five regular eigenstates $|\psi_k^m\rangle$ of $\hat{U}$ for $m = 0$ by $m_{\max} = 7$ in position representation. In figure 4.8 we illustrate the Husimi functions of the same states on a 1000×200 grid. The Husimi functions of the corresponding semiclassical states $|\psi_k^{\mathrm{sc},m}\rangle$ are shown in figure 4.9. We notice that the Husimi function of a regular eigenstate of $\hat{U}$ localizes on corresponding quantizing tori in all unit cells at the same time. The visible chaotic admixtures are a consequence of couplings with chaotic eigenstates of $\hat{U}$. Apart from these chaotic components, the comparison of the Husimi functions of the actual eigenstates $|\psi_k^m\rangle$ and their semiclassical approximations $|\psi_k^{\mathrm{sc},m}\rangle$ show a good agreement.
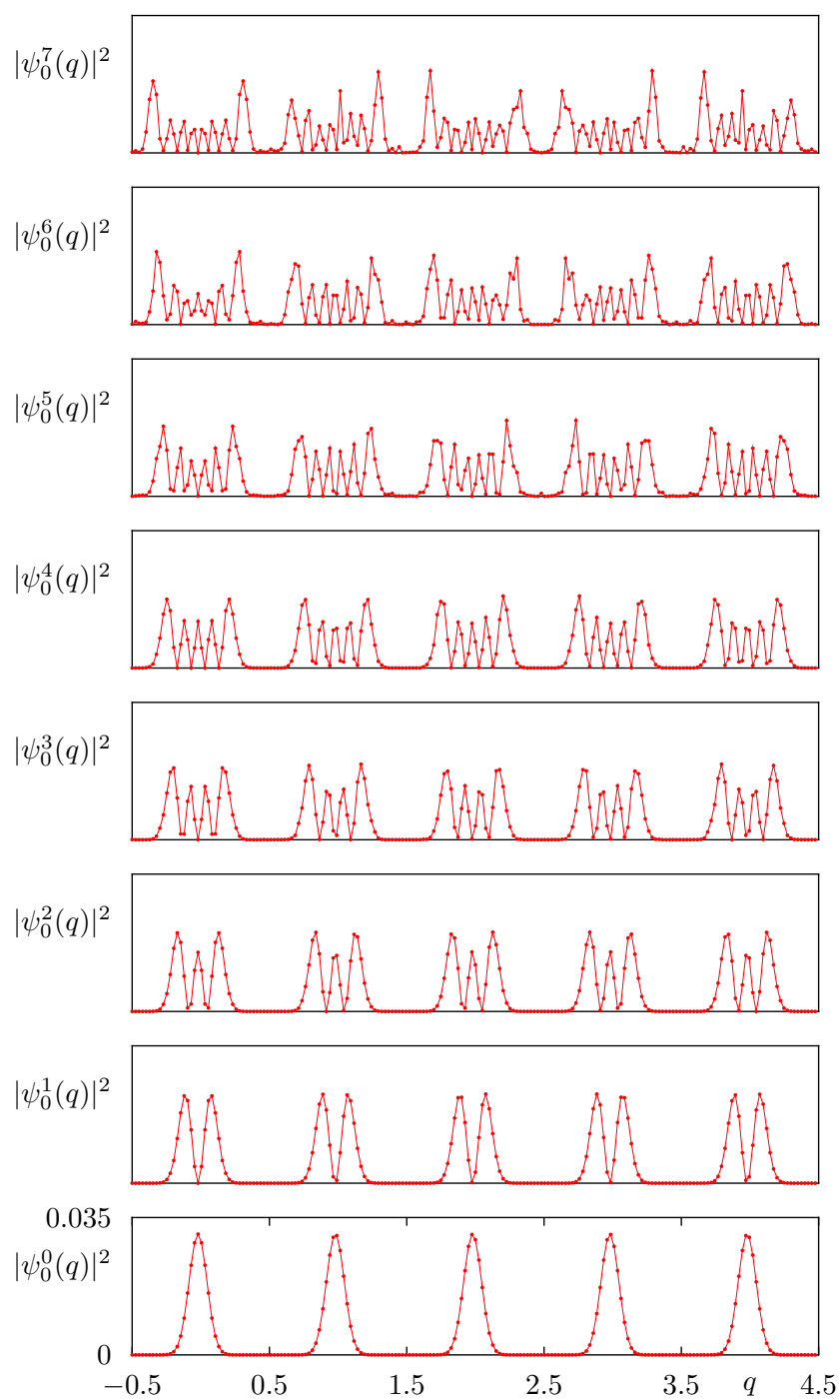
Figure 4.7: Square of the modulus of respectively one regular eigenstate $|\psi_k^m\rangle$ of $\hat{U}$ with $k = 0$ belonging to the quantum numbers $m = 0$ by $m_{\max} = 7$ in position representation for $M_q = 5$ and $N = 198$. The eigenstates are determined on the q grid given by equation (3.96). Successive discrete data points are connected by a line as a guide to the eye.
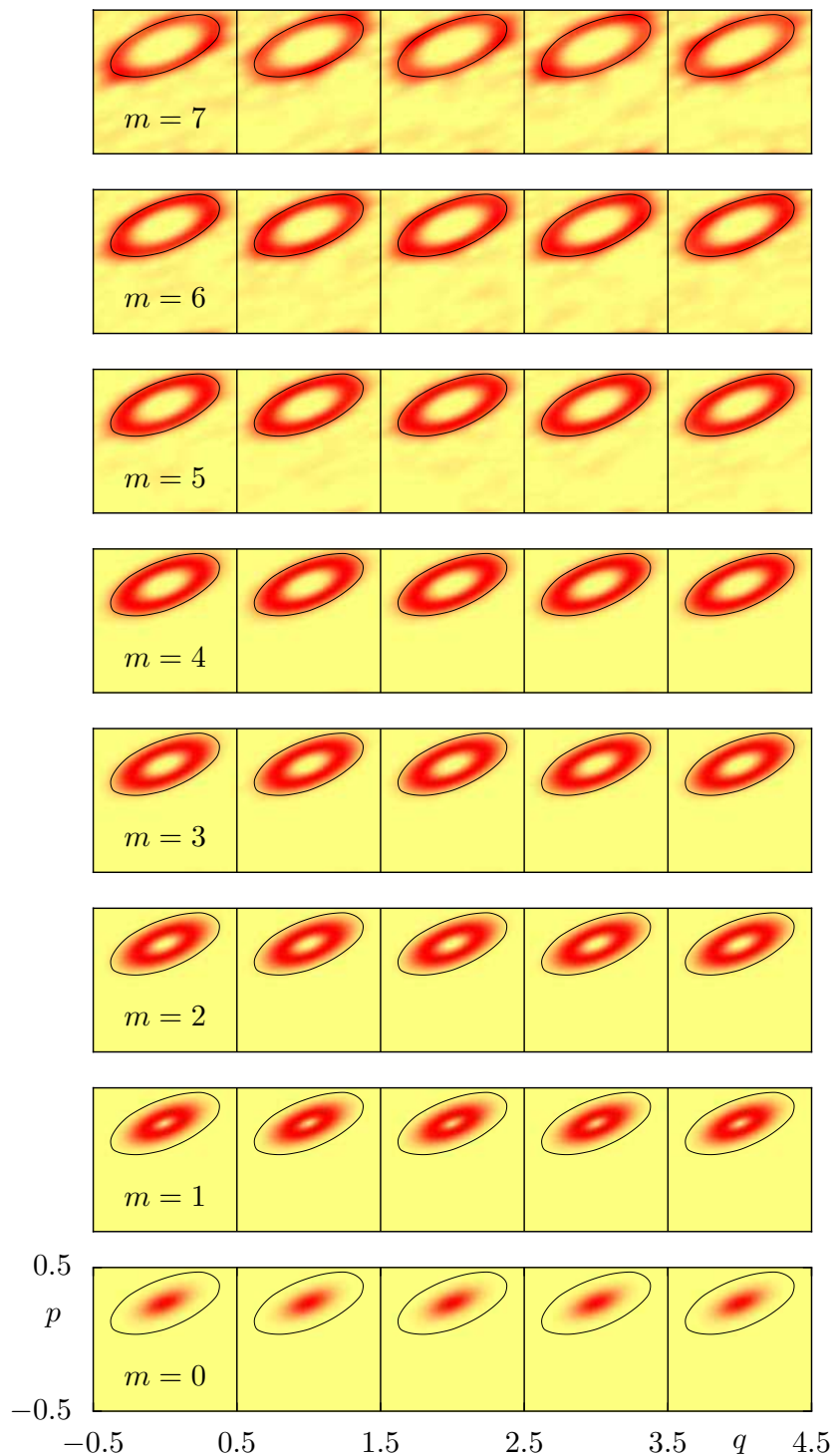
Figure 4.8: Husimi functions of the regular states $|\psi_k^m\rangle$ shown in figure 4.7. The approximate border of the regular island in each unit cell is additionally plotted as a guide to the eye.
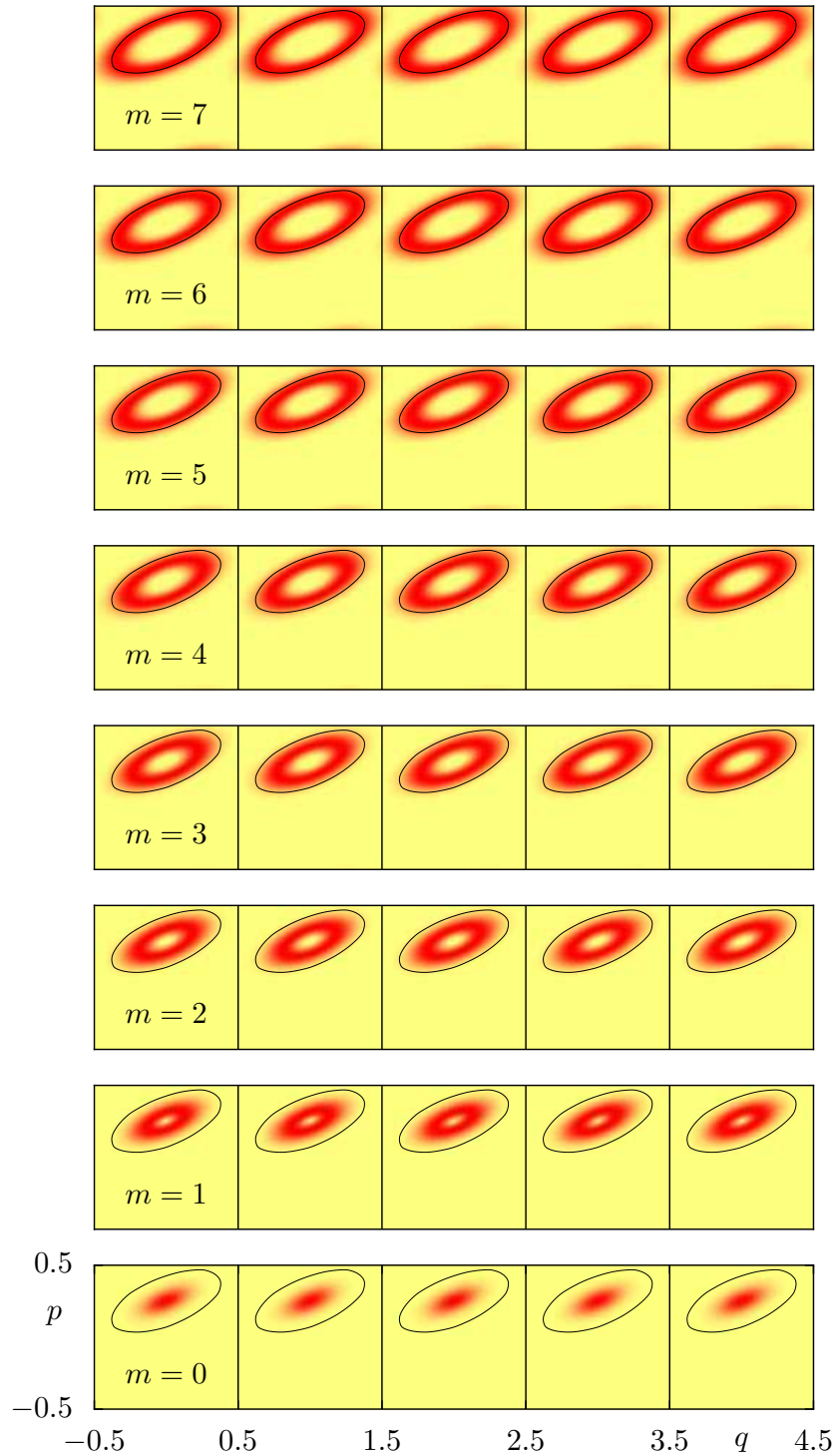
Figure 4.9: Husimi functions of the semiclassical approximations $\left|\psi_k^{\mathrm{sc},m}\right\rangle$ of the regular states shown in figure 4.7. The approximate border of the regular island in each unit cell is additionally plotted as a guide to the eye.
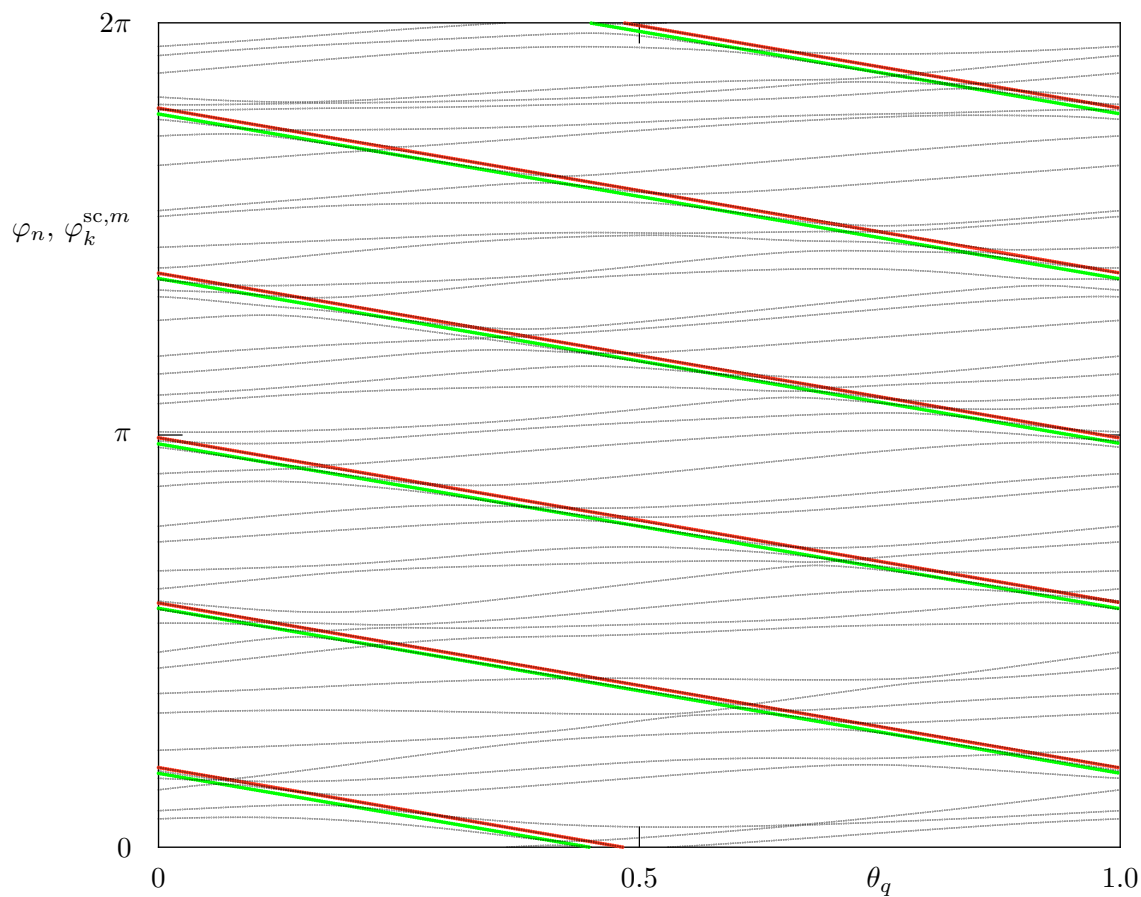
Figure 4.10: Quasi-energy spectrum φ_n of the time evolution operator $\hat{U}$ of the example map versus the Bloch phase θ_q for $N = 48$ and $M_q = 5$. The semiclassical approximation (4.103) is plotted in red for $m = 0$ and in green for $m = 1$. As $M_q = 5$, there are respectively five semiclassical curves $\varphi_k^{\mathrm{sc},m}$ for each value of the quantum number m according to $k = 0$ by $k = 4$.

5 Direct dynamical tunneling

In chapter 2 we recalled 1D tunneling through a static potential energy barrier. The concept of tunneling can be generalized to any classically forbidden transition between distinct phase space regions. Generic time dependent 1D Hamiltonian systems have a mixed phase space, where regular islands coexist with the chaotic sea [9]. An orbit, whose initial point is inside of a regular island, will never leave it. Similarly, the iterates of an orbit started in the chaotic sea cannot enter the regular phase space part. Transitions between a regular island and the chaotic sea are thus classically inhibited by a so-called dynamically generated barrier in contrast to a static insurmountable potential energy barrier in the 1D case. Quantum mechanically, transitions between these distinct phase space regions are allowed. Davis and Heller called them dynamical tunneling [4] due to the dynamically generated barrier. Dynamical tunneling has recently been observed experimentally by using cold atoms which propagate in periodically modulated optical lattices [5, 6].

The semiclassical study of dynamical tunneling between two distinct regular islands in phase space has attracted much attention in recent years by means of the chaos-assisted tunneling approach [10, 11]. Resonance island chains always appear within regular islands as an effect of non-linear perturbations. If they are resolvable by the effective Planck constant, they influence dynamical tunneling rates. The resonance assisted tunneling theory has investigated this influence and has provided semiclassical formulae which allow for the analytical determination of dynamical tunneling rates [26–29]. Its basic assumption is that a regular state is coupled via other regular states of the same island to the chaotic sea.

Numerical studies have shown that dynamical tunneling also takes place when resonance island chains cannot be resolved by the effective Planck constant. The resonance-assisted tunneling theory obviously fails to explain this, so that another dynamical tunneling process exists in addition to the resonance-assisted one. We will call it direct dynamical tunneling process in the following, because it couples a regular state directly, i.e. without other regular states, to the chaotic sea. A first approach to the understanding of direct dynamical tunneling was presented by Podolskiy and Narimanov in reference [33]. It is, however, only applicable to the regular ground state of an island. Furthermore, it fails to

explain our numerical results in the semiclassical limit.

In this chapter we consider direct dynamical tunneling in a phase space which contains one almost resonance-free regular island embedded in the chaotic sea. In section 5.1 we present the derivation of a new approach to the theoretical understanding of direct dynamical tunneling from a regular island to the surrounding chaotic sea. The result of this derivation is a formula which allows for the determination of direct dynamical tunneling rates for all regular states of an island irrespective of its shape. In order to investigate the accuracy of this formula, we evaluate it for a special class of kicked systems in section 5.2 and present its application to examples in section 5.3. A comparison with numerically determined tunneling rates is shown. Finally, two methods for the numerical determination of dynamical tunneling rates are presented in section 5.4.

5.1 A new approach

A mixed phase space contains regular islands which are embedded in the chaotic sea. As we are interested in direct dynamical tunneling from a regular island to the chaotic sea, we focus on a system whose phase space consists of one regular island surrounded by chaotic dynamics. In order to ensure that the direct dynamical tunneling process is not dominated by the resonance-assisted one, it is necessary to demand that the fine structure of the regular island cannot be resolved by the effective Planck constant within the domain of interest. For the following derivation we consider a periodically kicked system in 1D on a torus whose phase space has the previously mentioned properties. The corresponding quantum map is given by the time evolution operator $\hat{U}$ over one kicking period. For illustrations during the derivation we will use the example map P_{ex}, which was introduced in section 3.4. We remark that the ideas of the following derivation are not restricted to periodically kicked systems. Any other system, whose phase space contains one regular island with a negligible fine structure embedded in the chaotic sea, can in principle be used.

The investigation of the quasi-energy spectrum of $\hat{U}$ under the variation of a system-specific parameter κ reveals avoided crossings, e.g. the one between the quasi-energies $\varphi_+(\kappa)$ and $\varphi_-(\kappa)$ at $\kappa = \kappa^*$, which is sketched in figure 5.1(a) (black hyperbolae). Let us denote the eigenstates belonging to the quasi-energies $\varphi_+(\kappa)$ and $\varphi_-(\kappa)$ by $|\psi_+(\kappa)\rangle$ and $|\psi_-(\kappa)\rangle$. The smallest value of the difference between these two quasi-energies at the avoided crossing, $\Delta\varphi := \varphi_-(\kappa^*) - \varphi_+(\kappa^*)$, is, like in the case of 1D barrier tunneling, called as tunnel splitting. It is a measure of the effect of the coupling between the two eigenstates $|\psi_-(\kappa^*)\rangle$ and $|\psi_+(\kappa^*)\rangle$ involved in the avoided crossing. Our first aim is to

find an analytical expression for the tunnel splitting, by means of which a formula for the rates of direct dynamical tunneling transitions from the regular island to the chaotic sea will be derived in a second step.

The insets (g) and (h) of figure 5.1 show the Husimi functions of the eigenstates $|\psi_-(\kappa^*)\rangle$ and $|\psi_+(\kappa^*)\rangle$ at the avoided crossing. Both are almost identical. Inset (f) shows additionally a plot of the classical phase space. An integration of these two Husimi functions over the regular island and the chaotic sea yields the expected result: They have equal weights in both phase space regions. For $\kappa < \kappa^*$ the Husimi function of the state $|\psi_-(\kappa)\rangle$ has a larger weight in the regular island. In contrast to this, the Husimi function of $|\psi_+(\kappa)\rangle$ has its main weight in the chaotic sea. The state $|\psi_-(\kappa)\rangle$ is therefore regular for $\kappa < \kappa^*$, whereas the state $|\psi_+(\kappa)\rangle$ is chaotic. The opposite holds for $\kappa > \kappa^*$. The two eigenstates $|\psi_-(\kappa)\rangle$ and $|\psi_+(\kappa)\rangle$ thus interchange their properties at the avoided crossing [45].

These observations are similar to the case of tunneling in a 1D double well, if we associate the regular island and the chaotic sea with e.g. the left and the right well of the potential energy, respectively. A comparison of figure 5.1 with figure 2.7 supports this. It therefore might be helpful to proceed similar to the treatment of the 1D double well case. In chapter 2 we introduced a left and a right well Hamiltonian in order to find an analytical expression for the 1D tunnel splitting. In analogy to these two Hamiltonians we here introduce a regular and a chaotic quantum map: $\hat{U}_{\text{reg}}$ and $\hat{U}_{\text{ch}}$. The corresponding classical map of $\hat{U}_{\text{reg}}$ is constructed of the classical map of $\hat{U}$. The first step consists of an interpolation of the dynamics of the regular island in the mixed phase space. This interpolation is used in a second step for the continuation of the regular island to the chaotic sea. Figure 5.1(f) illustrates the mixed phase space. The phase space of the completely regular system is shown in figure 5.1(b). The chaotic system consists of a continuation of the chaotic sea to the regular island. It is, however, not clear how this can be performed, so that figure 5.1(c) can only be regarded as a sketch. We will later see that the chaotic map disappears from our consideration.

The normalized eigenstates of $\hat{U}_{\text{reg}}$ and $\hat{U}_{\text{ch}}$ fulfill the eigenequations

$$\hat{U}_{\text{reg}} |\psi_{\text{reg},k}(\kappa)\rangle \;\; = \;\; \mathrm{e}^{\mathrm{i}\varphi_{\text{reg},k}(\kappa)} |\psi_{\text{reg},k}(\kappa)\rangle \,, \tag{5.1}$$

$$\hat{U}_{\text{ch}} |\psi_{\text{ch},k}(\kappa)\rangle \;\; = \;\; \mathrm{e}^{\mathrm{i}\varphi_{\text{ch},k}(\kappa)} |\psi_{\text{ch},k}(\kappa)\rangle \tag{5.2}$$

for every parameter value κ. The eigenstates $|\psi_-(\kappa)\rangle$ and $|\psi_+(\kappa)\rangle$ of $\hat{U}$ fulfill

$$\hat{U} |\psi_\pm(\kappa)\rangle \;\; = \;\; \mathrm{e}^{\mathrm{i}\varphi_\pm(\kappa)} |\psi_\pm(\kappa)\rangle \,. \tag{5.3}$$

The quantum maps $\hat{U}_{\text{reg}}$ and $\hat{U}_{\text{ch}}$ possess by construction the property that respectively one of their quasi-energies, let us call them $\varphi_{\text{reg}}(\kappa)$ and $\varphi_{\text{ch}}(\kappa)$ with corresponding eigenstates $|\psi_{\text{reg}}(\kappa)\rangle$ and $|\psi_{\text{ch}}(\kappa)\rangle$, is an asymptote to the quasi-energies $\varphi_{\pm}(\kappa)$ of $\hat{U}$ sufficiently away from the avoided crossing. The functions $\varphi_{\text{reg}}(\kappa)$ and $\varphi_{\text{ch}}(\kappa)$ cross therefore at $\kappa = \kappa^*$, see the red and blue line in figure 5.1(a). This is an immediate consequence of the property that the regular and the chaotic quantum map are independent of each other.

Now we concentrate on the avoided crossing and define that $|\psi_-\rangle$, $|\psi_+\rangle$, $|\psi_{\text{reg}}\rangle$, and $|\psi_{\text{ch}}\rangle$ as well as φ_-, φ_+, φ_{reg}, and φ_{ch} are considered at $\kappa = \kappa^*$. The Husimi functions of the states $|\psi_{\text{reg}}\rangle$ and $|\psi_{\text{ch}}\rangle$ are shown as insets (d) and (e) in figure 5.1. Assuming that no other eigenstate of $\hat{U}$ lies energetically close to the eigenstates $|\psi_-\rangle$ and $|\psi_+\rangle$, the
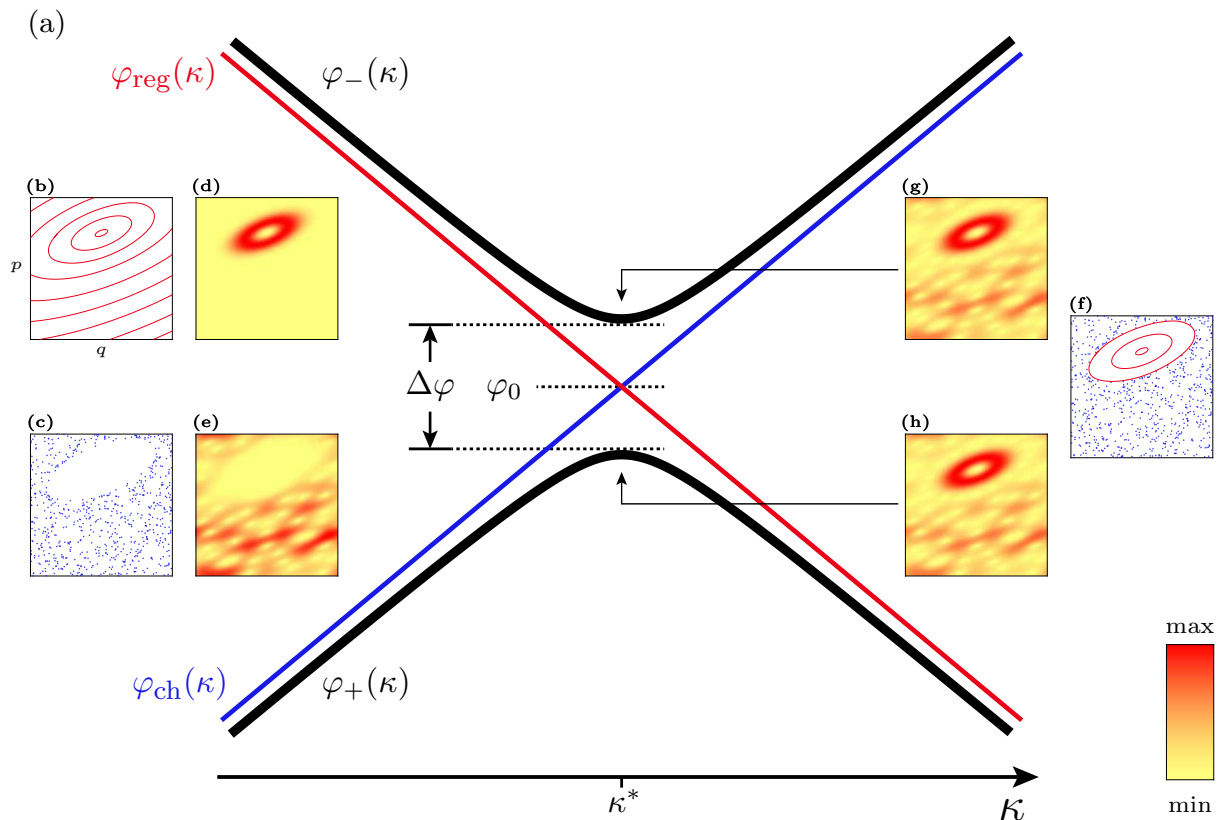
Figure 5.1: (a) Sketch of an avoided crossing between two quasi-energies $\varphi_{\pm}(\kappa)$ (black hyperbolae) of the quantum map $\hat{U}$ under the variation of a system-specific parameter κ. The quasi-energies $\varphi_{\text{reg}}(\kappa)$ (red) and $\varphi_{\text{ch}}(\kappa)$ (blue) of the quantum maps $\hat{U}_{\text{reg}}$ and $\hat{U}_{\text{ch}}$ cross at κ^* and are asymptotes to $\varphi_{\pm}(\kappa)$ sufficiently away from the avoided crossing. Insets in the left part of the figure: Phase space images of the regular (b) and chaotic (c) classical map. Husimi functions of the regular eigenstate $|\psi_{\text{reg}}(\kappa^*)\rangle$ (d) and the chaotic eigenstate $|\psi_{\text{ch}}(\kappa^*)\rangle$ (e). Insets in the right part: Phase space of the classical map belonging to $\hat{U}$ (f). Husimi functions of the eigenstates of $\hat{U}$ with the eigenvalues $\varphi_-(\kappa^*)$ (g) and $\varphi_+(\kappa^*)$ (h) at the avoided crossing.

coupling of these two states can, as in the 1D double well case, be described by a two-level system [45]. We then have

$$|\psi_\pm\rangle \;\approx\; \frac{1}{\sqrt{2}}\Big(\,|\psi_{\mathrm{reg}}\rangle \pm |\psi_{\mathrm{ch}}\rangle\,\Big) \tag{5.4}$$

in lowest perturbation order. With $\varphi_0 := \varphi_{\mathrm{reg}} = \varphi_{\mathrm{ch}}$ we have the eigenequations

$$\hat{U}_{\mathrm{reg}}\,|\psi_{\mathrm{reg}}\rangle \;=\; \mathrm{e}^{\mathrm{i}\varphi_0}\,|\psi_{\mathrm{reg}}\rangle\,, \tag{5.5}$$

$$\hat{U}_{\mathrm{ch}}\,|\psi_{\mathrm{ch}}\rangle \;=\; \mathrm{e}^{\mathrm{i}\varphi_0}\,|\psi_{\mathrm{ch}}\rangle\,, \tag{5.6}$$

and the tunnel splitting

$$\varphi_\pm \;=\; \varphi_0 \mp \frac{\Delta\varphi}{2}. \tag{5.7}$$

The insertion of equations (5.4) and (5.7) into equation (5.3) yields

$$\hat{U}\Big(\,|\psi_{\mathrm{reg}}\rangle + |\psi_{\mathrm{ch}}\rangle\,\Big) \;\approx\; \mathrm{e}^{\mathrm{i}\varphi_0}\mathrm{e}^{-\mathrm{i}\Delta\varphi/2}\Big(\,|\psi_{\mathrm{reg}}\rangle + |\psi_{\mathrm{ch}}\rangle\,\Big), \tag{5.8}$$

$$\hat{U}\Big(\,|\psi_{\mathrm{reg}}\rangle - |\psi_{\mathrm{ch}}\rangle\,\Big) \;\approx\; \mathrm{e}^{\mathrm{i}\varphi_0}\mathrm{e}^{\mathrm{i}\Delta\varphi/2}\Big(\,|\psi_{\mathrm{reg}}\rangle - |\psi_{\mathrm{ch}}\rangle\,\Big). \tag{5.9}$$

Now we perform a Taylor expansion of the respectively second exponential function appearing on the right-hand side of equations (5.8) and (5.9). This is justified, because $\Delta\varphi/2 \ll 1$ generally holds. Then, we take the sum of both equations and obtain

$$\hat{U}\,|\psi_{\mathrm{reg}}\rangle \;\approx\; \mathrm{e}^{\mathrm{i}\varphi_0}\left(\,|\psi_{\mathrm{reg}}\rangle - \mathrm{i}\frac{\Delta\varphi}{2}\,|\psi_{\mathrm{ch}}\rangle\right) \tag{5.10}$$

$$=\; \mathrm{e}^{\mathrm{i}\varphi_0}\,|\psi_{\mathrm{reg}}\rangle - \mathrm{i}\frac{\Delta\varphi}{2}\mathrm{e}^{\mathrm{i}\varphi_0}\,|\psi_{\mathrm{ch}}\rangle \tag{5.11}$$

$$\overset{(5.5)}{=}\; \hat{U}_{\mathrm{reg}}\,|\psi_{\mathrm{reg}}\rangle - \mathrm{i}\frac{\Delta\varphi}{2}\mathrm{e}^{\mathrm{i}\varphi_0}\,|\psi_{\mathrm{ch}}\rangle\,. \tag{5.12}$$

After a multiplication with $\langle\psi_{\mathrm{ch}}|$ we get

$$|v| \;:=\; \left|\frac{\Delta\varphi}{2}\right| \;\approx\; \left|\Big\langle\psi_{\mathrm{ch}}\Big|\hat{U} - \hat{U}_{\mathrm{reg}}\Big|\psi_{\mathrm{reg}}\Big\rangle\right| \tag{5.13}$$

for the modulus of the coupling matrix element v with respect to the states $|\psi_{\mathrm{reg}}\rangle$ and $|\psi_{\mathrm{ch}}\rangle$. It is similar to equation (2.64) in the 1D case. In the 1D case the corresponding contribution to $\langle\psi_{\mathrm{ch}}|\hat{U}_{\mathrm{reg}}|\psi_{\mathrm{reg}}\rangle$ becomes negligible in the semiclassical limit. But as we do not know, how the chaotic quantum map $\hat{U}_{\mathrm{ch}}$ with eigenstates $|\psi_{\mathrm{ch}}\rangle$ can be constructed, we cannot make a similar statement in the case of quantum maps. We therefore have

to keep the full expression (5.13). Even if the states $|\psi_{\text{reg}}\rangle$ and $|\psi_{\text{ch}}\rangle$ are not orthogonal, the analytical expression for the coupling matrix element (5.13) represents the minimal possible value. The proof is presented in appendix A.3.

Regular states are distinguished by their quantum number m. We will therefore write $|\psi_{\text{reg},m}\rangle$ instead of $|\psi_{\text{reg}}\rangle$ in the following. The value of the maximal possible quantum number is, on the basis of the relative size of the regular island, governed by the WKB like quantization condition (4.2) and the criterion (4.4). Due to the finite Hilbert space size, the total number of regular and chaotic states is finite. Let us denote the number of chaotic states by N_{ch}. In order to distinguish the chaotic states, we introduce an index j which is taken from the set $\{1, 2, ..., N_{\text{ch}}\}$ and write $|\psi_{\text{ch},j}\rangle$ instead of $|\psi_{\text{ch}}\rangle$ from now on. Equation (5.13) takes the coupling of the regular state $|\psi_{\text{reg},m}\rangle$ with a single chaotic state $|\psi_{\text{ch},j}\rangle$ into account

$$|\tilde{v}_{m,j}| \;\approx\; \left| \left\langle \psi_{\text{ch},j} \left| \hat{U} - \hat{U}_{\text{reg}} \right| \psi_{\text{reg},m} \right\rangle \right| \tag{5.14}$$

In order not to mix up the already dimensionless coupling matrix element (5.13) with the soon appearing dimensionful one, we introduced a tilde in equation (5.14). By means of the coupling matrix element (5.14) we now investigate the transition from the "initial" regular state $|\psi_{\text{reg},m}\rangle$ to the "final" chaotic state $|\psi_{\text{ch},j}\rangle$. As the number of chaotic states is finite, the spectrum of the chaotic quasi-energies must be discrete. If it had been continuous, the rate for the transition from the state $|\psi_{\text{reg},m}\rangle$ to $|\psi_{\text{ch},j}\rangle$ could have been determined via Fermi's golden rule. The number of chaotic states N_{ch} increases, however, in the semiclassical limit, what yields a more dense chaotic spectrum. We approximate the transition rate $\gamma_{m\to j}$ therefore by means of Fermi's golden rule, whose dimensionful version is taken from reference [48],

$$\gamma_{m\to j} \;\approx\; \frac{2\pi}{\hbar} \, |v_{m,j}|^2 \, \rho_{\text{ch}}(\varphi_{\text{ch}}), \tag{5.15}$$

where $\rho_{\text{ch}}(\varphi_{\text{ch}})$ denotes the density of the chaotic states. The effect of the coupling between the states $|\psi_{\text{reg},m}\rangle$ and $|\psi_{\text{ch},j}\rangle$ is maximal at the parameter value $\kappa = \kappa^*$. For every other of the remaining $N_{\text{ch}} - 1$ chaotic states there is a certain parameter value such that the effect of the coupling between it and $|\psi_{\text{reg},m}\rangle$ becomes also maximal. Actually we are not interested in the coupling of $|\psi_{\text{reg},m}\rangle$ to a special chaotic state, but rather in the coupling to the chaotic sea. We perform therefore an average over all transition rates belonging to these maximal couplings of the state $|\psi_{\text{reg},m}\rangle$ with the N_{ch} chaotic states at different

parameter values

$$\gamma_m \quad := \quad \frac{1}{N_{\text{ch}}} \sum_{j=1}^{N_{\text{ch}}} \gamma_{m \to j} \quad \approx \quad \frac{1}{N_{\text{ch}}} \sum_{j=1}^{N_{\text{ch}}} \frac{2\pi}{\hbar} \left| v_{m,j} \right|^2 \rho_{\text{ch}}(\varphi_{\text{ch}}). \tag{5.16}$$

The density $\rho_{\text{ch}}(\varphi_{\text{ch}})$ is given by

$$\rho_{\text{ch}}(\varphi_{\text{ch}}) \quad = \quad \sum_{j=1}^{N_{\text{ch}}} \delta(\varphi_{\text{ch}} - \varphi_{\text{ch},j}). \tag{5.17}$$

If the dynamics within the chaotic sea is ergodic, the chaotic quasi-energies follow the circular orthogonal ensemble statistics in the limit $N_{\text{ch}} \to \infty$ and are uniformly distributed. The density of the final chaotic states can then be assumed as constant. We remark that the tunnel splitting, which appears in the modulus of the coupling matrix element $|v_{m,j}| \approx |\Delta\varphi_{m,j}/2|$ in (5.16) is dimensionful. Before we continue with the evaluation of Fermi's golden rule, we focus on making it dimensionless. With the dimensionful kick period τ we have the following relation between dimensionful and dimensionless quasi-energies

$$\varphi \quad = \quad \frac{\hbar}{\tau} \tilde{\varphi}. \tag{5.18}$$

The same holds for $\Delta\varphi_{m,j}$ and $\Delta\tilde{\varphi}_{m,j}$. With a constant density ρ_{ch} we have

$$N_{\text{ch}} \quad = \quad \int_0^{h/\tau} \mathrm{d}\varphi \rho_{\text{ch}}$$

$$\Leftrightarrow \qquad \rho_{\text{ch}} \quad = \quad \frac{\tau}{h} N_{\text{ch}}. \tag{5.19}$$

Thus, ρ_{ch} is equal to the inverse mean level spacing of the chaotic states. With a characteristic time t_0 we define the dimensionless kick period according to equation (A.4) and the dimensionless transition or dynamical tunneling rate

$$\tilde{\gamma} \quad := \quad \gamma \, t_0. \tag{5.20}$$

As usual, we set $\tilde{\tau} = 1$ and finally find Fermi's golden rule in terms of dimensionless quantities

$$\tilde{\gamma}_m \quad \approx \quad \sum_{j=1}^{N_{\text{ch}}} |\tilde{v}_{m,j}|^2 . \tag{5.21}$$

In the following we will omit the tilde. The insertion of equation (5.14) yields

$$\gamma_m \approx \left\langle \psi_{\mathrm{reg},m} \left| \left(\hat{U}^\dagger - \hat{U}^\dagger_{\mathrm{reg}} \right) \left(\sum_{j=1}^{N_{\mathrm{ch}}} |\psi_{\mathrm{ch},j}\rangle \langle\psi_{\mathrm{ch},j}| \right) \left(\hat{U} - \hat{U}_{\mathrm{reg}} \right) \right| \psi_{\mathrm{reg},m} \right\rangle. \quad (5.22)$$

The term in the middle of the right-hand side of equation (5.22) is equal to the approximate projection operator onto the chaotic sea. As the corresponding classical dynamics of $\hat{U}_{\mathrm{reg}}$ is by construction equal to the dynamics within the regular island of the actual system, we expect that the Husimi function of the state

$$\left(\hat{U} - \hat{U}_{\mathrm{reg}} \right) |\psi_{\mathrm{reg},m}\rangle \quad (5.23)$$

has almost almost all of its weight in the chaotic sea of the mixed phase space. Figure 5.2 demonstrates this for the considered example system. It is thus justified to replace the approximate projection operator onto the chaotic sea in equation (5.22) by the identity operator $\hat{\mathbb{1}}$. This yields

$$\gamma_m \approx \left\| \left(\hat{U} - \hat{U}_{\mathrm{reg}} \right) \left| \psi_{\mathrm{reg},m} \right\rangle \right\|^2 \quad (5.24)$$

as final expression for the direct dynamical tunneling rate of the regular state $|\psi_{\mathrm{reg},m}\rangle$ from the regular island to the chaotic sea. Although formula (5.24) has been derived for a periodically kicked system, the main ideas of the derivation can also be transferred
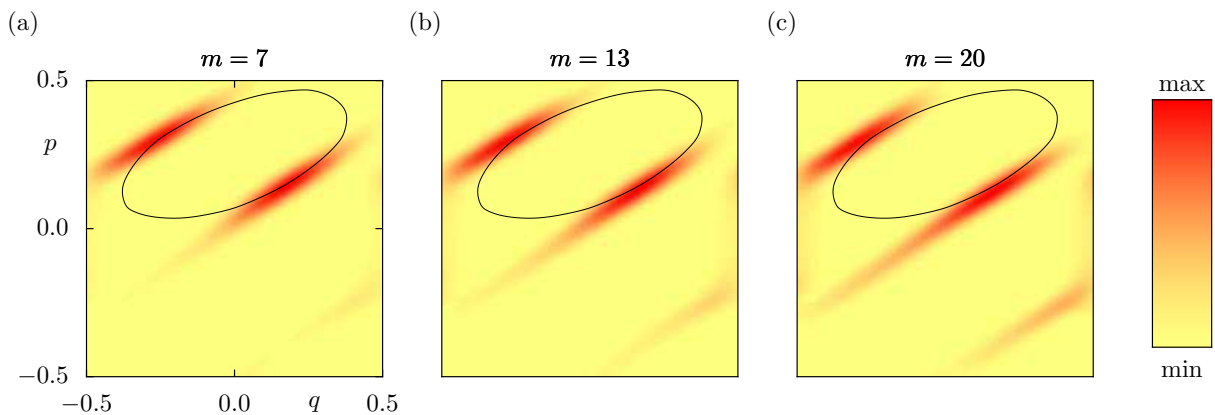
Figure 5.2: Husimi functions of equation (5.23) for the example system. The plots were determined for $h_{\mathrm{eff}} = 1/100$ and (a) $m = 7$, (b) $m = 13$, and $m = 20$. The numerically determined tunneling rates for $m < 7$ are smaller than 10^{-14}. The corresponding Husimi functions of equation (5.23) are therefore not trustworthy. The Husimi functions in this plot are determined on a 200 by 200 grid. The approximate border of the regular island of the classical map belonging to $\hat{U}$ is additionally plotted.

to other systems like e.g. billiards. The tunneling rate formula is therefore general. Its advantages are that the chaotic quantum map $\hat{U}_{\mathrm{ch}}$ and its eigenstates $|\psi_{\mathrm{ch}}\rangle$ do not appear. This is helpful, because the construction of the chaotic system is difficult, as has already been mentioned. The information about the chaotic sea itself is included in $\hat{U}$. The central quantity of the formula for the determination of direct dynamical tunneling rates is the regular system. Since it is constructed from the actual system by an interpolation of the regular dynamics with a final extrapolation to the chaotic sea, it seems to be natural that only one possible regular system exists. We will later encounter an example, where the existence of a unique regular system is obvious. Whether this is true in general, is, however, still an open question.

We remark that the tunneling rate γ_m is an exponentially small quantity. According to (5.24) it is obtained from the difference of the states $\hat{U}\,|\psi_{\mathrm{reg},m}\rangle$ and $\hat{U}_{\mathrm{reg}}\,|\psi_{\mathrm{reg},m}\rangle$. As these two states are by construction almost identical within the region of the regular island, the regular system needs to be known very precisely.

This observation and the fact that (5.24) still contains the complete quantum information, which is reflected by the dependence on the operator $\hat{U}$, imply that we should try to evaluate equation (5.24) further. Another aim is to find a general semiclassical formula, which expresses the tunneling rate γ_m as a function of the effective Planck constant h_{eff}, the quantum number m, and classical properties of the considered system like e.g. the area A_{reg} of the regular island or the rotation number R_m. Our studies have shown that this is difficult. In the following we will demonstrate how equation (5.24) can be evaluated further for a special class of kicked systems. Using the WKB ansatz we will demonstrate that it is possible to find a semiclassical tunneling rate formula for the case of an elliptic harmonic oscillator-like regular island.

5.2   Application to piecewise defined and smoothed kicked 1D systems

The quantum mechanical time evolution operator of a periodically kicked system over one kicking period has the simple structure

$$\hat{U} \;=\; \mathrm{e}^{-\frac{\mathrm{i}}{\hbar_{\mathrm{eff}}}V(\hat{q})}\mathrm{e}^{-\frac{\mathrm{i}}{\hbar_{\mathrm{eff}}}T(\hat{p})} \tag{5.25}$$

$$=:\; \hat{U}_{\mathrm{V}}\hat{U}_{\mathrm{T}}. \tag{5.26}$$

For kicked systems constructed of discontinuous piecewise defined derivatives of the kinetic and the potential energy, which are smoothed with a Gaussian, in order to obtain

analytical functions $T'(p)$ and $V'(q)$, regular functions $T_{\text{reg}}(p)$ and $V_{\text{reg}}(q)$ exist. The regular kinetic energy function $T_{\text{reg}}(p)$ is given by the continuation of that piece of the discontinuous function $T(p)$ to the real line, which covers the momentum domain of the regular island. Similarly, the regular potential energy function $V_{\text{reg}}(q)$ is obtained from the continuation of that piece of $V(q)$, which contains the position domain of the regular island. Furthermore, $\hat{U}_{\text{reg}} = \hat{U}_{V_{\text{reg}}}\hat{U}_{T_{\text{reg}}}$ holds, where $\hat{U}_{V_{\text{reg}}} := \exp\left(-2\pi i V_{\text{reg}}(\hat{q})/h_{\text{eff}}\right)$ and $\hat{U}_{T_{\text{reg}}} := \exp\left(-2\pi i T_{\text{reg}}(\hat{p})/h_{\text{eff}}\right)$. An example is the system whose stroboscopic classical dynamics is described by the example map P_{ex}, see section 3.4. The insertion of the regular time evolution operator into equation (5.24) yields

$$\gamma \;\approx\; \left\langle \psi_{\text{reg}} \left| \left(\hat{U}_T^\dagger \hat{U}_V^\dagger - \hat{U}_{T_{\text{reg}}}^\dagger \hat{U}_{V_{\text{reg}}}^\dagger\right)\left(\hat{U}_V\hat{U}_T - \hat{U}_{V_{\text{reg}}}\hat{U}_{T_{\text{reg}}}\right)\right| \psi_{\text{reg}} \right\rangle. \tag{5.27}$$

With the definitions

$$\hat{\varepsilon}_V \;:=\; \exp\left(-\frac{i}{\hbar_{\text{eff}}}\left(V(\hat{q}) - V_{\text{reg}}(\hat{q})\right)\right) - \hat{\mathbb{1}} \tag{5.28}$$

$$\hat{\varepsilon}_T \;:=\; \exp\left(-\frac{i}{\hbar_{\text{eff}}}\left(T(\hat{q}) - T_{\text{reg}}(\hat{q})\right)\right) - \hat{\mathbb{1}} \tag{5.29}$$

we have

$$
\begin{aligned}
\hat{U} - \hat{U}_{\text{reg}} \;&=\; \hat{U}_V\hat{U}_T - \hat{U}_{V_{\text{reg}}}\hat{U}_{T_{\text{reg}}} \\
&=\; \hat{U}_{V_{\text{reg}}}\hat{U}_{V_{\text{reg}}}^\dagger\left(\hat{U}_V\hat{U}_T - \hat{U}_{V_{\text{reg}}}\hat{U}_{T_{\text{reg}}}\right)\hat{U}_{T_{\text{reg}}}^\dagger\hat{U}_{T_{\text{reg}}} \\
&=\; \hat{U}_{V_{\text{reg}}}\left(\hat{U}_{V_{\text{reg}}}^\dagger\hat{U}_V\hat{U}_T\hat{U}_{T_{\text{reg}}}^\dagger - \hat{\mathbb{1}}\right)\hat{U}_{T_{\text{reg}}} \\
&=\; \hat{U}_{V_{\text{reg}}}\left[\exp\left(-\frac{i}{\hbar_{\text{eff}}}\left(V(\hat{q}) - V_{\text{reg}}(\hat{q})\right)\right)\right. \\
&\qquad\qquad \left.\cdot\exp\left(-\frac{i}{\hbar_{\text{eff}}}\left(T(\hat{q}) - T_{\text{reg}}(\hat{q})\right)\right) - \hat{\mathbb{1}}\right]\hat{U}_{T_{\text{reg}}} \\
&=\; \hat{U}_{V_{\text{reg}}}\left(\hat{\varepsilon}_V + \hat{\varepsilon}_T + \hat{\varepsilon}_V\hat{\varepsilon}_T\right)\hat{U}_{T_{\text{reg}}}.
\end{aligned} \tag{5.30}
$$

The vector $\left(\hat{U} - \hat{U}_{\text{reg}}\right)|\psi_{\text{reg},m}\rangle$ is equal to the quasimode-error-vector (4.59). Its norm is the quasimode error. According to equation (5.30), the quasimode error vector consists of the three contributions

$$|V_m\rangle \;:=\; \hat{U}_{V_{\text{reg}}}\hat{\varepsilon}_V\hat{U}_{T_{\text{reg}}}|\psi_{\text{reg},m}\rangle, \tag{5.31}$$

$$|T_m\rangle \;:=\; \hat{U}_{V_{\text{reg}}}\hat{\varepsilon}_T\hat{U}_{T_{\text{reg}}}|\psi_{\text{reg},m}\rangle, \tag{5.32}$$

$$|VT_m\rangle \;:=\; \hat{U}_{V_{\text{reg}}}\hat{\varepsilon}_V\hat{\varepsilon}_T\hat{U}_{T_{\text{reg}}}|\psi_{\text{reg},m}\rangle. \tag{5.33}$$

The operator $\hat{U}_{V_{reg}}$ corresponds to a rotation and a stretching in phase space. To avoid these effects, we also define

$$\left|\bar{V}_m\right\rangle \;\; := \;\; \hat{\varepsilon}_V \hat{U}_{T_{reg}} \left|\psi_{reg,m}\right\rangle, \tag{5.34}$$

$$\left|\bar{T}_m\right\rangle \;\; := \;\; \hat{\varepsilon}_T \hat{U}_{T_{reg}} \left|\psi_{reg,m}\right\rangle, \tag{5.35}$$

$$\left|\bar{V}T_m\right\rangle \;\; := \;\; \hat{\varepsilon}_V \hat{\varepsilon}_T \hat{U}_{T_{reg}} \left|\psi_{reg,m}\right\rangle. \tag{5.36}$$

In the considered special class of periodically kicked systems generally either the kinetic or the potential energy function governs the size of the regular island in phase space. One can realize this by the introduction of two different smoothing parameters. If respectively one of them is used for the smoothing of the derivative of the kinetic and the potential energy, their independent variation confirms this assumption. This should be reflected by the fact that either $|T_m\rangle$ or $|V_m\rangle$ is the dominating contribution to the quasimode error vector. In the example used throughout this chapter for the purpose of illustration, the kinetic energy is the decisive function. Figure 5.3 shows the norms of the three contributions to the quasimode error for the quantum numbers $m = 0$ and $m = 5$ as a function of $1/h_{eff}$. As expected, $\|\,|T_m\rangle\,\|$ is the dominating one. It is surprising that the second largest contribution is $\|\,|VT_m\rangle\,\|$ instead of $\|\,|V_m\rangle\,\|$. However, the latter two contributions are several orders of magnitude smaller than the dominating former one.

Figure 5.4 shows the Husimi functions of the quasimode error vector contributions $\left|\bar{T}_m\right\rangle$, $\left|\bar{V}_m\right\rangle$, and $\left|\bar{V}T_m\right\rangle$ for the quantum number $m = 10$ and $h_{eff} = 1/100$. They were determined on a 200 by 200 grid. The caption of each Husimi function plot contains the corresponding norm. The border of the regular island, which is additionally plotted as a guide to the eye, has a smaller distance to the edge of the unit cell in p direction. This reflects that the p dependent kinetic energy function governs the size of the regular island in this example. The Husimi function of the dominating contribution $\left|\bar{T}_m\right\rangle$, figure 5.4(a), has two equal maxima at the lower and the upper border of the regular island in p direction. If we had determined the Husimi function of $|T_m\rangle$, the additional operator $\hat{U}_{V_{reg}}$ would have effected a rotation and a stretching of the two maxima yielding a plot like in figure 5.2. In equations (5.34) by (5.36) only that part of $\hat{U}_{reg}$ which effects a free evolution, $\hat{U}_{T_{reg}}$, is applied to the regular state $|\psi_{reg,m}\rangle$. Correspondingly, we have to consider the classical map before the kick. This explains, why the border curves of the regular islands in figure 5.4 are mirrored with respect to the line $q = 0$ in contrast to e.g. figure 3.6.

Using the three contributions to the quasimode error vector equations (5.31) by (5.33)
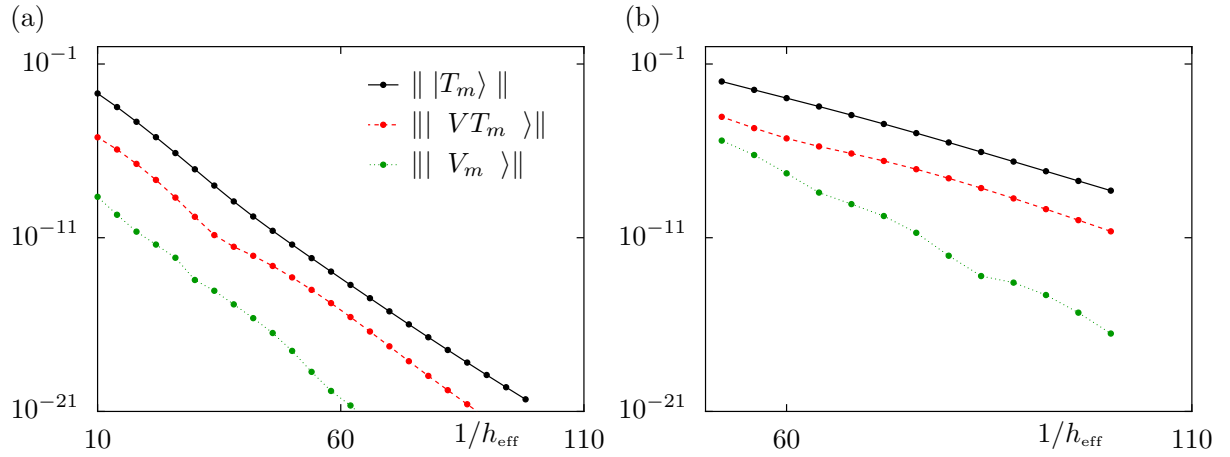
Figure 5.3: Norms of the states $|T_m\rangle$ (black), $|VT_m\rangle$ (red), and $|V_m\rangle$ (green) for the quantum numbers $m = 0$ (a) and $m = 5$ (b) versus $1/h_{\text{eff}}$. The lines, which connect successive disrete data points, are a guide to the eye.

we rewrite the direct dynamical tunneling rate formula (5.24)

$$
\begin{aligned}
\gamma_m &\approx \| \, |T_m\rangle + |V_m\rangle + |VT_m\rangle \, \|^2 \\
&= \langle T_m|T_m\rangle + \langle V_m|V_m\rangle + \langle VT_m|VT_m\rangle + \langle T_m|V_m\rangle + \langle T_m|VT_m\rangle \\
&\quad + \langle V_m|T_m\rangle + \langle V_m|VT_m\rangle + \langle VT_m|T_m\rangle + \langle VT_m|V_m\rangle.
\end{aligned} \tag{5.37}
$$

Since in general the kinetic or the potential energy function governs the size of the regular island, the first or the second contribution of (5.37) is the dominating one. The remaining seven contributions are expected to be orders of magnitude smaller and will thus be neglected. Using equations (5.28), (5.29), (5.31), and (5.32) we then have

$$
\begin{aligned}
\gamma_m &\approx \left\langle \psi_{\text{reg},m} \left| \hat{U}_{\text{T}_{\text{reg}}}^\dagger \hat{\varepsilon}_T^\dagger \hat{\varepsilon}_T \hat{U}_{\text{T}_{\text{reg}}} \right| \psi_{\text{reg},m} \right\rangle + \left\langle \psi_{\text{reg},m} \left| \hat{U}_{\text{T}_{\text{reg}}}^\dagger \hat{\varepsilon}_V^\dagger \hat{\varepsilon}_V \hat{U}_{\text{T}_{\text{reg}}} \right| \psi_{\text{reg},m} \right\rangle \\
&= \sum_{k=0}^{N-1} \left\langle \psi_{\text{reg},m} \left| e^{\frac{i}{\hbar_{\text{eff}}} T_{\text{reg}}(\hat{p})} \right| p_k \right\rangle 2 \left[1 - \cos\left(\frac{T(p_k) - T_{\text{reg}}(p_k)}{\hbar_{\text{eff}}} \right) \right] \\
&\quad \cdot \left\langle p_k \left| e^{-\frac{i}{\hbar_{\text{eff}}} T_{\text{reg}}(\hat{p})} \right| \psi_{\text{reg},m} \right\rangle \\
&\quad + \sum_{k=0}^{N-1} \sum_{l=0}^{N-1} \sum_{n=0}^{N-1} \left\langle \psi_{\text{reg},m} \left| e^{\frac{i}{\hbar_{\text{eff}}} T_{\text{reg}}(\hat{p})} \right| p_k \right\rangle \left\langle p_k | q_l \right\rangle 2 \left[1 - \cos\left(\frac{V(q_l) - V_{\text{reg}}(q_l)}{\hbar_{\text{eff}}} \right) \right] \\
&\quad \cdot \left\langle q_l | p_n \right\rangle \left\langle p_n \left| e^{-\frac{i}{\hbar_{\text{eff}}} T_{\text{reg}}(\hat{p})} \right| \psi_{\text{reg},m} \right\rangle
\end{aligned} \tag{5.38}
$$
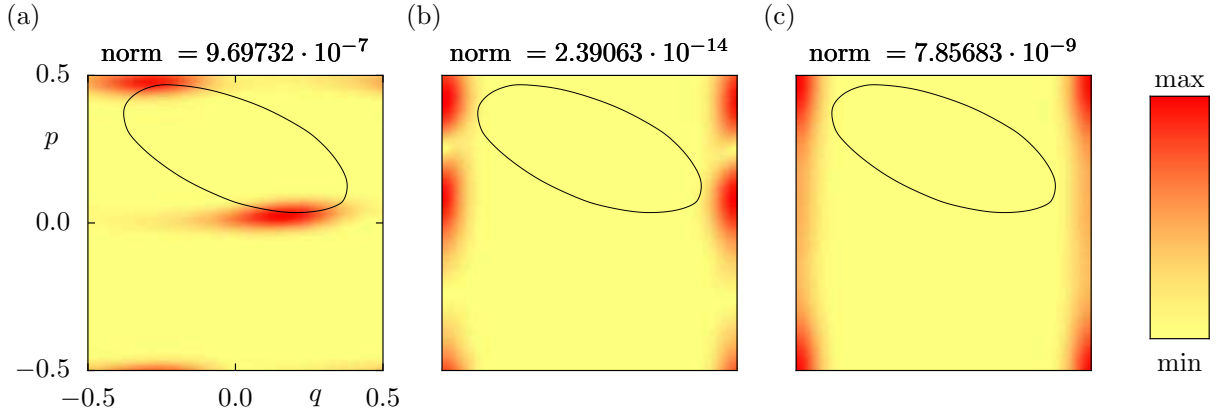
Figure 5.4: Husimi functions of the three quasimode error vector contributions (a) $\left|\bar{T}_m\right\rangle$, (b) $\left|\bar{V}_m\right\rangle$, and (c) $\left|\bar{V}T_m\right\rangle$ for $h_{\text{eff}} = 1/100$ and quantum number $m = 10$. The border of the regular island is plotted for a better comparison with the classical phase space.

$$\Leftrightarrow \quad \gamma_m \quad \approx \quad 2 \sum_{k=0}^{N-1} e^{\frac{i}{\hbar_{\text{eff}}} T_{\text{reg}}(p_k)} \left\langle \psi_{\text{reg},m} | p_k \right\rangle \left[1 - \cos\left(\frac{T(p_k) - T_{\text{reg}}(p_k)}{\hbar_{\text{eff}}} \right) \right]$$

$$e^{-\frac{i}{\hbar_{\text{eff}}} T_{\text{reg}}(p_k)} \left\langle p_k | \psi_{\text{reg},m} \right\rangle$$

$$+ 2 \sum_{l=0}^{N-1} \sum_{k=0}^{N-1} \sum_{n=0}^{N-1} e^{\frac{i}{\hbar_{\text{eff}}} T_{\text{reg}}(p_k)} \left\langle \psi_{\text{reg},m} | p_k \right\rangle \left\langle p_k | q_l \right\rangle \left[1 - \cos\left(\frac{V(q_l) - V_{\text{reg}}(q_l)}{\hbar_{\text{eff}}} \right) \right]$$

$$\cdot \left\langle q_l | p_n \right\rangle e^{-\frac{i}{\hbar_{\text{eff}}} T_{\text{reg}}(p_n)} \left\langle p_n | \psi_{\text{reg},m} \right\rangle$$

$$\overset{(3.64)}{=} \quad 2 \sum_{k=0}^{N-1} \left| \widehat{\psi}_{\text{reg},m}(p_k) \right|^2 \left[1 - \cos\left(\frac{T(p_k) - T_{\text{reg}}(p_k)}{\hbar_{\text{eff}}} \right) \right]$$

$$+ 2 \sum_{l=0}^{N-1} \left(\frac{1}{\sqrt{N}} \sum_{k=0}^{N-1} e^{\frac{i}{\hbar_{\text{eff}}} T_{\text{reg}}(p_k)} \widehat{\psi}^*_{\text{reg},m}(p_k) \, e^{-\frac{i}{\hbar_{\text{eff}}} p_k q_l} \right)$$

$$\left[1 - \cos\left(\frac{V(q_l) - V_{\text{reg}}(q_l)}{\hbar_{\text{eff}}} \right) \right]$$

$$\cdot \left(\frac{1}{\sqrt{N}} \sum_{n=0}^{N-1} e^{-\frac{i}{\hbar_{\text{eff}}} T_{\text{reg}}(p_n)} \widehat{\psi}_{\text{reg},m}(p_n) \, e^{\frac{i}{\hbar_{\text{eff}}} p_n q_l} \right)$$

$$= \quad 2 \sum_{k=0}^{N-1} \left| \widehat{\psi}_{\text{reg},m}(p_k) \right|^2 \left[1 - \cos\left(\frac{T(p_k) - T_{\text{reg}}(p_k)}{\hbar_{\text{eff}}} \right) \right]$$

$$+ 2 \sum_{l=0}^{N-1} \psi^*_{\text{reg},m}(q_l) \left[1 - \cos\left(\frac{V(q_l) - V_{\text{reg}}(q_l)}{\hbar_{\text{eff}}} \right) \right] \psi_{\text{reg},m}(q_l). \tag{5.39}$$

From (5.39) we then obtain

$$
\begin{aligned}
\gamma_m \;=\; & 2\sum_{k=0}^{N-1}\left|\widehat{\psi}_{\mathrm{reg},m}(p_k)\right|^2\left[1-\cos\left(\frac{T(p_k)-T_{\mathrm{reg}}(p_k)}{\hbar_{\mathrm{eff}}}\right)\right] \\
& + 2\sum_{k=0}^{N-1}\left|\psi_{\mathrm{reg},m}(q_k)\right|^2\left[1-\cos\left(\frac{V(q_k)-V_{\mathrm{reg}}(q_k)}{\hbar_{\mathrm{eff}}}\right)\right].
\end{aligned}
\tag{5.40}
$$

In the semiclassical limit $h_{\mathrm{eff}}\to 0$ we are allowed to replace the sums in equation (5.40) by integrals

$$
\begin{aligned}
\gamma_m \;\approx\; & 2\int_{p_{\min}}^{M_p+p_{\min}}\mathrm{d}p\;\left|\widehat{\psi}_{\mathrm{reg},m}(p)\right|^2\left[1-\cos\left(\frac{T(p)-T_{\mathrm{reg}}(p)}{\hbar_{\mathrm{eff}}}\right)\right] \\
& + 2\int_{q_{\min}}^{M_q+q_{\min}}\mathrm{d}q\;\left|\psi_{\mathrm{reg},m}(q)\right|^2\left[1-\cos\left(\frac{V(q)-V_{\mathrm{reg}}(q)}{\hbar_{\mathrm{eff}}}\right)\right].
\end{aligned}
\tag{5.41}
$$

We remark again that these steps, which modified the direct dynamical tunneling rate formula (5.24), are only valid for periodically kicked systems, which are constructed of discontinuous piecewise defined derivatives of the kinetic and the potential energy function. For these systems it is sure that the regular functions T_{reg} and V_{reg} exist and that the time evolution operator of the regular system can be decomposed into a kick and a free evolution contribution: $\hat{U}_{\mathrm{reg}}=\hat{U}_{\mathrm{V_{reg}}}\hat{U}_{\mathrm{T_{reg}}}$. In the following we will discuss some examples belonging to this class of special periodically kicked systems in order to check the accuracy of our modified formulae (5.40) and (5.41) for the determination of direct dynamical tunneling rates.

5.3 Examples

The simplest possible mixed system has a phase space which contains an elliptic almost resonance-free harmonic oscillator-like regular island embedded in the chaotic sea. In this case it is obvious, what the corresponding regular system is, see figure 4.5. The phase space of the system, whose dynamics is described by the example map P_{ex}, contains such a regular island. As this system is furthermore constructed of discontinuous piecewise defined derivatives $T'(p)$ and $V'(q)$, we can study it on the basis of the considerations presented in the previous section. We consider this system therefore as first example. The advantage of the simple elliptic shape of the regular island is that the direct dynamical tunneling rate formula (5.41) can analytically be transformed into a semiclassical

expression. This simple island shape is, however, not generic. One rather encounters systems with deformed regular islands. We therefore modify the first example finally such that the resonance-free regular island becomes deformed.

5.3.1 Harmonic oscillator-like regular island

We start our considerations with the example system which was introduced in section 3.4 for the case of one unit cell. The corresponding classical map is thus defined on the torus $[-1/2, 1/2] \times [-1/2, 1/2]$. The investigation of the three contributions (5.31) by (5.33) to the quasimode error vector of this system in figure 5.3 showed that $|T_m\rangle$ is the dominating one, so that

$$\gamma_m \quad \approx \quad \| \, |T_m\rangle \, \|^2 \tag{5.42}$$

holds. The momentum space integral in equation (5.41) is therefore the relevant one

$$\gamma_m \quad \approx \quad 2 \int\limits_{-1/2}^{1/2} \mathrm{d}p \, \left| \widehat{\psi}_{\mathrm{reg},m}(p) \right|^2 \left[1 - \cos\left(\frac{T(p) - T_{\mathrm{reg}}(p)}{\hbar_{\mathrm{eff}}} \right) \right]. \tag{5.43}$$

In our example the integrand of (5.43) is approximately symmetric with respect to the p coordinate of the center of the regular island, which is equal to $p_c = 1/4$. Furthermore, the wave function decreases rapidly in the chaotic sea, especially in the interval $[-1/2, 0)$, so that we approximately get

$$\gamma_m \quad \approx \quad 4 \int\limits_{1/4}^{1/2} \mathrm{d}p \, \left| \widehat{\psi}_{m,\mathrm{reg}}(p) \right|^2 \left[1 - \cos\left(\frac{T(p) - T_{\mathrm{reg}}(p)}{\hbar_{\mathrm{eff}}} \right) \right]. \tag{5.44}$$

The integrand of equation (5.44) contains the two factors $1 - \cos\left((T(p) - T_{\mathrm{reg}}(p))/\hbar_{\mathrm{eff}} \right)$ and $\left| \widehat{\psi}_{m,\mathrm{reg}}(p) \right|^2$. Figure 5.5 illustrates them and their product for the quantum number $m = 7$ and $m = 13$ at $h_{\mathrm{eff}} = 1/100$. We divided the wave functions in each case by their values at the border of the regular island. The intention of this rescaling will become clear soon. On the one hand the wave function $\widehat{\psi}_{m,\mathrm{reg}}(p)$ decreases rapidly in the chaotic sea, where $p > p_{\mathrm{border}}$, as is implied by the blue curves (i). The difference $T(p) - T_{\mathrm{reg}}(p)$ vanishes on the other hand by construction of the regular system within the regular island. The factor $1 - \cos\left((T(p) - T_{\mathrm{reg}}(p))/\hbar_{\mathrm{eff}} \right)$, green curves (ii), is therefore negligible within the regular island and the integrand in equation (5.43) does not have any considerable contribution up to the border p_{border} of the regular island. The main contribution comes therefore from

the region close to the border outside the island, red curves (iii). This implies that we need the regular system only within the regular island and in its immediate vicinity precisely. How it looks like elsewhere does obviously not matter. This is also supported by the observation that the Husimi function of the dominating contribution to the quasimode-error-vector localizes in the chaotic sea close the border of the regular island, see figures 5.2 and 5.4.

The regular wave function which appears in equation (5.44) can in the semiclassical limit be approximated by a WKB expression. For the turning point belonging to the WKB wave function with quantum number m, $p_{t,m}$, we always have $p_{t,m} < p_{\text{border}}$. Since the integral in (5.44) has only considerable contributions for $p > p_{\text{border}}$, it is sufficient to perform the integration over the classically forbidden region $p > p_{t,m}$. The corresponding momentum space WKB wave function analogue of equation (2.22) reads

$$\widehat{\psi}_{\text{WKB},m}(p) \;=\; \frac{C}{2\sqrt{|q(p)|}} \, \exp\left(-\frac{1}{\hbar_{\text{eff}}} \int\limits_{p_{t,m}}^{p} \mathrm{d}p' \, |q(p')| \right) \quad \text{with} \;\; C = const. \quad (5.45)$$

As the dominating contribution to the integral in (5.44) comes from a narrow region close to the border out of the regular island, we assume that the position as a function of the

(a)   (b)
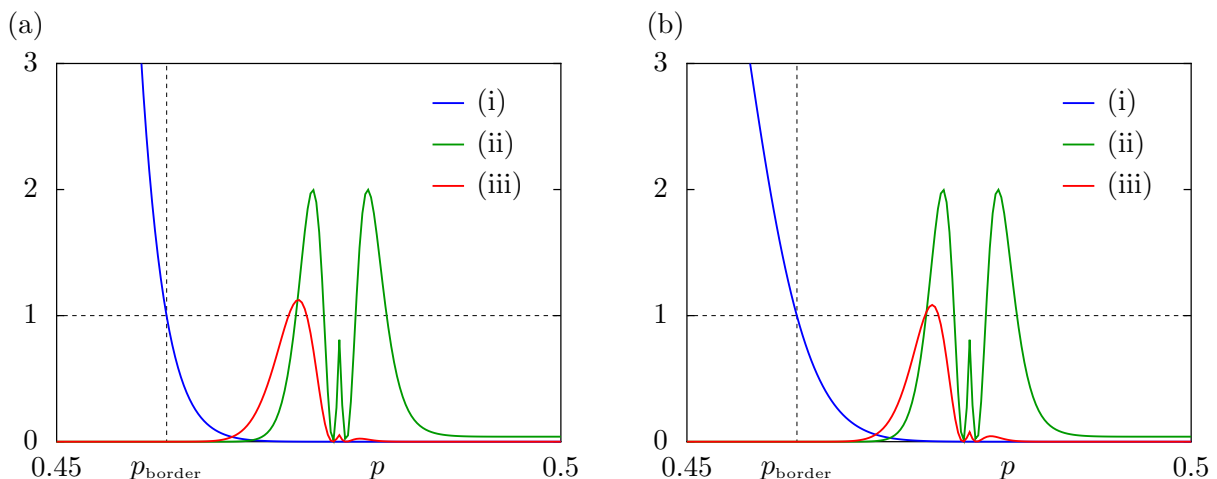
Figure 5.5: Illustration of the factors of the integrand appearing in equation (5.44). (i) Square of the modulus of the wave function $\widehat{\psi}_{m,\text{reg}}(p)$ divided by $\widehat{\psi}_{m,\text{reg}}(p_{\text{border}})$, (ii) $1 - \cos\big((T(p) - T_{\text{reg}}(p))/\hbar_{\text{eff}}\big)$ and (iii) the product of both factors at $h_{\text{eff}} = 1/100$ for the quantum numbers (a) $m = 7$ and (b) $m = 13$.

momentum is almost constant, $q(p) \approx q(p_{\text{border}})$,

$$\widehat{\psi}_{\text{WKB},m}(p) \quad \approx \quad \frac{C}{2\sqrt{|q(p_{\text{border}})|}} \; \exp\left(-\frac{1}{\hbar_{\text{eff}}} \int\limits_{p_{t,m}}^{p} \mathrm{d}p' \, |q(p_{\text{border}})|\right). \qquad (5.46)$$

Now we split the interval of integration into the two intervals $[p_{t,m}, \, p_{\text{border}}]$ and $[p_{\text{border}}, \, p]$

$$\widehat{\psi}_{\text{WKB},m}(p) \quad \approx \quad \frac{C}{2\sqrt{|q(p_{\text{border}})|}} \; \exp\left(-\frac{1}{\hbar_{\text{eff}}} \int\limits_{p_{t,m}}^{p_{\text{border}}} \mathrm{d}p' \, |q(p_{\text{border}})|\right)$$

$$\cdot \exp\left(-\frac{1}{\hbar_{\text{eff}}} \int\limits_{p_{\text{border}}}^{p} \mathrm{d}p' \, |q(p_{\text{border}})|\right)$$

$$\overset{(5.45)}{=} \quad \widehat{\psi}_{\text{WKB},m}(p_{\text{border}}) \; \exp\left(-\frac{1}{\hbar_{\text{eff}}} \int\limits_{p_{\text{border}}}^{p} \mathrm{d}p' \, |q(p_{\text{border}})|\right)$$

$$\approx \quad \widehat{\psi}_{\text{WKB},m}(p_{\text{border}}) \; \exp\left(-\frac{p - p_{\text{border}}}{\hbar_{\text{eff}}} \, |q(p_{\text{border}})|\right). \qquad (5.47)$$

According to equation (5.47), the WKB wave function is approximately proportional to its value at the border of the regular island. We therefore plotted $\left|\widehat{\psi}_{m,\text{reg}}(p)/\widehat{\psi}_{m,\text{reg}}(p_{\text{border}})\right|^2$ instead of $\left|\widehat{\psi}_{m,\text{reg}}(p)\right|^2$ in figure 5.5. We now insert the approximate momentum space WKB wave function (5.47) into equation (5.44)

$$\gamma_m \quad \approx \quad 4 \left|\widehat{\psi}_{\text{WKB},m}(p_{\text{border}})\right|^2 \int\limits_{1/4}^{1/2} \mathrm{d}p \; \exp\left(-2\frac{p - p_{\text{border}}}{\hbar_{\text{eff}}} \, |q(p_{\text{border}})|\right)$$

$$\cdot \left[1 - \cos\left(\frac{T(p) - T_{\text{reg}}(p)}{\hbar_{\text{eff}}}\right)\right]. \qquad (5.48)$$

As the considerable contribution to the integral comes from a small region close to the border of the regular island, we assume that the difference $T(p) - T_{\text{reg}}(p)$ is linear in $p - p_{\text{border}}$

$$T(p) - T_{\text{reg}}(p) \approx c_0(p - p_{\text{border}}) \qquad \text{with} \qquad c_0 \; \text{const.} \qquad (5.49)$$

Using the substitution $y := (p - p_{\text{border}})/\hbar_{\text{eff}}$, we find

$$
\gamma_m = 4\hbar_{\text{eff}} \left| \widehat{\psi}_{\text{WKB},m}(p_{\text{border}}) \right|^2 \int\limits_{(1/4-p_{\text{border}})/\hbar_{\text{eff}}}^{(1/2-p_{\text{border}})/\hbar_{\text{eff}}} \mathrm{d}y \ \exp(-2y|q(p_{\text{border}})|)
$$

$$
\cdot \left[1 - \cos\left(c_0 y \right) \right]. \tag{5.50}
$$

We then have

$$
\gamma_m = 4\frac{h_{\text{eff}}}{2\pi} \left| \widehat{\psi}_{\text{WKB},m}(p_{\text{border}}) \right|^2 \int\limits_{(1/4-p_{\text{border}})/\hbar_{\text{eff}}}^{(1/2-p_{\text{border}})/\hbar_{\text{eff}}} \mathrm{d}y \ \exp(-2y|q(p_{\text{border}})|)
$$

$$
\cdot \left[1 - \cos\left(c_0 y \right) \right] \tag{5.51}
$$

$$
= c_1 h_{\text{eff}} \left| \widehat{\psi}_{\text{WKB},m}(p_{\text{border}}) \right|^2 \qquad \text{with } c_1 = \text{const.} \tag{5.52}
$$

The integral in equation (5.51) is $\hbar_{\text{eff}}$ independent and therefore incorporated in the constant c_1. The WKB wave function is normalized as $\int_{-\infty}^{\infty} \mathrm{d}p \, |\widehat{\psi}_{\text{WKB},m}(p)|^2 = 1$. Numerically we consider the wave function on a discrete momentum grid. This requires a change of the normalization to $\sum_k |\widehat{\psi}_{\text{WKB},m}(p_k)|^2 = 1$. As $\Delta p = 1/N = h_{\text{eff}}$ holds for one unit cell $(M_q = M_p = 1)$, the factor h_{eff} in (5.52) vanishes. The tunneling rate is then proportional to the square of the modulus of the regular wave function evaluated at the border of the regular island in p direction

$$
\gamma_m = c_1 \left| \widehat{\psi}_{\text{WKB},m}(p_{\text{border}}) \right|^2. \tag{5.53}
$$

The insertion of the on a discrete momentum grid correctly normalized analogue of the WKB wave function (5.45) yields

$$
\gamma_m = \frac{c_2 h_{\text{eff}}}{|q(p_{\text{border}})|} \exp\left(-\frac{2}{\hbar_{\text{eff}}} \int\limits_{p_{t,m}}^{p_{\text{border}}} \mathrm{d}p' \, |q(p')| \right), \tag{5.54}
$$

where $c_2 = (c_1 C^2)/4$.

The dimensionless Hamiltonian of a harmonic oscillator reads

$$
H(q,p) = \frac{p^2}{2} + \frac{\omega^2 q^2}{2} \tag{5.55}
$$

in normal coordinates. The quantum mechanically allowed energies are $E_m = h_{\text{eff}}\,\omega(m + 1/2)$ with $m \in \mathbb{N}_0$. With this knowledge we obtain $p_{t,m} = \sqrt{2E_m}$ as classical turning points and $|q(p)| = \sqrt{p^2 - 2E_m}/\omega$ as modulus of the position in the classically forbidden region $p > p_{t,m}$. The aspect ratio of the elliptic invariant tori which belong to the Hamiltonian (5.55) is $\sigma = \omega$, what yields $A_{\text{reg}} = \pi p_{\text{border}}^2/\omega$ for the area of the regular island. Now we are well-prepared for the evaluation of the prefactor and the integral in the exponential function of equation (5.54) and obtain

$$\gamma_m = c\,\frac{h_{\text{eff}}}{\sqrt{1 - \alpha_m}}\,\exp\left(-2\,\frac{A_{\text{reg}}}{h_{\text{eff}}}\left[\sqrt{1 - \alpha_m} - \alpha_m\,\ln\left(\frac{1 + \sqrt{1 - \alpha_m}}{\sqrt{\alpha_m}}\right)\right]\right), \quad (5.56)$$

where

$$\alpha_m := \left(m + \frac{1}{2}\right)\left(\frac{A_{\text{reg}}}{h_{\text{eff}}}\right)^{-1}. \tag{5.57}$$

The constant $c := (c_2\sqrt{\pi\omega})/\sqrt{A_{\text{reg}}}$ in equation (5.56) contains the integral of equation (5.51) and can therefore in general not be expressed by a closed term. We thus have to treat c as a fit parameter. Equation (5.56) provides a semiclassical formula for the analytical determination of direct dynamical tunneling rates. It is, however, only applicable to harmonic oscillator-like regular islands. Semiclassically, the tunneling rates behave as $\gamma \sim e^{2A_{\text{reg}}/h_{\text{eff}}}$, yielding the value 2 for the constant C mentioned in the introduction.

Let us briefly sum up the results of the derivation up to this point. We started with the formula

$$\gamma_m \;\approx\; \left\|\left(\hat{U} - \hat{U}_{\text{reg}}\right)\big|\psi_{\text{reg},m}\big\rangle\right\|^2, \tag{5.58}$$

which followed from our new approach to the understanding of direct dynamical tunneling from a regular island to the chaotic sea. For periodically kicked systems, which are constructed of discontinuous piecewise defined derivatives $T'(p)$ and $V'(q)$, regular functions $T_{\text{reg}}(p)$ and $V_{\text{reg}}(q)$ exist. This enabled us to evaluate equation (5.58) further

$$
\begin{aligned}
\gamma_m \;\approx\; & 2\sum_{k=0}^{N-1}\left|\widehat{\psi}_{\text{reg},m}(p_k)\right|^2\left[1 - \cos\left(\frac{T(p_k) - T_{\text{reg}}(p_k)}{\hbar_{\text{eff}}}\right)\right] \\
& + 2\sum_{k=0}^{N-1}\left|\psi_{\text{reg},m}(q_k)\right|^2\left[1 - \cos\left(\frac{V(q_k) - V_{\text{reg}}(q_k)}{\hbar_{\text{eff}}}\right)\right].
\end{aligned}
\tag{5.59}
$$

A semiclassical consideration justified the replacement of the sums by integrals

$$\gamma_m \approx 2 \int\limits_{p_{\min}}^{M_p+p_{\min}} dp \left|\widehat{\psi}_{\mathrm{reg},m}(p)\right|^2 \left[1 - \cos\left(\frac{T(p) - T_{\mathrm{reg}}(p)}{\hbar_{\mathrm{eff}}}\right)\right]$$
$$+ 2 \int\limits_{q_{\min}}^{M_q+q_{\min}} dq \left|\psi_{\mathrm{reg},m}(q)\right|^2 \left[1 - \cos\left(\frac{V(q) - V_{\mathrm{reg}}(q)}{\hbar_{\mathrm{eff}}}\right)\right]. \qquad (5.60)$$

For an harmonic oscillator-like regular island, where the momentum space integral of equation (5.60) turned out to be the dominating one, we obtained

$$\gamma_m \approx c_1 \left|\widehat{\psi}_{\mathrm{WKB},m}(p_{\mathrm{border}})\right|^2 \qquad (5.61)$$

by inserting a semiclassical expression for the wave function $\widehat{\psi}_{m,\mathrm{reg}}(p)$ and finally

$$\gamma_m \approx c\, \frac{h_{\mathrm{eff}}}{\sqrt{1 - \alpha_m}}$$
$$\cdot \exp\left(-2\, \frac{A_{\mathrm{reg}}}{h_{\mathrm{eff}}} \left[\sqrt{1 - \alpha_m} - \alpha_m \ln\left(\frac{1 + \sqrt{1 - \alpha_m}}{\sqrt{\alpha_m}}\right)\right]\right), \qquad (5.62)$$

where c is a fit parameter and where the constant α_m is given by equation (5.57). Out of these five formulae (5.62) is the only semiclassical one. It can be evaluated analytically. The other formulae (5.58) by (5.61) are accessible to a numerical evaluation, only. In the following we will check the accuracy of all formulae by comparing them with numerically determined tunneling rates. The presentation of the methods which we used for this purpose is postponed to section 5.4.

Harmonic oscillator-like regular island: Parameter set 1

We consider the example map P_{ex} of section 3.4 for the parameters $A = 0$, $r = 0.65$, $s = 2.0$, and $\varepsilon = 0.002$ for the case of one unit cell. The almost resonance-free elliptic regular island in the phase space has then the size $A_{\mathrm{reg}} \approx 0.27$. Figure 5.6 gives an image of the Husimi functions of the eigenstates of $\hat{U}_{\mathrm{reg}}$ with the quantum numbers $m = 0$ by $m = 5$ at $h_{\mathrm{eff}} = 1/30$. Before we check the accuracy of the formulae for direct dynamical tunneling rates, we present the regular kinetic as well as the regular potential energy function, $T_{\mathrm{reg}}(p)$ and $V_{\mathrm{reg}}(q)$, in comparison with the smoothed functions $T(p)$ and $V(q)$ as well as the phase space of the original and the regular system in figure 5.7. The function $T_{\mathrm{reg}}(p)$ is obtained from the discontinuous kinetic energy function $t(p)$, which
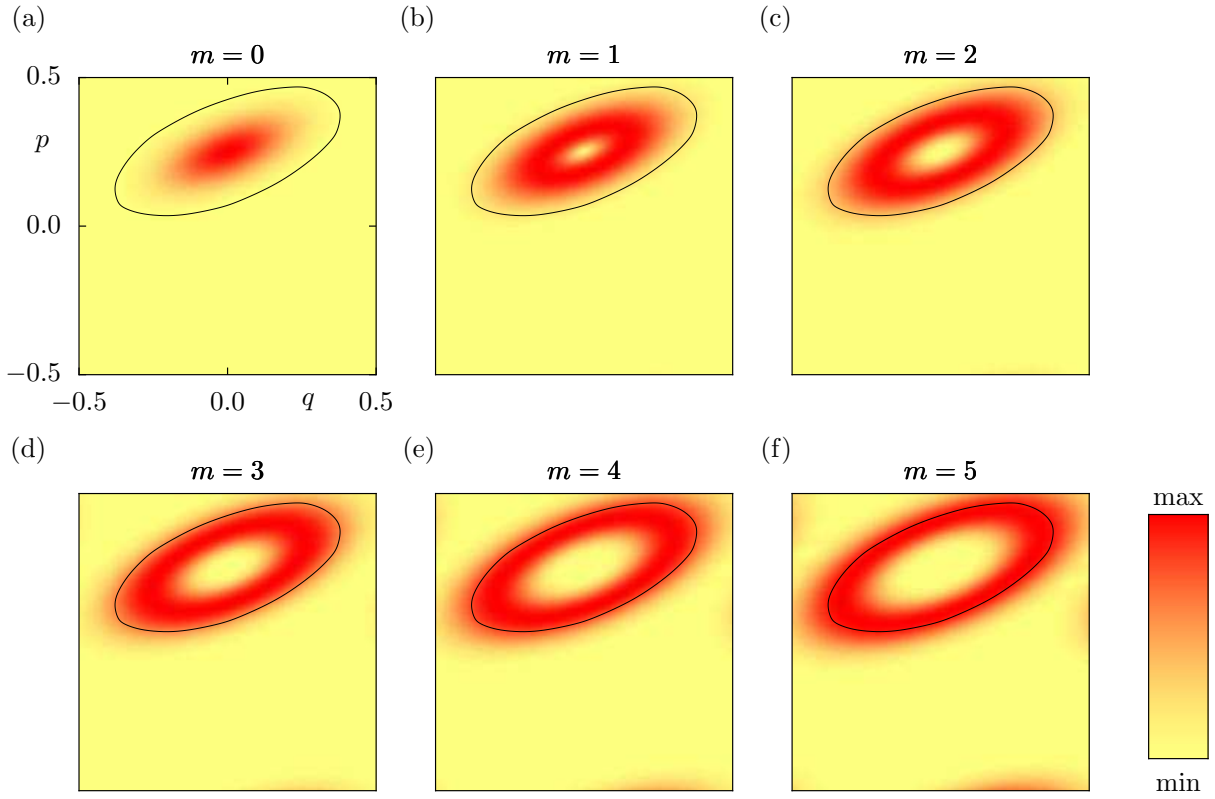
Figure 5.6: Husimi functions of the regular eigenstates of $\hat{U}_{\text{reg}}$ for $h_{\text{eff}} = 1/30$ and $m = 0$ (a) by $m = 5$ (f) for the parameters $A = 0$, $r = 0.65$, $s = 2.0$, and $\varepsilon = 0.002$. The approximate border of the regular island is plotted as a guide to the eye.

follows from an integration of its derivative (3.74). It is sufficient to take that piece of $t'(p)$ into account, which covers the domain of the momentum variables of the regular island. The extension of this piece to $[-1/2, 1/2]$ and a final integration yields

$$T_{\text{reg}}(p) = -p^2 + \frac{1}{2}p - \frac{1}{16}. \tag{5.63}$$

Similarly, we find

$$V_{\text{reg}}(q) = -\frac{13}{40}q^2 \tag{5.64}$$

from the discontinuous derivative of the potential energy (3.75). The integration constants in equations (5.63) and (5.64) are chosen such that both functions vanish at the center of the regular island $(q_{\text{c}}, p_{\text{c}}) = (0, 1/4)$.

The most important of the derived formulae for the determination of direct dynamical tunneling rates is (5.62), as it is a semiclassical one. In figure 5.8 we present the comparison of direct dynamical tunneling rates determined via this formula with numerically
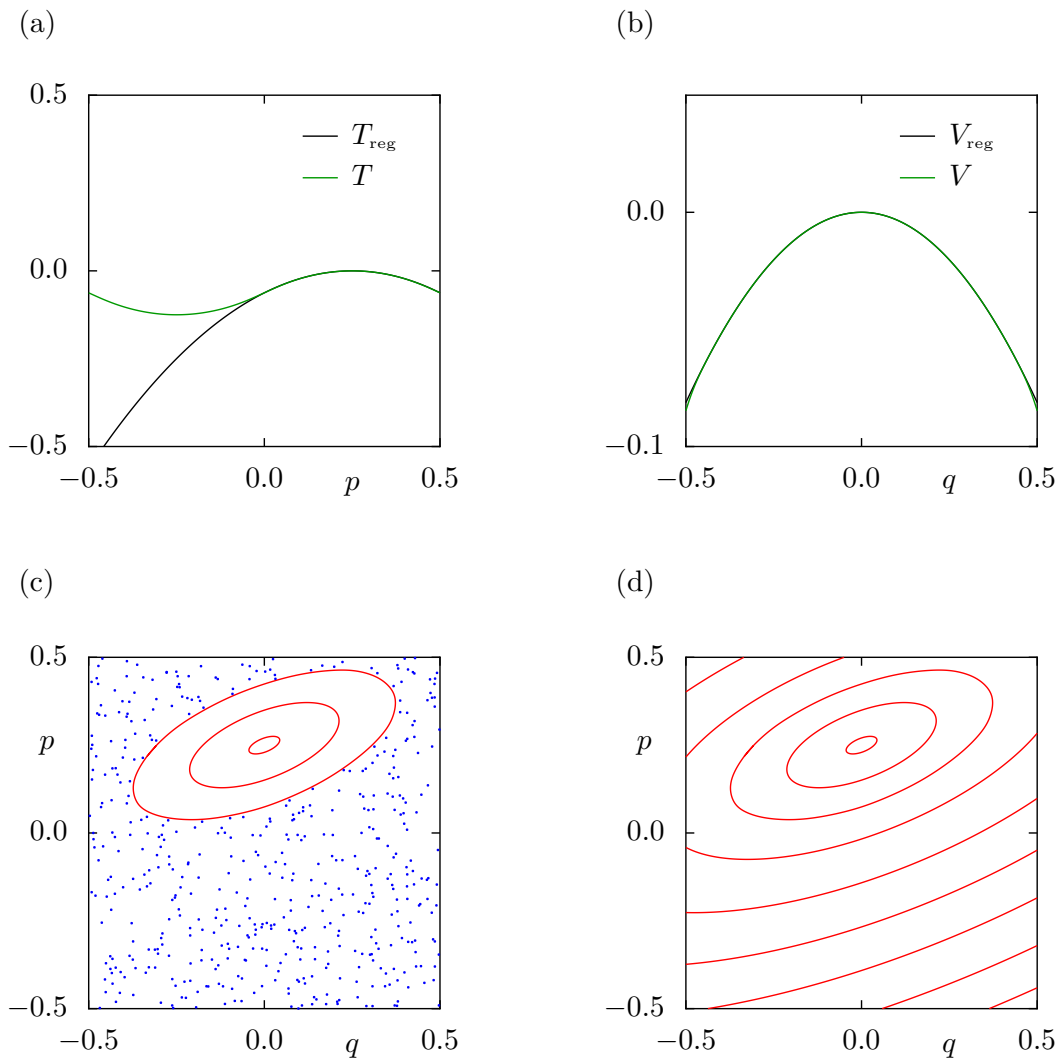
Figure 5.7: Comparison of the functions $T(p)$ and $T_{\text{reg}}(p)$ (a) as well as $V(q)$ and $V_{\text{reg}}(q)$ (b). Phase space of the original (c) and of the regular system (d).

determined data versus $1/h_{\text{eff}}$. We realize an agreement of the two data sets within a factor of two or even better over several orders of magnitude in the limit $h_{\text{eff}} \to 0$. This holds for the ground state with the quantum number $m = 0$, most left black data curves, as well as for the excited regular states.

The remaining formulae can only be numerically evaluated. We continue with the sum formula (5.59) and the integral formula (5.60). Their results are illustrated in figure 5.9. The prediction of the integral formula shows a very good agreement with the numerical data in the whole domain of $1/h_{\text{eff}}$, whereas the sum formula shows deviations for large h_{eff}. However, its prediction approaches the numerical data in the semiclassical limit. This has the following reason: For the Hilbert space size N the momentum grid, on which the sum in formula (5.59) is evaluated, has also the size N. As the effective Planck
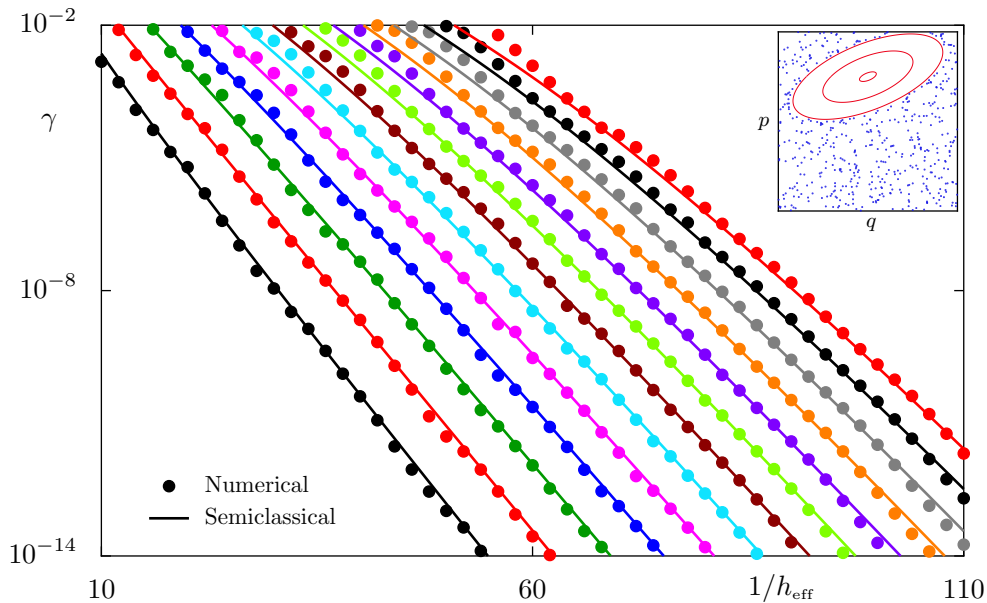
Figure 5.8: Comparison of numerically determined tunneling rates (dots) and the evaluation of the semiclassical formula (5.62) (lines). The value chosen for the fit parameter is $c = 0.19$. The most left black data curves belong to the quantum number $m = 0$, while the most right red curves represent the case $m = 12$. The inset shows an image of the classical phase space.

constant is given by $h_{\text{eff}} = 1/N$ for $M_q = M_p = 1$ according to equation (3.54), the grid is very coarse for large h_{eff}. The sum becomes consequently more precise for larger values of N, i.e. for $h_{\text{eff}} \to 0$. This explains why the agreement between the sum formula (5.59) and the numerical data becomes better in the semiclassical limit. As the integral formula (5.60) is continuously evaluated, this effect plays no role there. Its prediction is therefore acceptable in the whole $1/h_{\text{eff}}$ domain in figure 5.9.

It remains to compare the numerically determined tunneling rates with the evaluation of the border value formula (5.61), which is shown in figure 5.10. The agreement is again remarkably good over several orders of magnitude for all selected quantum numbers in the shown domain of $1/h_{\text{eff}}$.

Podolskiy and Narimanov investigate direct dynamical tunneling between two distinct regular islands embedded in the chaotic sea in reference [33]. They provide a formula which only allows for the determination of the ground state tunneling rate γ_0. The semiclassical expansion of Podolskiy's and Narimanov's tunnel splitting formula is presented

in reference [29]. Using a corrected version [34], we get

$$\gamma_0 = f h_{\text{eff}}^{5/2} \exp\left(-\frac{A_{\text{reg}}}{h_{\text{eff}}}(3 - \ln 4)\right) \qquad \text{with} \quad f = \text{const.} \qquad (5.65)$$

after the transfer of this ansatz to our situation with one regular island surrounded by the chaotic sea. The constant f is a fit parameter. The semiclassical formula (5.65) has a much simpler structure than equation (5.62). In figure 5.11 we compare the prediction of (5.65) with our numerical data. Furthermore, our semiclassical prediction given by formula (5.62) is shown. We realize that equation (5.65) describes the overall trend. Our formula agrees, however, much better with the numerically determined data, especially in the limit $h_{\text{eff}} \to 0$. A variation of the fit parameter f in (5.65) does not yield a better result. The better agreement with the numerically determined tunneling rates is the first advantage of our semiclassical formula (5.62). The second one is that it allows for the analytical determination of direct dynamical rates of all regular states belonging to a regular island with a very good precision.
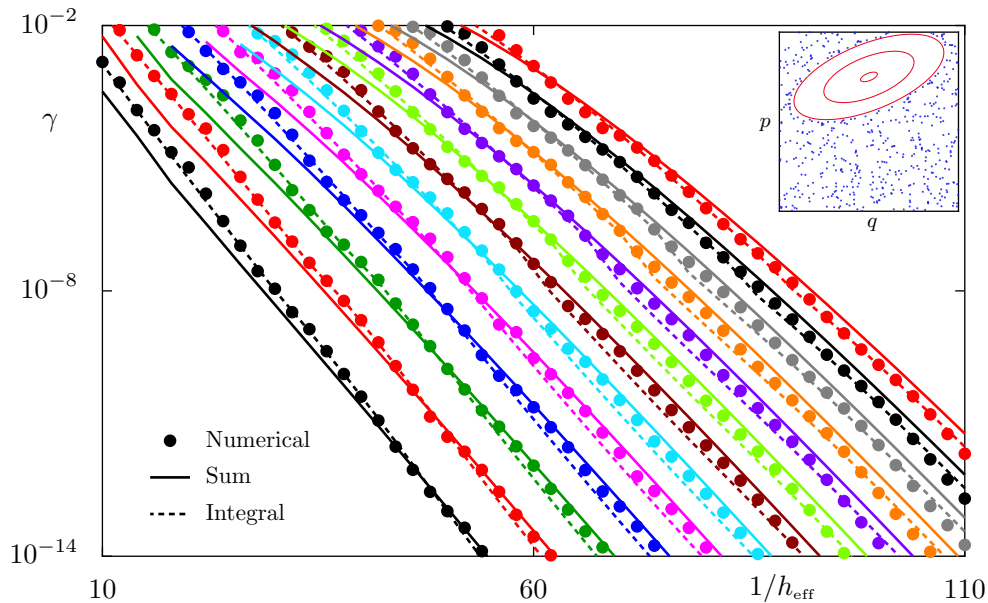
Figure 5.9: Comparison of numerically determined tunneling rates (dots) with the evaluation of the sum formula (5.59) (solid lines) and the integral formula (5.60) (dashed lines).
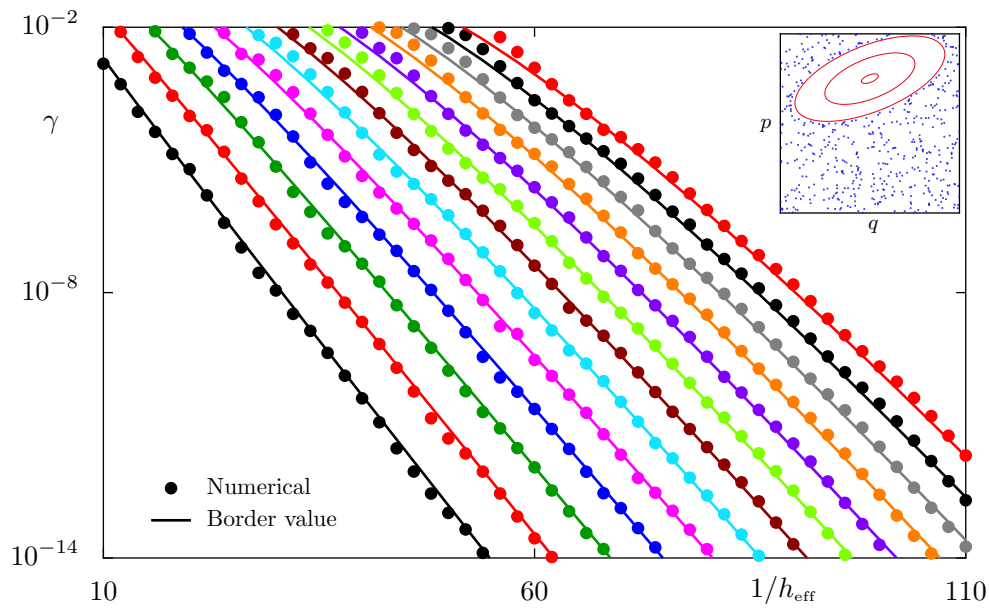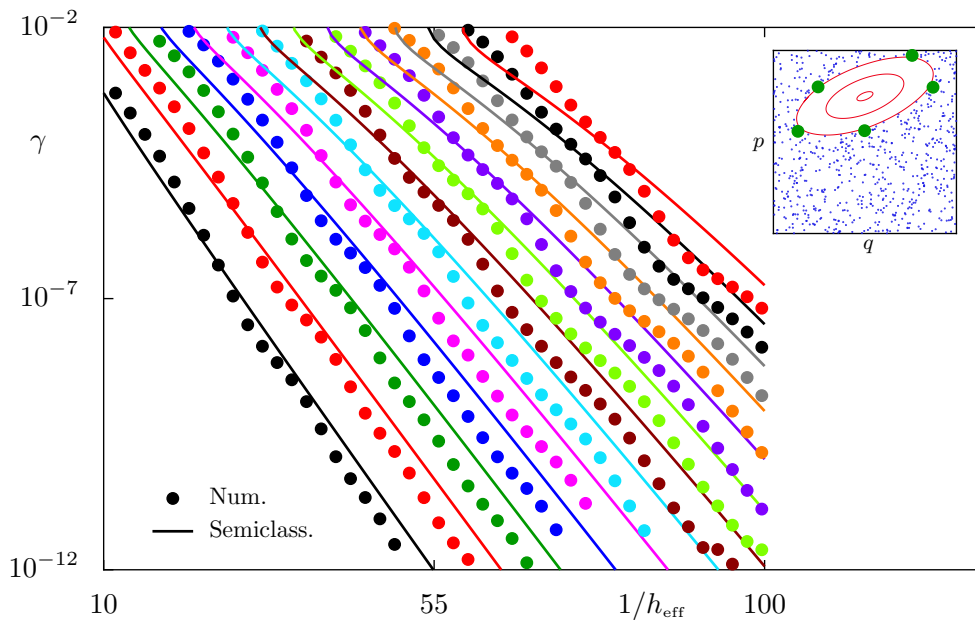
Figure 5.10: Comparison of numerically determined tunneling rates (dots) and the evaluation of the border value formula (5.61) (lines).
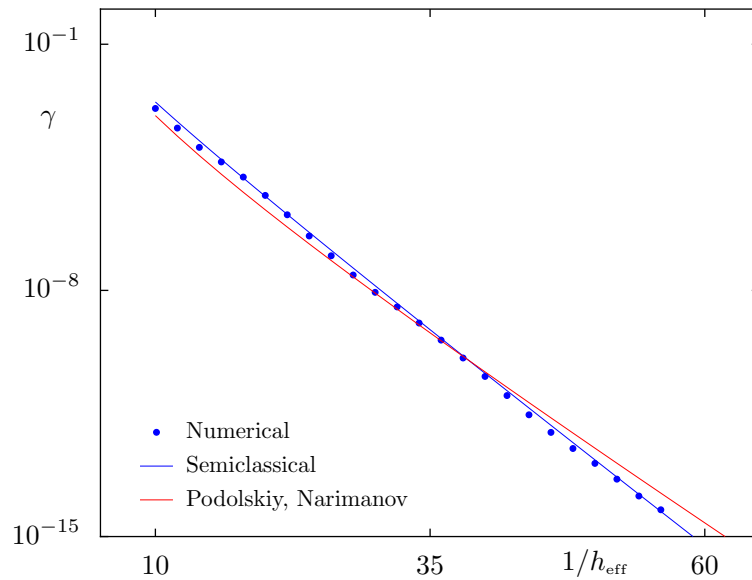
Figure 5.11: Comparison of numerically determined ground state tunneling rates (dots) with the evaluation of Podolskiy's and Narimanov's formula (5.65) (red line) and our formula (5.62) (blue line).

Harmonic oscillator-like regular island: Parameter set 2

Now we consider the same system as in the previous paragraph for the parameter set $A = 0$, $r = 0.65$, $s = 2.0$, and $\varepsilon = 0.015$. Here the smoothing parameter ε has a 7.5 times larger value than in the previous example. This is reflected by a smaller size of the regular island $A_{\text{reg}} \approx 0.215$. Let us consider the comparison of numerically determined tunneling rates with the semiclassical prediction following from equation (5.62). Figure 5.12 illustrates that the numerical data are described by the semiclassical formula for small quantum numbers m. The agreement is not as good as in the previous paragraph, but still acceptable. For increasing values of the quantum number m the numerical data show oscillations which are not reproduced by the semiclassical formula. This implies that our semiclassical formula is obviously not able to explain the behaviour for all quantum numbers appropriately. Figure 5.13 compares the tunneling rates shown in figure 5.12 with the regular quasi-energy spectrum. This comparison implies that the deviation of a numerically determined tunneling rate of a regular state with quantum number m from the semiclassical prediction seems to be correlated to the occurence of the $(m + 5j)$th, $j \in \mathbb{N}$, regular state at a large enough h_{eff}.

Figure 5.12: Comparison of numerically determined tunneling rates (dots) and the evaluation of the semiclassical formula (5.62) (lines). The value chosen for the fit parameter is $c = 0.12$. The inset shows an image of the classical phase space. The green dots represent an unstable orbit of period five.

The rotation number at the border of the regular island is close to $R = 1/5$, see section 3.4.1. Due to the smoothing of the discontinuous derivatives of the kinetic and the potential energy function of the system, equations (3.77) and (3.78), with a Gaussian, the border region of the regular island contains some fine structure.
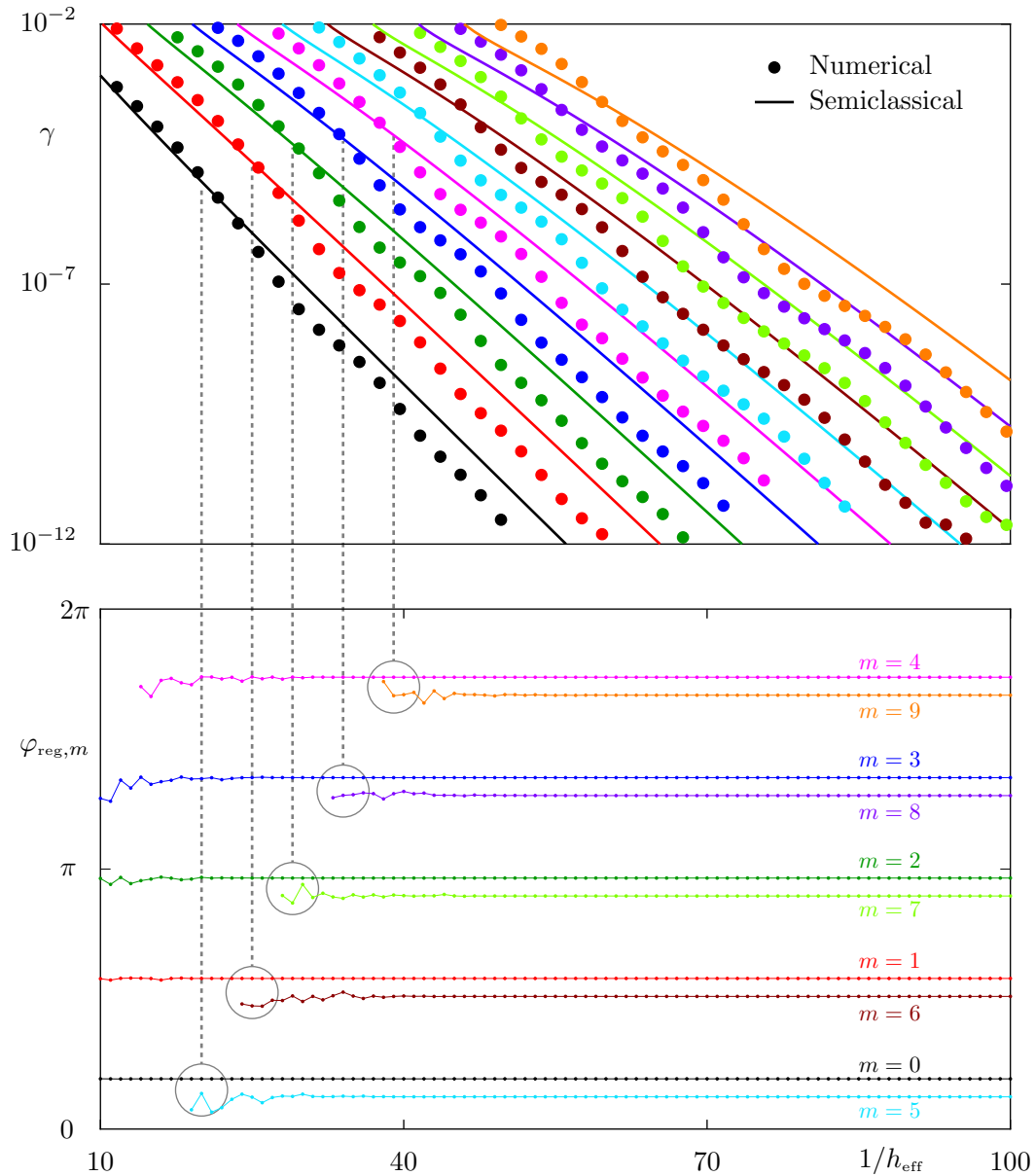
Figure 5.13: Part (a) of the figure contains the same information as figure 5.12. Part (b) shows the corresponding regular quasi-energy spectrum for the same values of the effective Planck constant as in (a).

Furthermore, several unstable fixed points exist in the chaotic sea. Five of them form an unstable orbit close to the border of the regular island. It is denoted by green dots in the inset of figure 5.12. This orbit might, similar to the influence of resonance island chains within regular islands in the resonance-assisted tunneling theory, be responsible for a possible coupling between the mth and the $(m+5j)$th regular state. As our semiclassical formula (5.62) does not account for such couplings, it cannot reproduce their influence on the dynamical tunneling rates. We emphasize that this is an assumption rather than an explanation.

A more thorough look at the numerically determined tunneling rates of the example in the previous paragraph also reveals oscillations. They are, however, much smaller. In this case also an unstable orbit with the period five exists in the vicinity of the regular island. But its distance to the border of the regular island is larger, so that its influence on tunneling from the regular island to the chaotic sea is assumed to be smaller. The application of our semiclassical formula (5.62) yields thus better results in that case.

5.3.2 Deformed regular island

Up to this point we restricted the application of our formulae for direct dynamical tunneling rates to a simple harmonic oscillator-like regular island. More generic is, however, the situation of a deformed regular island. This requires a new example system. As starting point we take the previous two examples. We modify the discontinuous derivative of the potential energy function (3.75) by adding a quadratic term

$$v'(q) = -rq + Rq^2, \tag{5.66}$$

where R is a new system-specific parameter. The derivative of the discontinuous kinetic energy function (3.74) is kept unchanged. Smoothing with a Gaussian, as is explained in section 3.4, yields again the analytical function $V'(q)$, and $V(q)$ after an integration. Here we consider the parameter set $A = 0$, $r = 0.26$, $s = 2.0$, $R = 0.4$, and $\varepsilon = 0.005$. Using these parameters and equation (5.66) we obtain

$$V_{\text{reg}}(q) = -\frac{13}{100}q^2 + \frac{2}{15}q^3 \tag{5.67}$$

for the regular potential energy function. Figure 5.14 shows $T_{\text{reg}}(p)$ and $V_{\text{reg}}(q)$ in comparison with the smoothed functions $T(p)$ and $V(q)$ as well as the phase space of the original and the regular system. As the border of the deformed but still almost resonance-free regular island is closer to the edge of the phase space unit cell in q direction, the function $V(q)$ governs the island size in this system.
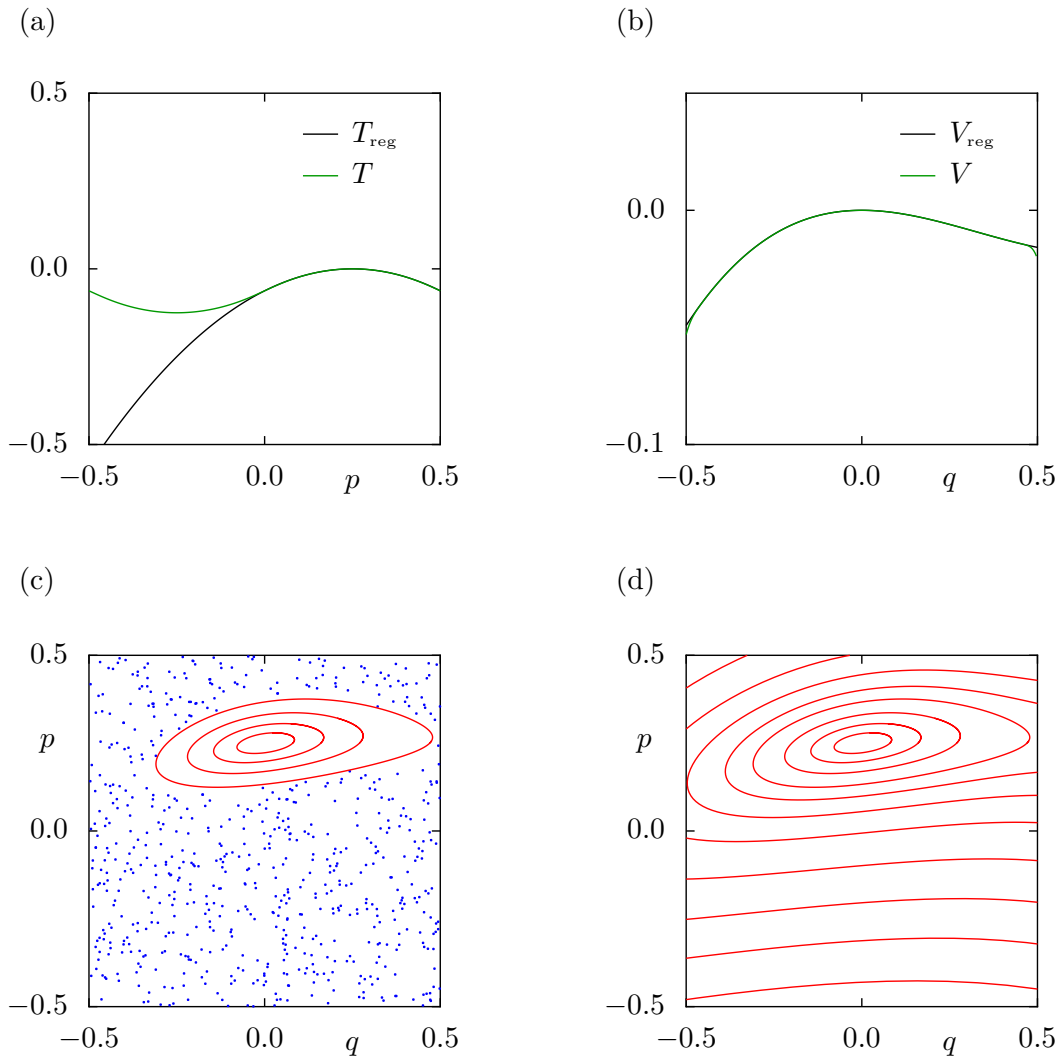
Figure 5.14: Comparison of the functions $T(p)$ and $T_{\text{reg}}(p)$ (a) as well as $V(q)$ and $V_{\text{reg}}(q)$ (b). Phase space of the original (c) and that of the regular system (d).

For tilted elliptic regular islands the eigenstates of a corresponding harmonic oscillator Hamiltonian turned out to be good regular states. In the case of a deformed regular island, regular states are analytically not available. They need to be constructed numerically. By means of e.g. the Lie transform method, which is described in appendix C.1, we can determine a time independent 1D Hamiltonian $\hat{H}_{\text{reg}}(q, p)$, which interpolates the dynamics within the regular island and which enables its continuation to the chaotic sea. The quantization of $\hat{H}_{\text{reg}}(q, p)$, e.g. by using the method which is described in appendix C.2, yields a Hamilton operator whose eigenstates $|\psi_{\text{reg},m}\rangle$ can be determined numerically. Figure 5.15 shows the Husimi functions of the regular states $|\psi_{\text{reg},m}\rangle$ for $m = 0$ by $m = 5$ at $h_{\text{eff}} = 1/50$. They look nice. Their comparison with the regular eigenstates of $\hat{U}$ within the domain of the regular island is, however, not promising. The precision is only of the
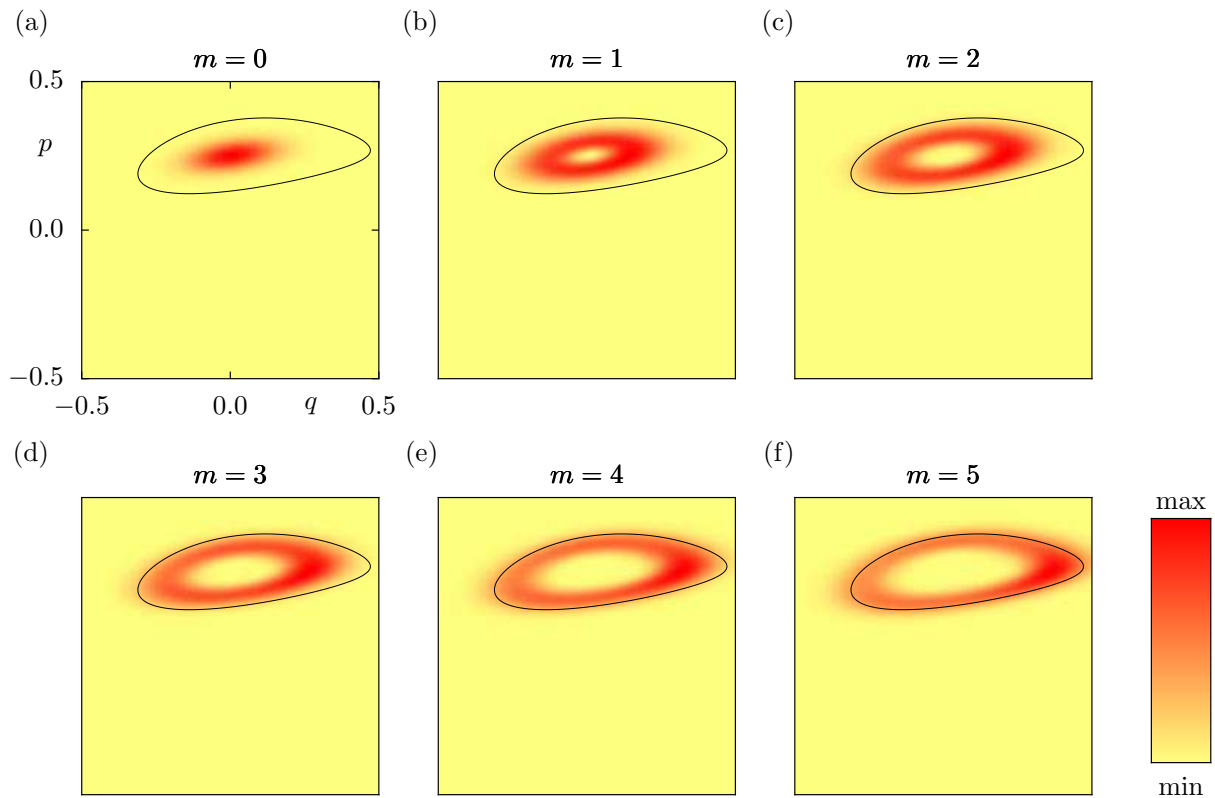
Figure 5.15: Husimi functions of regular states of the modified example map for $m = 0$ by $m = 5$ for $h_{\text{eff}} = 1/50$. The border of the deformed regular island is additionally plotted.

order $\sim 10^{-5}$. As e.g. formula (5.58) contains the difference of two states which are almost identical within the region of the regular island, it is essential to contstruct the regular states with an error smaller than the tunneling rate. A precision of the order $\sim 10^{-5}$ is obviously not sufficient.

Equation (5.59) contains the regular wave function as a factor of a product. The precision of the regular states is here sufficient for the evaluation of the formula. As the potential energy function determines the size of the regular island in this exmaple, the restriction to the sum in position space is sufficient

$$\gamma_m = 2 \sum_{k=0}^{N-1} |\psi_{\text{reg},m}(q_k)|^2 \left[1 - \cos \left(\frac{V(q_k) - V_{\text{reg}}(q_k)}{\hbar_{\text{eff}}} \right) \right]. \tag{5.68}$$

The resulting direct dynamical tunneling rates are compared with numerically determined ones in figure 5.16. Also in this case with a deformed regular island the agreement is remarkably good over several orders of magnitude. We believe that also a position space

analogue of equation (5.61),

$$\gamma_m \;=\; c\,|\psi_{\mathrm{reg},m}(q_{\mathrm{border}})|^2, \tag{5.69}$$

is valid here. Figure 5.17 confirms this. Using the general WKB ansatz [8]

$$\psi_{\mathrm{WKB},m}(q) = \sum_\alpha c_\alpha \psi_\alpha(q) \quad \text{with} \quad \psi_\alpha(q) = \left(\frac{\partial \hat{H}_{\mathrm{reg}}}{\partial p_\alpha}\right)^{-\frac{1}{2}} \exp\left(\frac{\mathrm{i}}{\hbar_{\mathrm{eff}}} \int\limits_{q_m}^{q} \mathrm{d}q'\, p_\alpha(q')\right) \tag{5.70}$$

with expansion coefficients c_α, momentum branches p_α and classical turning points q_m, where $(\partial \hat{H}_{\mathrm{reg}}/\partial p_\alpha)|_{p_\alpha(q_m)} = 0$ holds, it should in principle be possible to replace the regular position space wave functions in equations (5.68) and (5.69). The index α extends over all momentum branches. Since their number depends on the considered system, we neglect the borders of summation here. But, the general WKB function (5.70) can to our knowledge not be evaluated analytically. We are therefore currently not able to present a semiclassical formula for the analytical determination of direct dynamical tunneling rates for the case of a deformed regular island.
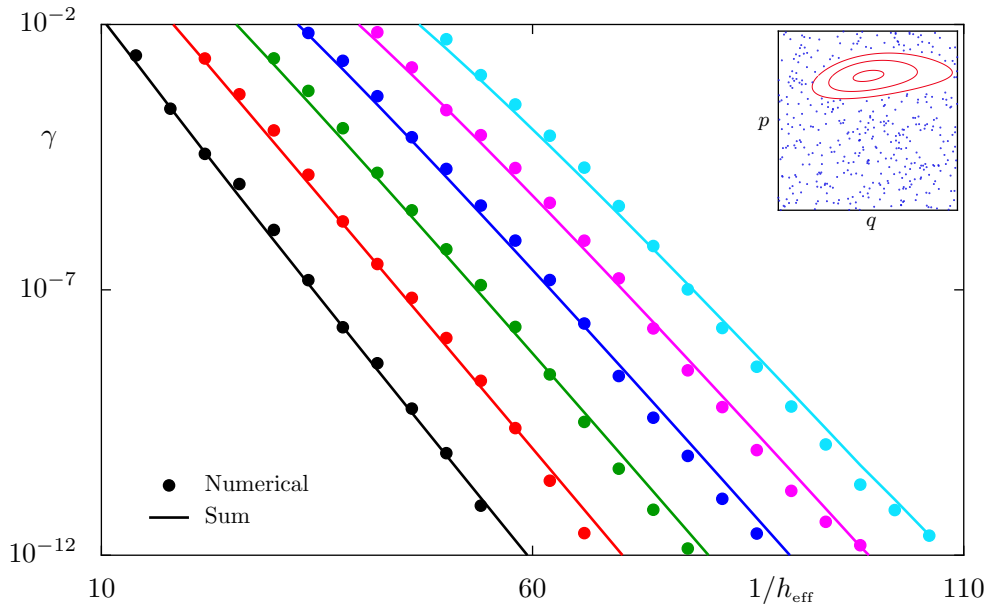
Figure 5.16: Comparison of numerically determined tunneling rates (dots) and the evaluation of the sum formula (5.68) (lines). The most left black data curves belong to the quantum number $m = 0$, while the most right light-blue curves represent the case $m = 5$. The inset shows an image of the classical phase space.
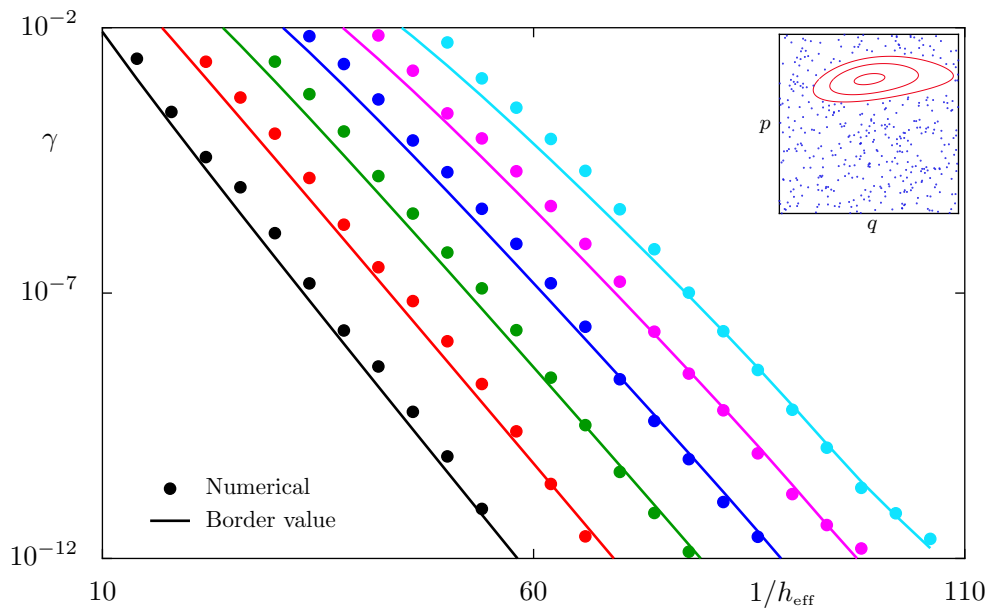
Figure 5.17: Comparison of numerically determined tunneling rates (dots) and the evaluation of the border value formula (5.69) (lines).

5.4 Methods for the numerical determination of dynamical tunneling rates

In the previous section we showed several plots containing numerically determined direct dynamical tunneling rates for transitions of regular states from an island of stability to the chaotic sea. We now introduce two methods which we used for their determination. The first one can be applied to systems with a chain of equal transporting regular islands and a chaotic sea with a mean drift against the direction of the regular transport. The second method is applicable to systems with and without transport.

5.4.1 Wave packet dynamics method

The wave packet dynamics method provides a possibility for the numerical determination of dynamical tunneling rates of regular states from an island of stability to the chaotic sea. Its applicability requires a chain of equal transporting regular islands and a chaotic sea with a mean drift against the regular transport. Before we explain this method, we focus on some important technical details.

Again, we perform the illustration of the derivation on the basis of the example system, which was introduced in section 3.4. Let us consider it for the parameter set $A = 1.0$,

$s = 2.0$, $r = 0.65$, and $\varepsilon = 0.015$ at first for one unit cell. We have already seen that the phase space is mixed with a large harmonic oscillator-like regular island surrounded by the chaotic sea, see e.g. figure 3.6. We now extend the phase space to $M_q > 1$ unit cells in q direction with the Hilbert space size $N \in \mathbb{N}$. According to equation (3.54) we have $h_{\text{eff}} = M_q/N$ as effective Planck constant. This means that e.g. each of the tuples $(M_q = 1, N = 20)$, $(M_q = 2, N = 40)$, or $(M_q = 10, N = 200)$ yields $h_{\text{eff}} = 1/20$. Let us study the quantized positions defined by equation (3.96). Since N is even and M_q is odd for each of the three tuples, we can set $\theta_p = 0$ according to equation (3.105)

$$q_n \quad = \quad n\frac{M_q}{N} - \frac{1}{2} \qquad \text{with} \qquad n \in \mathbb{Z}_N \; . \tag{5.71}$$

The last two tuples consist of commensurate numbers M_q and N. The borders of the M_q unit cells, $k - 1/2$ with $k \in \mathbb{Z}_{M_q}$, lie therefore on the q grid. This implies that the spatial period in q direction is actually one in each of the three cases.

The wave packet dynamics method requires sometimes an enlargement of the spatial period of the system in q direction with the constraint that the effective Planck constant needs to be kept constant. The reasoning up to this point shows, however, that this is not possible. A solution consists of finding rational approximants of $h_{\text{eff}} = 1/N$. We consider

$$h_{\text{eff}} \quad = \quad \frac{1}{N} \quad =: \quad \frac{1}{d+1} \quad \approx \quad \frac{1}{d+\sigma}, \tag{5.72}$$

where $d \in \mathbb{N}$ and $\sigma = (\sqrt{5} - 1)/2$ is the golden mean. It is the irrational number which is worst approximated by rationals. Considering its continued fraction

$$\sigma \quad = \quad \cfrac{1}{1 + \cfrac{1}{1 + \cfrac{1}{\dots}}} \tag{5.73}$$

we get approximants order by order. The third column of table 5.1 shows some approximants of σ. By inserting them into (5.72) we iteratively get approximants of h_{eff}. The last column of table 5.1 shows some of them for the case $h_{\text{eff}} = 1/20$ with $d = 19$. We emphasize that all approximants belong to slightly different values of the effective Planck constant - but, the spatial period in q direction is given by the numerator of the approximant, since numerator and denominator are incommensurate integers. We have thus the possibility to enlarge the spatial period in q direction by only changing the value of the effective Planck constant slightly. The approximant with $n = 26$ will later be used for an

example. The wave packet dynamics method uses the transport property of a chain of
equal regular islands for the determination of dynamical tunneling rates of regular states

| n	continued fraction	approximant of σ			$h_{\text{eff}} = M_q/N$
1	$[0, 1]$	$\frac{1}{1}$	$=$	1.00000000000	$\frac{1}{20}$
2	$[0, 1, 1]$	$\frac{1}{2}$	$=$	0.50000000000	$\frac{2}{39}$
3	$[0, 1, 1, 1]$	$\frac{2}{3}$	$\approx$	0.66666666667	$\frac{3}{59}$
4	$[0, 1, 1, 1, 1]$	$\frac{3}{5}$	$=$	0.60000000000	$\frac{5}{98}$
5	$[0, 1, 1, 1, 1, 1]$	$\frac{5}{8}$	$\approx$	0.62500000000	$\frac{8}{157}$
6	$[0, 1, 1, 1, 1, 1, 1]$	$\frac{8}{13}$	$\approx$	0.61538461538	$\frac{13}{255}$
7	$[0, 1, 1, 1, 1, 1, 1, 1]$	$\frac{13}{21}$	$\approx$	0.61904761905	$\frac{21}{412}$
8	$[0, 1, 1, 1, 1, 1, 1, 1, 1]$	$\frac{21}{34}$	$\approx$	0.61764705882	$\frac{34}{667}$
9	$[0, 1, 1, 1, 1, 1, 1, 1, 1, 1]$	$\frac{34}{55}$	$\approx$	0.61818181818	$\frac{55}{1079}$
10	$[0, 1, 1, 1, 1, 1, 1, 1, 1, 1, 1]$	$\frac{55}{89}$	$\approx$	0.61797752809	$\frac{89}{1746}$
11	$[0, 1, 1, 1, 1, 1, 1, 1, 1, 1, 1, 1]$	$\frac{89}{144}$	$\approx$	0.61805555556	$\frac{144}{2825}$
12	$[0, 1, 1, 1, 1, 1, 1, 1, 1, 1, 1, 1, 1]$	$\frac{144}{233}$	$\approx$	0.61802575107	$\frac{233}{4571}$
13	$[0, 1, 1, \ldots, 1, 1]$	$\frac{233}{377}$	$\approx$	0.61803713528	$\frac{377}{7396}$
14	$[0, 1, 1, \ldots, 1, 1]$	$\frac{377}{610}$	$\approx$	0.61803278689	$\frac{610}{11967}$
15	$[0, 1, 1, \ldots, 1, 1]$	$\frac{610}{987}$	$\approx$	0.61803444782	$\frac{987}{19363}$
16	$[0, 1, 1, \ldots, 1, 1]$	$\frac{987}{1597}$	$\approx$	0.61803381340	$\frac{1597}{31330}$
17	$[0, 1, 1, \ldots, 1, 1]$	$\frac{1597}{2584}$	$\approx$	0.61803405573	$\frac{2584}{50693}$
18	$[0, 1, 1, \ldots, 1, 1]$	$\frac{2584}{4181}$	$\approx$	0.61803396317	$\frac{4181}{82023}$
19	$[0, 1, 1, \ldots, 1, 1]$	$\frac{4181}{6765}$	$\approx$	0.61803399852	$\frac{6765}{132716}$
20	$[0, 1, 1, \ldots, 1, 1]$	$\frac{6765}{10946}$	$\approx$	0.61803398502	$\frac{10946}{214739}$
$\vdots$	$\vdots$	$\vdots$			$\vdots$
26	$[0, 1, 1, \ldots, 1, 1]$	$\frac{121393}{196418}$	$\approx$	0.61803398874	$\frac{196418}{3853335}$
$\vdots$	$\vdots$	$\vdots$			$\vdots$

Table 5.1:   First column: counting variable, second column: continued fraction decom-
position, third column: rational approximants of the golden mean σ, last column: rational
approximants of $h_{\text{eff}} = 1/20$.

from a regular island to the chaotic sea. For a certain value of the effective Planck constant we take an approximant with incommensurate integers N and M_q according to the introductory remarks. All of the M_q unit cells contain equal regular islands.

Figure 5.18(a) shows the modulus of the time evolution operator $\hat{U}$ in position representation for the fifth approximant of $h_{\mathrm{eff}} = 1/20$ in table 5.1, ($M_q = 8, N = 157$), on the $N \times N$ grid. Part (b) of this figure illustrates a cut along the red diagonal of (a). We clearly see the banded structure of $\hat{U}$ with width B. The bands below the main diagonal of $\hat{U}$ are responsible for the regular transport one cell to the right according to $A = 1.0$, and the bands above the diagonal yield the transport of chaotic wave function components to the left. The entries in the lower left and upper right corner ensure the periodic boundary conditions in q direction.

The basic idea of the wave packet dynamics method is to start with the semiclassical state $\big|\tilde{\phi}_k^{\mathrm{sc},m}\big\rangle$ belonging to an allowed quantum number m, whose Husimi function localizes on the mth quantizing torus of the regular island in unit cell k.

The wave packet $\big|\tilde{\phi}_k^{\mathrm{sc},m}\big\rangle$ mainly excites the regular state living on the mth quantizing torus in the regular island of unit cell k. It has a certain initial weight $w(0)$ within this island. But this state is no eigenstate of $\hat{U}$. The application of $\hat{U}$ to $\big|\tilde{\phi}_k^{\mathrm{sc},m}\big\rangle$ does therefore not only lead to a state living in unit cell $(k+1) \bmod M_q$ according to (4.68), but also to its decay from the regular island to the chaotic sea. Thus, the weight of $\hat{U}\big|\tilde{\phi}_k^{\mathrm{sc},m}\big\rangle$ within the regular island of unit cell $(k+1) \bmod M_q$, denoted by $w(1)$, is smaller than the original weight $w(0)$ of the state $\big|\tilde{\phi}_k^{\mathrm{sc},m}\big\rangle$ in the regular island of unit cell k. The iterated application of $\hat{U}$ to the time evolved wave packet enables the determination of the weight
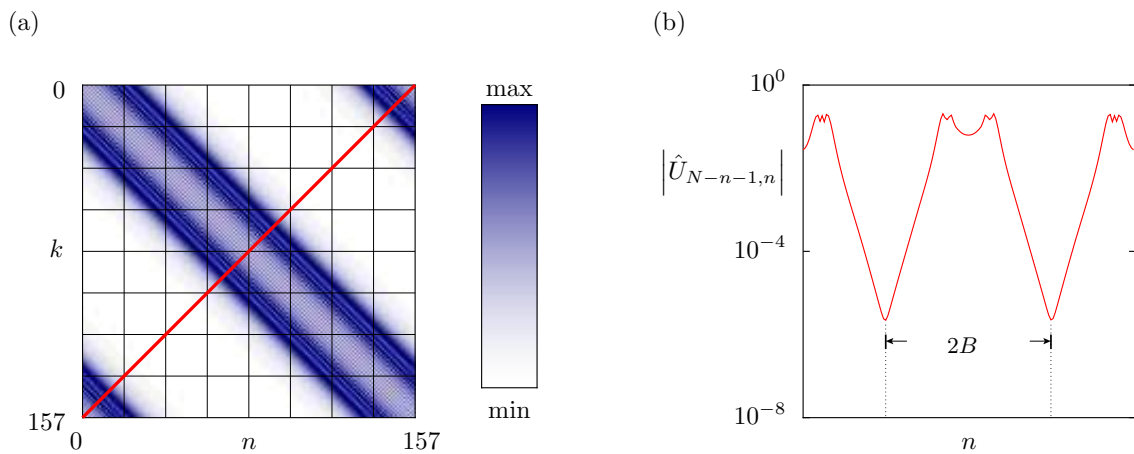
Figure 5.18: (a) The modulus of the time evolution operator $\hat{U}$ with the elements $\hat{U}_{k,n}$ in position representation for $M_q = 8$ and $N = 157$ on the $N \times N$ grid. For a better orientation an 8×8 grid is given in the background. (b) Cut along the red diagonal of (a). $\hat{U}$ has a banded structure with width B.

as a function of natural valued times t: $w(t)$. With increasing t the weight of the initial semiclassical state decreases in the regular phase space part. It increases at the same in the chaotic sea. In order to prevent the return of chaotic components into the regular island of unit cell $(k + t + 1) \bmod M_q$ after the $(t + 1)$st application of $\hat{U}$, it is necessary to transport them against the regular transport direction, i.e to the left. Now we see, why the requirement of a chaotic sea with a mean drift to the left is essential for the applicability of the wave packet dynamics method.

Decay processes are theoretically described by an exponential law,

$$w(t) = w(0)\mathrm{e}^{-\gamma_m t}, \tag{5.74}$$

where γ_m is the decay rate of the regular state with quantum number m. For the determination of the weight $w(t)$ we have two possibilities:

1. We can compute the Husimi function of $\big|\tilde{\phi}^{\mathrm{sc},m}_{(k+t)\bmod M_q}\big\rangle = \hat{U}^t\big|\tilde{\phi}^{\mathrm{sc},m}_k\big\rangle$. It has its main contribution in the unit cell $(k + t) \bmod M_q$. An integration of the Husimi function over the regular island of this cell yields $w(t)$. In order to simplify the procedure, the initial Husimi function should be normalized such that its integral over the whole phase space $[-1/2, M_q - 1/2] \times [-1/2, 1/2]$ is equal to one.

2. Since $\big|\tilde{\phi}^{\mathrm{sc},m}_{(k+t)\bmod M_q}\big\rangle$ has its main contribution in the unit cell $(k + t) \bmod M_q$, the weight $w(t)$ is also given by the projection of $\big|\tilde{\phi}^{\mathrm{sc},m}_{(k+t)\bmod M_q}\big\rangle$ onto the initial state $\big|\tilde{\phi}^{\mathrm{sc},m}_k\big\rangle$ translated t unit cells on the same q grid to the right:
   $w(t) = \big\langle \hat{T}(t,0)\tilde{\phi}^{\mathrm{sc},m}_k \big| \tilde{\phi}^{\mathrm{sc},m}_{(k+t)\bmod M_q}\big\rangle$.

Compared to the second method, the first one is very time consuming due to the necessary repeated Husimi function determinations.

Since $\big|\tilde{\phi}^{\mathrm{sc},m}_k\big\rangle$ is no eigenstate of the time evolution operator $\hat{U}$, it can apart from the regular state living on the mth quantizing torus within the island of unit cell k also excite states with other quantum numbers. Quantizing tori of regular states with larger quantum numbers as m enclose a larger area within the regular island and lie therefore closer to the border of the island. Their tunneling rates are obviously larger and their influence becomes relevant during the first wave packet dynamics steps. After the sufficient decay of these states, the decay of the mth regular state is the dominating one. When the mth regular state is nearly completely decayed, the excited regular state with the next smaller quantum number begins to dominate. This can be seen in the functions $w(t)$, if the Husimi function method is used for the weight determination. Figure 5.19 shows them as semi-logarithmic plots for an example. Since the initial semiclassical wave packets $\big|\tilde{\phi}^{\mathrm{sc},m}_k\big\rangle$ belonging to different quantum numbers are approximately orthogonal to each

other, (4.67), the function $w(t)$ determined via the projection method shows only the decay of the mth regular state. Figure 5.20 illustrates this by showing the functions $w(t)$ for the same parameters as in figure 5.19. The decay rates, which are given by the slopes of the linear parts, are of course identical. In order to visualize the decay processes belonging to other quantum numbers than m, we can additionally compute the overlap $\langle \hat{T}(t,0)\tilde{\phi}_k^{\mathrm{sc},n} | \tilde{\phi}_{k+t}^{\mathrm{sc},m}\rangle$, where $m \neq n$. The two methods for the determination of the weight $w(t)$ have therefore both, advantages and disadvantages.

We have already seen that the transport property of the chaotic sea to the left is essential for not disturbing the decay process of the regular states to the chaotic sea. With $A_{\mathrm{reg}} \approx 0.215$ as relative area of the regular island in one unit cell and $v_{\mathrm{reg}} = 1$ as regular transport velocity, we have $v_{\mathrm{ch}} \approx -0.274$ as mean drift velocity of the chaotic sea to the left according to equation (3.95). Due to the spatial periodicity after M_q cells in q direction chaotic components are moved to the right end of the system when they reach the left one. For regular components the opposite holds, when they reach the right end of the system. The chaotic components reach therefore after

$$t_{\mathrm{critical}} \approx \frac{M_q}{|v_{\mathrm{reg}}| + |v_{\mathrm{ch}}|} \tag{5.75}$$
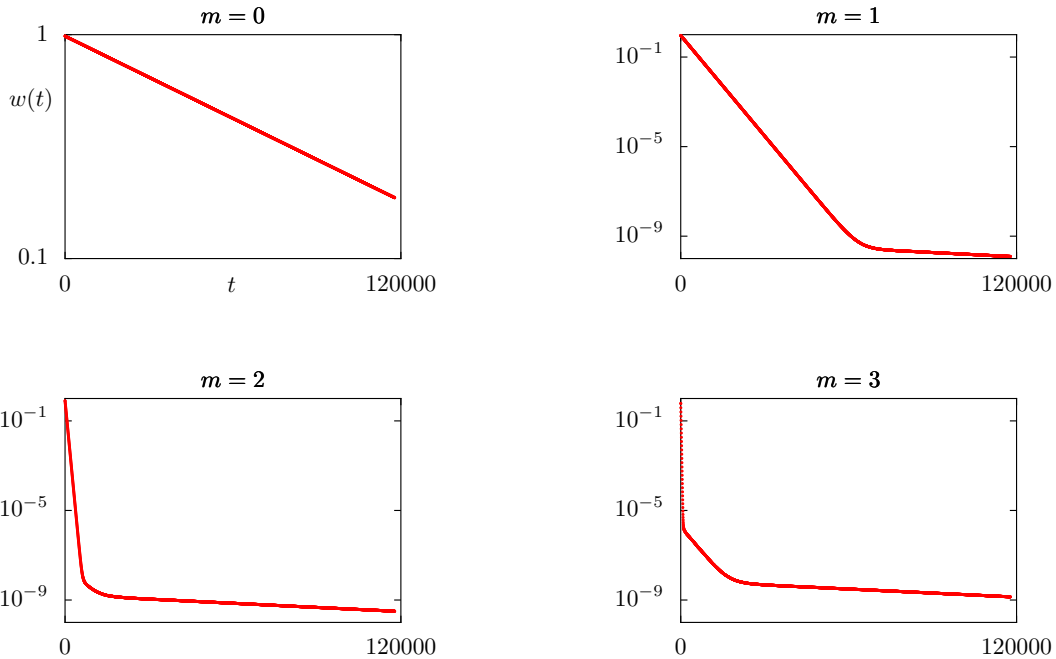
Figure 5.19: Weight w as a function of time for $h_{\mathrm{eff}} = 196418/3853335 \approx 1/20$ for the quantum numbers $m = 0$ by $m = 1$. The weights were determined using the Husimi function method. We clearly see different decays in the plots.
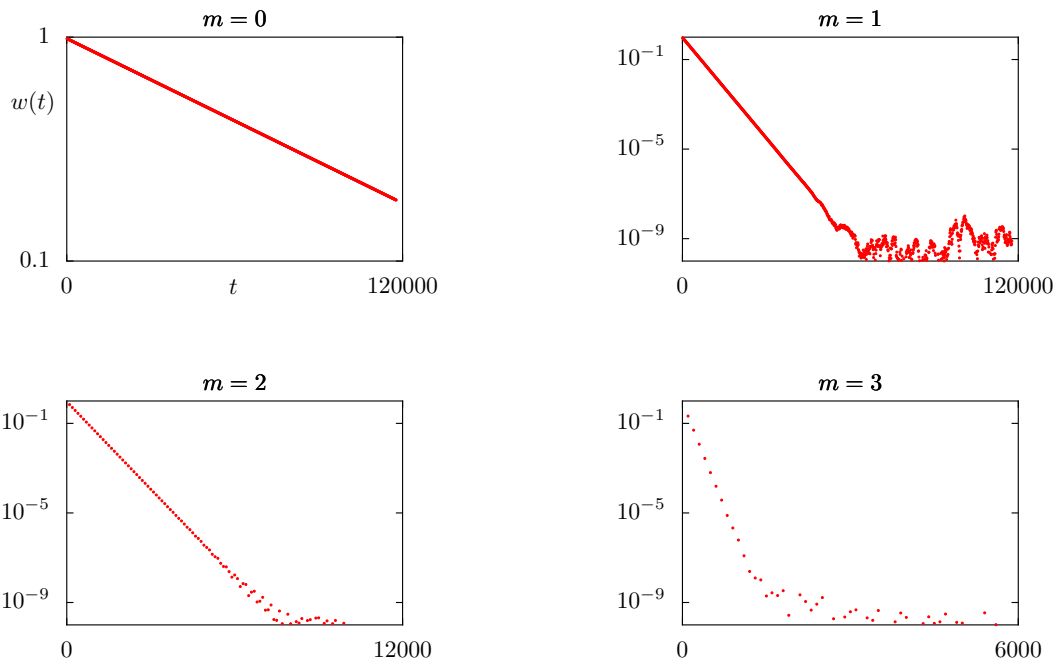
Figure 5.20: Same situation as in figure 5.19. Here we used the projection method in order to determine the function $w(t)$. In contrast to figure 5.19 we see one decay per plot due to the approximate orthogonality of the initial wave packets.

the unit cell in which the regular weight of the wave packet is currently being determined. A return of weight from the chaotic sea to the regular island can then no longer be prevented. It is thus useless to continue the wave packet dynamics beyond t_{critical}. Figure 5.21 illustrates the return of weight from the chaotic sea to the regular island for $t > t_{\text{critical}}$. If we needed the weight for times $t > t_{\text{critical}}$, we could take another rational approximant of h_{eff} with a larger numerator M_q yielding a negligibly different value of h_{eff}.
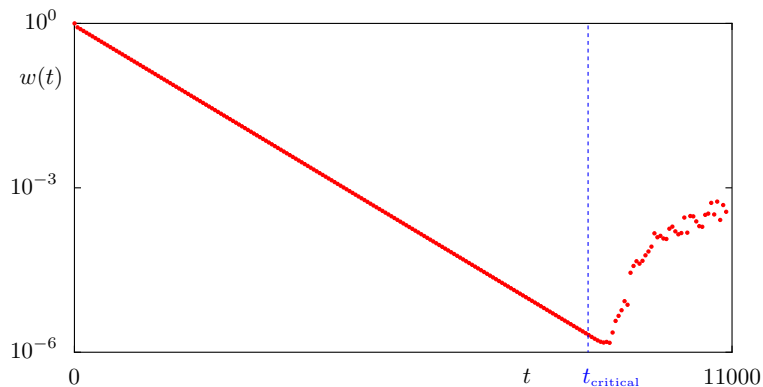

Figure 5.21: The return of weight to the regular island for times larger than the critical time t_{critical} (5.75). The shown example belongs to the case $M_q = 10946$ and $N = 105279$ with $t_{\text{critical}} \approx 8600$.

5.4.2 Projector method

We let N be the size of the Hilbert space. The unitary position space time evolution operator $\hat{U}$ of a system, which is quasi-periodic in q as well as in p direction, is represented by the $N \times N$ matrix (3.69) with elements $\hat{U}_{k,n}$, where $k, n \in \mathbb{Z}_N$. The phase space of the system is equal to the torus $[q_{\min}, q_{\min} + M_q] \times [p_{\min}, p_{\min} + M_p]$. Figure 5.22(a) shows the modulus of the matrix elements $\hat{U}_{k,n}$ for the example system, which was introduced in section 3.4, for the case $M_q = 5$, $M_p = 1$, and $N = 250$. The matrix elements in the lower left and upper right corner reflect the periodic boundary condition in q direction. The coarse grid in the background is a guide to the eye and indicates the five unit cells. Let us now modify this system such that there is no quasi-periodicity in q direction. The momentum variable p of the new system cannot be quantized and the effective Planck constant h_{eff} is not only restricted to discrete values. Furthermore, the corresponding position space time evolution operator, denoted by $\hat{U}^{(2,\infty)}$, is infinite dimensional, but still unitary. It reads

$$\hat{U}_{k,n}^{(2,\infty)} = \frac{1}{M_p} \mathrm{e}^{-\frac{2\pi \mathrm{i}}{h_{\mathrm{eff}}}V(q_k)} \int\limits_{p_{\min}}^{M_p+p_{\min}} \mathrm{d}p \; \mathrm{e}^{\frac{2\pi \mathrm{i}}{h_{\mathrm{eff}}}(q_k-q_n)p} \; \mathrm{e}^{\frac{2\pi \mathrm{i}}{h_{\mathrm{eff}}}(q_k-q_n)p_{\min}} \tag{5.76}$$
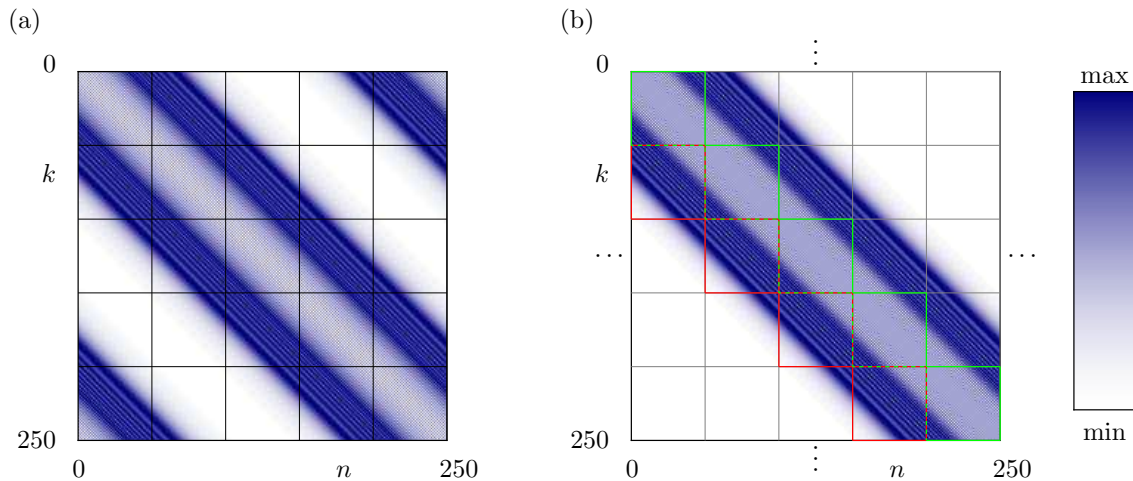
Figure 5.22: (a) Modulus of the matrix elements of $\hat{U}$ with the elements $\hat{U}_{k,n}$ of the example system evaluated in position space for $M_q = 5$ and $N = 250$. The coarse grid in the background is a guide to the eye and indicates the unit cells. (b) Modulus of the matrix elements of $\hat{U}^{(2,\infty)}$. The cells with red frames contain the elements which are responsible for the regular transport one unit cell to the right.

e.g. on the q grid

$$q_n = \frac{h_{\text{eff}}}{M_p}(n + \theta_p) + q_{\text{min}} \qquad \text{with} \qquad n \in \mathbb{Z}. \qquad (5.77)$$

Using an appropriate choice of h_{eff} we can achieve that the q grid (3.67)

$$q_n = \frac{M_q}{N}(n + \theta_p) + q_{\text{min}} \qquad \text{with} \qquad n \in \mathbb{Z}_N, \qquad (5.78)$$

on which the original time evolution operator $\hat{U}$ is determined, is containd in the infinite grid (5.77). We assume this for the following consideration. Figure 5.22(b) illustrates the modulus of the matrix elements of $\hat{U}^{(2,\infty)}$ on this adapted q grid. As we cannot plot an infinite matrix, only that part of $\hat{U}^{(2,\infty)}$ is shown which corresponds to the q grid (5.78). The remaining part is indicated by dots.

This infinite system is similar to a scattering system, as its phase space contains an infinitely large chaotic sea. States with a small decay probability, which live for a long time within the regular phase space part of a scattering system, are quasi-stationary. The spectrum of these states is quasi-discrete and consists of a large number of smeared energy levels with a width $\Gamma = h_{\text{eff}}/\tau$, where τ denotes the life time of the quasi-stationary state [1]. 2D scattering states are described by outgoing planar waves in the infinity. A consideration of the Schrödinger equation for these scattering states shows that their eigenvalues cannot be real. One rather has

$$E = E_0 - \mathrm{i}\frac{\Gamma}{2\hbar_{\text{eff}}} \qquad \text{with} \qquad E_0 \in \mathbb{R},\ \Gamma \in \mathbb{R}^+, \qquad (5.79)$$

and

$$|\psi(t)\rangle \sim \mathrm{e}^{\frac{\mathrm{i}}{\hbar_{\text{eff}}}E_0 t - \frac{\Gamma}{2\hbar_{\text{eff}}}t}|\psi(0)\rangle \qquad (5.80)$$

for the time evolution of an initial quasi-stationary state $|\psi(0)\rangle$. The square of the modulus of the time evolved state $|\psi(t)\rangle$ decreases as $\mathrm{e}^{\Gamma t/\hbar_{\text{eff}}} \approx 1 - \Gamma t/\hbar_{\text{eff}}$, where $\Gamma t/\hbar_{\text{eff}} \ll 1$. Consequently, Γ can be identified with a tunneling rate.

We now return to the quantum map which is described by the infinite time evolution operator $\hat{U}^{(2,\infty)}$. Our example system shows, also without quasi-periodicity in q direction, regular transport to the right with the velocity $v_{\text{reg}} = 1$ for the parameter $A = 1$. This transport is effected by the red boxed parts of $\hat{U}^{(2,\infty)}$ in figure 5.22(b), since they contain the transport bands below the main diagonal. As every unit cell of the example system shows an equal regular island, we slice one of these red boxes out of $\hat{U}^{(2,\infty)}$ and call

this sliced time evolution operator $\hat{U}^{(2)}$. If the example system does not show regular transport, $A = 0$, we use one of the green cells of $\hat{U}^{(2,\infty)}$ along the main diagonal as sliced operator $\hat{U}^{(2)}$. In contrast to $\hat{U}^{(2,\infty)}$ the sliced operator $\hat{U}^{(2)}$ is not unitary and its eigenvalues do consequently not lie on the unit circle. With $\left|\psi_n^{(2)}\right\rangle$ as an eigenstate of $\hat{U}^{(2)}$, we have the eigenvalue equation

$$\hat{U}^{(2)}\left|\psi_n^{(2)}\right\rangle = z_n\left|\psi_n^{(2)}\right\rangle \tag{5.81}$$

with the eigenvalue

$$z_n := \mathrm{e}^{\frac{\mathrm{i}}{\hbar_{\mathrm{eff}}}\left(\varphi_n + \mathrm{i}\frac{\Gamma_n}{2}\right)} \qquad \text{with} \qquad \varphi_n \in [0, 2\pi],\ \Gamma_n \in \mathbb{R}^+. \tag{5.82}$$

We let $\left|\psi_m^{(2)}\right\rangle$ be a regular eigenstate of $\hat{U}^{(2)}$ with norm one. The norm of the time evolved state $\hat{U}^{(2)}\left|\psi_m^{(2)}\right\rangle$ must be smaller than one, since $\hat{U}^{(2)}$ is not unitary. The loss of norm can be associated with the weight which tunneled from the regular island to the chaotic sea. We therefore assume

$$\gamma_m \approx 1 - \left\|\hat{U}^{(2)}\left|\psi_m^{(2)}\right\rangle\right\|^2 \tag{5.83}$$

for the corresponding tunneling rate. The insertion of equations (5.81) and (5.82) yields the relation between the width Γ_m and the tunneling rate γ_m

$$\gamma_m = 1 - \mathrm{e}^{-\frac{\Gamma_m}{\hbar_{\mathrm{eff}}}} \approx 1 - \left(1 - \frac{\Gamma_m}{\hbar_{\mathrm{eff}}}\right) = \frac{\Gamma_m}{\hbar_{\mathrm{eff}}}. \tag{5.84}$$

For the modulus of the eigenvalue z_m we have

$$|z_m| = \mathrm{e}^{-\frac{\Gamma_m}{2\hbar_{\mathrm{eff}}}} \overset{(5.84)}{=} \mathrm{e}^{-\frac{\gamma_m}{2}} \approx 1 - \frac{\gamma_m}{2}. \tag{5.85}$$

This implies that the tunneling rate γ_m is approximately twice the distance of the eigenvalue z_m from the unit circle

$$\gamma_m \approx 2\left(1 - |z_m|\right). \tag{5.86}$$

The opening of the actually considered system has a larger influence on the chaotic states. Furthermore, the influence on a regular state becomes smaller, the smaller its coupling to the chaotic sea is. Thus, sorting the eigenvalues of the non unitary operator $\hat{U}^{(2)}$ by their distance from the unit circle should yield the tunneling rates of all regular states with increasing quantum number m, see the example shown in figure 5.23.
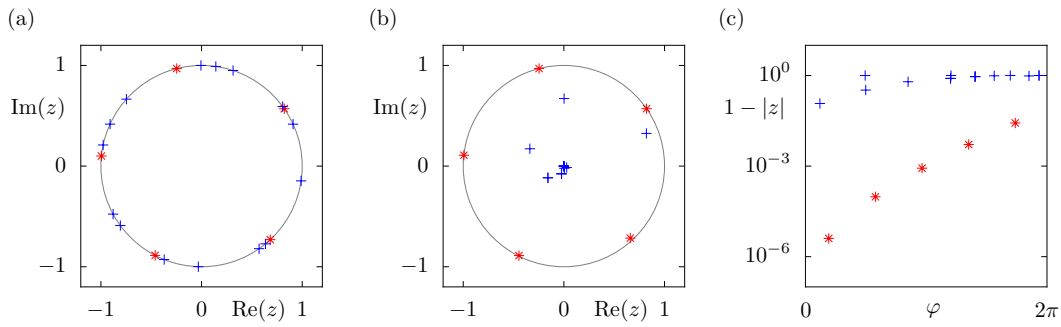
Figure 5.23: (a) The eigenvalues of the quantum map $\hat{U}$ lie on the unit circle due to unitarity. Eigenvalues belonging to regular states are shown with red colour, whereas chaotic ones are blue coloured. (b) $\hat{U}^{(2)}$ is not unitary. Its eigenvalues therefore do not lie on the unit circle. (c) The opening of the actual system mainly influences chaotic eigenvalues. The smaller the quantum number of a regular state is, the less this state is influenced.

Let us make some final remarks on the interpretation of this method for the determination of direct dynamical tunneling rates on the basis of the example map P_{ex}. We concentrate on the unit cell $[-1/2, 1/2] \times [-1/2, 1/2]$ and neglect all periodic boundary conditions. Figure 5.24(a) illustrates what happens, if the classical map is applied once to points within this unit cell. Those phase space points, which move one cell to the right, are green coloured, and those, which are mapped more than one cell to the right, are blue coloured. Phase space points, which stay in the considered cell or which are mapped to
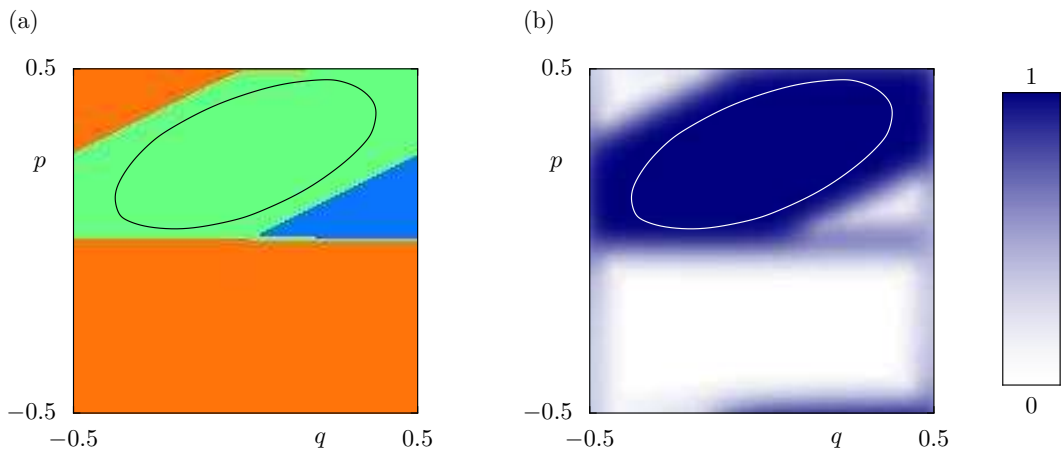
Figure 5.24: (a) Application of the example map without periodic boundary conditions to the phase space points in the unit cell $[-1/2, 1/2] \times [-1/2, 1/2]$. Green: The points are mapped one cell to the right; blue: Mapping more than one cell to the right; orange: The points stay in the considered unit cell or are mapped to the left. (b) The quantity $g(q, p)$, equation (5.87), is equal to one, where the neglection of the periodic boundary conditions does not have a relevant influence. Anywhere else it is almost zero.

the left, are indicated by orange colour. In order to check, how this behaviour is reflected on the quantum level, we consider the quantity

$$g(q, p) \quad := \quad \left\| \hat{U}^{(2)} \left| \chi_{q,p} \right\rangle \right\|, \tag{5.87}$$

where $\chi_{q,p}$ is a periodized coherent state with center (q, p). Figure 5.24(b) illustrates the function $g(q, p)$. Its value is equal to zero (white) in those phase space regions, where the periodic boundary conditions are essential. A comparison with figure 5.24(a) shows that these are the orange and blue coloured regions. The function $g(q, p)$ has the value equal to one (blue), where the classical phase space points are mapped one cell to the right (green). Since this region contains the regular island, this reflects the regular transport to the right. The blue and orange coloured parts of figure 5.24(a) lie in the chaotic sea. The neglection of the periodic boundary conditions, which is performed in order to obtain the non-unitary operator $\hat{U}^{(2)}$ from $\hat{U}^{(2,\infty)}$, influences therefore mainly chaotic states. Their eigenvalues must consequently have a large distance from the unit circle, as can be seen in figure 5.23(b). Regular states localizing in the green coloured part of the phase space are only influenced so far by the neglection of the periodic boundary conditions as they couple to chaotic states - but this coupling is related to the tunneling rate: The smaller the quantum number m is, the smaller is the coupling and consequently the distance of its eigenvalue from the unit circle. These considerations based on figure 5.24 imply that

$$\hat{U}^{(2)} \quad \equiv \quad \hat{P}\hat{U} \tag{5.88}$$

holds like in [70], with a projection operator $\hat{P}$ fulfilling

$$\hat{P}^\dagger \quad = \quad \hat{P}, \tag{5.89}$$

$$\hat{P}^2 \quad = \quad \hat{P}. \tag{5.90}$$

By using the eigenequations of the operators $\hat{U}$ and $\hat{U}^{(2)}$,

$$\hat{U} \left| \psi_n \right\rangle \quad = \quad e^{i\varphi_n} \left| \psi_n \right\rangle, \tag{5.91}$$

$$\hat{U}^{(2)} \left| \psi_n^{(2)} \right\rangle \quad = \quad z_n \left| \psi_n^{(2)} \right\rangle, \tag{5.92}$$

and defining

$$\left| \psi_n^{(2)} \right\rangle \quad := \quad \frac{\hat{P} \left| \psi_n \right\rangle}{\left\| \hat{P} \left| \psi_n \right\rangle \right\|}, \tag{5.93}$$

we have

$$\hat{U}^{(2)} \left| \psi_n^{(2)} \right\rangle \left\| \hat{P} \left| \psi_n \right\rangle \right\| \;=\; \hat{P}\hat{U}\hat{P} \left| \psi_n \right\rangle \tag{5.94}$$

$$=\; z_n \hat{P} \left| \psi_n \right\rangle . \tag{5.95}$$

A multiplication with $\langle \psi_n |$ yields

$$\left\langle \psi_n \left| \hat{P}\hat{U}\hat{P} \right| \psi_n \right\rangle \;=\; z_n \left\langle \psi_n \left| \hat{P} \right| \psi_n \right\rangle \tag{5.96}$$

$$\overset{(5.90),(5.93)}{\Leftrightarrow} \qquad \left\langle \psi_n^{(2)} \left| \hat{U} \right| \psi_n^{(2)} \right\rangle \;=\; z_n \left\langle \psi_n^{(2)} \middle| \psi_n^{(2)} \right\rangle . \tag{5.97}$$

Taking the square of the modulus of (5.97) and using equation (5.85), we finally find

$$\gamma_m \approx 1 - \left| \left\langle \psi_m^{(2)} \left| \hat{U} \right| \psi_m^{(2)} \right\rangle \right|^2 \tag{5.98}$$

for the tunneling rates of the regular states. A similar formula can be obtained from our dynamical tunneling rate formula (5.22), if we replace the projection operator onto the chaotic sea by $\sum_{j=1}^{N_{\mathrm{ch}}} |\psi_{\mathrm{ch},j}\rangle\langle\psi_{\mathrm{ch},j}| = \hat{\mathbb{1}} - \sum_{m=0}^{m_{\max}} |\psi_{\mathrm{reg},m}\rangle\langle\psi_{\mathrm{reg},m}|$. If the direct dynamical tunneling process dominates, couplings between different regular states are negligible. We then have $\left| \left\langle \psi_{\mathrm{reg},m} \left| \hat{U} \right| \psi_{\mathrm{reg},k} \right\rangle \right| \ll \gamma_m$ with $k \neq m$ and get

$$\gamma_m \;\approx\; 1 - \left| \left\langle \psi_{\mathrm{reg},m} \left| \hat{U} \right| \psi_{\mathrm{reg},m} \right\rangle \right|^2 . \tag{5.99}$$

The regular eigenstates of the operator $\hat{U}^{(2)}$ are obviously similar to the regular eigenstates $\left| \psi_{\mathrm{reg},m} \right\rangle$ of $\hat{U}_{\mathrm{reg}}$. Equations (5.98) and (5.99) have the form $\gamma_m \sim 1 - x$. As the quantity x is itself almost equal to 1, this shows again that we need the regular states with a very high precision in order to determine the exponentially small tunneling rate γ_m.

In this section we described two methods which allow for the numerical determination of dynamical tunneling rates. On the one hand the wave packet dynamics method is illustrative. It is on the other hand, however, very time consuming due to the repeated determinations of weights of the time evolved wave packet in a regular island or due to the computation of overlaps with the translated initial wave packet. In contrast to this, the projector method is very fast as it only consists of the diagonalization of a matrix with an additional sorting of its eigenvalues. Nevertheless we used both methods in order to crosscheck our obtained numerical data.

6 Summary and outlook

The first main result of this thesis is the generalization of the already known semiclassical quantization of regular islands of quantum maps, whose corresponding classical maps are defined on $\mathbb{R}^2$, to the case of equal transporting regular islands. Based on it, we incorporated the periodic boundary conditions of a torus. For a single non-transporting and transporting regular island on a torus as well as for a chain of equal transporting regular islands, also on a torus, we found a good agreement between semiclassically constructed quasimodes and numerically determined eigenfunctions and quasi-energies. These results will be summarized in reference [72]. An interesting open question in this context is, in how far a modification is necessary for the semiclassical quantization of resonance island chains within regular islands.

In this thesis we have furthermore studied direct dynamical tunneling in a mixed phase space with a focus on the transition of regular states from an almost resonance-free regular island to the surrounding chaotic sea. The investigations were based on periodically kicked 1D systems defined on a torus, whose quantum time evolution is described by the operator $\hat{U}$ over one kicking period. Tunneling in a 1D double well shaped potential energy can semiclassically be described by means of a left and a right well Hamiltonian. This encouraged us to consider dynamical tunneling from a regular island to the chaotic sea in a similar manner. We introduced two new classical systems. The phase space of the first one consists of a continuation of the regular island in the mixed phase space to the chaotic sea and is thus completely regular. The second system is completely chaotic. Its phase space shows the same chaotic sea as the actual system, but somehow continued to the regular island. The quantization of both new systems yielded the time evolution operators $\hat{U}_{\mathrm{reg}}$ and $\hat{U}_{\mathrm{ch}}$. As the regular island and the chaotic sea are quantum mechanically connected by dynamical tunneling, the quasi-energy spectrum of $\hat{U}$ shows avoided crossings under the variation of a system-specific parameter. Those two eigenstates of $\hat{U}$, which are involved in an avoided crossing, are by construction approximately equal to respectively one of the eigenstates of $\hat{U}_{\mathrm{reg}}$ and $\hat{U}_{\mathrm{ch}}$ sufficiently away from the avoided crossing. A consideration of the corresponding eigenvalue equations of $\hat{U}$, $\hat{U}_{\mathrm{reg}}$, and $\hat{U}_{\mathrm{ch}}$

at the avoided crossing yielded finally the formula

$$\gamma_m \;\approx\; \left\| \left(\hat{U} - \hat{U}_{\text{reg}} \right) \middle| \psi_{\text{reg},m} \right\rangle \right\|^2 . \tag{6.1}$$

It allows for the determination of the tunneling rate of the regular eigenstate $|\psi_{\text{reg},m}\rangle$ of $\hat{U}_{\text{reg}}$, whose Husimi function localizes on the mth quantizing torus in the island, to the surrounding chaotic sea for all quantum numbers m at a given value of the effective Planck constant. An important observation is that (6.1) does not depend on the chaotic system. This is helpful, as it is still not clear how the chaotic system can practically be constructed.

Formula (6.1) has on the one hand a simple structure. On the other hand its evaluation turned out to be difficult: Since $\hat{U}|\psi_{\text{reg},m}\rangle$ and $\hat{U}_{\text{reg}}|\psi_{\text{reg},m}\rangle$ are by construction almost identical within the regular island and since the tunneling rate is in general an exponentially small quantity, the regular system needs to be known very precisely.

For the class of periodically kicked 1D systems, which are constructed of piecewise defined discontinuous derivatives of the kinetic and the potential energy, we were able to evaluate the dynamical tunneling rate formula (6.1) further. The result is a formula which relates the tunneling rate to the square of the modulus of the mth regular wave function at the border of the regular island either in position or in momentum direction, depending on, whether the q dependent potential energy function or the p dependent kinetic energy function governs the size of the regular island. We obtained e.g.

$$\gamma_m \;=\; c_0 \, |\psi_{\text{reg},m}(p_{\text{border}})|^2 , \tag{6.2}$$

where c_0 is a fit parameter. The relation of the tunneling rate to the value of the regular wave function at the border of the regular island is somehow natural and confirms what we have expected from the very beginning of our studies. The replacement of the regular wave function by a semiclassical WKB expression yields in principle a semiclassical expression for the tunneling rate γ_m in a certain system. For the case of a harmonic oscillator-like elliptic regular island one knows a corresponding analytical semiclassical WKB wave function. Using it we found

$$\gamma_m = c \, \frac{h_{\text{eff}}}{\sqrt{1 - \alpha_m}} \, \exp\left(-2 \frac{A_{\text{reg}}}{h_{\text{eff}}} \left[\sqrt{1 - \alpha_m} - \alpha_m \, \ln\left(\frac{1 + \sqrt{1 - \alpha_m}}{\sqrt{\alpha_m}} \right) \right] \right), \tag{6.3}$$

with

$$\alpha_m := \left(m + \frac{1}{2} \right) \left(\frac{A_{\text{reg}}}{h_{\text{eff}}} \right)^{-1} ,$$

where c is also a fit parameter. The comparison of this analytical prediction with numerically determined tunneling rates showed a good agreement within a factor of two or even better over several orders of magnitude in a large domain of the effective Planck constant.

Whereas it is obvious, what the corresponding regular system of a mixed system with an elliptic regular island embedded in the chaotic sea is, this is not clear for a generic deformed regular island. The Lie transform provides a method for the continuation of a deformed regular island. It performs the continuation via the determination of an interpolating time independent 1D Hamilton operator $\hat{H}_{\mathrm{reg}}$. Its diagonalization yields the regular states $|\psi_{\mathrm{reg},m}\rangle$. Their comparison with the regular eigenstates of $\hat{U}$ showed only a precision of $\sim 10^{-5}$ in our studies. This precision is surely sufficient for many applications, but obviously not for the evaluation of the exponentially small tunneling rate γ_m using equation (6.1), where the difference of two almost equal terms is determined. Here the error needs to be smaller than the tunneling rate. The quantum normal form analysis might yield a better precision of the regular states [71] than the Lie transform.

Since the regular wave function appears only as a factor in equation (6.2), the precision of the regular states determined via the Lie transform is sufficient for its evaluation. The comparison of this analytical prediction with numerically determined tunneling rates showed also for a generic deformed regular island a good agreement over several orders of magnitude in a large domain of the effective Planck constant.

An unsolved question of our approach to the theoretical understanding of direct dynamical tunneling from a regular island to the chaotic sea is, whether the continuation of the regular island to the chaotic sea, i.e. the regular system, is unique. Provided that the regular dynamics within the island is perfectly known, we believe that the answer is "yes". This statement is supported by the situation of an elliptic regular island, where the existence of only one continuation is obvious. As the main ideas of the derivation of (6.1) can also be transferred to other systems, like e.g. 2D billiards, an answer can perhaps be found by their investigation.

Moreover, it would be nice to have a general semiclassical formula for the determination of direct dynamical tunneling rates similar to (6.3). The WKB ansatz can to our knowledge, however, not be evaluated analytically for deformed regular islands, so that we did not manage to derive a general semiclassical theory. Our results represent nevertheless an important progress compared to previous works, especially compared to reference [33]. This is supported by the good agreement of the predictions of our formulae with numerically determined data over several orders of magnitude not only for the ground state, but also for excited states. Our results on direct dynamical tunneling from an almost resonance-free regular island to the surrounding chaotic sea will finally be summarized in reference [73].

A Derivations and remarks

A.1 Dimensionless quantities

The introduction of dimensionless quantities reduces the number of system parameters. In the following we will consider a particle with mass m and demonstrate, how the quantities of a 1D system with the kinetic energy $T(p) = p^2/2m$ and the potential energy $V(q)$ can be made dimensionless. At first, we introduce a characteristic length q_0 and a characteristic energy V_0. By means of them we define a dimensionless length

$$\tilde{q} \; := \; \frac{q}{q_0} \tag{A.1}$$

and a dimensionless potential energy

$$\tilde{V}(\tilde{q}) \; := \; \frac{V(q)}{V_0}. \tag{A.2}$$

We remark that the choices of q_0 and V_0 are not unique. The definition of the energy scale, however, automatically fixes the length scale due to equation (A.2). The characteristic quantities q_0 and V_0 can be used to make all lengths and energies, which appear in the considered problem, dimensionless. We use

$$p_0 \; = \; \sqrt{mV_0} \tag{A.3}$$

as characteristic momentum, what is implied by the dimensionless kinetic energy $\tilde{T}(\tilde{p}) := T(p)/V_0 = p^2/2mV_0$, yielding $\tilde{p} := p/p_0$ for the dimensionless momentum. The characteristic time t_0 follows from the quantities, which have been derived up to this point,

$$t_0 \; = \; \frac{q_0\, m}{p_0} \; = \; q_0\,\sqrt{\frac{m}{V_0}}, \tag{A.4}$$

and leads to the the dimensionless time $\tilde{t} := t/t_0$. The dimensionless expression of Planck's constant, which is usually called effective Planck constant, can be deduced from the

dimensionless Hamilton operator,

$$\hat{\tilde{H}} \quad := \quad -\frac{1}{2}\,\frac{\hbar^2}{m\,V_0\,q_0^2}\,\frac{\mathrm{d}^2}{\mathrm{d}\tilde{q}^2} + \tilde{V}(\hat{\tilde{q}}), \tag{A.5}$$

yielding

$$h_{\mathrm{eff}} \quad := \quad \frac{h}{q_0\,\sqrt{m\,V_0}} \quad \overset{(\mathrm{A.3})}{=} \quad \frac{h}{q_0\,p_0}. \tag{A.6}$$

Finally, we have to rescale the wave functions, e.g. in position representation,

$$\tilde{\psi}(\tilde{q}) \quad := \quad \sqrt{q_0}\psi(q), \tag{A.7}$$

in order to keep the normalization condition

$$1 \quad \overset{!}{=} \quad \int\limits_{-\infty}^{\infty} \mathrm{d}q\,|\psi(q,t)|^2 \quad = \quad \int\limits_{-\infty}^{\infty} \mathrm{d}\tilde{q}\,\left|\tilde{\psi}(\tilde{q},\tilde{t})\right|^2. \tag{A.8}$$

We realize that only the parameter h_{eff} remains in the dimensionless formulation.

A.2 Proof of energy-action formula

In section 2.1.3 we used the formula

$$E_m \quad = \quad \int\limits_0^{b_m} \mathrm{d}q\,\frac{1}{T(q)}\,\frac{\mathrm{d}S(q)}{\mathrm{d}q}, \tag{A.9}$$

in order to assign a WKB energy to the mth quantizing torus. This formula will be proved in the following.

The upper integration limit in equation (A.9), b_m, is equal to the right turning point of the closed invariant torus which belongs to the energy E_m, whereas T denotes the period of an invariant torus which encloses the action S. Let us consider an arbitrary 1D Hamiltonian $H(q,p)$ which generates a regular island with center (q_c, p_c) in phase space. Figure A.1 gives an image of its invariant tori. The invariant torus, which consists only of one point, is defined as the center of the island. Every other invariant torus possesses two turning points. If the right turning point q_t is given, the left one, $\bar{q}_t$, is automatically fixed by the dynamics of the system: $\bar{q}_t = \bar{q}_t(q_t)$. These turning points are connected by the two momentum branches $p_+(q_t, q)$ (green colour) and $p_-(q_t, q)$ (red colour). For the
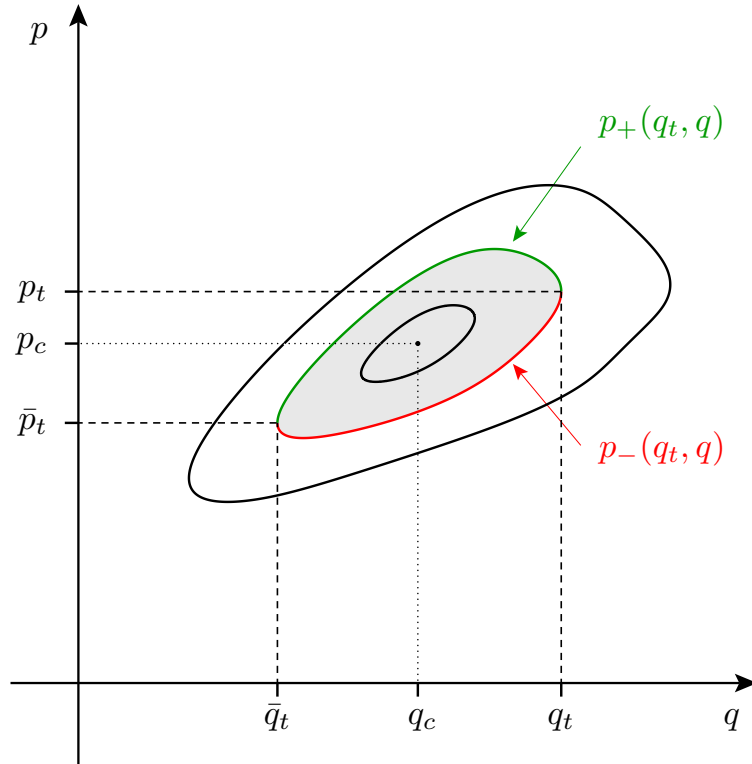
Figure A.1: A regular island in phase space. Except for its center, every invariant torus possesses two turning points q_t and $\bar{q}_t(q_t)$, which are connected by the momentum branches $p_+(q_t, q)$ (green) and $p_-(q_t, q)$ (red). The grey coloured area, which is enclosed by the invariant torus, is equal to the action $S(q_t)$.

following we define

$$p_t \quad := \quad p_+(q_t, q_t) = p_-(q_t, q_t), \tag{A.10}$$

$$\bar{p}_t \quad := \quad p_+(q_t, \bar{q}_t) = p_-(q_t, \bar{q}_t). \tag{A.11}$$

From the action which is enclosed by the invariant torus,

$$S(q_t) \quad = \quad \int_{\bar{q}_t}^{q_t} \mathrm{d}q'\, p_+(q_t, q') - \int_{\bar{q}_t}^{q_t} \mathrm{d}q'\, p_-(q_t, q'), \tag{A.12}$$

we find

$$
\begin{aligned}
\frac{\mathrm{d}S(q_t)}{\mathrm{d}q_t} &= \underbrace{p_+(q_t, q_t)}_{p_t} - \underbrace{p_+(q_t, \bar{q}_t)}_{\bar{p}_t} + \int\limits_{\bar{q}_t}^{q_t} \mathrm{d}q \frac{\partial p_+(q_t, q)}{\partial q_t} \\
&\quad - \underbrace{p_-(q_t, q_t)}_{p_t} + \underbrace{p_-(q_t, \bar{q}_t)}_{\bar{p}_t} - \int\limits_{\bar{q}_t}^{q_t} \mathrm{d}q \frac{\partial p_-(q_t, q)}{\partial q_t} \\
&= \int\limits_{\bar{q}_t}^{q_t} \mathrm{d}q \left[\frac{\partial p_+(q_t, q)}{\partial q_t} - \frac{\partial p_-(q_t, q)}{\partial q_t} \right].
\end{aligned}
\tag{A.13}
$$

We let

$$
E(q_t) = H\big(p_\pm(q_t, q), q\big),
\tag{A.14}
$$

be the energy, which is associated with the considered invariant torus and have

$$
\begin{aligned}
\frac{\mathrm{d}E(q_t)}{\mathrm{d}q_t} &= \frac{\partial H(p_\pm(q_t, q), q)}{\partial p_\pm(q_t, q)} \frac{\partial p_\pm(q_t, q)}{\partial q_t} \\
&= v_\pm(q_t, q) \frac{\partial p_\pm(q_t, q)}{\partial q_t},
\end{aligned}
\tag{A.15}
$$

where $v_\pm(q_t, q)$ are the velocities of the particle along the two branches $p_\pm(q_t, q)$. The insertion of equation (A.15) into (A.13) yields

$$
\begin{aligned}
\frac{\mathrm{d}S(q_t)}{\mathrm{d}q_t} &= \frac{\mathrm{d}E(q_t)}{\mathrm{d}q_t} \int\limits_{\bar{q}_t}^{q_t} \mathrm{d}q \left[\frac{1}{v_+(q_t, q)} - \frac{1}{v_-(q_t, q)} \right] \\
&= \frac{\mathrm{d}E(q_t)}{\mathrm{d}q_t} \big(T_+(q_t) + T_-(q_t) \big) \\
&= \frac{\mathrm{d}E(q_t)}{\mathrm{d}q_t} T(q_t).
\end{aligned}
\tag{A.16}
$$

The quantities $T_\pm(q_t)$ denote the times which the particle requires to pass the branches $p_\pm(q_t, q)$ in phase space. Consequently, $T(q_t)$ is the period which is associated with the considered invariant torus. By solving for $\mathrm{d}E(q_t)/\mathrm{d}q_t$ and performing an integration we finally obtain

$$
E(q_t) = E(q_c) + \int\limits_{q_c}^{q_t} \mathrm{d}q' \frac{\mathrm{d}S(q')}{\mathrm{d}q'} \frac{1}{T(q')}.
\tag{A.17}
$$

After the replacements $q_c = 0$, $q_t = b_m$, and $E(q_t) \rightarrow E_m$ we obtain formula (A.9), except for the constant $E(q_c)$. But we can set it equal to zero, since it does not influence the dynamics.

A.3 Remarks on the coupling matrix element of quantum maps

The modulus of the coupling matrix element v of quantum maps between regular and chaotic states is given by equation (5.13) and reads

$$
\begin{aligned}
|v| &\approx \left| \left\langle \psi_{\mathrm{ch}} \left| \hat{U} - \hat{U}_{\mathrm{reg}} \right| \psi_{\mathrm{reg}} \right\rangle \right| \\
&\overset{(5.5)}{=} \left| \left\langle \psi_{\mathrm{ch}} \left| \hat{U} \right| \psi_{\mathrm{reg}} \right\rangle - \mathrm{e}^{\mathrm{i}\varphi_0} \hat{\mathbb{1}} \left\langle \psi_{\mathrm{ch}} \middle| \psi_{\mathrm{reg}} \right\rangle \right|.
\end{aligned}
\tag{A.18}
$$

If the constructed states $|\psi_{\mathrm{ch}}\rangle$ and $|\psi_{\mathrm{reg}}\rangle$ were orthogonal, the second term on the right-hand side of equation (A.18) would vanish and we would have a coupling matrix element similar to the 1D case, see equation (2.67). In the following we will demonstrate that equation (A.18) is indeed minimal, even if the states $|\psi_{\mathrm{ch}}\rangle$ and $|\psi_{\mathrm{reg}}\rangle$ are not orthogonal.

The eigenstates belonging to the quasi-energies φ_+ and φ_-, $|\psi_+\rangle$ and $|\psi_-\rangle$, build an orthogonal basis of a subspace of the actual Hilbert space. The states $|\psi_{\mathrm{ch}}\rangle$ and $|\psi_{\mathrm{reg}}\rangle$ are a basis of the same subspace. If they were also orthogonal, we would have

$$
|\psi_\pm\rangle = \frac{1}{\sqrt{2}} \left(|\psi_{\mathrm{ch}}\rangle \pm |\psi_{\mathrm{reg}}\rangle \right).
\tag{A.19}
$$

Let us now assume that $\delta := \langle \psi_{\mathrm{reg}} | \psi_{\mathrm{ch}} \rangle \neq 0$ holds. Equation (A.19) can no longer be valid, so that a more general ansatz is required

$$
|\psi_+\rangle := \frac{1}{\sqrt{N_+}} \left(|\psi_{\mathrm{reg}}\rangle + \alpha \, |\psi_{\mathrm{ch}}\rangle \right),
\tag{A.20}
$$

$$
|\psi_-\rangle := \frac{1}{\sqrt{N_-}} \left(|\psi_{\mathrm{reg}}\rangle + \beta \, |\psi_{\mathrm{ch}}\rangle \right),
\tag{A.21}
$$

where N_+ and N_- are real, and α and β are complex coefficients. Now we exploit that the states $|\psi_+\rangle$ and $|\psi_-\rangle$ are normalized

$$
\begin{aligned}
1 = \langle \psi_+ | \psi_+ \rangle &= \frac{1}{N_+} \left(1 + |\alpha|^2 + \alpha\delta + \alpha^*\delta^* \right) \\
\Leftrightarrow \qquad N_+ &= 1 + |\alpha|^2 + \alpha\delta + \alpha^*\delta^*,
\end{aligned}
\tag{A.22}
$$

$$1 \; = \; \langle\psi_-|\psi_-\rangle \;\; = \;\; \frac{1}{N_-}\left(1 + |\beta|^2 + \beta\delta + \beta^*\delta^*\right)$$

$$\Leftrightarrow \qquad\qquad N_- \;\; = \;\; 1 + |\beta|^2 + \beta\delta + \beta^*\delta^*. \qquad\qquad\text{(A.23)}$$

From the orthogonality we have

$$0 \; = \; \langle\psi_-|\psi_+\rangle \;\; = \;\; \frac{1}{\sqrt{N_+ N_-}}\left(1 + \alpha\delta + \beta^*\delta^* + \alpha\beta^*\right), \qquad\qquad\text{(A.24)}$$

which yields the function

$$\beta(\alpha) \;\; = \;\; -\frac{1 + \alpha^*\delta^*}{\alpha^* + \delta}. \qquad\qquad\text{(A.25)}$$

This implies that the modulus of the coupling matrix element is a function of the parameter α: $|v| = |v(\alpha)|$. Since $|\psi_+\rangle$ and $|\psi_-\rangle$ are eigenstates of the time evolution operator $\hat{U}$, we have the eigenequations

$$\hat{U}|\psi_+\rangle \;\; = \;\; e^{i(\varphi_0 - |v(\alpha)|)}|\psi_+\rangle, \qquad\qquad\text{(A.26)}$$

$$\hat{U}|\psi_-\rangle \;\; = \;\; e^{i(\varphi_0 + |v(\alpha)|)}|\psi_-\rangle. \qquad\qquad\text{(A.27)}$$

After a multiplication of equation (A.26) with $\sqrt{N_+}$ and equation (A.27) with $\sqrt{N_-}$ and taking the difference we have

$$\hat{U}\left(\sqrt{N_+}|\psi_+\rangle - \sqrt{N_-}|\psi_-\rangle\right) \stackrel{\text{(A.20),(A.21)}}{=} (\alpha - \beta)\hat{U}\,|\psi_{\text{ch}}\rangle \qquad\qquad\text{(A.28)}$$

for the left-hand side and

$$
\begin{aligned}
\hat{U}&\left(\sqrt{N_+}|\psi_+\rangle - \sqrt{N_-}|\psi_-\rangle\right) \\
&= \; e^{i\varphi_0}\left(e^{-i|v(\alpha)|}\sqrt{N_+}|\psi_+\rangle - e^{i|v(\alpha)|}\sqrt{N_-}|\psi_-\rangle\right) \\
&= \; e^{i\varphi_0}\left(\left[e^{-i|v(\alpha)|} - e^{i|v(\alpha)|}\right]|\psi_{\text{reg}}\rangle + \left[\alpha e^{-i|v(\alpha)|} - \beta e^{i|v(\alpha)|}\right]|\psi_{\text{ch}}\rangle\right) &&\text{(A.29)} \\
&\approx \; e^{i\varphi_0}\left(-2i|v(\alpha)|\,|\psi_{\text{reg}}\rangle + (\alpha - \beta - i|v(\alpha)|(\alpha + \beta))\,|\psi_{\text{ch}}\rangle\right). &&\text{(A.30)}
\end{aligned}
$$

for the right-hand side of the resulting equation. In the step from equation (A.29) to (A.30) the exponentials $\exp\left(i|v(\alpha)|\right)$ were expanded into Taylor series up to first order with respect to $|v(\alpha)| = 0$. This is possible, because $|v(\alpha)| \ll 1$ usually holds. The multiplication of equation (A.28) with $\langle\psi_{\text{reg}}|$ yields

$$\left\langle\psi_{\text{reg}}\left|(\alpha - \beta)\hat{U}\right|\psi_{\text{ch}}\right\rangle \;\; \approx \;\; e^{i\varphi_0}\left(-2i|v(\alpha)| + [\alpha - \beta - i|v(\alpha)|(\alpha + \beta)]\delta\right). \qquad\text{(A.31)}$$

We then get

$$\left\langle \psi_{\text{reg}} \left| \hat{U} - \mathrm{e}^{\mathrm{i}\varphi_0} \hat{\mathbb{1}} \right| \psi_{\text{ch}} \right\rangle \;\approx\; -\frac{\mathrm{i}\mathrm{e}^{\mathrm{i}\varphi_0}|v(\alpha)|}{\alpha - \beta}\bigl(2 + (\alpha + \beta)\delta\bigr) \tag{A.32}$$

from equation (A.31) and with

$$f(\alpha, \delta) \;:=\; \left| \frac{2 + (\alpha + \beta)\delta}{\alpha - \beta} \right| \tag{A.33}$$

we obtain

$$|v(\alpha)| \;\approx\; \left| \left\langle \psi_{\text{reg}} \left| \hat{U} - \mathrm{e}^{\mathrm{i}\varphi_0} \hat{\mathbb{1}} \right| \psi_{\text{ch}} \right\rangle \right| f(\alpha, \delta)^{-1} \tag{A.34}$$

for the coupling matrix element. Using the function $\beta(\alpha)$, equation (A.25), yields

$$\alpha - \beta \;=\; \alpha + \frac{1 + \alpha^*\delta^*}{\alpha^* + \delta} \;=\; \frac{1 + |\alpha|^2 + 2\mathrm{Re}(\alpha\delta)}{\alpha^* + \delta}, \tag{A.35}$$

$$\alpha + \beta \;=\; \alpha - \frac{1 + \alpha^*\delta^*}{\alpha^* + \delta} \;=\; \frac{-1 + |\alpha|^2 + 2\mathrm{i}\,\mathrm{Im}(\alpha\delta)}{\alpha^* + \delta}. \tag{A.36}$$

We thus have

$$\begin{aligned}
f(\alpha, \delta) \;&=\; \left| \frac{2 + \delta\frac{-1+|\alpha|^2+2\mathrm{i}\,\mathrm{Im}(\alpha\delta)}{\alpha^*+\delta}}{\frac{1+|\alpha|^2+2\mathrm{Re}(\alpha\delta)}{\alpha^*+\delta}} \right| \\
&\approx\; \frac{\sqrt{(2\alpha^* + \delta(1 + |\alpha|^2))\,(2\alpha + \delta^*(1 + |\alpha|^2))}}{1 + |\alpha|^2 + 2\mathrm{Re}(\alpha\delta)}.
\end{aligned} \tag{A.37}$$

The terms $\delta\mathrm{Im}(\alpha\delta)$ are of $O(\delta^2)$ and were neglected. We are interested in the extremal values of $f(\alpha, \delta)$. The expression $\mathrm{Re}(\alpha\delta)$ will be therefore replaced by its extremal values $\pm|\alpha||\delta|$ in the following. With the abbreviations $a := |\alpha|$ and $d := |\delta|$ equation (A.37) becomes

$$\begin{aligned}
f(a, d) \;&=\; \frac{\sqrt{4a^2 \pm 4ad(1 + a^2) + d^2(1 + a^2)^2}}{1 + a^2 \pm 2ad} \tag{A.38} \\
&=\; \frac{2a \pm d(1 + a^2)}{1 + a^2 \pm 2ad}. \tag{A.39}
\end{aligned}$$

Performing a Taylor expansion in the variable d with respect to $d = 0$ yields

$$f(a, d) \;=\; \frac{2a}{1 + a^2} \pm \frac{(1 - a^2)^2}{(1 + a^2)^2}d + O(d^2). \tag{A.40}$$

The parameter d will be kept constant in the following, whereas a will be varied: $f(a) :=$ $f(a, d = \text{const.})$. We want to determine those values a_i which minimize the function $f(a)$. We differentiate equation (A.40) therefore with repsect to the variable a and set it equal to zero

$$0 \overset{!}{=} \left. \frac{\mathrm{d}f(a)}{\mathrm{d}a} \right|_{a=a_i} = \frac{2(1-a_i^2)}{(1+a_i^2)^3}(1 + a_i^2 \mp 4a_i d), \tag{A.41}$$

with

$$a_0 = 1 \quad \text{and} \quad a_{1,2} = \pm 2d \pm \sqrt{4d^2 - 1}. \tag{A.42}$$

Since $d \ll 1$, the radicand of the latter two solutions $a_{1,2}$ is negative. $a_{1,2}$ are thus complex. This is, however, not possible by the definiton of a. Consequently, $a_{1,2}$ are not physical solutions of equation (A.41). The only remaining physical extremal position is $a_0 = 1$. We have $\left. \frac{\mathrm{d}f(a)}{\mathrm{d}a} \right|_{a=1-\varepsilon} > 0$ and $\left. \frac{\mathrm{d}f(a)}{\mathrm{d}a} \right|_{a=1+\varepsilon} < 0$ for $\varepsilon \ll 1$. The function $f(a)$ is consequently maximized at $a = 1$, i.e. $f(a)^{-1}$ becomes minimal at this position. The phases of the complex coefficients α and β are irrelevant. We choose $\alpha = 1$, which yields $\beta(\alpha = 1) = -1$ and $f(\alpha = 1, \delta) = 1$ according to equations (A.25) and (A.33).

We conclude therefore that the minimal coupling matrix element, resulting from equation (A.34), reads

$$|v| \approx \left| \left\langle \psi_{\text{ch}} \left| \hat{U} - \mathrm{e}^{\mathrm{i}\varphi_0} \hat{\mathbb{1}} \right| \psi_{\text{reg}} \right\rangle \right|. \tag{A.43}$$

It is equal to equation (A.18).

B Tilted harmonic oscillator

B.1 Aspect ratio, inclination angle, and monodromy matrix

We consider the invariant tori of a harmonic oscillator with the Hamiltonian

$$H(q', p') \;=\; \frac{1}{2}\frac{(q' - q_0')^2}{(\Delta q')^2} + \frac{1}{2}\frac{(p' - p_0')^2}{(\Delta p')^2} \tag{B.1}$$

with $\Delta q'$, $\Delta p' \in \mathbb{R}^+$ in an orthonormal coordinate system S' spanned by the axes q' and p'. For any energy E we get an ellipse with center (q_0', p_0'), semi-axes $\Delta q'\sqrt{2E}$ and $\Delta p'\sqrt{2E}$, and real valued aspect ratio $\sigma' = \Delta p'/\Delta q'$. With the creation operator

$$\hat{a}^\dagger \;=\; \frac{1}{\sqrt{2}}\left(\frac{\hat{q}'}{\Delta q'} - \mathrm{i}\frac{\hat{p}'}{\Delta p'}\right) \tag{B.2}$$

and with the complex coordinate

$$z' \;=\; \frac{1}{\sqrt{2}}\left(\frac{q_0'}{\Delta q'} + \mathrm{i}\frac{p_0'}{\Delta p'}\right) \tag{B.3}$$

a coherent state centered around (q_0', p_0'), which is adapted to the invariant tori of the harmonic oscillator Hamiltonian (B.1), is defined as

$$|z'\rangle \;=\; \mathrm{e}^{-|z'|^2/2}\mathrm{e}^{z'\hat{a}^\dagger}|0\rangle, \tag{B.4}$$

where $|0\rangle$ denotes the harmonic oscillator ground state (see equations 5.79 and 5.413 in [56]). For simplicity we set $q_0' = p_0' = 0$ from now on, so that S' coincides with the normal coordinate system of the elliptical invariant tori. Let us assume that S' is rotated by an angle θ with respect to another orthonormal coordinate system S, see figure B.1. The coordinates of S and S' are connected by
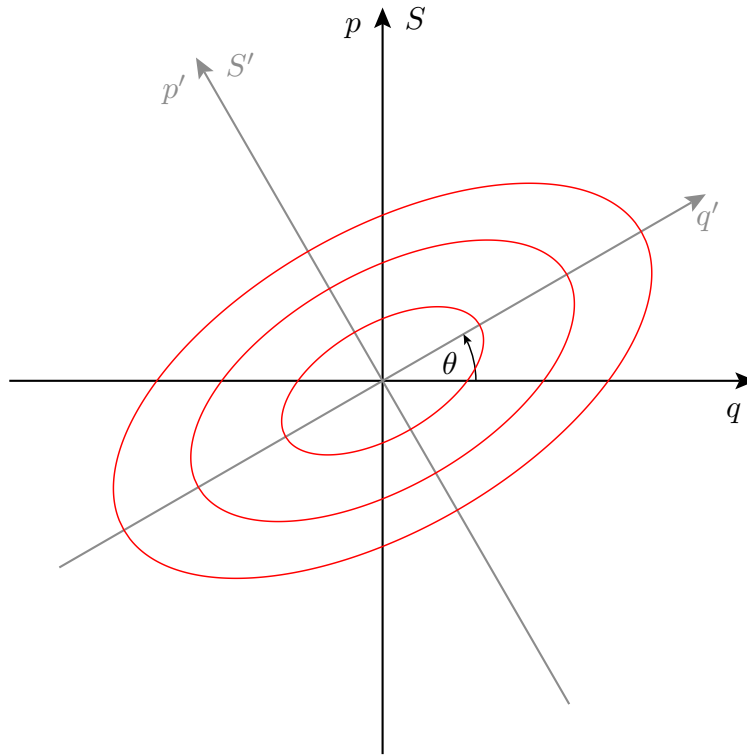
Figure B.1: Elliptic invariant tori of the harmonic oscillator Hamiltonian (B.1) with $q'_0 = p'_0 = 0$ in the normal coordinate system S' (primed variables). The coordinate system S' is rotated by an angle θ with respect to another system S (unprimed variables).

$$q' = \cos(\theta)\,q + \sin(\theta)\,p, \tag{B.5}$$

$$p' = -\sin(\theta)\,q + \cos(\theta)\,p. \tag{B.6}$$

In order to find an expression for the aspect ratio σ in the system S, we replace $\hat{q}'$ and $\hat{p}'$ in (B.2) by the operator analogues of (B.5) and (B.6), and find

$$\hat{a}^{\dagger} = \frac{1}{\sqrt{2}}\left[\left(\frac{\cos(\theta)}{\Delta q'} + \mathrm{i}\,\frac{\sin(\theta)}{\Delta p'}\right)\hat{q} - \mathrm{i}\left(\frac{\cos(\theta)}{\Delta p'} + \mathrm{i}\,\frac{\sin(\theta)}{\Delta q'}\right)\hat{p}\right]. \tag{B.7}$$

Equation (B.7) is equal to the creation operator in the system S with complex parameters Δq and Δp

$$\hat{a}^{\dagger} = \frac{1}{\sqrt{2}}\left(\frac{\hat{q}}{(\Delta q)^*} - \mathrm{i}\,\frac{\hat{p}}{(\Delta p)^*}\right). \tag{B.8}$$

A comparison of (B.8) with (B.7) yields expressions for Δq and Δp. We obtain

$$\mathrm{Re}(\sigma) \;=\; \frac{1}{\frac{1}{\sigma'}\cos^2(\theta)+\sigma'\sin^2(\theta)}, \tag{B.9}$$

$$\mathrm{Im}(\sigma) \;=\; \mathrm{Re}(\sigma)\left(\sigma'-\frac{1}{\sigma'}\right)\sin(\theta)\cos(\theta), \tag{B.10}$$

for the real and imaginary part of the aspect ratio $\sigma = \Delta p/\Delta q$ in the system S. It depends on the still unknown aspect ratio σ' in the normal coordinate system and the rotation angle θ. A classical area-preserving map $P : \mathbb{R}^2 \to \mathbb{R}^2$, which iterates an initial point along an elliptic invariant curve around a stable elliptic fixed point, is described by a 2×2 matrix

$$M \;=\; \begin{pmatrix} M_{11} & M_{12} \\ M_{21} & M_{22} \end{pmatrix}. \tag{B.11}$$

Since P is area-preserving, $\det(M) = 1$ must hold. In order to have elliptic invariant tori around the fixed point, the eigenvalues of M

$$\begin{aligned}
\lambda_\pm &\;=\; \frac{\mathrm{Tr}(M)}{2} \pm \sqrt{\left(\frac{\mathrm{Tr}(M)}{2}\right)^2 - 1} \\
&\;=\; \frac{\mathrm{Tr}(M)}{2} \pm \mathrm{i}\sqrt{1-\left(\frac{\mathrm{Tr}(M)}{2}\right)^2} \;=:\; \mathrm{e}^{\pm\mathrm{i}\alpha}
\end{aligned} \tag{B.12}$$

must be complex. This is fulfilled for $|\mathrm{Tr}(M)| < 2$. We furthermore find

$$\vec{v}_\pm \;=\; \frac{1}{\sqrt{M_{12}\left(M_{12}-M_{21}\right)}}\begin{pmatrix} M_{12} \\ \mathrm{e}^{\pm\mathrm{i}\alpha}-M_{11} \end{pmatrix} \tag{B.13}$$

for the corresponding normalized eigenvectors of M. We remark that $\lambda_+ = \lambda_-^*$ and $\vec{v}_+ = \vec{v}_-^*$ hold. Now we consider the mapping of a point $\vec{r}_0 := c_+\vec{v}_+ + c_-\vec{v}_-$, where $c_- = c_+^*$ due to the reality of $\vec{r}_0$. The index 0 denotes the initial time. The nth iterate, $n \in \mathbb{N}$, is obtained by the n-fold application of the matrix M to $\vec{r}_0$

$$\begin{aligned}
\vec{r}_n &\;=\; M^n\vec{r}_0 \\
&\;=\; c_+ M^n\vec{v}_+ + c_+^* M^n\vec{v}_- \\
&\;=\; c_+ \lambda_+^n\vec{v}_+ + c_+^*\left(\lambda_+^*\right)^n\vec{v}_- \\
&\;=\; c\,\mathrm{e}^{\mathrm{i}\gamma}\mathrm{e}^{\mathrm{i}n\alpha}\begin{pmatrix} M_{12} \\ \mathrm{e}^{\mathrm{i}\alpha}-M_{11} \end{pmatrix} + c\,\mathrm{e}^{-\mathrm{i}\gamma}\mathrm{e}^{-\mathrm{i}n\alpha}\begin{pmatrix} M_{12} \\ \mathrm{e}^{-\mathrm{i}\alpha}-M_{11} \end{pmatrix}.
\end{aligned} \tag{B.14,B.15}$$

In the step from (B.14) to (B.15) the expansion coefficients were replaced by their polar coordinate expressions. The normalization factors of the eigenvectors (B.13) were absorbed by the constant c. We therefore have

$$q_n \;=\; 2cM_{12}\cos(n\alpha+\gamma), \tag{B.16}$$

$$p_n \;=\; 2c\left[\cos((n+1)\alpha+\gamma) - M_{11}\cos(n\alpha+\gamma)\right]. \tag{B.17}$$

If α is not commensurable with π, the iterated points (q_n, p_n) fill an ellipse. The inclination angle and the aspect ratio of this ellipse are independent of the initial point, c, and γ. We are therefore free to choose $c = 1/2$ and $\gamma = 0$. Furthermore, we use the parametrization $\omega := n\alpha$ with $0 \le \omega < 2\pi$

$$q \;=\; M_{12}\cos(\omega), \tag{B.18}$$

$$p \;=\; \left(\cos(\alpha) - M_{11}\right)\cos(\omega) - \sin(\alpha)\sin(\omega). \tag{B.19}$$

Equations (B.18) and (B.19) can be combined to a quadratic form

$$M_{21}\,q^2 + (M_{22} - M_{11})\,q\,p - M_{12}\,p^2$$
$$-M_{12}\left[M_{12}M_{21} + \left(\frac{M_{22} - M_{11}}{2}\right)^2\right] + M_{12}\sin^2(\alpha) \;=\; 0. \tag{B.20}$$

Formula (B.1) is the equation of an ellipse in the normal coordinate system S' with aspect ratio $\sigma' = \Delta p'/\Delta q'$ and semi-axes $\Delta q'\sqrt{2E}$ and $\Delta p'\sqrt{2E}$. Using the coordinate rotation equations (B.5) and (B.6), we find the equation of the same ellipse in the coordinate system S, where $q_0' = p_0' = 0$ is assumed,

$$\left(\frac{\cos^2(\theta)}{2E\,(\Delta q')^2} + \frac{\sin^2(\theta)}{2E\,(\Delta p')^2}\right)q^2 + 2\left(\frac{1}{2E\,(\Delta q')^2} - \frac{1}{2E\,(\Delta p')^2}\right)\sin(\theta)\cos(\theta)q\,p$$
$$+ \left(\frac{\sin^2(\theta)}{2E\,(\Delta q')^2} + \frac{\cos^2(\theta)}{2E\,(\Delta p')^2}\right)p^2 - 1 \;=\; 0. \tag{B.21}$$

It must be equal to (B.20), so that a term by term comparison yields $\Delta q'\sqrt{2E}$, $\Delta p'\sqrt{2E}$ and θ as functions of the entries of the matrix M. Using the definition of the aspect ratio,

$\sigma' := \Delta p'/\Delta q'$, we finally find

$$
\theta \;=\; \frac{1}{2}\arctan\left(\frac{M_{22} - M_{11}}{M_{12} + M_{21}}\right), \tag{B.22}
$$

$$
\sigma' \;=\; \sqrt{\frac{(M_{21} - M_{12})\operatorname{sign}(M_{12} + M_{21}) - \sqrt{(M_{12} + M_{21})^2 + (M_{22} - M_{11})^2}}{(M_{21} - M_{12})\operatorname{sign}(M_{12} + M_{21}) + \sqrt{(M_{12} + M_{21})^2 + (M_{22} - M_{11})^2}}}\,. \tag{B.23}
$$

Thus, we are able to determine the aspect ratio σ' in the normal coordinate system and the rotation angle θ from the geometric information about the elliptic invariant tori of the area preserving-map P, which is represented by the matrix M.

B.2 Annihilation and creation operators, and eigenstates

The derivation of the eigenstates of the harmonic oscillator Hamilton operator in the normal coordinate system S' is well-known. The basic idea is the introduction of an annihilation and a creation operator, $\hat{a}$ and $\hat{a}^\dagger$,

$$
\hat{a} \;:=\; \frac{1}{\sqrt{2}}\left(\frac{\hat{q}'}{\Delta q'} + \mathrm{i}\frac{\hat{p}'}{\Delta p'}\right), \tag{B.24}
$$

$$
\hat{a}^\dagger \;:=\; \frac{1}{\sqrt{2}}\left(\frac{\hat{q}'}{\Delta q'} - \mathrm{i}\frac{\hat{p}'}{\Delta p'}\right), \tag{B.25}
$$

which allow for a compact notation of the Hamilton operator belonging to the Hamiltonian (B.1) with $q'_0 = p'_0 = 0$

$$
\hat{H} \;=\; \frac{1}{2}\frac{\hat{q}'^2}{(\Delta q')^2} + \frac{1}{2}\frac{\hat{p}'^2}{(\Delta p')^2} \tag{B.26}
$$

$$
\;=\; \frac{1}{2}\left(\hat{a}^\dagger\hat{a} + \hat{a}\hat{a}^\dagger\right). \tag{B.27}
$$

Instead of the special choice for the annihilation (B.24) and the creation operator (B.25), we can use the general ansatz

$$
\hat{a} \;:=\; \frac{1}{\sqrt{2}}\left(\frac{\hat{q}}{\Delta q} + \mathrm{i}\frac{\hat{p}}{\Delta p}\right), \tag{B.28}
$$

$$
\hat{a}^\dagger \;:=\; \frac{1}{\sqrt{2}}\left(\frac{\hat{q}}{(\Delta q)^*} - \mathrm{i}\frac{\hat{p}}{(\Delta p)^*}\right), \tag{B.29}
$$

for the system S, where

$$\Delta q \;=\; |\delta q| \mathrm{e}^{\mathrm{i}\alpha_q} \qquad \text{and} \qquad \Delta p \;=\; |\delta p| \mathrm{e}^{\mathrm{i}\alpha_p} \tag{B.30}$$

are complex numbers with phases α_q and α_p. Using the abbreviation
$\hbar_{\mathrm{eff}} := \hbar\,\mathrm{Re}\,(1/\Delta q\,\Delta p^*)$, these general operators fulfill the commutation relation

$$\left[\hat{a}, \hat{a}^\dagger\right] \;=\; \hbar_{\mathrm{eff}}\,\hat{\mathbb{1}}. \tag{B.31}$$

Without loss of generality we can assume $\mathrm{Re}\,(1/\Delta q\,\Delta p^*) > 0$. If it was zero, the operators
(B.28) and (B.29) would commute and a creation of states would not be possible. And
if it was negative, the role of the two operators would be exchanged. Since the condition
$\mathrm{Re}\,(1/\Delta q\,\Delta p^*) > 0$ is equal to $\mathrm{Re}(\sigma) = \mathrm{Re}(\Delta p/\Delta q) = \cos(\alpha_p - \alpha_q) > 0$, we have $-\pi/2 <$
$\alpha_p - \alpha_q < \pi/2$. Here we encounter the aspect ratio of the tilted ellipse in the system S
again. The insertion of (B.28) and (B.29) into (B.27) yields

$$\hat{H} \;=\; \frac{1}{2}\frac{\hat{q}^2}{|\Delta q|^2} + \frac{1}{2}\frac{\hat{p}^2}{|\Delta p|^2} + \frac{1}{2}\frac{\sin(\alpha_p - \alpha_q)}{|\Delta q||\Delta p|}\,(\hat{q}\hat{p} + \hat{p}\hat{q})\,, \tag{B.32}$$

which is the Hamilton operator in the coordinate system S. In the following $\hat{H}$ will denote
the Hamilton operator with respect to the coordinate system S, in which the elliptical
invariant tori are tilted. In addition to (B.31) we also find the commutation relations

$$\left[\hat{H}, \hat{a}\right] \;=\; -\hbar_{\mathrm{eff}}\,\hat{a}, \tag{B.33}$$

$$\left[\hat{H}, \hat{a}^\dagger\right] \;=\; \hbar_{\mathrm{eff}}\,\hat{a}^\dagger. \tag{B.34}$$

With their help we can start to derive the eigenstates of the tilted harmonic oscillator in
the system S. If $|\lambda\rangle$ is an eigenstate of $\hat{H}$, $\hat{H}|\lambda\rangle = \lambda|\lambda\rangle$, the eigenvalue λ must be real
due to the hermiticity of the Hamilton operator. Furthermore, we realize that

$$\hat{H}\left(\hat{a}^\dagger|\lambda\rangle\right) \;=\; (\lambda + \hbar_{\mathrm{eff}})\left(\hat{a}^\dagger|\lambda\rangle\right), \tag{B.35}$$

$$\hat{H}\left(\hat{a}|\lambda\rangle\right) \;=\; (\lambda - \hbar_{\mathrm{eff}})\left(\hat{a}|\lambda\rangle\right), \tag{B.36}$$

hold, what leads to

$$\hat{a}^\dagger|\lambda\rangle \;=\; c_\lambda^+|\lambda + \hbar_{\mathrm{eff}}\rangle, \tag{B.37}$$

$$\hat{a}|\lambda\rangle \;=\; c_\lambda^-|\lambda - \hbar_{\mathrm{eff}}\rangle. \tag{B.38}$$

From the analytical consideration of the expectation values $\langle\lambda|2\hat{H}|\lambda\rangle$ and $\langle\lambda\,|\hat{a}\hat{a}^{\dagger}|\,\lambda\rangle$ we find

$$\left|c_{\lambda}^{\pm}\right|^{2} \;\; = \;\; \lambda \pm \frac{1}{2}\hbar_{\text{eff}}\;. \tag{B.39}$$

These considerations show that the values of λ are quantized and that the lowest possible value is $\hbar_{\text{eff}}/2$. Thus,

$$\hat{a}|0\rangle \;\; = \;\; 0 \tag{B.40}$$

must hold. After replacing $|\lambda\rangle$ by $|n\rangle$ we finally find

$$\hat{H}|n\rangle \;\; = \;\; \left(n+\frac{1}{2}\right)\hbar_{\text{eff}}|n\rangle \qquad \text{with} \qquad n\in\mathbb{N}_{0} \tag{B.41}$$

and

$$\hat{a}|n\rangle \;\; = \;\; \sqrt{\hbar_{\text{eff}}\,n}\,|n-1\rangle, \tag{B.42}$$
$$\hat{a}^{\dagger}|n\rangle \;\; = \;\; \sqrt{\hbar_{\text{eff}}\,(n+1)}\,|n+1\rangle. \tag{B.43}$$

From equations (B.42) and (B.43) we derive

$$|n\rangle \;\; = \;\; \frac{\left(\hat{a}^{\dagger}\right)^{n}|0\rangle}{\sqrt{\hbar_{\text{eff}}^{n}\,n!}}, \tag{B.44}$$

and the orthonormality relation

$$\langle m|n\rangle = \delta_{m,n} \tag{B.45}$$

follows from equations (B.40) and (B.44).

B.3 Eigenstates in position representation

Now we derive the eigenstates of the tilted harmonic oscillator in position representation. In order to find the ground state $\langle q|0\rangle$, we perform the following consideration

$$0 \;=\; \langle q\,|\hat{a}|\,0\rangle \;=\; \frac{1}{\sqrt{2}}\left(\frac{1}{\Delta q}\,\langle q\,|\hat{q}|\,0\rangle + \frac{\mathrm{i}}{\Delta p}\,\langle q\,|\hat{p}|\,0\rangle\right)$$

$$\Leftrightarrow \qquad 0 \;=\; \frac{q}{\Delta q}\langle q|0\rangle + \frac{\hbar}{\Delta p}\frac{\mathrm{d}\langle q|0\rangle}{\mathrm{d}q}$$

$$\Rightarrow \qquad \langle q|0\rangle \;=\; \left(\frac{\mathrm{Re}(\sigma)}{\pi\hbar}\right)^{\frac{1}{4}} \mathrm{e}^{-\frac{\sigma}{\hbar}\frac{q^2}{2}}$$

In the last step we used the definition of the aspect ratio, $\sigma = (\Delta p/\Delta q)$, in the coordinate system S. Here we see again the necessity that $\mathrm{Re}(\Delta p/\Delta q) > 0$ must hold.

Equation (B.44) tells us, how the excited states can be obtained from the ground state. The only thing that we need to know is the action of the general creation operator (B.29) in position representation. With an arbitrary state $|\psi\rangle$ we have

$$\begin{aligned}
\langle q\,|\hat{a}^\dagger|\,\psi\rangle &\;=\; \frac{1}{\sqrt{2}}\left(\frac{1}{(\Delta q)^*}\,\langle q\,|\hat{q}|\,\psi\rangle - \frac{\mathrm{i}}{(\Delta p)^*}\,\langle q\,|\hat{p}|\,\psi\rangle\right) \\
&\;=\; \frac{1}{\sqrt{2}}\left(\frac{q}{(\Delta q)^*} - \frac{\hbar}{(\Delta p)^*}\frac{\mathrm{d}}{\mathrm{d}q}\right)\langle q\,|\,\psi\rangle
\end{aligned} \qquad (\text{B}.46)$$

which gives

$$\begin{aligned}
\langle q\,|\,n\rangle &\;=\; \frac{1}{\sqrt{[2\hbar\,\mathrm{Re}(1/\Delta q(\Delta p)^*)]^n\,n!}}\left(\frac{q}{(\Delta q)^*} - \frac{\hbar}{(\Delta p)^*}\frac{\mathrm{d}}{\mathrm{d}q}\right)^n \langle q\,|\,0\rangle \qquad (\text{B}.47) \\
&\;=\; \left(2^n n!\sqrt{\pi}\left[\frac{|\Delta p|}{\hbar|\Delta q|}\cos(\alpha_p - \alpha_q)\right]^{n-1/2}\right)^{-1/2} \\
&\qquad \cdot \left(\frac{\Delta p^*}{\hbar\Delta q^*}q - \frac{\mathrm{d}}{\mathrm{d}q}\right)^n \mathrm{e}^{-\frac{\sigma}{\hbar}\frac{q^2}{2}}\,\mathrm{e}^{\mathrm{i}n\alpha_p} \qquad (\text{B}.48)
\end{aligned}$$

in combination with (B.44). With the nth Hermite polynonial H_n and a modified version of Rodrigues' formula (for the usual version see equation 8.959(1), 1. in [74]),

$$H_n\left(\sqrt{\frac{b+c}{2}}\,q\right) = \left(\frac{2}{b+c}\right)^{\frac{n}{2}} \mathrm{e}^{\frac{c}{2}q^2}\left(bq - \frac{\mathrm{d}}{\mathrm{d}q}\right)^n \mathrm{e}^{-\frac{c}{2}q^2} \quad \text{with} \quad b,c > 0, \qquad (\text{B}.49)$$

we finally find

$$\langle q \,|\, n \rangle = \frac{\mathrm{e}^{\mathrm{i}n\alpha_p}}{\sqrt{2^n n!}} \left(\frac{\mathrm{Re}(\sigma)}{\pi\hbar} \right)^{\frac{1}{4}} H_n \left(\sqrt{\frac{\mathrm{Re}(\sigma)}{\hbar}} \, q \right) \mathrm{e}^{-\frac{\sigma}{\hbar} \frac{q^2}{2}} \tag{B.50}$$

for the nth excited state of the tilted harmonic oscillator in position representation. This result is similar to the well-known eigenstates in the normal coordinate system. The main difference is the dependence on the complex aspect ratio σ. The phase α_p can be set equal to zero without loss of generality.

B.4   Eigenstates in momentum representation

In order to derive the eigenstates of the tilted harmonic oscillator in momentum representation, we have two possibilities. The first one is a Fourier transform of the position space result (B.50), which is, however, very elaborate. We prefer the second alternative, which repeats the steps performed in the previous section in momentum space. Since we would not learn anything new, we restrict ourselves to the presentation of the result

$$\langle p \,|\, n \rangle = \frac{\mathrm{e}^{\mathrm{i}n(\alpha_q - \pi/2) - \mathrm{i}/2(\alpha_p - \alpha_q)}}{\sqrt{2^n n!}} \left(\frac{\mathrm{Re}(1/\sigma)}{\pi\hbar} \right)^{\frac{1}{4}} H_n \left(\sqrt{\frac{\mathrm{Re}(1/\sigma)}{\hbar}} \, p \right) \mathrm{e}^{-\frac{1}{\sigma\hbar} \frac{p^2}{2}}. \tag{B.51}$$

C 1D Hamiltonians and their quantization

C.1 Lie transform method

The derivation in this appendix follows the textbook by Lichtenberg and Liebermann [75]. For a more detailed review see the diploma thesis by S. Löck [76].

We let $H_0(\mathbf{q}, \mathbf{p})$ be the Hamilton operator of an integrable system in k dimensions. If one adds a small non linear perturbation to it, $H(\mathbf{q}, \mathbf{p}) = H_0(\mathbf{q}, \mathbf{p}) + \varepsilon H_1(\mathbf{q}, \mathbf{p})$ with $\varepsilon \ll 1$, the resulting perturbed system can be approximated by a completely integrable one, e.g. by means of the Lie transform method. It is helpful to start with autonomous systems. One defines $\mathbf{x} := (\mathbf{q}, \mathbf{p})$ as vector of the generalized positions and momenta representing a single point in phase space and considers a generating function $w(\bar{\mathbf{x}}, \varepsilon)$ fulfilling the equation

$$\frac{\mathrm{d}\bar{\mathbf{x}}}{\mathrm{d}\varepsilon} = \{\bar{\mathbf{x}},\, w\}, \tag{C.1}$$

with the Poisson bracket

$$\{a,\, b\} := \sum_{i,j=1}^{k} \left(\frac{\partial a}{\partial q_i} \frac{\partial b}{\partial p_j} - \frac{\partial a}{\partial p_i} \frac{\partial b}{\partial q_j} \right). \tag{C.2}$$

For every ε equation (C.1) generates a canocial transform: $\bar{\mathbf{x}} = \bar{\mathbf{x}}(\mathbf{x}, \varepsilon)$ with $\{\bar{q}_i,\, \bar{q}_j\} = \{\bar{p}_i,\, \bar{p}_j\} = 0$ and $\{\bar{q}_i,\, \bar{p}_j\} = \delta_{i,j}$. Furthermore, one introduces an operator T, which evaluates every function g at the transformed coordinates $\bar{\mathbf{x}}(\mathbf{x}, \varepsilon)$. Additionally T should return a function in the original coordinates: $f = Tg$. If g is the identity, one has $g(\mathbf{x}) = \mathbf{x}$ and

$$\bar{\mathbf{x}} = T\mathbf{x}. \tag{C.3}$$

In order to find the operator T, one introduces the so-called Lie operator $L = [w, \cdot]$. Then,

$$\frac{\mathrm{d}T}{\mathrm{d}\varepsilon} = -TL \tag{C.4}$$

follows from (C.1) and (C.3). Every canonical transform has the property that the Hamiltonian expressed in terms of the new variables is equal to the Hamiltonian expressed in terms of the old ones

$$\bar{H}(\bar{\mathbf{x}}(\mathbf{x}, \varepsilon)) = H(\mathbf{x}, \varepsilon). \tag{C.5}$$

This property can be expressed by using the operator T: $\bar{H} = T^{-1}H$.

In contrast to autonomous systems, w, L und T do explicitly depend on time in non-autonomous systems and one has

$$\bar{H} = T^{-1}H + T^{-1} \int_0^\varepsilon \mathrm{d}\varepsilon' \, T(\varepsilon') \frac{\partial w(\varepsilon')}{\partial t}. \tag{C.6}$$

In order to enable a pertubative approach, one expands the quantities w, L, T, T^{-1}, H, and $\bar{H}$ into series of powers of the parameter ε

$$w = \sum_{n=0}^{\infty} \varepsilon^n w_{n+1} \,, \tag{C.7}$$

$$L = \sum_{n=0}^{\infty} \varepsilon^n L_{n+1} \,, \tag{C.8}$$

$$T = \sum_{n=0}^{\infty} \varepsilon^n T_n \,, \tag{C.9}$$

$$T^{-1} = \sum_{n=0}^{\infty} \varepsilon^n T_n^{-1} \,, \tag{C.10}$$

$$H = \sum_{n=0}^{\infty} \varepsilon^n H_n \,, \tag{C.11}$$

$$\bar{H} = \sum_{n=0}^{\infty} \varepsilon^n \bar{H}_n. \tag{C.12}$$

The insertion of equations (C.8) and (C.9) into equation (C.4) and recalling $L_n = [w_n, \cdot]$ yields

$$T_n = -\frac{1}{n} \sum_{m=0}^{n-1} T_m L_{n-m}. \tag{C.13}$$

By differentiating TT^{-1} one finds

$$T_n^{-1} = \frac{1}{n} \sum_{m=0}^{n-1} L_{n-m} T_m^{-1}. \tag{C.14}$$

Finally, a multiplication of (C.6) with T, differentiating by ε, and the insertion of the power series yields the expression for the perturbation series in nth order

$$\frac{\partial w_n}{\partial t} = n\bar{H}_n - \sum_{m=0}^{n-1} L_{n-m} \bar{H}_m - \sum_{m=1}^{n} m T_{n-m}^{-1} H_m. \tag{C.15}$$

By writing down the first term of the first sum and the last one of the second sum and by using the definition $D_0 := \partial/\partial t + [\cdot, H_0]$, one obtains the more aesthetic result

$$D_0 w_n = n \left(\bar{H}_n - H_n \right) - \sum_{m=1}^{n-1} \left(L_{n-m} \bar{H}_m + m T_{n-m}^{-1} H_m \right). \tag{C.16}$$

With the initial values $w_0 = L_0 = 0$ and $T_0 = \mathbb{1}$ one can determine all coefficients for the new time independent Hamiltonian $\bar{H}(\bar{\mathbf{x}})$, which interpolates the regular dynamics of the system given by the original Hamiltonian $H(\mathbf{x}, \varepsilon)$.

The Lie transform provides therefore a method for the continuation of a regular island of a map to the chaotic sea by means of the Hamiltonian

$$H(q, p) = \sum_{n=0}^{N} \varepsilon^n H_n(q, p), \tag{C.17}$$

where N is the maximum order, which is taken into account. The bars are omitted in equation (C.17) for simplicity. Figure C.1 shows two examples. The dynamics of the original system is plotted in grey, whereas the interpolation is shown in red. The first example, figure C.1(a), contains an almost resonance-free regular island. In this case the effect of non linear resonances is very small which is reflected by a very good interpolation of the dynamics within the original regular island. The regular island in figure C.1(b) possesses large resonance islands. As they represent large perturbations, they cannot be interpolated by the Lie transform method. Figure C.2 shows the convergence behaviour

for an example as a function of the order N.

Every kicked 1D system contains resonance islands. The regular dynamics of the initial system can therefore in general not be reproduced with any given accuracy by the Lie transform method. It can happen that the accuracy of the method becomes smaller at a certain order of the expansion.
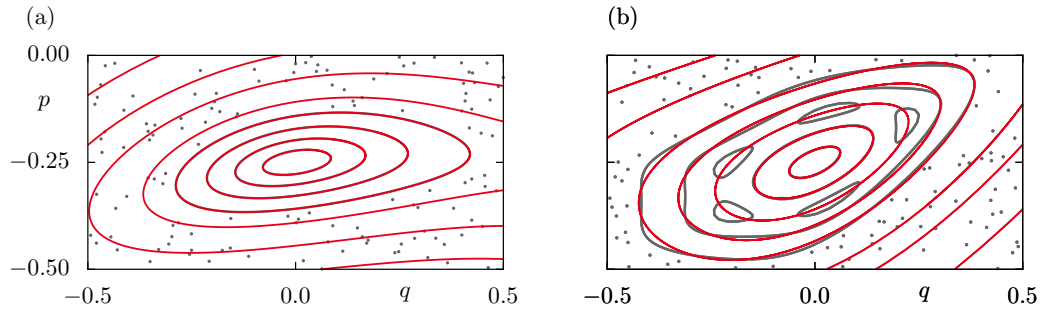
Figure C.1: The iterates of the actually considered classical 1D kicked system are grey coloured. The red coloured lines represent the invariant tori of the time-independent interpolating Hamiltonian (C.15) obtained using the Lie transform method. (a) The phase space consists of a distorted almost resonance-free regular island embedded in the chaotic sea. (b) The regular island contains large resonance islands which cannot be interpolated. This figure is taken from reference [76].
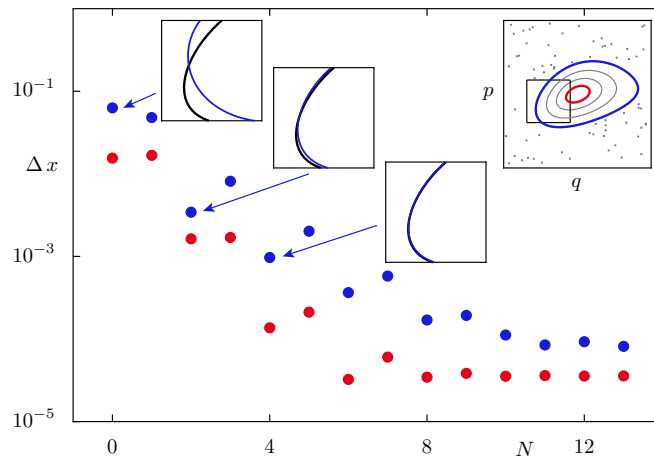
Figure C.2: Deviation of the dynamics of the actual Hamiltonian from the dynamics of the interpolating system obtained using the Lie transform method for a regular island without visible resonance islands as a function of the maximum used order N. The upper right inset shows the full phase space. Highlighted are a red and a blue invariant torus within the regular island. The main plot shows the along these two closed curves averaged distance Δx between the points $(q,p)_{\text{Lie}}$ and $(q,p)_{\text{map}}$. The remaining insets illustrate the convergence of $(q,p)_{\text{Lie}}$ to $(q,p)_{\text{map}}$ for the blue invariant torus. This figure is taken from reference [76].

C.2 Quantization of a 1D Hamiltonian and its diagonalization

In order to quantize a 1D Hamiltonian of order M,

$$H(q,p) \; = \; \sum_{n=0}^{M} \sum_{k=0}^{n} h_{k,n-k}\, q^k p^{n-k}, \tag{C.18}$$

with certain coefficients $h_{k,n-k}$, one has to symmetrize it at first

$$H(q,p) \; = \; \frac{1}{2} \sum_{n=0}^{M} \sum_{k=0}^{n} h_{k,n-k}\, (q^k p^{n-k} + p^{n-k} q^k). \tag{C.19}$$

In general one has $q \in \mathbb{R}$ and $p \in \mathbb{R}$. The replacement of q and p by the quantum mechanical operators $\hat{q}$ and $\hat{p}$ yields the corresponding Hamilton operator

$$\hat{H}(\hat{q},\hat{p}) \; = \; \frac{1}{2} \sum_{n=0}^{M} \sum_{k=0}^{n} h_{k,n-k}\, (\hat{q}^k \hat{p}^{n-k} + \hat{p}^{n-k} \hat{q}^k). \tag{C.20}$$

One can consider it e.g. in position representation. Due to a finite computing capacity it is not possible to perform a quantization along the infinite real line. One needs therefore a restriction to a certain grid

$$q_i \; = \; q_{\min} + i\,\frac{q_{\max} - q_{\min}}{N-1} \; =: \; q_{\min} + i\Delta q \qquad \text{with } i \in \mathbb{Z}_N, \tag{C.21}$$

where N denotes the size of the grid. The minimum and maximum positions $q_{\min}$ and $q_{\max}$ have to be chosen such that the eigenfunctions $\psi(q)$ of the Hamilton operator (C.20) vanish there approximately. With the position space expression of the momentum operator, $\hat{p} = -\mathrm{i}\hbar_{\mathrm{eff}}\,\mathrm{d}/\mathrm{d}q$, one finds the eigenvalue equation

$$\hat{H}\left(\hat{q}, \frac{\hbar_{\mathrm{eff}}}{\mathrm{i}} \frac{\mathrm{d}}{\mathrm{d}q}\right) \psi_n(q) \; = \; E_n \psi_n(q). \tag{C.22}$$

It remains to approximate the derivatives in this equation on the position space grid (C.21). One can take e.g.

$$\frac{\mathrm{d}\psi_n(q)}{\mathrm{d}q}\bigg|_{q=q_i} \; \approx \; \frac{\psi_n(q_i + \Delta q) - \psi(q_i - \Delta q)}{2\Delta q}$$

$$=: \; \frac{\psi_{n,i+1} - \psi_{n,i-1}}{2\Delta q} \tag{C.23}$$

for the first derivative of the function $\psi_n(q)$. The limit $\Delta q \to 0$ would yield the exact derivative. After the replacement of all derivatives in the Hamilton operator by similar difference quotients one obtains a band matrix, where the main diagonal and l secondary diagonals are occupied. The number l represents the maximum power of the momentum operator. Thus, one has the discretized eigenvalue equation

$$
\begin{pmatrix}
\ddots & \ddots & & & 0 \\
\ddots & \ddots & \ddots & & \\
& \ddots & \ddots & \ddots & \\
& & \ddots & \ddots & \ddots \\
0 & & & \ddots & \ddots
\end{pmatrix}
\begin{pmatrix}
\psi_{n,0} \\
\\
\vdots \\
\\
\psi_{n,N-1}
\end{pmatrix}
= E_n
\begin{pmatrix}
\psi_{n,0} \\
\\
\vdots \\
\\
\psi_{n,N-1}
\end{pmatrix} .
\tag{C.24}
$$

The diagonalization of this band shaped Hamiltonian yields the eigenenergies E_n and the corresponding eigenfunctions $\psi_n(q)$. The error of this method originates from the replacement of the derivatives by finite difference quotients. It is of the order $(\Delta q)^2$ and becomes therefore smaller with an increasing grid size N.

Bibliography

[1] L. D. Landau and E. M. Lifschitz: *Lehrbuch der theoretischen Physik: Qunaten-mechanik*, Akademie-Verlag, Berlin, 9th edn., (1979).

[2] M. Wilkinson: *Tunneling between tori in phase space*, Physica D **21** (1986) 341–354.

[3] M. Wilkinson and J. H. Hannay: *Multidimensional tunneling between excited states*, Physica D **27** (1987) 201–212.

[4] M. J. Davies and E. J. Heller: *Quantum dynamical tunnelling in bound states*, J. Chem. Phys. **75** (1981) 246–254.

[5] W. K. Hensinger et al.: *Dynamical tunnelling of ultracold atoms*, Nature **412** (2001) 52–55.

[6] D. A. Steck, W. H. Oskay and M. B. Raizen: *Observation of chaos-assisted tunneling between islands of stability*, Science **293** (2001) 274–278.

[7] S. Creagh in: *Tunneling in Complex Systems*, edited by S. Tomsovic (World Scientific, Singapore, 1998).

[8] S. Creagh: *Tunnelling in multidimensional systems*, J. Phys. A **27** (1994) 4969–4993.

[9] L. Markus and K. Meyer: *Generic Hamiltonian Dynamical Systems are neither Integrable nor Chaotic*, no. 114 in Mem. Amer. Math. Soc., American Mathematical Society, Providence, Rhode Island, (1974).

[10] O. Bohigas, S. Tomsovic and D. Ullmo: *Manifestations of classical phase space structures in quantum mechanics*, Phys. Rep. **223** (1993) 43–133.

[11] S. Tomsovic and D. Ullmo: *Chaos-assisted tunneling*, Phys. Rev. E **50** (1994) 145–162.

[12] E. Doron and S. D. Frischat: *Semiclassical description of tunneling in mixed systems: the case of the annular billiard*, Phys. Rev. Lett. **75** (1995) 3661–3664.

[13] S. D. Frischat and E. Doron: *Dynamical tunneling in mixed systems*, Phys. Rev. E **57** (1998) 1421–1443.

[14] S. Tomsovic: *Chaos-assisted tunnelling in the absence of reflexion symmetry*, J. Phys. A **31** (1998) 9469–9481.

[15] F. Grossmann, T. Dittrich, P. Jung and P. Hänggi: *Coherent destruction of tunneling*, Phys. Rev. Lett. **67** (1991) 516–519.

[16] V. Averbukh, S. Osovski and N. Moiseyev: *Controlled Tunneling of Cold Atoms: From Full Suppression to Strong Enhancement*, Phys. Rev. Lett. **89** (2002) 253201 (4 pages).

[17] A. Shudo and K. S. Ikeda: *Complex Classical Trajectories and Chaotic Tunneling*, Phys. Rev. Lett. **74** (1994) 682–685.

[18] T. Onishi, A. Shudo, K. S. Ikeda and K. Takahashi: *Tunneling mechanism due to chaos in a complex phase space*, Phys. Rev. E **64** (2001) 025201 (4 pages).

[19] A. Ishkawa, A. Tanaka and A. Shudo: *Strong Enhancement of Tunneling Amplitude due to Destruction of Coherence in Chaotic Tunneling Trajectories*, unpublished (2006).

[20] A. Shudo, Y. Ishii and K. S. Ikeda: *Chaos Attracts Tunneling Trajectories: A Universal Mechanism of Chaotic Tunneling*, unpublished (2006).

[21] J. Zakrzewski, D. Delande and A. Buchleitner: *Ionization via chaos assisted tunneling*, Phys. Rev. E **57** (1998) 1458–1474.

[22] V. A. Podolskiy and E. E. Narimanov: *Chaos-assisted tunneling in dielectric microcavities*, Opt. Lett. **30** (2005) 474–476.

[23] C. Dembowski, H.-D. Gräf, A. Heine, R. Hofferbert, H. Rehfeld, and A. Richter: *First experimental evidence for chaos-assisted tunneling in a microwave annular billiard*, Phys. Rev. Lett. **84** (200) 867–870.

[24] R. Hofferbert, H. Alt, C. Dembowski, H.-D. Gräf, H. L. Harney, A. Heine, H. Rehfeld and A. Richter: *Experimental investigations of chaos-assisted tunneling in a microwave annular billiard*, Phys. Rev. E **71** (2005) 046201 (21 pages).

[25] L. Bonci, A. Farusi, P. Grigolini and R. Roncaglia: *Tunneling rate fluctuations in-duced by nonlinear resonances: A quantitative treatment based on semiclassical ar-guments*, Phys. Rev. E **58** (1998) 5689–5692.

[26] O. Brodier, P. Schlagheck and D. Ullmo: *Resonance-Assisted Tunneling in Near-Integrable Systems*, Phys. Rev. Lett. **87** (2001) 64101.

[27] O. Brodier, P. Schlagheck and D. Ullmo: *Resonance-Assisted Tunneling*, Ann. Phys. **300** (2002) 88–136.

[28] C. Eltschka and P. Schlagheck: *Resonance- and Chaos-Assisted Tunneling in Mixed Regular-Chaotic Systems*, Phys. Rev. Lett. **94** (2005) 14101 (4 pages).

[29] P. Schlagheck, C. Eltschka and D. Ullmo: *Resonance- and Chaos-Assisted Tunneling*, arXiv:cond-mat/0508024 (2005).

[30] J. D. Hanson, E. Ott and T. M. Antonsen: *Influence of finite wavelength on the quantum kicked rotator in the semiclassical regime*, Phys. Rev. A **29** (1984) 819–825.

[31] M. Sheinman, S. Fishman, I. Guarneri and L. Rebuzzini: *Decay of Quantum Accel-erator Modes*, Phys. Rev. A **73** (2006) 052110 (12 pages).

[32] J. Feist, A. Bäcker, R. Ketzmerick, S. Rotter, B. Huckestein and J. Burgdörfer: *Nano-wires with surface disorder: Giant localization lengths and quantum-to-classical crossover*, Phys. Rev. Lett. **97** (2006) 116804 (4 pages).

[33] V. A. Podolskiy and E. E. Narimanov: *Semiclassical description of chaos-assisted tunneling*, Phys. Rev. Lett. **91** (2003) 263601 (4 pages).

[34] M. Sheinman: *Decay of Quantum Accelerator Modes*, Ph.D. thesis, Technion, Haifa, Israel, (2004).

[35] A. Zwaan: *Intensitäten im Ca-Funkenspektrum*, Ph.D. thesis, University of Utrecht, (1929).

[36] S. C. Miller and R. H. Good: *A WKB-Type Approximation to the Schrödinger Equa-tion*, Phys. Rev. **91** (1953) 174–179.

[37] R. B. Dingle: *The method of comparison equations in the solution of linear second-order differential equations (generalized W.K.B. method)*, Appl. Sc. Res. **B5** (1956) 345–367.

[38] M. V. Berry and K. E. Mount: *Semiclassical approximations in wave mechanics*, Rep. Prog. Phys. **35** (1972) 315–397.

[39] H. Abramowitz and I. A. Stegun: *Handbook of Mathematical Functions*, Dover Publications, Inc., New York, 9th edn., (1970).

[40] H. Jeffreys: *On certain approximate solutions of linear differential equations of the second order*, Proc. Lond. Math. Soc. **23** (1923) 428–436.

[41] H. A. Kramers: *Wellenmechanik und halbzahlige Quantisierung* (in German), Z. Physik **39** (1926) 828–840.

[42] J. Vaníček: *Uniform semiclassical methods and their applications*, Ph.D. thesis, Harvard University, (2003).

[43] R. E. Langer: *On the Connection Formulas and the Solutions of the Wave Equation*, Phys. Rev. **51** (1937) 669–676.

[44] E. Merzbacher: *Quantum mechanics*, Wiley, New York, (1998).

[45] J. von Neumann and E. Wigner: *Über das Verhalten von Eigenwerten bei adiabatischen Prozessen*, Physik. Zeitschr. **30** (1929) 467–470.

[46] S. J. Gustafson and I. M. Israel: *Mathematical concepts of quantum mechanics*, Springer-Verlag, Berlin Heidelberg, (2003).

[47] W. Nolting: *Quantenmechanik - Methoden und Anwendungen*, Springer Verlag, Berlin, (2004).

[48] C. Cohen-Tannoudji, B. Diu and F. Laloë: *Quantenmechanik Teil 2*, Walter de Gruyter, Berlin, 2nd edn., (1999).

[49] M. Nakahara: *Geometry, Topology and Physics*, Graduate Student Series in Physics, Institue Of Physics Publishing, Bristol, (1990).

[50] M. Tabor: *Chaos and Integrability in Nonlinear Dynamics: An Introduction*, John Wiley & Sons, New York, (1989).

[51] M. V. Berry: *Regular and irregular motion*, vol. 46 of *AIP Conference Proceedings*, American Institute of Physics, (1978), reprinted in [77].

[52] J. M. Greene: *Two–dimensional measure–preserving mappings*, J. Math. Phys. **20** (1968) 760–768.

[53] B. V. Chirikov: *A universal instability of many-dimensional oscillator systems*, Physics Reports **52** (1979) 263–379.

[54] M. Brown and W. D. Neumann: *Proof of the Poincaré-Birkhoff fixed point theorem*, Michigan Math. J. **24** (1977) 21–31.

[55] H. J. Stöckmann: *Quantum chaos. An introduction*, Cambridge University Press, Cambridge, 2nd edn., (2000).

[56] C. Cohen-Tannoudji, B. Diu and F. Laloë: *Quantenmechanik Teil 1*, Walter de Gruyter, Berlin, 2nd edn., (1999).

[57] I. C. Percival: *Regular and irregular spectra*, J. Phys. B **6** (1973) L229–L232.

[58] M. V. Berry: *Regular and irregular semiclassical wavefunctions*, J. Phys. A **10** (1977) 2083–2091.

[59] A. Voros: *Semi-classical ergodicity of quantum eigenstates in the Wigner representation*, in: *Stochastic Behavior in Classical and Quantum Hamiltonian Systems*, no. 93 in Lecture Notes in Physics, 326–333, Springer-Verlag, Berlin, (1979).

[60] S.-J. Chang and K.-J. Shi: *Evolution and exact eigenstates of a resonant quantum system*, Phys. Rev. A **34** (1986) 7–22.

[61] L. Hufnagel, R. Ketzmerick, M.-F. Otto and H. Schanz: *Eigenstates ignoring regular and chaotic phase-space structures*, Phys. Rev. Lett. **89** (2002) 154101 (4 pages).

[62] J. Laskar: *Frequency analysis for multidimensional systems. Global dynamics and diffusion*, Physica D **67** (1993) 357–281.

[63] J. Laskar and C. F. ad A. Celletti: *The measure of chaos by the numerical analysis of fundamental frequencies. Application to the standard mapping*, Physica D **56** (1992) 253–269.

[64] H. Schanz, T. Dittrich and R. Ketzmerick: *Directed chaotic transport in Hamiltonian ratchets*, Phys. Rev. E **71** (2005) 026228.

[65] M. V. Berry, N. L. Balazs, M. Tabor and A. Voros: *Quantum maps*, Annals of Physics **122** (1979) 26–63.

[66] A. Bäcker, R. Ketzmerick and A. G. Monastra: *Flooding of chaotic eigenstates into regular phase space islands*, Phys. Rev. Lett. **94** (2005) 054102 (4 pages).

[67] V. F. Lazutkin: *KAM theory and semiclassical approximations to eigenfunctions*, Springer-Verlag, Berlin, (1993).

[68] M. V. Berry and N. L. Balazs: *Evolution of semiclassical quantum states in phase space*, J. Phys. A **12** (1979) 625–642.

[69] A. G. Monastra: *private communication*.

[70] J. P. Keating, M. Noaves, S. D. Prado and M. Sieber: *Semiclassical structure of chaotic resonance eigenfunctions*, Phys. Rev. Lett. **97** (2006) 150406 (4 pages).

[71] R. Schubert: *private communication*.

[72] A. Bäcker, R. Ketzmerick, A. Monastra and L. Schilling: *Semiclassical quantization of regular islands of quantum maps (in preparation)*.

[73] A. Bäcker, R. Ketzmerick, S. Löck and L. Schilling: *Direct dynamical tunneling in a mixed phase space (in preparation)*.

[74] I. S. Gradshteyn and I. M. Ryzhik: *Table of Integrals, Series, and Products*, Academic Press, London, 6th edn., (2000).

[75] A. J. Lichtenberg and M. A. Lieberman: *Regular and Chaotic Motion*, vol. 38 of *Applied Mathematical Sciences*, Springer-Verlag, New York, 2nd edn., (1992).

[76] S. Löck: *Dynamisches Tunneln im gemischten Phasenraum*, Diploma thesis, Technische Universität Dresden, (2006).

[77] R. S. MacKay and J. D. Meiss: *Hamiltonian Dynamical Systems*, Adam Hilger, Bristol and Philadelphia, (1987), (reprint selection).

Acknowledgments

Erklärung

Hiermit versichere ich, dass ich die vorliegende Arbeit ohne unzulässige Hilfe Dritter und ohne Benutzung anderer als der angegebenen Hilfsmittel angefertigt habe. Die aus fremden Quellen direkt oder indirekt übernommenen Gedanken sind als solche kenntlich gemacht. Die Arbeit wurde bisher weder im Inland noch im Ausland in gleicher oder ähnlicher Form einer anderen Prüfungsbehörde vorgelegt.

Die vorliegende Arbeit habe ich unter der Betreuung von Prof. Dr. Roland Ketzmerick am Institut für Theoretische Physik angefertigt. Ich erkenne die Promotionsordnung der Fakultät Mathematik und Naturwissenschaften vom 20. März 2000 an.

Dresden, den 11. Dezember 2006